Pendulum Impact Machines

Procedures and Specimens for Verification

Thomas A. Siewert and
A. Karl Schmieder, editors

STP 1248

STP 1248

Pendulum Impact Machines: Procedures and Specimens for Verification

Thomas A. Siewert and A. Karl Schmieder, Editors

ASTM Publication Code Number (PCN):
04-012480-23

ASTM
1916 Race Street
Philadelphia, PA 19103
Printed in the U.S.A.

Library of Congress Cataloging-in-Publication Data

Pendulum impact machines: procedures and specimens
for verification/Thomas A. Siewert and A. Karl
Schmieder, editors.
p. cm.--(STP; 1248)
"ASTM publication code number (PCN): 04-012480-23"
Includes bibliographical references and index.
ISBN 0-8031-2018-4
1. Impact--Testing--Equipment and supplies. 2.
Pendulum. 3. Notched bar testing--Equipment and
supplies. I. Siewert, T. A. II. Schmieder, A. Karl
(Albert Karl), 1919-- . III. Series: ASTM special
technical publication; 1248.
TA418.34.P46 1995
620.1'123--dc20

95-13999
CIP

Peer Review Policy

Each paper published in this volume was evaluated by three peer reviewers. The authors addressed all of the reviewers' comments to the satisfaction of both the technical editor(s) and the ASTM Committee on Publications.

The quality of the papers in this publication reflects not only the obvious efforts of the authors and the technical editor(s), but also the work of these peer reviewers. The ASTM Committee on Publications acknowledges with appreciation their dedication and contribution to time and effort on behalf of ASTM.

Printed in Fredericksburg, VA
May 1995

Foreword

This publication, *Pendulum Impact Machines: Procedures and Specimens for Verification,* contains papers presented at the symposium of the same name held in Montreal, Quebec, Canada, on 18–19 May 1994. The symposium was sponsored by ASTM Committee E-28 on Mechanical Testing and its Subcommittee E28.07 on Impact Testing. The symposium was chaired by Tom Siewert, National Institute of Standards and Technology, and Karl Schmieder, consultant on mechanical testing.

Contents

Overview

This was the sixth symposium published by ASTM on the topic of impact testing. The five previous symposia, *Proceedings of ASTM,* Vol. 22-II (1922), *Proceedings of ASTM,* Vol. 38-II (1938), STP 176 (1956), STP 466 (1970), and STP 1072 (1990), were sponsored by ASTM Subcommittee E28.07 (prior to 1969 known as E-1.7). These symposia covered a broad range of topics and occurred rather infrequently. The period before 1985 might be characterized as one in which the Charpy test procedure was broadly accepted and changing very slowly. However, the last symposium (1989), "Charpy Impact Test: Factors and Variables," was driven by new forces: a recognition within ISO Technical Committee 164 (Mechanical Testing) Subcommittee 4 (Fracture) of shortcomings in the procedure and a desire to know the basis for the requirements. Although most of the requirements and procedure details were considered quite reasonable and still valid, there was a desire by the late 1980s to restudy a few of the relationships. Some felt that changes in materials and energy ranges (from those under which the original relationships were developed) might justify slight revisions to the procedures. Also, some other standards and users in other countries had adopted different procedures, which raised questions about comparison of data developed under these different procedures.

Authors from five countries presented a broad variety of test data at the 1989 Symposium, which encouraged spirited discussion and comparison of the results. The twelve papers in the proceedings (STP 1072) and another paper in the *Journal of Testing and Evaluation* provided a review of the effects of procedural and specimen variables in Charpy impact testing. The data proved to be of interest to many general users of the test, but was of particular interest to the members of ASTM Subcommittee E28.07 (the subcommittee responsible for Standard E-23 on the Charpy test). During the past five years, the data presented at the symposium have been the single most important factor in determining whether to change various requirements in Standard E-23. The data have also been useful in supporting tolerances and procedural details during the reballoting of ISO Standard 442 on Charpy testing.

By 1991, the E28 Subcommittee on Symposia suggested that it was time to schedule another symposium on Charpy impact testing. One reason was because the 1989 symposium did not answer certain questions about the choice of tolerances in the specifications. Indeed, several of the papers appeared to reach conflicting conclusions about the effect of certain variables.

The Call for Papers for the 1994 Symposium specifically invited studies on the issues of procedures and specimens for machine verification. The following paragraphs describe our success in attracting papers that study the procedural details and suggest changes in the tolerances in ASTM and ISO standards.

This publication includes three papers comparing the 8-mm and the 2-mm radius striker designs. These papers (Nanstad and Sokolov; Siewert and Vigliotti; and Tanaka et al.) confirm that the data taken with the two strikers are not interchangeable and suggest that the 8-mm radius typically produces higher energies below about 20 J and that the 2-mm radius striker produces higher energies above 100 J. In the intermediate range, the results are less consistent. During the final discussion period, we tried to find ways to resolve the use of different striker radii between countries. It became clear that there is no easy solution because each country has developed a large statistical database with their own striker design (8- or 2-mm radius). These data have been incorporated in a complex web of other standards and requirements. However, it was very encouraging to learn that the European standards (EN series) may add the 8-mm striker in the next revision (in about four years) and that the ASTM subcommittee plans to add the 2-mm striker in their next revision of E23. Unfortunately, there does not seem to be a similar activity in Japan.

We heard about the development of standardized specimens for indirect verification of machine performance to supplement direct measurements (primary physical characteristics of the machines). Papers by Hida and by Galban et al. described the development of standardized specimens for Japan and France, respectively. Building on the statistical calculations contained in these two papers, a paper by Splett and Wang provided more details on the determination of the quality of standardized specimens.

In the area of machine and specimen tolerances, we learned about the effect of machine alignment on second strike marks (Schmieder et al.), the effect of specimen edge squareness (Marsh), striker geometry tolerances (Ruth), striker surface finish (Ruth et al.), subsize speciments (Alexander et al. and Manahan et al.), and reconstitution of specimens (Williams et al.).

The topic of machine verification is becoming important for nonmetallic materials as well. The Call for Papers was developed in discussions with ASTM Subcommittee D20.10 (Mechanical Properties of Plastics) and Section D20.10.02 (Impact Properties of Plastics) to include papers on Charpy and Izod testing of plastics. We received a paper by Mackin and Tognarelli on calibration of an impact machine for plastics and one by Kalthoff and Wilde on instrumented impact testing of polymeric materials.

Other papers covered the use of load-displacement curves for obtaining more information from impact tests (KarisAllen and Matthews and McCowan et al.) and the kinetic energy of the specimen being tossed from the machines (Chandavale and Dutta for an unbroken specimen; Kalthoff and Wilde for the two broken halves).

Many people commented that they found the information presented in this symposium to be particularly interesting. One reason for this may be that the 1994 symposium attracted contributions from many countries. Twenty-one of the forty-two authors and coauthors are from outside the U.S., an even broader participation that in the 1989 symposium. We believe that this is due partly to wide distribution of the Call for Papers at international meetings and because of the current importance of this topic in international commerce.

Although the 1994 symposium provided much useful information that will allow us to improve impact testing standards, it also identified other differences between standards and will require further study before a decision can be made. The following topics should be considered for inclusion in the Call for Papers for a future symposium:

1. The theoretical effect of striker contact radius on the state of elastic stress at or near the root of a Charpy specimen notch.
2. The use of instrumented strikers to separate the energies of crack initiation and of crack propagation for machines with 8-mm and 2-mm striker radii in the range below 25 J Charpy V-notch absorbed energy.
3. Correlation of results of static tests for plane-strain fracture toughness to those for Charpy V-notch impact tests at different temperatures, using both the ISO and the ASTM striker.
4. By finite element or other analytical techniques, determine the striker form that will minimize the plastic work of crushing and bending the specimen.
5. Compare the absorbed energy as measured by machines with C-type pendulums to U-type, including materials with high yield strength and absorbed energy less than 20 J.

Acknowledgments

We appreciate the assistance of E28.07 members, many of whom helped by chairing the sessions and by reviewing the manuscripts. We particularly appreciate the assistance of J. M. Holt who (in his role and Chairman of Subcommittee E28.93 on Symposia) helped us obtain sponsorship of the Symposium and provided valuable advice on the arrangements, and who (in his role as the U.S. delegate to ISO Committee 164-TC4) encouraged international participation. We also received wise advice from a large number of the ASTM staff on symposium arrangements, selection of reviewers, and the other myraid of details necessary for a successful symposium.

The Specimen

A. Karl Schmieder[1], Patrick T. Purtscher[2], and Daniel P. Vigliotti[2]

THE ROLE OF STRIKE MARKS ON THE REPRODUCIBILITY OF CHARPY IMPACT TEST RESULTS*

REFERENCE: Schmieder, A.K., Purtscher, P.T., and Vigliotti, D.P., "The Role of Strike Marks in the Study of Reproducibility of the Results of Charpy Impact Tests," Pendulum Impact Machines: Procedures and Specimens for Verification, ASTM STP 1248, T.T. Siewert and A.K. Schmieder, Eds., American Society for Testing and Materials, Philadelphia, 1995.

ABSTRACT: Charpy V-notch specimens from one lot of high-strength steel were tested using three machines to determine reference values for three measures of toughness: absorbed energy, lateral expansion, and height of shear lips. The broken specimens were examined to determine the location and magnitude of changes in specimen features made during testing. The features of interest were the height and location of the shear lips, the location of the lateral expansion projections ranked by height, and the location, length, width, and angle of the first- and second-strike marks. Changes in these features were compared to the changes in average absorbed energy for each of the machines in its standard condition. To correlate changes in these features with intentional machine modifications, ten series of tests were made on a fourth machine. Patterns which could predict the direction of change in absorbed energy for most modifications were observed. The trends indicated by these data are: (1) each modification resulted in an increase in absorbed energy, (2) the distance between second-strike marks is a measure of the compliance of the striking edge and anvil, (3) the offset of the first-strike marks is largely due to lift-off of the specimen at the moment the striker hits the specimen, (4) offset and the angle of second-strike marks are measures of general asymmetry of loading, and (5) lateral expansion and shear lips are valuable as means to detect scale errors and excess losses not related to the work of fracture.

KEYWORDS: Absorbed energy, Charpy V-notch, high-strength steel, high-speed photography, impact machine, lateral expansion, shear lips, strike marks

[1]Consultant, Mechanical Testing, Scotia, NY 12302

[2]Physical Scientist and ASTM Charpy Program Coordinator respectively, NIST, Boulder, Colorado 80303

*Contribution of NIST, not subject to copyright.

NOMENCLATURE

composite postfracture energy -- a measure of the work done to create the fracture surface, excluding energy expended in shock losses, toss losses, and work to form depressions in the specimen at points of contact.

lift-off -- the momentary loss of contact between the specimen and the anvils, which occurs immediately after first contact.

offset -- the horizontal distance from the striking edge to the notch.

reference value -- a value obtained from tests made by a machine in standard condition.

specimen locations -- when the specimen is in the position for testing.

in direction of swing:
(N)[3] notched surface -- the surface parallel to the notch root and nearest it.
(S) struck surface -- the surface parallel to notch root and farthest from it.

vertically:
(U) upper horizontal surface.
(L) lower horizontal surface.

transversely:
(I) inboard half -- portion of specimen originally between the striking edge and the machine column.
(O) outboard half -- the portion originally adjacent to the inboard half.

first-strike mark -- the mark made on the specimen by the anvils before fracture (see Fig. 1).

second-strike mark -- the mark made on the specimen if the broken halves fly away from the pendulum and strike the anvils (see Fig. 1).

third-strike mark -- additional mark made on the specimen after fracture by striking a machine part or other solid object in the vicinity.

types of second-strike marks:

line -- the second-strike mark which completely crosses the notched surface (see Fig. 2, codes A, I and J).

nick -- a second-strike mark which impacts both edges, but not in the center, of the notched surface (see Fig. 2, codes B and F).

others -- a nick at one edge only, or a nick on one half and a line on the other half, or no second-strike marks on one half.

INTRODUCTION

Relative to hardness and tension tests of metal, impact tests have poor reproducibility. This is economically important since it requires more tests to ensure a given degree of precision. This testing

[3]Letters are abreviations used in Tables.

problem has been long recognized [1-4]. Although significant improvements have been made during the last three decades [5], limited reproducibility remains one of the principal disadvantages of impact testing. The objective of this study is to reduce the variability of impact test results by identifying machine deficiencies through inspection of the broken specimens.

This inspection included the usual measurement of absorbed energy, lateral expansion, and shear lips. In addition, another less well-known measurement was made, the characterization of subsequent strike marks. The process of forming the marks is shown schematically in Fig. 1. High-speed photographs confirm the transverse flight of the broken halves and the strike against the anvils. Enlarged photographs in Fig. 2 show various types of first- and second-strike marks.

EXPERIMENTAL PROCEDURES

Specimens

All specimens were drawn at random from a large lot of verification-grade specimens. The material specification is published in ASTM Standard Practice for Qualifying Charpy Verification Specimens of Heat Treated Steel, E 1271, Appendix X1. The specimen dimensions were those for Type A shown in Fig. 6 of ASTM Standard Methods for Notched Bar Impact Testing of Metallic Materials E 23 except that the tolerances are smaller.

Machines

The first three machines, which were used to determine the reference values, were manufactured by different companies to meet the specifications of ASTM E 23. All had capacities of 300 J (220 ft·lbf) or more. All were directly verified within a year of making the tests

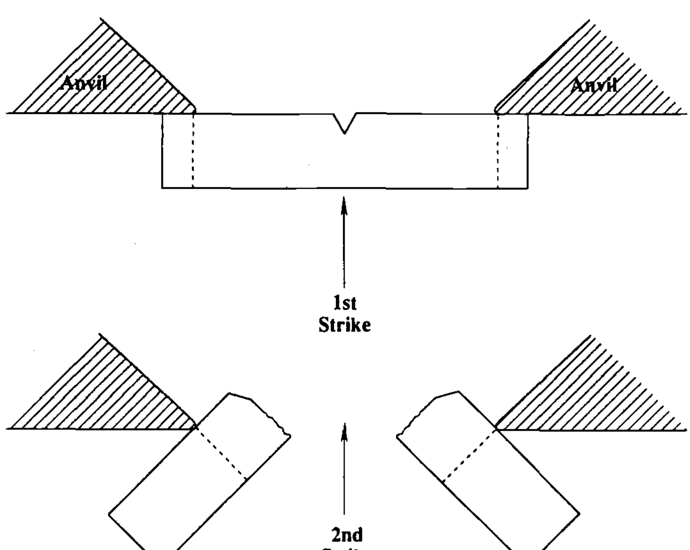

Fig. 1 -- Schematic diagram shows how the first- and second-strike marks are produced.

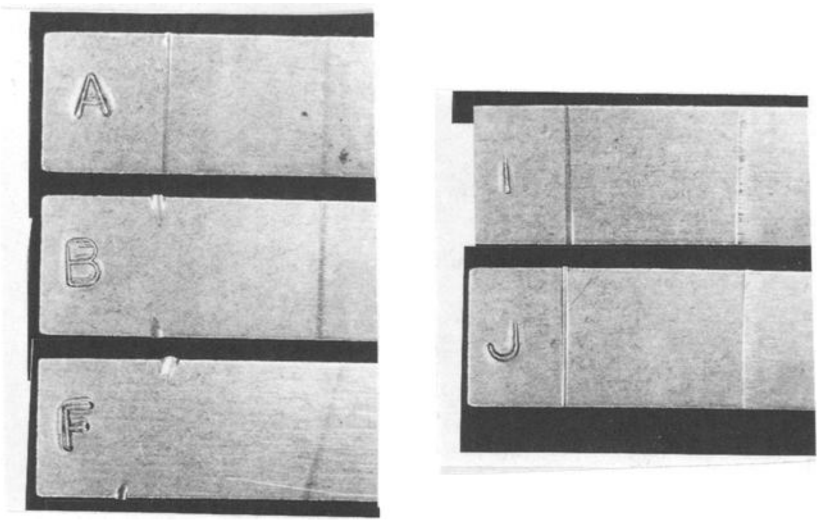

Fig. 2 -- Photographs of the struck surfaces on a broken half from each of the following series: A, B, F, I, and J. The first-strike marks are on the right-hand side and the second-strike marks are on the left-hand side.

reported here. The fourth machine, which was modified during these tests, had less than half the capacity of the others. The machine designations used in this study, the pendulum types (as described in ASTM E 23, Fig. 1), and the scale errors in percentage of the reading are:

Designation	R1C	R1U	R2U	M1C
Type of pendulum	C	U	U	C
Scale error	-3.0%	-0.8%	-0.3%	0.0%

All reported values are corrected for the scale errors that are known. A method to estimate the scale error for M1C is discussed later. The modifications made to Machine M1C are given letter designations and are listed below. The same letters are used to identify the test series in the tables of results.

A. As received. History of prior use unknown. Tightness of bolts unknown.

B. Old anvils replaced by new anvils. Bolts tightened to 100 J (75 ft·lbf) at each installation.

C. Old anvils reinstalled.

D. Place specimen on the supports so that they are offset 2 mm toward the machine pedestal.

E. New taller supports installed to raise the specimen 10.6 mm above the standard position. During this and each subsequent replacement of the supports, the bolts were tightened to 27 J (20 ft·lbf).

F. Reinstall the original inboard support only.

G. Remove both supports so the specimen is 10.9 mm below the standard position.

H. Shorten and grind the top surface of the new supports so that the specimen is slanted upward toward the anvil at one degree with the horizontal and reinstall.

I. Reinstall the original standard supports. Remove old anvils and grind the face which bears against the specimen so that it has an angle of 10:1000 to the original surface, measured in a vertical plane when installed. Restore the corner radii and surface finish. Reinstall modified anvils.

J. Remove anvils and restore contact faces to original condition, also reduce the thickness in the direction of swing by 5 mm. Reinstall modified anvils.

K. Reinstall new anvils, restoring the machine to standard condition. Photograph specimen half as it flies transversely and strikes the anvil.

Methods of Testing

All specimens were tested at -40°C (-40°F) in accordance with ASTM E 23. The lateral expansion of the broken specimens was measured as prescribed in ASTM E 23-93a, Section 12.4.2.

The location, length, and width of the strike marks were measured with an optical comparator in the reflective mode. Magnifications of 10X and 20X were used for the first- and second-strike marks, respectively.

Many of the first-strike marks had poorly defined outer boundaries. To be consistent, we reported the distance from the notch root center-line to the inner boundary of the mark. For a few marks, both boundaries were poorly defined and no dimension was recorded.

The high-speed photographs were taken at 2000 frames per second with a video system. The lighting system included two banks of incandescent lights arranged around the outboard side of the impact machine, for a total of 1500 watts of power.

Methods of Calculation

The statistical calculations were made according to the mathematical definitions of the average and standard deviation. The lateral expansion was measured as prescribed by ASTM E 23, that is, by the sum of the two highest of the projections at the ends of the pendulum strike marks on both broken halves. This method is based on test results which correlate lateral expansion and absorbed energy over a wide range, mostly at energies higher than those reported here. Some information is available in the range of these tests [6].

Since four measurements are taken in any case, they were added to see if the correlation with absorbed energy was improved in the range of these tests. To make the results compatible with the standard value, the sum of the four measurements is divided by two when reported.

The composite postfracture energy index reported is calculated by dividing the average value for a series by the average of all specimens tested during the program. This is repeated for each of the three types of measurements of postfracture energy, and then the three values are averaged. The result is a dimensionaless number for each series which allows the series to be compared but does not indicate the magnitude or units of the energy measurement. To allow comparison to other published results, the composite number is multiplied by the average value for all tests for the lateral expansion measured according to ASEM E 23. The average values for all tests are shown on the bottom line of Table 1 and the values for Series R1C on the top line. Using these values, the composite postfracture index for Series R1C is

$$0.133\left[\frac{\left(\frac{0.12}{0.133}\right)+\left(\frac{0.11}{0.111}\right)+\left(\frac{1.35}{1.403}\right)}{3}\right] = 0.126\ mm.$$

The distance reported as a measure of position of second-strike marks is the distance from the centerline of the notch to the centerline of the mark. The offset is equal to one half of the difference between first-strike marks, measured on the inboard and the outboard halves. Unless stated otherwise, the distances at the upper and lower surfaces are averaged before the difference is calculated.

RESULTS

Table 1 shows averages and standard deviations of energy measurements for some single series and for combinations of related series. Table 2 shows the energy measurements for all of the series as a dimensionless ratio to the average values for Machine M1C. This permits comparison of quantities, such as lateral expansion to absorbed energy, which have different units and magnitudes varying by a factor of over one hundred.

TABLE 1 -- Weighted average values for for quantities which are given as a single number for both broken ends.

Machine or Class	Absorbed Energy J, ft·lbf	Lateral Expansion[a]		Sum of Shear Lips, mm
		E 23, mm	Sum/2, mm	
R1C	15.9, 11.7 (0.3%)[b]	0.12 (0.01)[c]	0.11 (0.01)[c]	1.35 (0.11)[c]
R1U	17.2, 12.7 (0.5)	0.14 (0.03)	0.12 (0.01)	1.43 (0.14)
R2U	17.5, 12.9 (0.5)	0.14 (0.03)	0.12 (0.01)	1.40 (0.13)
M1C-A	15.2, 11.2 (0.6)	0.11 (0.10)	0.09 (0.01)	1.36 (0.09)
A,B,C,K	15.3, 11.3 (0.2)	0.13 (0.02)	0.10 (0.01)	1.34 (0.04)
M1C-Others	15.9, 11.7 (0.3)	0.14 (0.01)	0.11 (0.01)	1.45 (0.09)
All RXX	16.9, 12.4 (0.6)	0.13 (0.01)	0.12 (0.09)	1.39 (0.04)
All XXU	17.4, 12.8 (0.2)	0.14 (0.00)	0.12 (0.00)	1.40 (0.04)
All Std.C[d]	15.5, 11.4 (0.2)	0.13 (0.00)	0.10 (0.00)	1.34 (0.01)

[a] E 23 is sum of two highest projections. "Sum/2" is one half the sum of the four readings.
[b] Values in parenthesis are coefficients of variation.
[c] Values are standard deviation in mm.
[d] Values from R1C and M1C: Series A,B,C,K.

TABLE 2 -- Deviations[a] of energy-related measurements in Table 1 from the corresponding values for Machine R1C.

ID[b]	Absorbed Energy	Lateral Expansion		Height of Shear Lip
		E 23 method	Sum of Four	
R1C (10)	0.0 (0.0)	0.0 (0.0)	0.0 (0.0)	0.0 (0.0)
R1U (10)	8.5 (0.7)	14.6 (2.7)	12.5 (0.9)	15.9 (0.3)
R2U (10)	10.3 (0.7)	15.2 (1.6)	15.9 (0.6)	2.4 (0.3)
M1C-A (6)	-4.5 (1.1)	-6.3 (0.7)	-14.0 (0.3)	0.7 (-0.2)
B (6)[c]	-5.3 (0.4)	5.7 (5.4)	-1.5 (3.5)	0.7 (0.5)
C (5)[c]	-3.0 (0.2)	13.3 (-0.6)	15.1 (-0.4)	-4.8 (0.1)
D (5)	2.6 (0.6)	28.5 (0.2)	1.1 (0.4)	14.1 (0.7)
E (5)	-1.7 (0.5)	5.3 (1.4)	-4.2 (0.7)	3.0 (-0.3)
F (6)	-2.7 (0.6)	7.8 (-0.4)	-4.5 (0.5)	3.0 (0.1)
G (5)	-0.9 (0.6)	12.1 (2.8)	6.8 (1.3)	3.0 (0.9)
H (5)	1.7 (0.0)	18.4 (1.4)	13.9 (0.2)	4.4 (0.9)
I (5)	1.3 (1.1)	20.5 (0.6)	4.6 (0.8)	0.7 (-0.2)
J (5)	3.4 (0.2)	18.4 (3.3)	16.3 (0.2)	10.8 (0.2)

[a] Deviation of measured quantities are shown as percentages, deviation of the coefficient of variation of that quantity as a ratio.
[b] Machine identification, series, and number of specimens.
[c] One of the halves not available for measurement.

Table 3 presents the various second-strike measurements. Table 4 is a tally showing the number of occurrences of various deformations at specified locations. Its primary use is to identify asymmetrical conditions. Table 5 presents statistics on first- and third-strike marks and compares absorbed energy to the composite postfracture energy.

DISCUSSION

Significance and Limitations of Various Measurements

One of the main objectives of the impact test is to measure the energy required to produce the fracture surface. The loss of potential energy of the pendulum during the swing is reported as absorbed energy, but it also includes:

A. friction losses due to pendulum motion,

B. shock losses due to vibration and displacement of the machine parts,

TABLE 3a -- For the reference machines, average values and coefficients of variation for position, width, and direction of second-strike marks.

ID[a]	Distance from Notch to Mark[b]				Line Width,[c] mm	Angle with Upper Edge, deg.			
	Outboard		Ratio 0/I			Outboard		Inboard	
	Lines	Others	Lines	Other		Lines	Others	Lines	Others
R1C	0.94 (0.04)[d]	0.94 (0.04)	1.03 (0.08)	1.06 (0.09)	1.22/1.12[e] (0.38)	0.3 (0.7)	3.2 (0.4)	0.2 (1.0)	0.5 (0.4)
R1U	0.94 (....)	0.93 (0.04)	0.98 (....)	1.03 (0.07)	0.28/0.34 (0.31)	1.0 (...)	2.0 (0.3)	0.2 (...)	0.2 (0.5)
R2U	1.06 (0.02)	0.99 (0.04)	1.05 (0.06)	0.99 (0.03)	1.25/1.22 (0.37)	1.6 (0.5)	2.7 (0.8)	0.8 (1.3)	0.2 (1.1)

[a] Machine identification and type of pendulum.
[b] Dimensionless ratio of distance to width of specimen, which is 10 mm.
[c] Width of all specimens in a series combined statistically.
[d] Value in parentheses is ratio of standard deviation to average.
[e] Upper surface/lower surface.

C. crushing work to form the depressions on the surfaces struck by the pendulum and the anvils simultaneously, and

D. the kinetic energy of the broken halves after fracture.

<u>Absorbed energy</u> -- ASTM E 23 includes a correction for (a) which adequately removes this amount of work from the reported absorbed energy [7]. The other losses are included in the reported value. Measurements of lateral expansion remove all of the above except the crushing work at the struck surface. The shear-lip-height method excludes all of the losses. However, that does not mean that the machine has no influence on the results from these alternative measures of energy. These tests indicate that the different machines impose different conditions of force, displacement, and loading points which influence the work done at or near the fracture; therefore, the resulting numbers are not solely material properties. Attempts to separate these machine dependent contributions by measurements of the broken specimen halves is discussed further in other sections.

<u>Lateral expansion</u> -- The principal use of lateral expansion in this study is to provide a measure of the work to produce a fracture without depending on the energy measurement scale of an impact machine. In order to estimate its discriminatory capability in a single series, a regression analysis was made with inputs of the average absorbed energy and lateral expansion from each of the fourteen series unweighted for the number of specimens in each series. The regression of series averages showed regression coefficients 0.534 for the ASTM method, 0.644 for the sum method, and 0.552 the composite postfracture energy, respectively.

TABLE 3b -- For Machine M1C, average values and coefficients of variation for position, width, and direction of second-strike marks.

ID[a]	Distance from Notch to Mark[b]		Line Width,[c] mm	Angle with Upper Edge,	
	Outboard	Ratio O/I		Outboard	Inboard
A	0.94 (0.02)	1.01 (0.05)	0.49 (0.16)	1.3 (0.8)	1.2 (1.1)
B	0.90 (0.06)	1.04 (0.06)	0.65 (0.30)	2.5 (0.4)	2.1 (0.7)
C	0.90 (0.07)	1.00 (0.07)	0.57 (0.50)	1.5 (0.9)	1.9 (1.0)
D	1.09[e] (0.01)	... (...)	0.56[e] (0.11)	1.6[e] (0.4)	... (...)
E	0.89 (...)	0.98 (...)	0.64 (0.10)	0.9 (0.5)	1.4 (0.8)
F	0.83[f] (0.05)	... (...)	1.21[f] (0.10)	... (...)	19.0 (0.3)
G	0.86 (0.04)	0.95 (...)	0.67 (0.29)	2.6 (0.4)	... (...)
H	0.86 (0.05)	0.99 (0.05)	0.84 (0.28)	2.8 (0.7)	4.7 (0.4)
I	0.89 (0.03)	1.05 (0.06)	0.56 (0.15)	1.3 (0.9)	1.1 (0.6)
J	0.86 (0.06)	1.04 (0.11)	0.49 (0.17)	1.8 (0.8)	1.0 (0.7)

[a] Series identification.
[b] Dimensionless ratio of distance to width of specimen, which is 10 mm.
[c] Width of all specimens in a series combined statistically.
[d] Value in parentheses is ratio of standard deviation to average.
[e] Outboard values. No strike marks on inboard halves.
[f] No strike marks on upper outboard halves.

Shear-lip heights -- The shear-lip height has the advantage of less proportional reading error than lateral expansion; the shear-lip heights were about 10 times greater than the lateral expansions. This difference would seem to compensate for the differences in the reference surfaces for the two methods, a fracture surface for the former and a ground surface for the latter. Another disadvantage of the shear-lip height is that a maximum is sought along the crest of the lip by measuring at various distances from the notch. A much more serious source of error is that most crests were flattened by various amounts from contact with a hard plane surface.

A regression analysis of the ten individual specimens vs. the absorbed energy of each showed that the shear-lip height was superior to the lateral expansion method for a single series. The regression coefficients were 0.81 for the R1C machine, 0.56 for R1U, and 0.46 for the R2U machine. Corresponding values for lateral expansion were all less than 0.25.

First-strike marks -- The accuracy of the measurements can be judged by comparing the distance between first-strike marks on the inboard and outboard halves to the specified distance between anvils. For the three reference machines, the distance between marks are 41.0 ± 0.2 mm for R1C, 41.1 ± 0.1 mm for R1U, and 41.1 ± 0.2 mm for R2U. The specified

TABLE 4 -- Evaluation of machine asymmetry by number of deformations at various locations.

ID[a]	Start of Second-Strike Marks[b]						Shear Lips		Lateral Expansion Projections[c]							
	Line		Nick		None[d]				Upper Surface				Lower Surface			
	U	L	U	L	U	L	U	L	A	B	C	D	A	B	C	D
R1C																
-O	6/1[e]	6/4	4/2	4/3	0	0	5/2	4/3	2	3	1	4	3	2	2	3
-I	7/2	7/5	3/1	2/1	0	1	5/3	6/2	2	4	1	3	4	4	1	1
R1U																
-O	6/6	6/0	2/0	4/4	2	0	3/2	6/1	2	2	1	3	4	2	1	1
-I	3/1	3/2	6/2	6/5	1	1	7/4	4/3	1	3	2	2	1	3	3	1
R2U																
-O	6/6	6/0	4/1	4/3	0	0	5/3	5/2	5	2	2	1	3	3	4	0
-I	6/5	6/1	4/3	4/1	0	0	5/3	5/2	3	3	2	2	1	2	0	7
M1C																
A-O	2/2	2/1	2/1	3/1	1	0	4/2	3/1	1	2	2	1	3	3	0	0
A-I	6/4	6/2	0	0	0	0	3/2	3/0	2	1	1	2	2	0	1	3
M1C																
B-O	2/2	2/0	2/1	3/1	1	0	2/1	0	2	1	2	0	2	0	1	2
B-I	1/1	1/0	4/0	5/0	1	0	3/1	6/3	1	1	1	2	2	1	1	1
M1C																
D-O	5/5	5/0	0	0	0	0	1/0	4/1	0	1	1	2	0	3	1	0
D-I	0	0	0	0	0	0	4/3	1/1	0	0	1	3	1	2	0	1
M1C																
H-O	3/2	3/1	2/1	2/1	0	0	3/2	3/2	2	1	2	0	0	3	2	0
H-I	1/0	1/1	3/1	4/2	1	0	2/0	2/1	2	0	1	2	1	1	2	1
M1C																
J-O	3/3	3/0	2/2	2/0	0	0	2/1	3/2	1	1	0	3	3	1	1	0
J-I	5/3	5/2	0	0	0	0	3/1	2/1	1	0	2	2	1	2	2	0

[a]Machine identification - Position of half before fracture.
[b]Where first contact between the specimen and the anvil occurs, "U" designates upppermost surface in position for testing, "L" the opposite.
[c]Letters indicate ranking of heights at four locations. A is highest projection. If two are equal, both receive the same rank and the next lowest is omitted.
[d]Indicates no second strike mark at that location.
[e]Numerator is total number of occurrences at that location. Denominator is the number of highest values included in the numerator.

Table 5 -- Absorbed energy, index of fracture work, first-strike dimensions, and frequency of occurrence of third-strike marks.

ID	Absorbed Energy, J	Composite Index of Fracture, mm	First-Strike Marks			Third-Strike Marks[a]			
			Offset	Angle, deg		Fracture End			
			mm	O	I	Lips[b]	Corner	Surface	Edge
R1C	15.9 (2.5)[c]	0.126	0.1 (0.5)	0.4° (0.7)	0.2° (1.5)	67	13	7	27
R1U	17.2 (4.0)	0.140	0.2 (0.7)	0.4 (1.5)	0.1 (2.1)	55	22	11	27
R2U	17.5 (3.9)	0.140	0.3 (0.9)	0.2 (1.8)	0.4 (1.0)	50	...	...	45
- A	15.2 (5.6)	0.113	0.1 (0.9)	0.6 (0.9)	0.2 (1.6)	109	72	55	45
- B	15.0 (3.6)	0.128	0.1 (0.8)	0.1 (...)	0.9 (1.6)	110	20	80	10
- C	15.4 (3.0)	0.135	0.1 (0.4)	0.3 (1.2)	0.3 (1.5)	89	22	67	44
- D	16.3 (3.9)	0.144	2.1 (1.3)	0.2 (1.4)	0.1 (2.2)	0	0	0	0
- E	15.6 (3.7)	0.128	0.0 (0.4)	0.2 (1.4)	0.2 (1.4)	55	18	36	64
- F	15.4 (4.1)	0.127	0.5 (0.5)	12.8 (0.1)	14.3 (0.1)	40	20	60	10
- G	15.7 (4.0)	0.135	0.1 (0.4)	1.1 (0.7)	1.3 (0.8)	83	8	50	33
- H	16.1 (2.5)	0.141	0.1 (0.3)	0.3 (0.9)	0.5 (1.1)	70	...	70	20
- I	16.1 (5.2)	0.136	0.1 (0.9)	0.3 (0.9)	0.6 (0.7)	67	...	44	44
- J	16.4 (2.8)	0.145	0.2 (0.5)	0.2 (1.4)	0.3 (0.9)	22	22	22	22

[a]Values shown are number of occurrences as a percent of the number of specimen halves examined.
[b]Flattening of the tip of the shear lip, therby reducing the height.
[c]Values shown in parentheses are standard deviations as percentages of the value.

gap between anvils is 40.0 ± 0.05 mm and the distance between tangent points (gap + radius of curvature) is approximately 42.0 mm. The average of the values for the three machines differs from the average of the specified dimensions by 0.2 mm or 0.5 percent, indicating that the distance measurements have better precision than any other measurements presented in this report. The angle measurements are derived trigonometrically from the distance measurements. Their accuracy is estimated at 0.3 deg.

For the thirteen series of tests reported in Table 5, the average offset of first-strike marks was typically less than 0.3 mm; four values are less than 0.1 mm, indicating that the specimens had been positioned very precisely. One explanation for higher offsets is operator carelessness, but that would not account for the fact that the angles, which the operator does not control, vary just as much. Even more puzzling is the fact that the angles on each end of the specimen differ, in some cases, by more than the estimated inaccuracy. An explanation is that after the first contact with the striker, the specimen bends and loses contact with the anvils momentarily. Furthermore, when contact is restored, one anvil may touch before the other, allowing the specimen to continue tilting until the second anvil makes contact. The published records of force vs. time during the first contact between the specimen and the striking edge of a high-strength steel specimen show the force decreasing, approaching zero for a short period, thus indicating that lift-off occurs [8,9].

Second-strike marks -- The second-strike marks provide more measurements related to asymmetry than the other reported characteristics of the broken halves. The most conspicuous is whether the marks are lines or nicks. A less obvious but just as useful difference is the width of the strike mark, the edge showing the widest mark having struck the anvil first.

The feature found most useful for quantitative analysis is the sum of the distance between second-strike marks, obtained by adding the distance from notch to mark for the outboard half of the specimen to that for the inboard half. This distance seems to be a measure of compliance of anvils and frame. The test series did not contain a comparison of directly controlled compliance, but Series I and J have partial contact between the specimen and the anvils during the initial loading, thus, simulate the slower rate of force increase of a less stiff system. The average distance between marks for the same machine and the same anvils in normal condition (Series A and C) was 36.9 mm while that for the less stiff anvils (Series I and J) was 35.8 mm or a decrease of 3 percent. The corresponding increase in absorbed energy was 15.3 to 16.2 J or an increase of 3 percent, both changes being larger than those due to other modifications. Bluhm has demonstrated that the absorbed energy increases with a decrease in machine stiffness [10].

Third-strike marks -- For Type-C machines, the specimen halves can leave the machines transversely without again being near the moving pendulum. For Type-U machines, the specimens rebound from the shrouds and approach the moving pendulum. With this in mind, we expected that the Type -U machines would have more third-strike marks. This expectation is not confirmed by the test results shown in Table 5.

The reported effectiveness of shrouds in reducing jamming was confirmed by these tests [5]. Only one specimen half showed marks due to jamming. Even in this case, an increase in absorbed energy was not clearly demonstrated. One specimen of the ten in the series had greater absorbed energy than the jammed specimen.

Evaluating asymmetry of machines -- At the beginning of this study, we assumed that a properly adjusted machine would produce a uniform line as a second-strike mark on the specimen. Misalignment would result in asymmetrical second-strike marks. The data indicate that the absorbed energy increases as deliberate asymmetry is introduced, but the rate of increase for a given asymmetry is small. Furthermore, the marks and features of the broken halves are also asymmetrical. When the specimens show second-strike marks, there are several features that can be used to measure symmetry. Among these are:

A. whether lines or nicks are formed on the two halves,

B. the distance from the notch on each half,

C. the angle of the strike mark with the specimen edge, and

D. whether the upper or lower edge struck the anvils first.

Table 4 shows the tally for these dimensions. Examples of how the second-strike marks are useful will be presented in the discussion of the results that follow.

Components of absorbed energy -- The simplest estimate of the effect of a modification is to subtract the absorbed energy of tests with the modification from that without the modification. This is effective if other variables not obviously related to the controlled variable remain unchanged. To decrease the proportional effect of the uncontrolled variables, the controlled variable was changed by an amount five to ten times the specified tolerance on the controlled variable. An exception is for specimen elevation relative to the striking edge, which could be changed only to the limits of the specified tolerance. Then the difference in absorbed energy was divided by the change in the controlled variable to measure the rate of change, assuming a linear relationship. For example, the effect of offset was calculated to be +0.44 J/mm, that of the angle of strike to be 0.02 J/deg, and that of compliance as measured by the change in the distance between second-strike marks to be -0.92 J/mm.

The second approach was to make a regression analysis of individual specimens from a set which showed an above average range of that variable. That approach showed much larger values of slope; for example, 4.0 J/mm for offset. The 4.0 J/mm estimated the change between some modifications better than 0.44 J/mm. However, the higher value is not due to offset alone; other uncontrolled factors must be present that influence the result that we measure.

Comparison of Pendulum Types

Table 2 shows that the average value for absorbed energy measured by R1U and R2U is 9 percent greater than that measured by R1C. This is greater than the change in absorbed energy due to deliberate modifications to exceed the specified tolerance beyond what would be expected in machines in use. Considering the magnitude of difference due to pendulum type, this effect will be analyzed in detail.

Comparison of different measures of the energy to produce fracture -- As shown in Table 5, on average, the composite postfracture energy, as measured after testing, is 10 percent higher for tests made using the Type-U machines than for those using the Type-C machine. Each method of measurement in Table 1 indicates that the Type-C machines produce lower values than for the Type-U machines. Therefore, the difference in absorbed energy is not due to the means of measurement.

Differences in the striking edge -- We know that the stiffness of the loading system affects the absorbed energy and that the difference can be measured fairly easily [8,10]. The striking edge of the type-C pendulum is supported along its whole length by the massive disk of the tup while that for the Type U is a short, relatively slender cantilever beam. The stiffness of the latter is no doubt less than the former so the rate of increase of the force on the specimen is smaller and less uniform from the upper side of the specimen to the lower.

Another factor to consider is the distance between second-strike marks. For a specimen that is loaded more rapidly, we expect that the halves would have greater velocity after fracture and, thus, the second-strike marks would be closer together. The distance between second-strike marks for the specimens broken in the Type-C machine average 19.0 mm, those broken by R1U average 18.6 mm, and those from R2U average 21.8 mm. The 2.8 mm average difference between machines R1C and R2U would lead to a predicted increase in energy of about 16 percent for R2U compared to R1C; a 10 percent increase was measured (see Table 2). The results for R1U do not follow the generally observed trend.

Energy loss due to shrouds -- The more complicated flight path for specimens tested in shrouded machines would be a convenient explanation for an increase in the number of third-strike marks when compared to the Type-C machine. However, the tallies in Table 5 show that the numbers are approximately equal. In any case, unless the mark involves contact with the pendulum, it cannot affect the absorbed energy.

Summary -- Of the three uncontrolled variables (energy loss to shroud, difference in striking edge, and means of measurement), the difference of striking edge appears to be the major factor that relates to the difference between pendulum type.

Effects of Modifications to Machine M1C

The scale of the modified machine was graduated in ft·lbf, and the readings were recorded to the nearest 0.25 ft·lbf, which is about 2 percent of the typical value obtained during the tests described in this paper. Modifications producing changes of greater than 2 percent are regarded as significant and are discussed below.

Offsetting specimen 2 mm -- Series D shows that the effect of the offset on the different measures of toughness (see Tables 2 and 5) was measurable. In Table 4, the effect of the offset on appearance of the broken halves is consistent. None of the inboard halves (shorter from anvil to notch) showed second-strike marks. All of the outboard halves had second-strike lines. The 2-mm offset shows the most conspicuous relationship between the type of modification and the appearance of the broken specimens.

Relative to the normal condition of the machine in Series C, the effect of the offset is to increase the absorbed energy by 0.9 J or about 6 percent, an amount exceeded by only one other modification in the series of eleven. The rate of 0.44 J/mm is consistent with previous experience. Again, the rate of 4.0 J/mm quoted earlier in the discussion is not due to the offset, but rather is the result of uncontrolled variables.

Tilting the specimen supporting surface -- Series H consists of tests made after the new supports were machined to position the specimen at the standard height but with the horizontal surface sloped upward toward the anvils. The effect on absorbed energy was a 0.7 J or 5 percent increase when compared to the machine in its last standard condition. The composite postfracture energy (Table 5) increases slightly from 5.3 to 5.6 mm, indicating that the change is relatively insignificant.

Comparing the distance between second-strike marks shows values of 18.1 and 17.5 mm, respectively, for the reference Series C and Series H. Multiplying the difference by -0.92 J/mm (the previously determined slope) predicts a +0.6 J change in absorbed energy due to the reduced stiffness of the modified system. Therefore, the change in absorbed energy can be predicted from the appearance of second-strike marks in this case.

Remachining the anvils to slant the contact faces -- Table 5 shows that Series I averages 0.7 J or 4 percent more than Series C. The misalignment of 10 parts in 1000 is about 0.6 deg, less than that tested in Series H where the support was angled 1 deg. The distance between second-strike marks is 17.8 mm. The 0.3 mm decrease in distance between second-strike marks would account for a 0.3 J increase in absorbed energy, again consistent with the analysis in the previous section.

Reducing the horizontal thickness of the anvils -- Table 2 shows that when the anvils are moved in the direction of swing by 5 mm (Series J), the absorbed energy is increased by 6 percent relative to the machine in standard condition (Series C). This is larger than the corresponding value for any other modification made during these tests. The physical effect of this on fracture work is that it causes a change in the angle between the specimen and the striking edge, similar to Series H and I. In this case, the angle is about 5 parts in 1000 and the distance between second-strike marks is 17.5 mm (0.6 mm decrease from that found in series C). The predicted change in absorbed energy is inconsistent with the predictions in the previous two sections. However, the change in absorbed energy is consistent with the change in composite postfracture energy reported in Table 5.

CONCLUSIONS

Among the effects of the thirteen variations tested, the largest was a difference between the absorbed energy as measured on a machine with a Type-C pendulum and two machines with Type-U pendulums, the latter indicating values 9 percent higher. The intentional modifications to M1C indicate that further tightening of machine tolerance would have marginal utility for normal testing. The alternative energy-related measurements were helpful as additional information to substantiate our conclusions. These conclusions may only be applicable to tests on high-strength steels with fracture energies below 20 J.

For similar investigations in the future, we recommend that a set size of at least ten specimens be used, and that the energy indicator on the machine should be readable to 1 percent variations in the absorbed energy.

ACKNOWLEDGEMENTS

The authors are grateful to N. V. Gjaja for permission to use the measuring instruments at the Schenectady Materials and Processes Laboratory and to T.P. Quinn and R.B. Madigan (NIST) for assisting with the high-speed photography.

REFERENCES

1. Kahn, N.A., and Imbembo, E.A., "Reproducibility of the Single-Blow Charpy Notched-Bar Test," ASTM Bulletin, May, 1947, pp. 66-74.

2. Fry, N.L., "An Inquiry into the Reproducibility of Impact Test Results," ASTM Bulletin, January, 1953, pp. 61-66.

3. Driscoll, D.E., "Reproducibility of Charpy Impact Test," Symposium on Impact Testing, STP 176, American Society for Testing Materials, Philadelphia, 1955.

4. Rickett, R.L., et.al, "A Comparison of Impact Testing Machines in the 20 to 30 Ft-Lb Range," Proceedings ASTM, Vol. 53, pp. 739-754, 1953.

5. Fahey, N.H., "Effect of Variables in Charpy Impact Testing," Materials Research & Standards, November, 1961, pp. 872-876.

6. Orner, G.M., "Charpy Brittle Fracture Transition by the Lateral Expansion-Energy Relationship," Welding Journal, May, 1958, pp. 201s-205s.

7. Schmieder, A.K., "Comparison of Metrological Techniques for Charpy Impact Machine Verification," Charpy Impact Test-Factors and Variables, ASTM STP 1072, J. M. Holt, Ed., American Society for Testing and Materials, Philadelphia, 1990, pp. 20-34.

8. Porro, F., Trippodo, R., Bertozzi, R., Garagnani, G., "Impact Tester Compliance: Significance, Sensitivity and Evaluation," Charpy Impact Test: Factors and Variables, ASTM STP 1072, J. M. Holt, Ed., American Society for Testing and Materials, Philadelphia, 1990, pp. 7-19.

9. M.P. Manahan, R.B. Stonesifer, Y. Soong, and J.M. Burger, "Miniaturized Notch Test Specimen and Test Machine Design," this volume.

10. Bluhn, J.I., "The Influence of Pendulum Flexibilities on Impact Energy Measurements," Symp. on Impact Testing STP 176, Am. Soc. for Testing Materials, Philadelphia, 1955.

Francis J. Marsh[1]

EFFECT OF SQUARENESS TOLERANCE ON CHARPY V-NOTCH IMPACT ENERGY

REFERENCE: Marsh, F. J., "**Effect of Squareness Tolerance on Charpy V-Notch Impact Energy**", Pendulum Impact Machine: Procedures and Specimens for Verification, ASTM STP 1248, Thomas A. Siewert and A. Karl Schmieder, Eds., American Society for Testing and Materials, Philadelphia, 1995.

ABSTRACT: The need for a tight squareness tolerance (90° ±10 min) of adjacent sides of Charpy V-notch impact specimens has been questioned by Quality Assurance personnel in the metals industry. An experiment has been designed to evaluate the effect of the squareness tolerance greater than required in ASTM E23-93a, Standard Test Methods for Notched Bar Impact Testing of Metallic Materials [1]. Material used to manufacture impact standards of low, high and super high energy levels was heat-treated, and the notched surface and surface opposite the notch were machined to 90° +20 min, 90° +40 min and 90° +60 min. The sides adjacent to the notch were held flat and parallel. A control set of samples was machined to meet current squareness requirements given in ASTM E 23. The results were statistically analyzed. The analysis shows when out-of-squareness is ≥ 20 min, energy ranges, mean energy values and associated standard deviations at the low and high energy levels are statistically different when compared to the same information derived from SRMs.

KEYWORDS: impact energy, low energy, high energy, super high energy, jamming, squareness tolerance, SRM specimens, spinning and tumbling, statistical analysis, t-Test

It was reported by N. H. Fahey [2] that out-of-squareness greater than ±10 min does not cause erroneous impact energies, but does govern spinning of the broken specimen parts and may cause jamming. At that time, he recommended the 10 min squareness tolerance in ASTM E 23 be maintained to minimize jamming. Since Fahey's investigation over 30 years ago, ASTM E 23 has required the installation of shrouds at the anvil area to reduce the probability of jamming after fracture. As this machine revision is effective, Quality Assurance personnel in the metals industry have questioned the validity of the tight tolerance requirement. A relaxation of the out-of-squareness tolerance could result in significant savings in machining time and cost. If test results from

[1]Research Engineer, Homer Research Laboratories, Mechanical Test Lab, Bethlehem Steel Corporation, Bethlehem, PA 18016-7699.

out-of-tolerance specimens show that impact energies are not statistically affected, the current squareness tolerance could be relaxed. The following experiment was designed to determine the effect of specimen out-of-squareness on impact energy.

EXPERIMENT DESIGN

Material

Test material was chosen to span the energy ranges of the lower and upper shelf Charpy behavior. The low and high energy specimens came from the same heat of E-4340 VIM-VAR material. The super high energy specimens came from Vascomax T-200 material. Each specimen was uniquely identified and then heat-treated with the appropriate lot of material for each specific energy range. To significantly reduce material variability, the specimens in the study were fabricated and processed according to Standard Reference Material (SRM) specifications [3]. All specimens were finish ground within the tolerances specified in ASTM E 23. The low energy specimens (Code BL-1) were part of SRM lot LL-45, the high energy specimens (Code HL-1) were part of SRM lot HH-45 and the super high energy specimens (Code BSH-1) were part of SRM lot SH-3. The identities of the specimens are shown in Table 1.

Table 1--Identification of test specimens

OOS (min)	Low Energy		High Energy		Super High Energy	
	Code	Serial Number	Code	Serial Number	Code	Serial Number
20 40 60	BL-1	001-010 011-020 021-030	HL-1	001-010 011-020 021-030	BSH-1	001-010 011-020 021-030

Figure 1 shows the out-of-squareness dimensions used in the experiment.

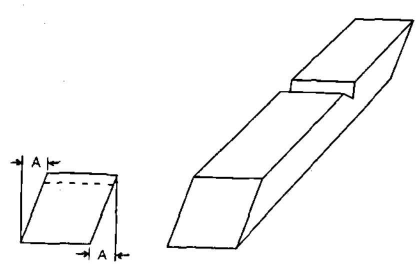

20 min out-of-square = 0.0582 mm (Dimension A)
40 min out-of-square = 0.1164 mm (Dimension A)
60 min out-of-square = 0.1747 mm (Dimension A)

Maximum allowable out-of-square = 0.0279 mm.

FIG. 1--Out-of-square dimensions

Test procedure

It was decided to use the results of verification specimens (SRMs) as a basis of comparison of results derived from the 20, 40 and 60 min out-of-squareness conditions. The National Institute of Standards and Technology (NIST) uses three reference machines to characterize each SRM lot. Twenty-seven verification specimens were tested on each reference machine (i.e., a total of 81 specimens at each energy level) according to ASTM E 1271 [3]. The energies and standard deviations of the SRMs used in this experiment were calculated from tests conducted on a reference machine equipped with a U-type hammer. The results are shown in Table 2.

Table 2--Results of SRM tests

Out of Squareness (min)	Low Energy Test Temp. -40°C			High Energy Test Temp. -40°C			Super High Energy Test Temp. 24.2°C		
	Spec. No.	Impact Energy (J)	Mean Energy (J)	Spec. No.	Impact Energy (J)	Mean Energy (J)	Spec. No.	Impact Energy (J)	Mean Energy (J)
	1	18.6		1	103.0		1	199.3	
	2	17.6		2	96.9		2	219.6	
	3	18.3		3	97.3		3	191.2	
	4	17.6		4	98.3		4	193.9	
	5	18.0		5	95.2		5	204.7	
	6	18.3		6	99.6		6	199.3	
	7	18.6		7	104.1		7	234.6	
	8	18.6		8	96.9		8	210.2	
	9	17.6		9	99.6		9	200.0	
	10	17.6		10	97.6		10	215.9	
	11	17.3		11	98.0		11	229.1	
	12	18.3		12	95.6		12	196.9	
	13	19.3		13	97.6		13	211.5	
0	14	18.3	18.2	14	99.0	98.6	14	204.1	206.9
	15	18.0		15	99.3		15	215.9	
	16	18.3		16	94.9		16	221.0	
	17	18.0		17	101.0		17	217.9	
	18	17.6		18	102.4		18	212.9	
	19	18.6		19	100.7		19	206.8	
	20	18.6		20	96.6		20	198.6	
	21	18.0		21	96.3		21	196.6	
	22	18.6		22	99.0		22	207.4	
	23	18.6		23	97.3		23	208.1	
	24	18.6		24	103.0		24	193.9	
	25	18.0		25	97.6		25	206.8	
	26	18.0		26	100.3		26	203.3	
	27	18.6		27	96.3		27	191.8	

Ten specimens each with 20 min, 40 min and 60 min out-of-squareness were tested at each energy level on the same reference machine by the same operator on the same day, i.e., a total of 30 specimens were tested at each energy level. The low and high energy specimens were tested at -40°C, the super high energy specimens were tested at 24.2°C [1]. The results are shown in Table 3.

Table 3--Results of tests

Out of Squareness (min)	Low Energy Test Temp. -40°C			High Energy Test Temp. -40°C			Super High Energy Test Temp. 24.2°C		
	Spec. No.	Impact Energy (J)	Mean Energy (J)	Spec. No.	Impact Energy (J)	Mean Energy (J)	Spec. No.	Impact Energy (J)	Mean Energy (J)
20	1	18.6	18.5	1	100.3	104.5	1	221.7	208.1
	2	18.6		2	105.8		2	212.9	
	3	18.6		3	105.8		3	206.8	
	4	18.3		4	104.4		4	214.4	
	5	18.6		5	107.1		5	201.7	
	6	18.6		6	103.7		6	193.2	
	7	17.6		7	105.8		7	212.2	
	8	18.6		8	105.1		8	215.6	
	9	18.3		9	103.7		9	195.9	
	10	19.0		10	103.0		10	207.2	
40	11	18.3	18.1	11	103.0	103.1	11	195.2	206.4
	12	17.3		12	105.8		12	219.6	
	13	18.3		13	102.4		13	212.2	
	14	17.6		14	108.5		14	199.3	
	15	18.3		15	102.4		15	204.7	
	16	18.0		16	104.4		16	212.9	
	17	18.3		17	101.7		17	210.8	
	18	18.6		18	104.4		18	197.9	
	19	18.3		19	101.0		19	200.7	
	20	18.3		20	97.6		20	210.2	
60	21	18.6	19.1	21	101.7	102.0	21	200.7	202.5
	22	18.3		22	100.3		22	204.0	
	23	18.6		23	104.4		23	210.2	
	24	20.3		24	101.0		24	204.0	
	25	19.3		25	101.7		25	202.0	
	26	19.3		26	104.4		26	189.8	
	27	19.0		27	97.6		27	208.8	
	28	19.0		28	102.4		28	191.8	
	29	19.3		29	101.0		29	204.7	
	30	19.0		30	105.1		30	208.8	

RESULTS AND ANALYSIS

Plots of absorbed energy vs. out-of-squareness (FIGs. 2, 3 and 4) show the test results for the low, high and super high energy impact specimens. Each figure shows three groups of 10 specimens at 20, 40 and 60 min out-of-square plus the NIST SRM value at 0 min out-of-square. The horizontal lines represent the upper and lower limits allowed for the SRM samples per ASTM E 1271.

A statistical analysis (the t-Test) was applied to the low, high and super high energy specimens with each level considered as a separate problem. Within a given problem, the t-Test compared two sample means with unequal sample size less than 30, unknown population mean and unequal population variances (Equation 1) [4]

$$t = \frac{(\bar{X}_1 - \bar{X}_2)}{\sqrt{\frac{S_1^2}{N_1 - 1} + \frac{S_2^2}{N_2 - 1}}} \qquad (1)$$

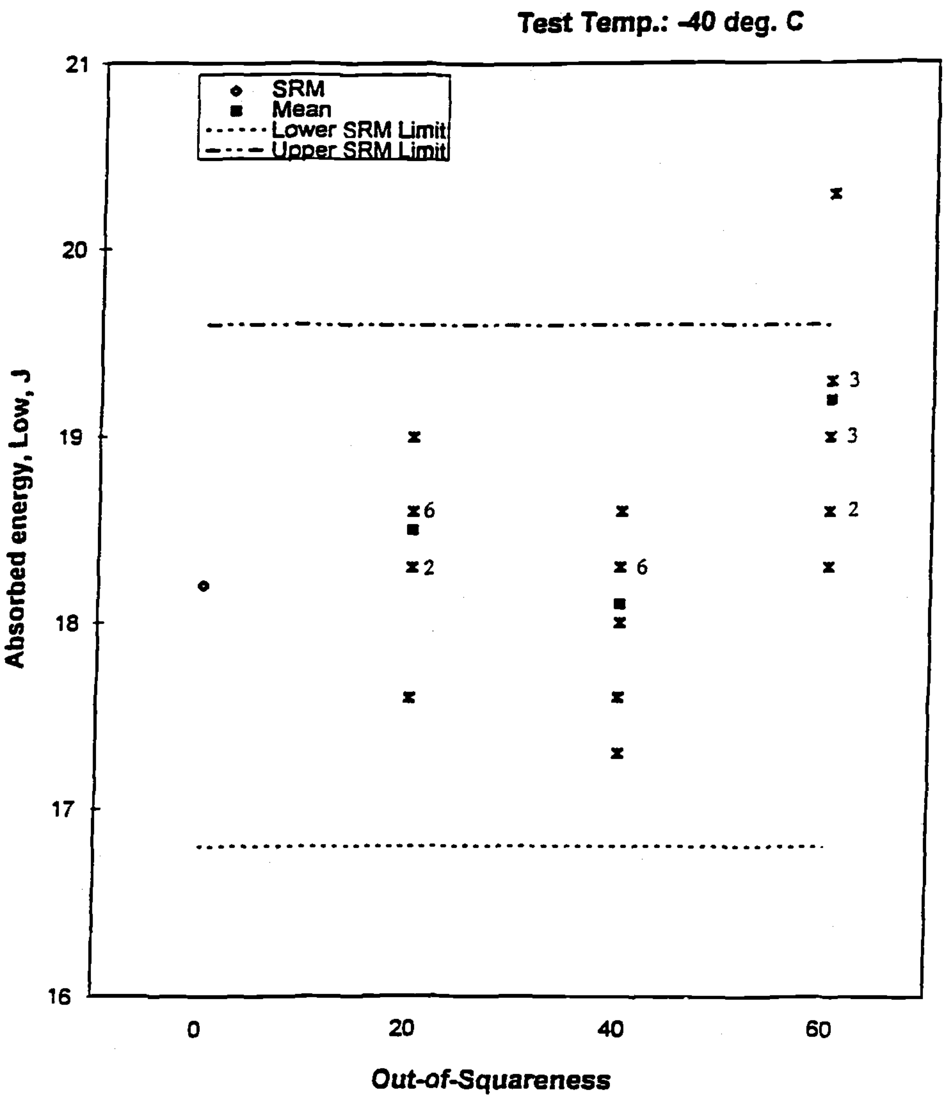

FIG. 2— Absorbed energy (low) vs. out-of-squareness

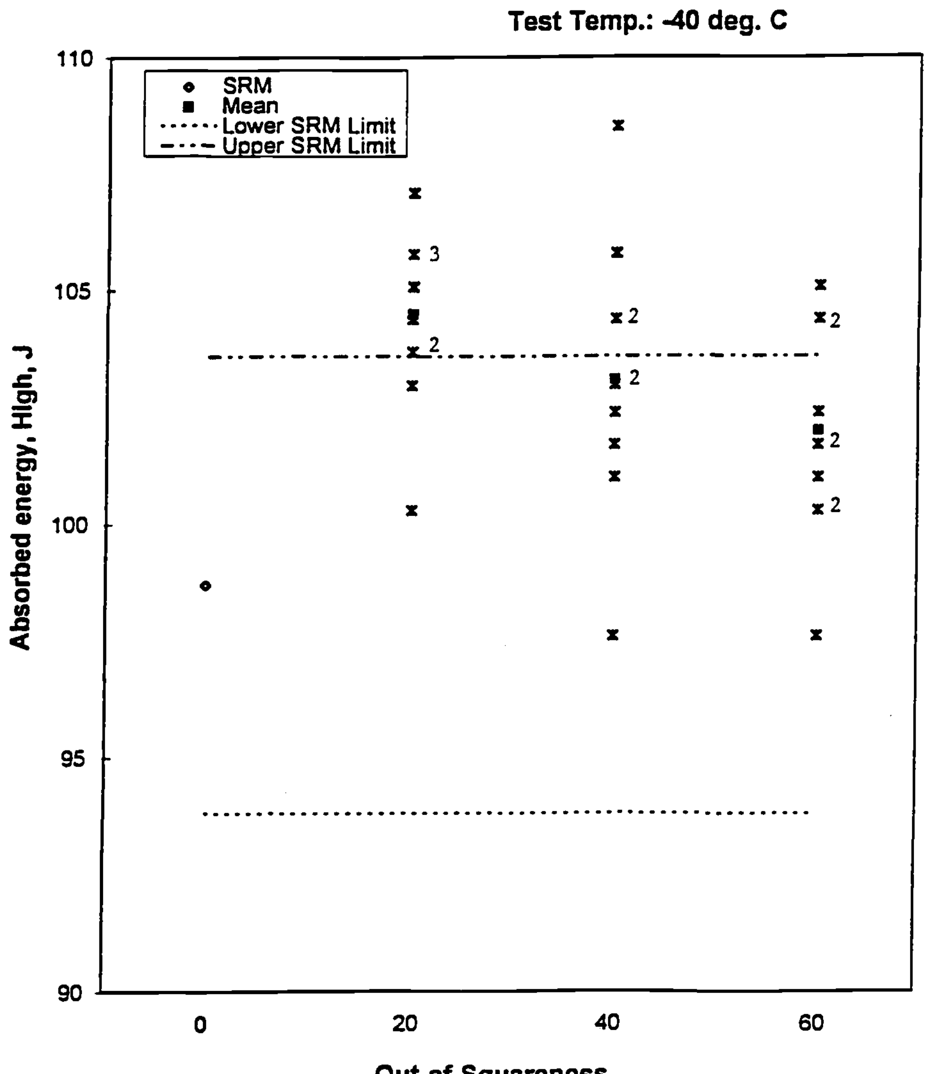

FIG. 3-- Absorbed energy (high) vs. out-of-squareness

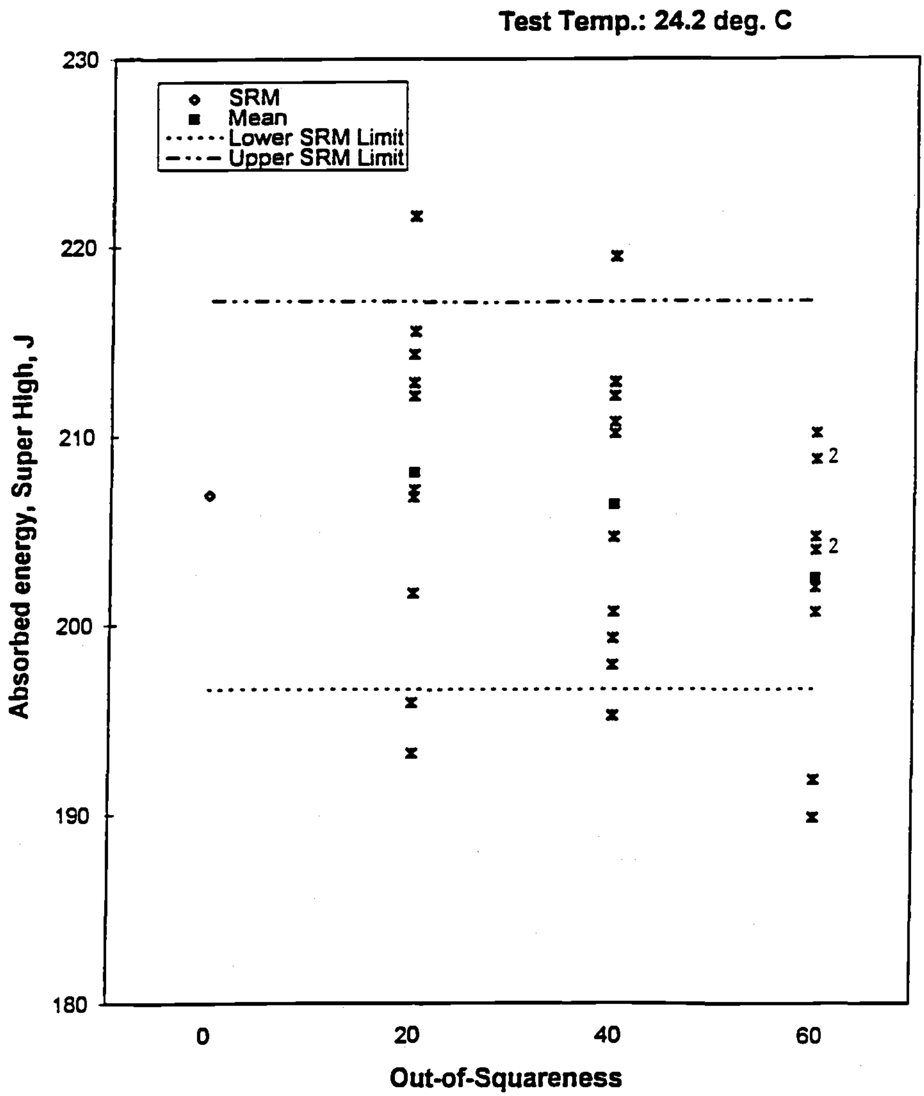

FIG. 4— Absorbed energy (super high) vs. out-of-squareness

where $\overline{X}_1$ and S_1 are the mean and standard deviation for 10 specimens out-of-square condition within a given energy level, and $\overline{X}_2$ and S_2 are the mean and standard deviation for 27 specimens at each energy level.

Table 4--Derived t-values from equation 1

	Low Energy	High Energy	Super High Energy
20 min	2.056	7.793	0.337
40 min	-0.639	4.403	-0.151
60 min	4.325	3.920	-1.445

The t-Test values calculated from Equation 1 are shown in Table 4. The unequal sample sizes (10 and 27) necessitated the use of Equation 2 to calculate the weighted critical t value at the 95% confidence level [4].

$$t_{critical_{95}} = \frac{\left(\frac{S_1^2}{N_1} \times t_1 + \frac{S_2^2}{N_2} \times t_2\right)}{\left(\frac{S_1^2}{N_1} + \frac{S_2^2}{N_2}\right)} \tag{2}$$

The weighted critical t values for the low, high and super high energy levels are 1.79, 1.79 and 1.78, respectively, where N_1, S_1, N_2 and S_2 are the same values used in Equation 1. The values t_1 and t_2 were taken from a standard statistical t-table for 9 and 26 degrees of freedom, respectively.

In this experiment, the t-Test is designed to measure the statistical significance of the hypothesis that out-of-squareness would cause higher impact energies when the results would be compared to NIST verification specimens with 0 min out-of-squareness. Two hypotheses were tested:

Ho: Null Hypothesis

There is no significant difference between the specimen sample mean and the NIST SRM mean.

Ha: Alternative Hypothesis

There is a significant difference between the sample mean and the NIST SRM mean.

The goal of this analysis is to determine if the evidence resulting from each group of 10 specimens within a given energy level is strong enough to reject the null hypothesis. If the result of a t-Test at the 95% confidence level exceeds the critical t-value for a given energy level, the null hypothesis will be rejected and the alternative hypothesis is accepted. Conversely, if the t-Test does not exceed the critical t-value for a given energy level, we cannot say the null hypothesis is true - we can only state the evidence is insufficient to reject the null hypothesis.

The sample statistics from Table 5 are graphed for each test case in FIGs. 5, 6 and 7. The mean of the SRM and the 20 min, 40 min and 60 min means are represented by a solid square. The upper and lower limits are ±2 sigma from the mean. The 0 min entries in Table 2 were calculated from 27 tests at each energy level.

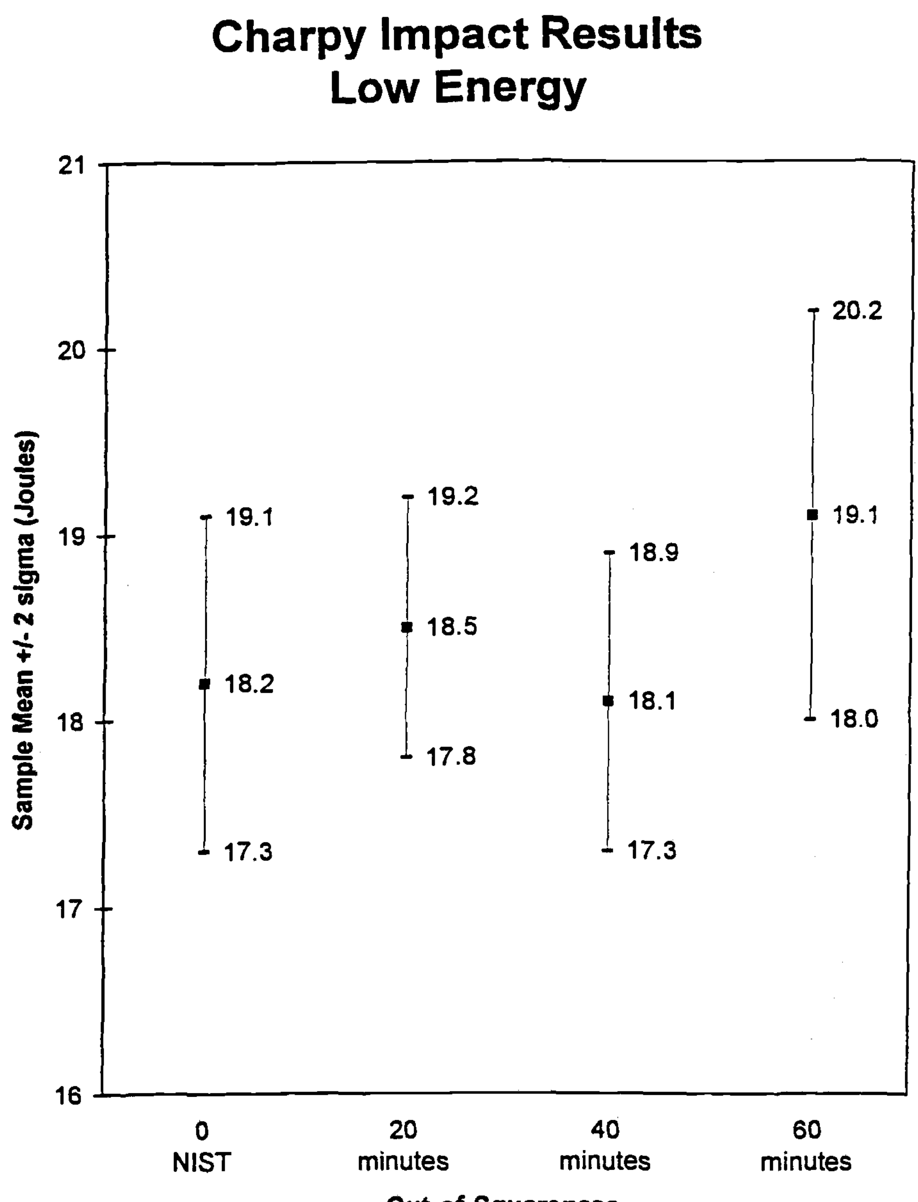

FIG. 5--Sample means and ranges vs. out-of-squareness

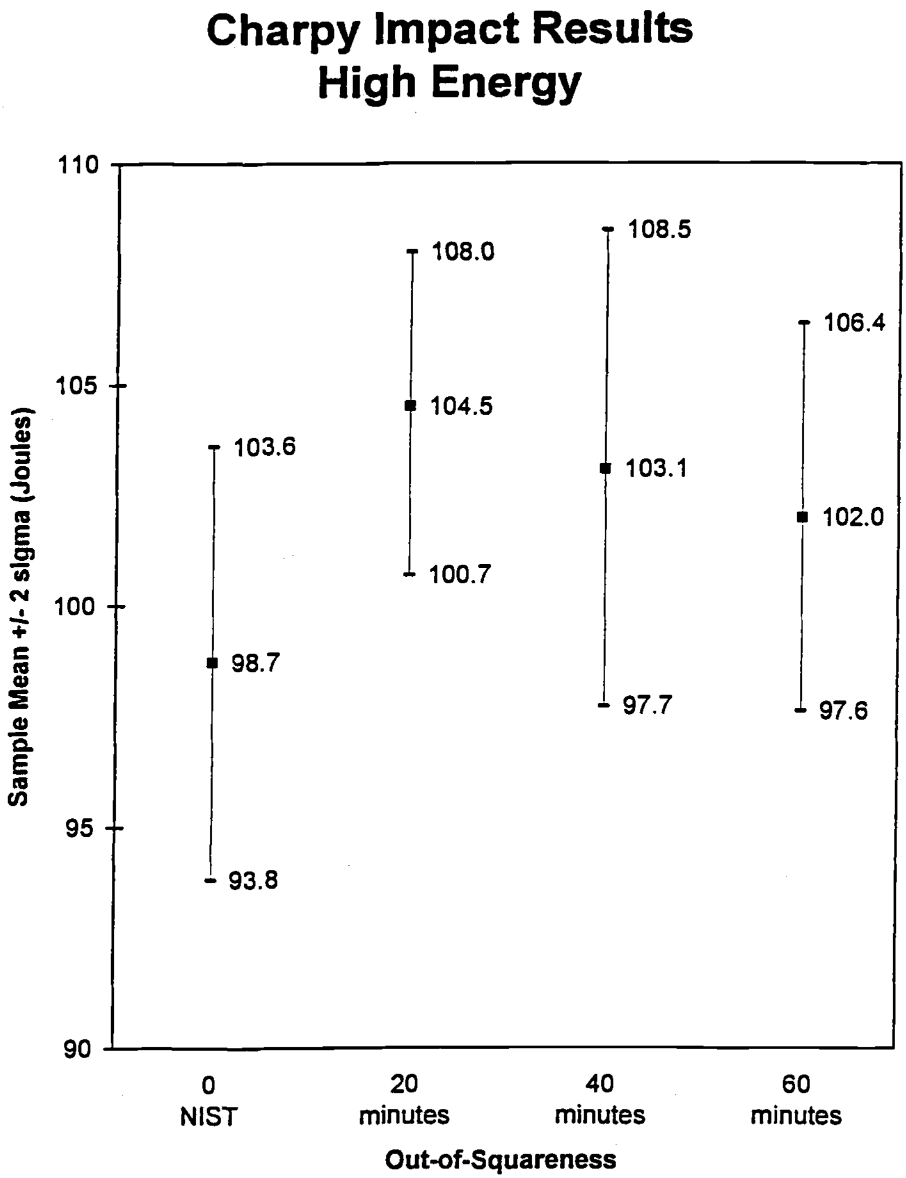

FIG. 6--Sample means and ranges vs. out-of-squareness

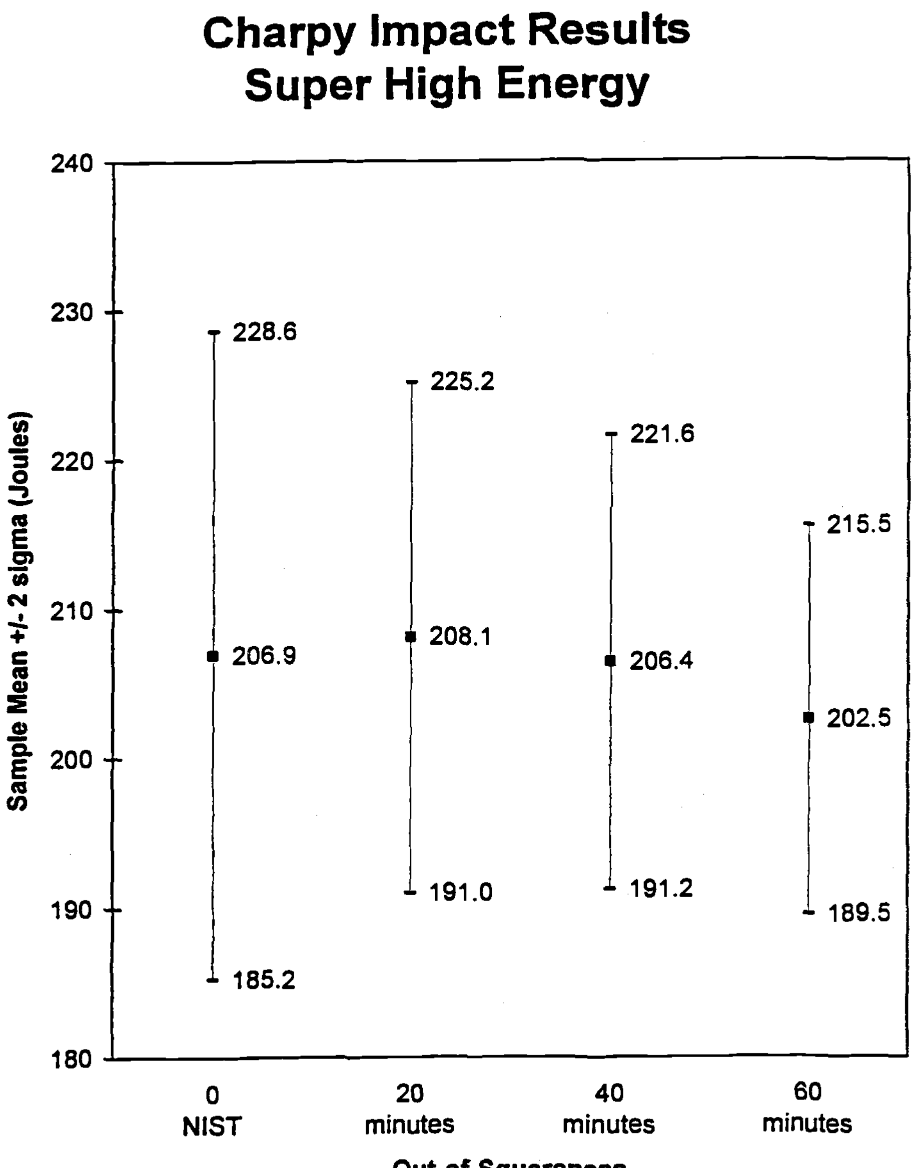

FIG. 7--Sample means and ranges vs. out-of-squareness

Table 5--Charpy impact results and associated statistical data

	Low Energy	High Energy	Super High Energy
0 min	18.2 0.46	98.7 2.44	206.9 xbar 10.85 sigma
20 min	18.5 0.34	104.5 1.76	208.1 xbar 8.54 sigma
40 min	18.1 0.38	103.1 2.71	206.4 xbar 7.59 sigma
60 min	19.1 0.56	102.0 2.17	202.5 xbar 6.51 sigma

As out-of-squareness increases, an increase in tumbling and spinning of the broken Charpy pieces immediately after impact would be expected, causing the broken pieces to strike the hammer a second time. These secondary sample-to-hammer collisions would be expected to impede hammer movement thereby increasing apparent absorbed energy. The data plotted in FIGs. 5 and 6 (with the exception of the 40 min data in FIG. 5) support this expectation, i.e., out-of-squareness increases the mean absorbed energy. Additionally, inspection of the low energy specimens by NIST confirmed that as out-of-squareness increased, the number of second strike impressions also increased. However, the super high energy data plotted in FIG. 7 show little dependence on out-of-squareness. It is believed that the different specimen behavior can be explained in the available kinetic energy remaining after specimen fracture. The total available energy of the test system is fixed and is governed by the design of the test machine. In the case of the low energy specimens, very little energy is absorbed in sample fracture leaving high kinetic energy available to promote sample movement.

In the high energy samples, although more energy is absorbed in sample fracture, sufficient kinetic energy is available to promote sample tumbling. However, for the super high specimens most of the energy available in the test system is absorbed in sample fracture leaving little kinetic energy available for sample tumbling. The results of the statistical analysis confirm these observations. Table 4 shows that the critical value of 1.79 is exceeded and therefore significant at the 20 and 60 min out-of-squareness conditions for the low energy level and at the 20, 40 and 60 min out-of-squareness conditions for the high energy level. The critical value of 1.78 was not exceeded and therefore is not significant for any super high energy level condition. These findings are summarized in Table 6.

Table 6--Conclusions of testing

	Low Energy	High Energy	Super High Energy
20 min	Significant	Significant	Not Significant
40 min	Not Significant	Significant	Not Significant
60 min	Significant	Significant	Not Significant

CONCLUSION

The t-Test results show that the out-of-squareness does make a statistically significant difference for low and high energy specimens when compared to NIST SRM verification specimens. For the super high energy specimens, the t-Test results show the evidence to be insufficient to reject the null hypothesis.

Based on the results of this experiment, it is recommended the ±10 min out-of-squareness be retained when machining impact specimens for testing under ASTM E 23. Future experimentation should consider use of high speed video to investigate the spinning and tumbling of broken specimens to further validate the results of this work.

ACKNOWLEDGMENTS

The author wishes to acknowledge S. Barcus, Sure Tool & Engineering, Inc. for heat-treating and machining the specimens, D. P. Vigliotti, NIST - Boulder, Material Reliability Division, for testing the specimens and critiquing the results, and D. D. Newhart, Bethlehem Steel Corp., for the statistical evaluations.

REFERENCES

[1] ASTM E 23, **Standard Test Methods for Notched Bar Impact Testing of Metallic Materials**, 1993 Annual Book of ASTM Standards, Vol. 03.01.

[2] Fahey, N. H., "Effects of Variables in Charpy Impact Testing," Materials Research & Standards, Vol. 1, No. 11, Nov. 1961, pp 872-876.

[3] ASTM E 1271, **Standard Practice for Qualifying Charpy Verification Specimens of Heat-Treated Steel**, 1993 Annual Book of ASTM Standards, Vol. 03.01.

[4] Shannan, R. E., "Systems Simulation the Art and Science," Prentice-Hall, Inc., 1975, pp. 219-222 and 375.

David J. Alexander,[1] William R. Corwin,[1] and Thomas D. Owings[2]

THE PRODUCTION OF CALIBRATION SPECIMENS FOR IMPACT TESTING OF SUBSIZE CHARPY SPECIMENS

REFERENCE: Alexander, D. J., Corwin, W. R.,and Owings, T. D., **"The Production of Calibration Specimens for Impact Testing of Subsize Charpy Specimens,"** *Pendulum Impact Machines: Procedures and Specimens for Verification, ASTM STP 1248,* Thomas A. Siewert and A. Karl Schmieder, Eds., American Society for Testing and Materials, Philadelphia, 1995.

ABSTRACT: Calibration specimens have been manufactured for checking the performance of a pendulum impact testing machine that has been configured for testing subsize specimens, both half-size (5.0 × 5.0 × 25.4 mm) and third-size (3.33 × 3.33 × 25.4 mm). Specimens were fabricated from quenched-and-tempered 4340 steel heat treated to produce different microstructures that would result in either high or low absorbed energy levels on testing. A large group of both half- and third-size specimens were tested at −40°C. The results of the tests were analyzed for average value and standard deviation, and these values were used to establish calibration limits for the Charpy impact machine when testing subsize specimens. These average values plus or minus two standard deviations were set as the acceptable limits for the average of five tests for calibration of the impact testing machine.

KEYWORDS: impact testing, calibration, subsize specimens

Extensive characterization of the impact properties of a variety of materials is conducted at Oak Ridge National Laboratory (ORNL). Base metal, heat-affected zone, and weldments of ferritic pressure vessel steels and stainless steels are often studied, as well as newly developed alloys such as nickel and iron aluminides and low-activation ferritic/martensitic steels. The

---

[1]Oak Ridge National Laboratory, Metals and Ceramics Division, 4500S, MS-6151, P.O. Box 2008, Oak Ridge, TN 37831-6151.

[2]Retired from Oak Ridge National Laboratory.

effects of irradiation on the ductile-to-brittle transition temperature and the upper-shelf energy level are also examined. To allow a greater number of specimens to be irradiated within a given capsule, subsize specimens are frequently used. In addition, these smaller specimens allow data to be produced from small heats of developmental alloys. As a result, subsize specimen testing is a significant fraction of the impact testing conducted at ORNL.

The use of these small specimens necessitates changes in the test system to accommodate the reduced specimen dimensions [1]. As a result, changes in the calibration procedures for the test machine are necessary. After the test system is set up and calibrated with full-size specimens, it must be modified with a smaller tup and relocation of the anvils to test the subsize specimens. This change in critical components of the system would raise concerns about the previous calibration. Therefore, it was decided to develop subsize calibration specimens analogous to the full-size specimens presently supplied by the National Institute for Standards and Technology (NIST) and previously supplied by the Army Materials and Mechanics Research Center (AMMRC) in Watertown, Massachusetts. Both half-size (5 × 5 × 25.4 mm long) and third-size (3.33 × 3.33 × 25.4 mm long) specimens are used in irradiation programs at ORNL. To allow equipment to be set up in a remote hot cell for the appropriate specimen size, and thus reduce the number of cell entries, calibration specimens of both sizes were fabricated.

The use of the subsize calibration specimens is not intended to serve as the primary calibration of the Charpy impact machine. That is accomplished in the usual manner as prescribed by ASTM Standard Test Methods for Notched Bar Impact Testing of Metallic Materials (E 23) using full-size calibration specimens from NIST. The original purpose and principal value of the subsize specimens is to provide a direct means of checking the reproducibility of the Charpy machine after it has been reconfigured to test subsize specimens.

EXPERIMENTAL PROCEDURE

With the aid of information supplied by AMMRC,[1] aircraft-quality vacuum arc remelted 4340 steel was selected. This steel was purchased as bars 14.3 by 14.3 mm (0.56 by 0.56 in.) that were machined into pieces 11.4 × 11.4 × 57.2 mm long (0.45 × 0.45 × 2.25 in.). The bars were the excess portion of a lot produced for AMMRC for their use in manufacturing standard full-size calibration specimens. These bars were heat treated to produce microstructures that would provide either high or low energy levels. The bars

---

[1]Roy, W. N., Chief, NDT Training and Certification Office, Army Materials and Mechanics Research Center, Watertown, MA 02172, personal communication with W. R. Corwin, Oak Ridge National Laboratory, Oak Ridge, TN 37831, March 1981.

were held in wire racks so that a suitable gap was present around each bar. All of the bars were normalized for 1 h at 899° C (1650° F) followed by an air cool, and then austenitized for 1 h at 871° C (1600° F) with an oil quench. The bars for high-energy specimens were tempered for 1.25 h at 593° C (1100° F) and oil quenched. The bars for low energy specimens were tempered for 1.5 h at 399° C (750° F) and oil quenched. These heat treatments were those specified by AMMRC for their own fabrication of full-size calibration specimens.[1]

Eight specimens were sectioned from each of the heat-treated bars. The half-size specimens were 5.0 × 5.0 × 25.4 mm long (0.197 × 0.197 × 1.00 in.) with a 0.76-mm-deep (0.030-in.) 45°-included-angle notch with a 0.08-mm (0.003-in.) root radius. The third-size specimens were 3.33 × 3.33 × 25.4 mm (0.131 × 0.131 × 1.00 in.) with a 0.51-mm-deep (0.020-in.) 30°-included-angle notch with a 0.08-mm (0.003-in.) root radius.

In order to verify the performance of the testing system, the calibration of the impact tester was checked with full-size specimens supplied by AMMRC. The anvils and tup were then changed to allow subsize specimens to be tested [1]. Fifty low-energy and fifty-one high-energy half-size specimens were tested, with twenty-five each of the third-size high- and low-energy specimens. Specimens were tested in a semiautomated test system adapted for testing subsize specimens [1,2]. The testing machine had a capacity of 407 J (300 ft-lb). The absorbed energies were indicated by a digital readout and recorded to the nearest 0.1 ft-lb. All data were originally recorded in English units, and have been converted to metric values. Gas from liquid nitrogen was used for cooling. Specimens were tested at −40°C, as are full-size specimens. The subsize specimens were slightly undercooled to compensate for their rapid warming during the interval between their removal from the cooling chamber and the hammer impact (less than 5 s), based on temperature readings taken on dummy specimens instrumented with surface and buried thermocouples.

RESULTS

The results of the testing are shown in Figs. 1 and 2 as histograms for the half- and third-size specimens, respectively, and are summarized in Table 1. The data have been plotted in columns of equal width to allow a fair comparison of the histograms. Since twice as many half-size as third-size specimens were tested, the vertical axes for the half-size specimens have been doubled.

---

[1]Roy, W. N., Chief, NDT Training and Certification Office, Army Materials and Mechanics Research Center, Watertown, MA 02172, personal communication with W. R. Corwin, Oak Ridge National Laboratory, Oak Ridge, TN 37831, March 1981.

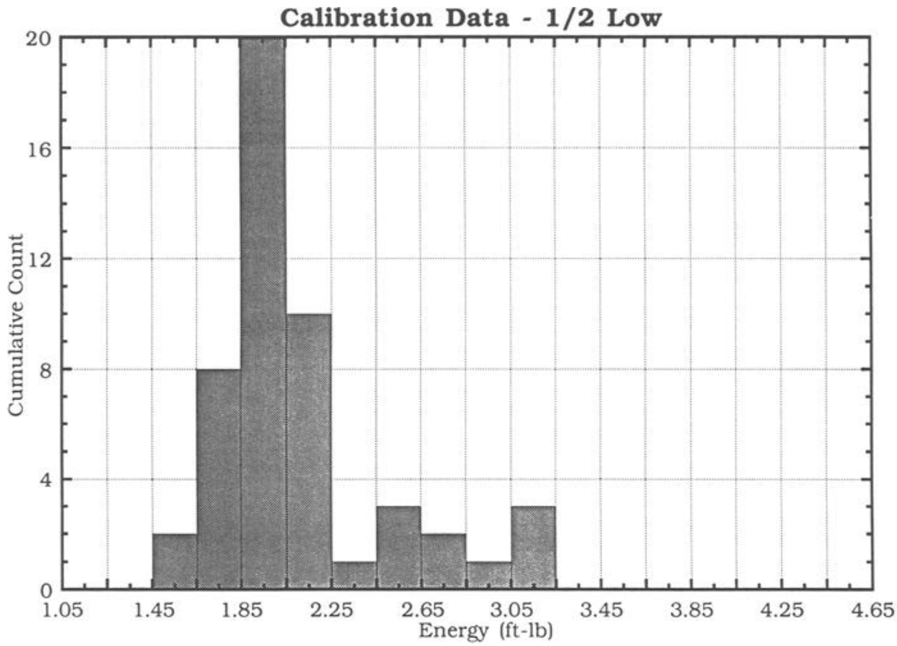

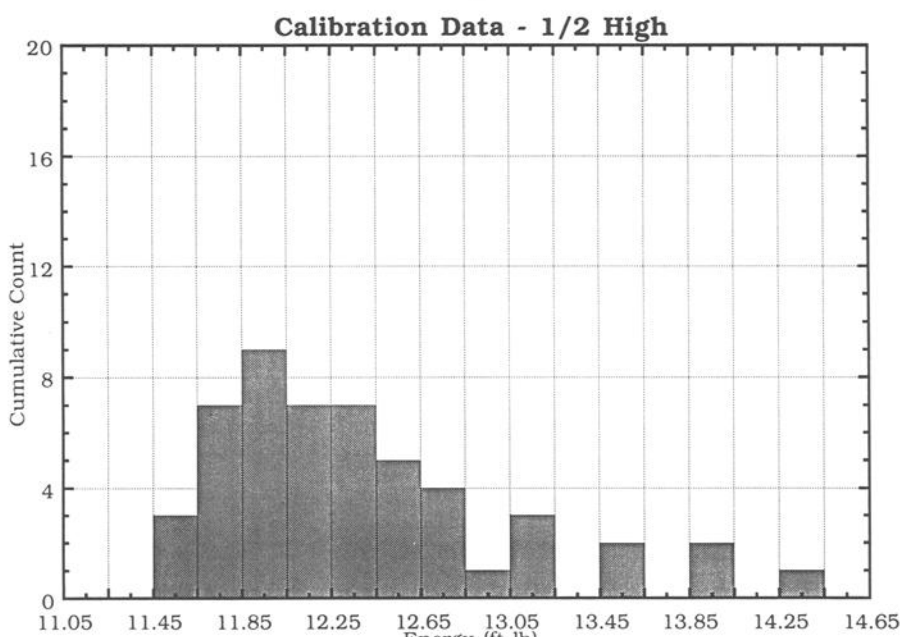

Fig. 1. Results from testing of half-size calibration specimens. Top: low-energy specimens. Bottom: high-energy specimens.

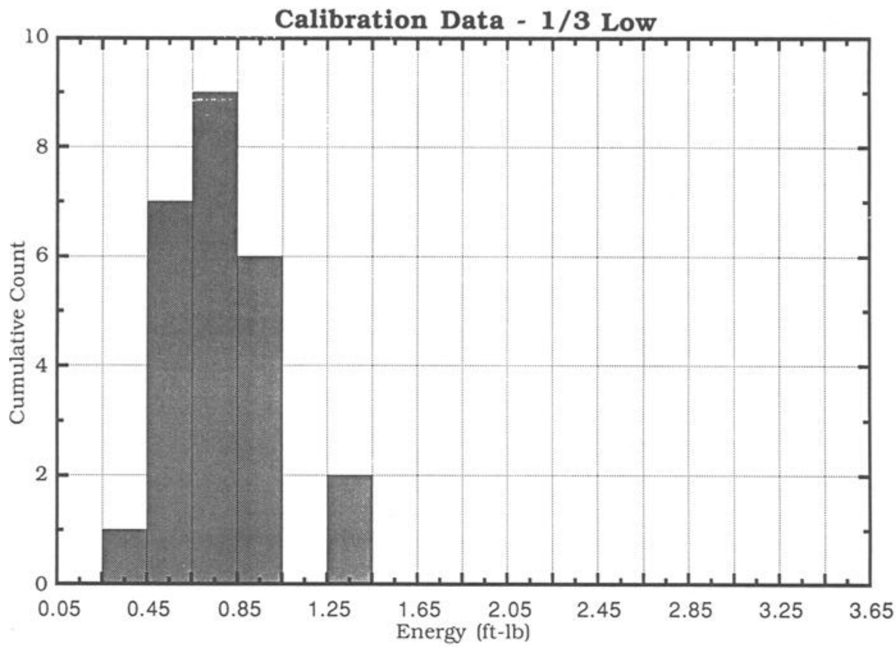

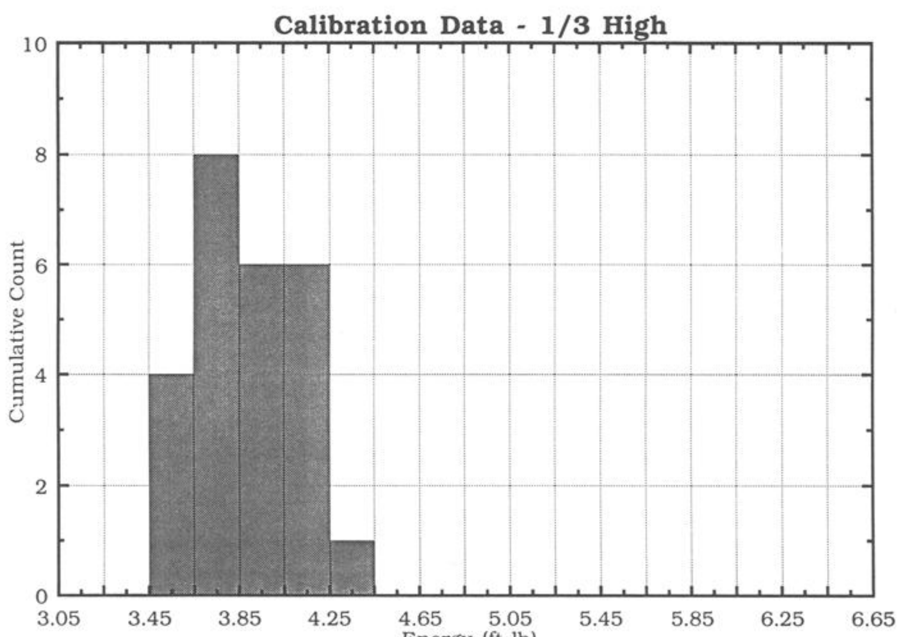

Fig. 2. Results from testing of third-size calibration specimens. Top: low-energy specimens. Bottom: high-energy specimens.

Table 1. Summary of subsize Charpy calibration specimen results

Specimen size	Energy level	Number of specimens	Average energy (J)	Standard deviation (J)	Coefficient of variation
Half	High	51	16.79	0.88	0.05
	Low	50	2.85	0.54	0.19
Third	High	25	5.28	0.31	0.06
	Low	25	1.04	0.31	0.30

For the half-size specimens, the average energy level for the low-energy material was 2.85 J (2.10 ft-lb) with a standard deviation of 0.54 J (0.40 ft-lb). The high-energy material gave an average value of 16.79 J (12.38 ft-lb) and a standard deviation of 0.88 J (0.65 ft-lb). For the third-size specimens, the averages and standard deviations were 1.04 and 0.31 J (0.76 and 0.23 ft-lb) for the low-energy material, and 5.28 and 0.31 J (3.89 and 0.23 ft-lb) for the high-energy material, respectively.

DISCUSSION

The histograms show that the half-size specimens exhibit longer tails and more spread in the data than do the third-size specimens. The standard deviations for the half-size specimens are much larger also.

The average value plus or minus two standard deviations has been chosen for use as the criterion to evaluate the test machine performance. Therefore, the allowable range for the half-size specimens is 1.75 to 3.94 J (1.29 to 2.91 ft-lb) and 15.03 to 18.54 J (11.09 to 13.68 ft-lb) for the low- and high-energy specimens, respectively. Similarly, the allowable range for the third-size specimens is 0.42 to 1.65 J (0.31 to 1.22 ft-lb) and 4.66 to 5.90 J (3.43 to 4.35 ft-lb) for the low- and high-energy specimens, respectively. The calibration of the test system is checked by testing five specimens of each energy level at −40°C. The average of these five tests must fall within these limits for both energy levels.

The subsize calibration specimens are now in routine use at ORNL. They have been used in both laboratory and hot cell machines, in both specimen sizes. No problems have been encountered in their use. They have successfully demonstrated that the impact machines are reproducibly measuring impact energies when configured to test subsize specimens.

There is a need within the technical community at large to establish some means of calibrating the testing machines used for subsize impact testing. There are currently a wide range of testing techniques, specimens, and types of impact machines that are being utilized to obtain data on impact properties of materials. The need for standardization for testing full-size Charpy specimens has long been recognized and is jointly addressed by ASTM E 23 and the NIST calibration specimens. Unfortunately, neither of these means of standardization have an established counterpart for subsize impact specimens. Ongoing efforts in ASTM Committee E 28 are aimed at formulating standards for testing techniques of subsize specimens. It would be very useful to establish a subsize counterpart to the NIST calibration specimens in support of these standardization activities as well as to provide a more reliable means for accurate comparisons of the data produced by the various subsize specimens currently in use.

CONCLUSIONS

Subsize Charpy impact specimens have been produced from 4340 steel heat treated to produce microstructures that will absorb either high or low energies when tested in impact. These specimens have been successfully used to check the operation of impact machines in both laboratory and hot cell locations.

ACKNOWLEDGMENTS

This work was funded in part by the Office of Fusion Energy, U.S. Department of Energy, and the Office of Nuclear Regulatory Research, U.S. Nuclear Regulatory Commission, under Interagency Agreement DOE 1886-8109-8L with the U.S. Department of Energy, under contract DE-AC05-84OR21400 with Martin Marietta Energy Systems, Inc. We would like to thank S. K. Iskander and R. L. Klueh for their helpful reviews of the manuscript, which was prepared by J. L. Bishop.

REFERENCES

[1] Corwin, W. R. and Hougland, A. M., "Effect of Specimen Size and Material Condition on the Charpy Impact Properties of 9Cr-1Mo-V-Nb Steel," *The Use of Small-Scale Specimens for Testing Irradiated Material, ASTM STP 888*, W. R. Corwin and G. E. Lucas, Eds., American Society for Testing and Materials, Philadelphia, 1986, pp. 325-38.

[2] Alexander, D. J., Nanstad, R. K., Corwin, W. R., and Hutton, J. T., "A Semiautomated Computer-Interactive Dynamic Testing System," *Applications of Automation Technology to Fatigue and Fracture Testing, ASTM STP 1092*, A. A. Braun, N. E. Ashbaugh, and F. M. Smith, Eds., American Society for Testing and Materials, Philadelphia, 1990, pp. 83-94.

Michael P. Manahan, Sr.[1], Randall B. Stonesifer[2], Yang Soong[3], James M. Burger[4]

MINIATURIZED NOTCH TEST SPECIMEN AND TEST MACHINE DESIGN

REFERENCE: Manahan, M. P., Stonesifer, R. B., Soong, Y., and Burger, J. M., "Miniaturized Notch Test Specimen and Test Machine Design," Pendulum Impact Machines: Procedures and Specimens for Verification, ASTM STP 1248, Thomas A. Siewert and Karl Schmieder, Eds., American Society for Testing and Materials, Philadelphia, 1995.

ABSTRACT: Charpy V-notch specimens are widely used within the nuclear industry to monitor the effects of neutron damage to the reactor pressure vessel (RPV) beltline region. There is an ever-increasing need to obtain more notched bar impact data as plants age. Many plants will require more specimens for surveillance during the license renewal period. Other plants have experienced more embrittlement than originally anticipated, and it will be necessary to develop plant-specific Charpy shift trend curve models to ensure continued safe operation. Since physically based trend curves have not yet been validated, the use of plant-specific data will save the utilities operations costs since overly (arbitrarily) conservative models are no longer needed. Miniature specimens have also been used to characterize the material condition after vessel annealing. The use of miniaturized specimens which can be fabricated from previously tested full sized specimens offers one solution to this need for more fracture data.

Experiments performed using side-grooved miniaturized notch test (MNT) specimens have demonstrated that 1/16 scale miniature specimens can be designed to yield transitional fracture behavior and that the fracture appearance and energy-temperature curves can be quantitatively related to the conventional ASTM E23 specimen data. This paper presents the results of a study focused on designing an optimized MNT specimen and test machine. A combination of literature review, metallurgical analysis, and finite element analysis was used to consider such design parameters as minimum specimen cross-section, specimen length, notch acuity, the use of side grooves, side groove geometry, support span, and striker geometry. Two dimensional and three dimensional, elastic-plastic, large deformation, finite element analyses were used to compare stress/strain fields for standard and miniaturized specimens. Specimen and test machine geometries have been developed to ensure continuum requirements are met, the MNT specimen stress fields simulate those of the conventional specimen, and scatter for the miniature data is minimized.

---

[1]President, MPM Research & Consulting, 915 Pike Street, P.O. Box 840, Lemont, PA 16851

[2]President, Computational Mechanics, Inc., Rt. 2, Box 64, Julian, PA 16844

[3]Consultant, 6414 Terese Terrace, Jamesville, NY 13078

[4]Program Manager, ESEERCO, 1515 Broadway, 43rd Floor, New York, NY 10036

KEYWORDS: Charpy, miniaturized specimen testing, impact test, fracture appearance, lateral expansion, ductile-brittle transition temperature, upper shelf energy

---

INTRODUCTION

Neutron irradiation of nuclear reactor pressure vessel (RPV) materials results in embrittlement which must be accounted for in the fracture mechanics evaluation to determine Pressure-Temperature (P-T) operating limits. At present, the ASME K_{IR} curve is shifted by the Charpy V-notch (CVN) shift indexed at 41 J (ΔT_{41}) to account for neutron damage. Many plants require additional Charpy data to support license renewal, to provide plant-specific data, and, in several plants in Europe, to confirm the beneficial effects of vessel annealing. The use of miniaturized specimens which can be prepared from the broken halves of previously tested full sized specimens offers one solution to this need for additional data.

In the past, qualitative [1, 2, 3] interpretations of miniature Charpy data have been proposed to explain differences between the miniature specimen data and the ASTM E23 standard specimen results. The first successful quantitative interpretation of miniature Charpy data was reported in Reference [4]. The key elements of this approach are reviewed in the following section of this paper. The recently released ASTM STP 1204 [5] contains several papers focused on quantification of the miniature Charpy test [6, 7, 8, 9, 10]. Review of the work presented in References [5, 11] shows that there are presently widely differing miniature Charpy test approaches and data interpretations reported in the open literature. In support of miniature Charpy standardization work, a focused design study has been performed to optimize the miniaturized notched test (MNT) for nuclear RPV applications. The MNT is a dynamic three point bend test which has been designed to yield data which are quantitatively the same as those obtained in conventional Charpy testing. The key elements of this study are presented here. It is intended that the international standardization effort will lead to accepted standard practices related to miniature specimen geometry, test machine parameters, and data analysis. It is important to emphasize that the specimen size recommendations reported herein are only applicable to the U.S. RPV materials. Application to other classes of material must begin with an in-depth understanding of the material microstructure. The appropriate size and specimen geometry can then be determined using a similar approach.

BACKGROUND

Prior to performing a comprehensive design study, limited scope experiments were performed to demonstrate the feasibility of achieving transitional fracture behavior using specimens which are 1/16 of the volume of conventional Charpy specimens. These experiments have been reported in References [12, 4, 13, 14] and the key results are briefly discussed here.

An important limitation in miniaturizing any specimen is the extent of the material's microstructural inhomogeneities. The usual guideline dictates that the specimen be at least five to ten times as large as the characteristic heterogeneity dimension. Material for this work was taken from a special heat of ASTM A508 steel provided by Oak Ridge National Laboratory (ORNL) for crack arrest research as part of the Heavy Section Steel Technology (HSST) Program [15]. Microscopy analysis indicated that carbon segregates in slender bands about 0.25 *mm* wide with a mean separation of 0.5 mm-1.0 mm. As a result of these findings, the minimum specimen cross section dimension was 5 mm.

Early MNT static tests demonstrated that 1/16 volume miniature Charpy specimens, when tested in the transition region or upper shelf, yield data which cannot be properly analyzed nor related to conventional Charpy data (severe nonplanar fracture surfaces were observed). These nonplanar failures in the miniature specimens were due to their plastic collapse load being smaller than their fracture load. This behavior is consistent with the well known tendency for smaller fracture specimens to behave in a more ductile manner than larger specimens of similar geometry. This behavior is basically due to the fact that stress intensity factors scale with the square root of the specimen size. For example, a half scale specimen will require about 1.41 (i.e., $\sqrt{2}$) higher applied stress than a full scale specimen to achieve the same stress intensity factor level. This behavior was perhaps exaggerated in these miniature specimens due to their very short lengths resulting in relatively larger shear stress to bending stress ratios than found in proportionally scaled specimens. This failure mode problem was overcome by adding side grooves to the specimens. The side grooves offset the loss of constraint associated with the increase in plastic deformation and stress levels to achieve fracture in the smaller specimens.

As discussed in Ref [4], either percent shear or percent post maximum load energy (PMLE) can be used as valid MNT parameters. However, it is essential that the ductile-to-brittle transition temperature (DBTT) be determined using an index which accurately represents the actual fracture process. In particular, for a given index, the fracture mode in the miniature specimen should be identical to that in the conventional specimen. Therefore, tracking embrittlement using percent shear data obtained from miniature specimens is ideal. Since the regulations within the nuclear industry are based on the 41 J index with absorbed energy as the parameter, the PMLE is preferable since it can be related directly to the conventional specimen absorbed energy. Figure 1 provides the correlation for obtaining these indices for both specimen dimensions for A508 steel. This technique can be used to relate any specimen geometries that yield notched specimen fracture transition data. For example, for the A508 steel used in this study, a Charpy energy level of 41 J corresponds to about 4% shear fracture appearance in the unirradiated condition. Referring to Fig. 1, this level of shear corresponds to about 15% PMLE. Thus, when fracture appearance is used as the MNT parameter, the corresponding index is 4% shear for this particular steel. When PMLE is chosen as the MNT parameter, a value of 15% PMLE is used as the index. Either index accurately tracks the miniature specimen Charpy shift at 4% shear and will provide 41 J Charpy shift data which is identical to the conventional specimen ΔT_{41}.

On comparing the miniature and conventional DBTTs, correction factors due to rate effect and size effect were obtained. The average shift due to rate effect for the conventional CVN is 45.3°C. This shift was determined by averaging the static to dynamic shift at the 41-J level for the three materials using conventional Charpy specimens. This is in reasonable agreement with the correlation presented in Ref. [16]. These data can be used to relate the MNT data with conventional, dynamic Charpy data for the ASTM A508 steel. The dynamic 41-J transition temperature is obtained by adding the rate effect shift (45.3°C) and the size effect shift (21.3°C) to yield a 41-J dynamic conventional Charpy transition temperature. Based on the successful experimental feasibility demonstration, an in-depth experimental design study was performed to develop appropriate size ranges for key parameters in the MNT.

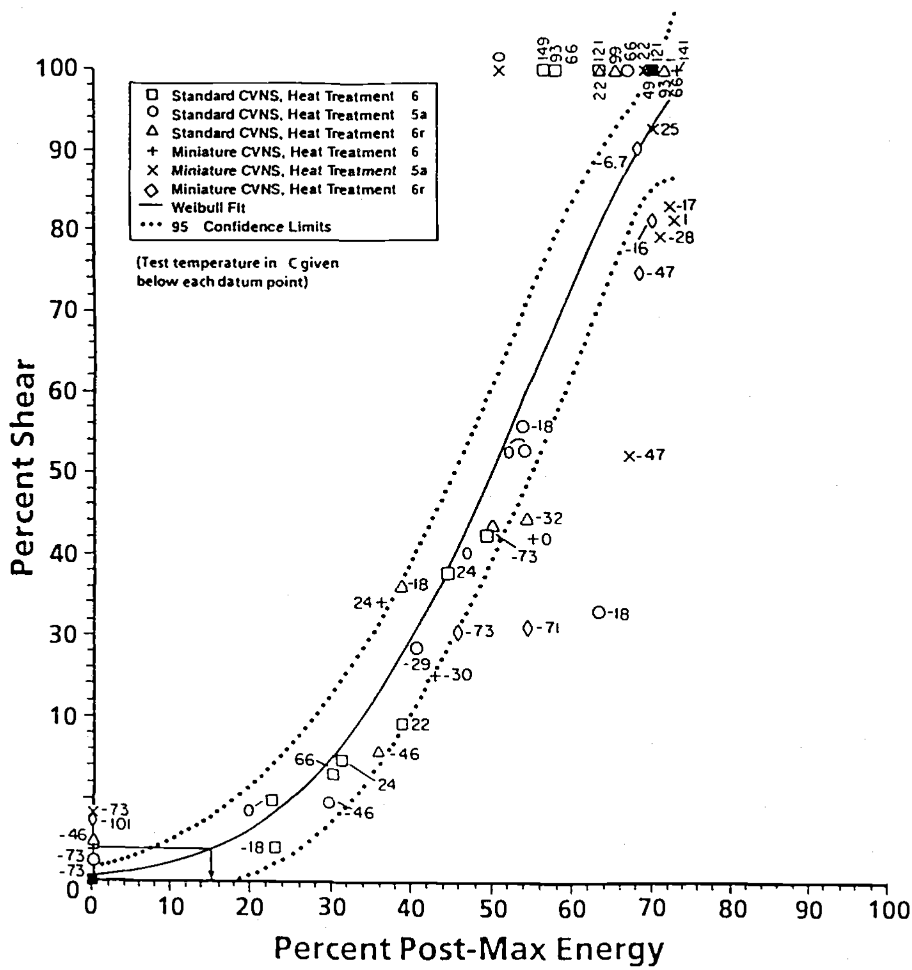

FIG. 1--Percent PME as a fracture transition criterion (miniature and standard specimen sizes)

MNT EXPERIMENTAL DESIGN

Miniature Specimen Cross Section

It is, of course, possible to perform an in-depth microstructural study for each material for which a miniaturized Charpy test is conducted. However, a more effective approach would be to define a specimen size which is adequate for determining MNT properties for a defined class of materials. This latter approach has been pursued and will form the basis for recommendation to the standards committees.

To adequately sample a representative volume of an RPV steel when using MNT specimens, one must know the scale, or mean separation, of the inhomogeneities that exist in the steel plate from which the pressure vessel is fabricated. The term inhomogeneity as used here refers to such compositional and microstructural characteristics as: solute segregation during solidification which leads to bands of variation in mean chemical composition and stringers of inclusions; grain boundaries (grain size); colonies of transformation products; precipitates; and the presence of Fe and alloy carbides. The scale of the inhomogeneities depends upon both compositional and processing variables. Base, weld, and heat-affected zone (HAZ) materials were analyzed for the U.S. vessel steels to determine the cross sectional dimensions which will ensure adequate material sampling. This analysis was performed to provide a conservative estimate of the minimum MNT specimen cross sectional dimensions so that microstructural measurements are not required for each heat of nuclear reactor pressure vessel material tested.

Base Plate--The size scale of various microstructural features considered for U.S. RPV steels are shown in Table 1. It is concluded that the coarsest inhomogeneity in the base plate is chemical banding that occurs especially in high-Mn steels. The variation in Mn content across the banding leads to the formation of a range of transformation products, and thus a range of properties throughout the plate cross section. Therefore, the band separation will be the factor which controls minimum specimen size in RPV plates. An approximate relation for the spacing of bands (L) based on the casting size and the total reduction from ingot to plate is: $L = 0.116\ \theta_f$ (mm), where θ_f is the

TABLE 1--Size scale of various microstructural features in reactor pressure vessel steels

Inhomogeneity Type	Scale (mm)
Chemical banding	0.5-1
Inclusion stringers	~0.5
Austenite grain size (TE)	0.06-0.2
Ferrite grain/pearlite colony size	0.01-0.08
Bainite/martensite colony size	~0.05
Carbide spacing in	
pearlite	0.0001-0.005
bainite	~0.002
martensite	≤0.0001

plate thickness (expressed in inches) [17]. Accordingly, high-Mn RPV plates which are typically 4 to 10 inches thick are predicted to contain chemical bands with an average separation of 0.5 to 1.1 mm. Observations on a section of forged A508 plate confirm these predictions [14]. Stringers of inclusions, which are concentrated in the chemical bands, are the next coarsest inhomogeneity in RPV plate. The primary effect of inclusions (sulfides, oxides, oxy-sulfides) is a loss of ductility (manifested as a decrease in the upper shelf energy (USE)) because of the weakness of the interface between metal and inclusion, and because of the brittleness of the inclusions. The separation of inclusion stringers is somewhat finer than that of the bands since the stringers can form at any point within the rather diffuse band width. Thus, tensile and Charpy specimens designed to sample a volume that will include chemical banding will of necessity include an adequate sample of inclusion stringers.

Other chemical and microstructural inhomogeneities in the plate are on a finer scale than either the bands or stringers and thus will be adequately sampled by specimens designed to include the coarser inhomogeneities. Accordingly, the cross sectional dimension of mini-specimens cut from base plate, assuming that five times the coarsest inhomogeneity will provide an adequate sampling, will be dictated by the banding separation which varies with plate thickness. From the above analysis, specimen cross sections will range from 2.5 mm for 4-inch plate to 5 mm for 10-inch plate.

HAZ--Throughout most of the HAZ, there is no massive redistribution of solute during the very short dwell time at high temperature experienced during the weld thermal cycle. Austenite grain size in the coarse grain HAZ (CGHAZ) may approach 0.5 mm in plates of all thicknesses depending on heat input and peak temperature. Thus the scale of temper embrittlement (TE) may be on the same order as the banding (~0.5 mm), and would therefore require specimens taken from the CGHAZ to have a cross section dimension of at least 2.5 mm. Therefore, the spacing of chemical banding present in the base plate (0.5-1 mm) still remains the controlling factor in determining the cross sectional dimension of mini-specimens cut from the HAZ.

Weld Bead--In the weld bead the grain structure is columnar, the width of the columns being 0.2-0.5 mm. In addition, centerline segregation of impurities often occurs. Specimens should therefore be notched at the centerline and have a cross section dimension on the order of 2.5 mm or greater.

Miniature Specimen Length

Based on microstructural considerations, miniature Charpy specimens cut from RPV materials should have minimum cross sectional dimensions of 5 mm x 5 mm, unless a smaller size can be justified by thorough microstructural characterization. Using the scale factor of 1/2 that was selected for designing the miniature specimen cross-section to select the specimen length would allow 8 miniature specimens (each 27.5 mm long) to be fabricated from the material of one standard Charpy specimen. The experimental work described earlier used specimens with half of this scaled length and therefore allowed 16 miniature specimens (each 13.75 mm long) to be obtained from the material of one standard specimen. Although the experimental data showed good characterization of the transitional fracture behavior, it is not clear that the stress field of the 13.75 mm long miniature specimen adequately simulates that of the conventional specimen. Therefore, the bending-to-shear stress ratio analysis described below was performed to determine the optimal specimen length.

In discussing the effect of length on specimen behavior, it is convenient to refer to the bending-to-shear stress ratio. This is just the ratio of the nominal peak bending stress to the shear stress that results from a simple strength of materials analysis of a smooth bar with the same overall dimensions as the fracture specimen. For simply supported rectangular bars, the bending-to-shear stress ratio is 3S/D, where S is the distance between supports, and D is the specimen depth. For the standard Charpy specimen, the ratio is 12. For the 1/16 volume miniature specimens [4], the ratio is 7.1. Proportional scaling of cross-sectional dimensions and length by a factor of 1/2 results in the scaled specimen having the same ratio as the standard Charpy specimen.

If the bending-to-shear ratio is sufficiently large, then the form and intensity of the notch and subsequent crack tip fields are effectively determined by the applied bending moment. For smaller specimen span-to-depth ratios, the load required to achieve a given bending moment is increased. For a four point loaded specimen, these larger loads would tend to be of little consequence since the notch region would be under pure bending and the stress and strain concentrations around the load points would be remote to the fracture plane. For the three point bending configuration of the Charpy specimen, however, the striker contact region stress field and associated plastic zone can begin to interact with that of the notch (or crack) if the load levels are sufficiently large. Decreasing the specimen span-to-depth ratio would result in such interaction effects occurring at a lower applied moment. Even with the same span-to-depth ratio, a smaller specimen will require a larger applied load (relative to the yield load for example) than a full scale specimen to achieve the same applied J level. Therefore, even with the same span-to-depth ratio, the interaction between the notch/crack tip fields and the tup contact related fields will occur at a lower level of crack field intensity for the smaller specimen. Using a smaller span-to-depth ratio in a smaller specimen would just compound this undesirable behavior.

The tendency for the miniature specimens that were used in previous studies to fail outside the intended fracture plane when side grooves were not used could have been increased by using a smaller bending-to-shear ratio. The failure of these specimens apparently involved plastic slip along the plastic zone that resulted from the notch region plastic zone linking up with the plastic zone formed in the tup contact region. The contact stresses for a given moment and notch/crack field intensity would have been larger due to the decreased span-to-depth ratio. This would result in correspondingly more intense contact region plastic zones. Another contributing factor to this undesirable failure mode would be the increased level of average shear stress acting in the region where the plastic zones link (average shear stress on the section is proportional to the applied load). This shear stress would tend to promote the type of slip that resulted in the observed failure mode.

As the above discussion shows, the only benefit to using a shorter specimen is the ability to get more miniature specimens from a given amount of material. Since it seems likely that weld reconstitution will allow the benefits of a smaller length (i.e., more specimens), while still allowing the benefits of a proportionately scaled standard specimen, a scale factor of 1/2 was recommended for designing the miniature specimen length.

The Plane Strain Nature of 3D Notch Region Stresses

To determine the degree to which the 3D notch region stresses are plane strain in nature, the stress distributions in the fracture plane were compared to the 2D plane strain solution. The ABAQUS general purpose non-linear finite element code was used to perform these calculations. A typical finite element mesh and coordinate system are shown in Figure 2. Eight-noded brick elements were used in the analysis and finite strain theory was included in all calculations. The material flow curve was idealized as piece-wise linear. In the discussion which follows, general yield load is defined as the load at which yielding has spread across the entire uncracked ligament. This load corresponds to the "knee" in the load-deflection curve. In the cases where side-grooves were analyzed, a 45 degree included angle was modelled with 20% depth.

Figures 3 through 5 show the notch region stress field comparisons for the three applied displacement levels of 0.2 (near general yield), 1.5, and 3.0 mm (near peak load). In order to determine the dependence of the behavior on position along the notch front, stresses from the 3D midplane (solid line) are plotted as well as stresses from a position about half way between the midplane and the surface plane (dashed line).All three normal stress components are plotted in addition to the hydrostatic stress. The hydrostatic stress is the average of the three normal stresses and is considered to be an effective measure of constraint.

Figure 4 compares the 2D and 3D fracture plane stress distributions at a displacement of 1.5 mm which is about 8 times the displacement at general yield. At this load level, the peak σ_{yy} stresses occur at about 2.5 times the initial notch root radii from the notch surface. Except for the effect on the through thickness stress (σ_{zz}), the increased plasticity associated with this load level has led to very little loss of plane strain behavior compared to that at general yield. To the extent that the hydrostatic stress behavior is believed to be a more important measure of plane strain behavior than the through thickness stress, it can be reasonably argued that the center half of the 3D specimen notch fronts are still predominately plane strain. At this load level, the side grooves are again seen to provide an improvement of the σ_{zz} distributions.

Figure 3 compares the 2D and 3D fracture plane stress distributions for a full size standard specimen at about the general yield load. The stress distributions are plotted versus the distance from the notch tip, where the notch tip is normalized by the original notch tip radius (0.25 mm). The portion of the stress distribution important to fracture behavior is that between the notch tip and the peak stress (σ_{yy}) location. For this load level, the peak stress location is about 1.5 notch root radii from the notch surface. At least the center half thickness of both 3D geometries (with side grooves and without) is very near to plane strain conditions. At this load level, even the through thickness stress (σ_{zz}) is very close to that of the 2D plane strain solution. The side grooves provide a slight improvement of the σ_{zz} distribution at the intermediate plane.

Figure 5 compares the 2D and 3D fracture plane stress distributions at a displacement of 3.0 mm which is about 15 times the displacement at general yield. At this load level, the peak σ_{yy} stresses occur at about 3.5 times the initial notch root radii from the notch surface. The "bump" in the σ_{yy} stress distributions near the notch surface is believed to be the result of excessive distortion in the finite elements near the notch tip. To the extent that the element distortion affects the 2D and 3D solutions similarly, it is believed that this numerical anomaly does not impact the conclusions to be drawn from these solutions. Again, except for the effect on the through thickness stress (σ_{zz}), the increased plasticity associated with this load level has led to very little loss of plane strain behavior at the examined sections. The improvement in the σ_{zz} stress distribution for the side grooved specimen at higher loads is apparent in Figure 5. The

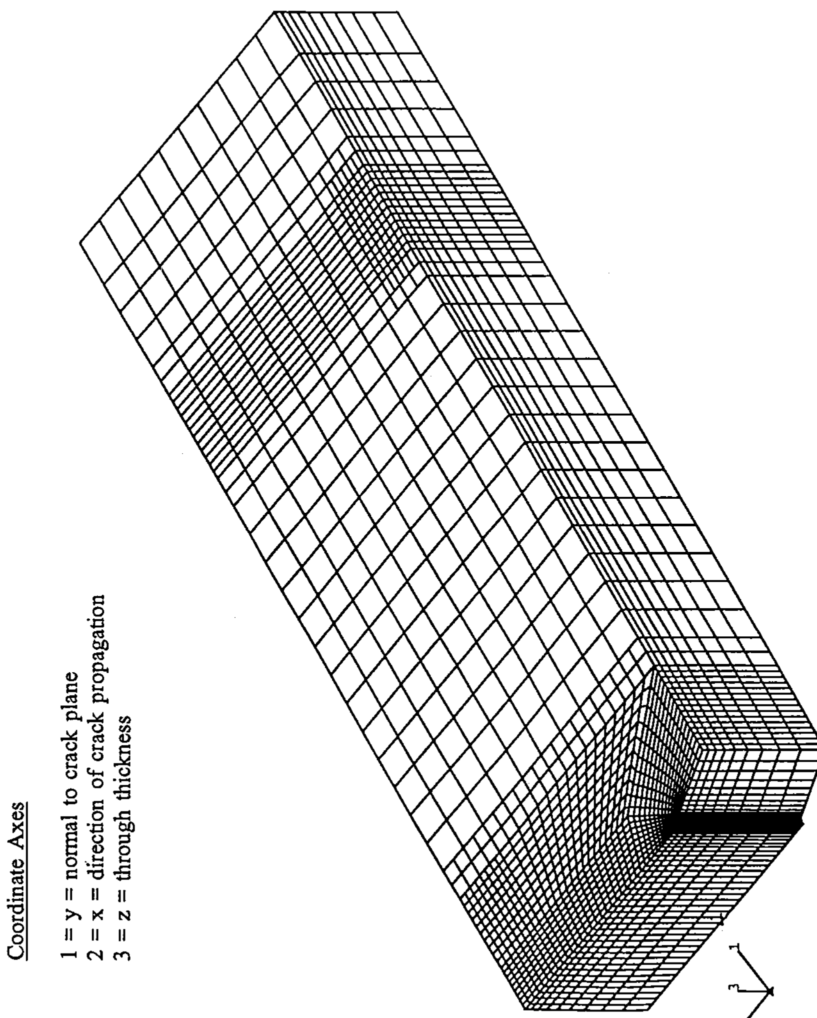

FIG. 2--Refined 3D finite element grid of the standard Charpy specimen

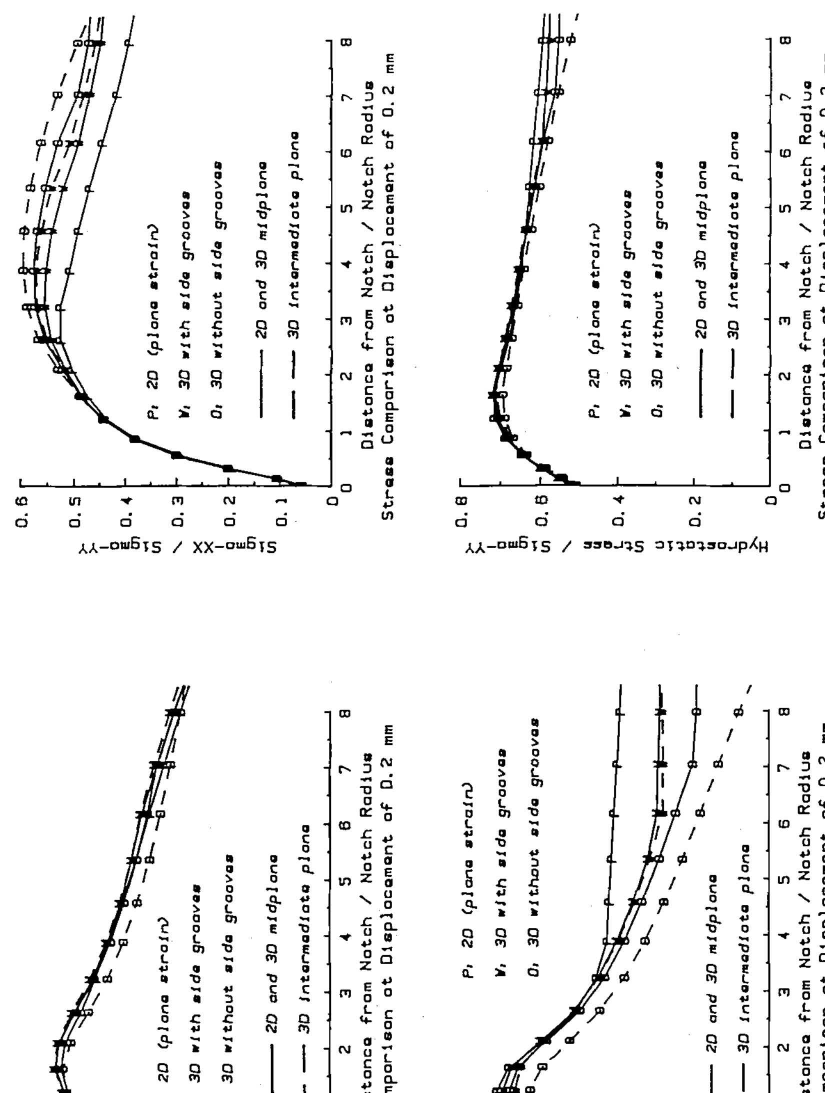

FIG. 3--2D and 3D model notch region stress behavior at an applied displacement level of 0.2 mm (general yield load conditions)

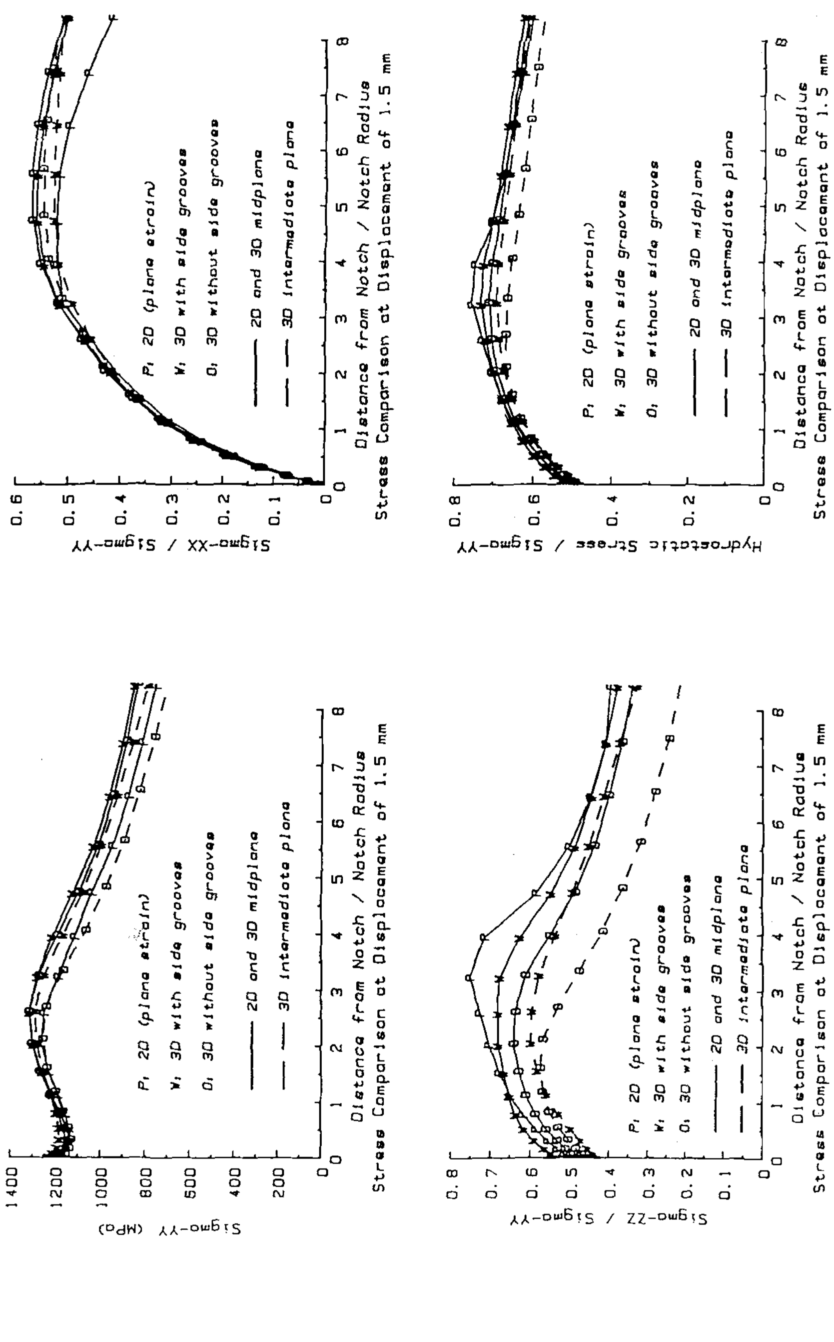

FIG. 4--2D and 3D model notch region stress behavior at an applied displacement level of 1.5 mm

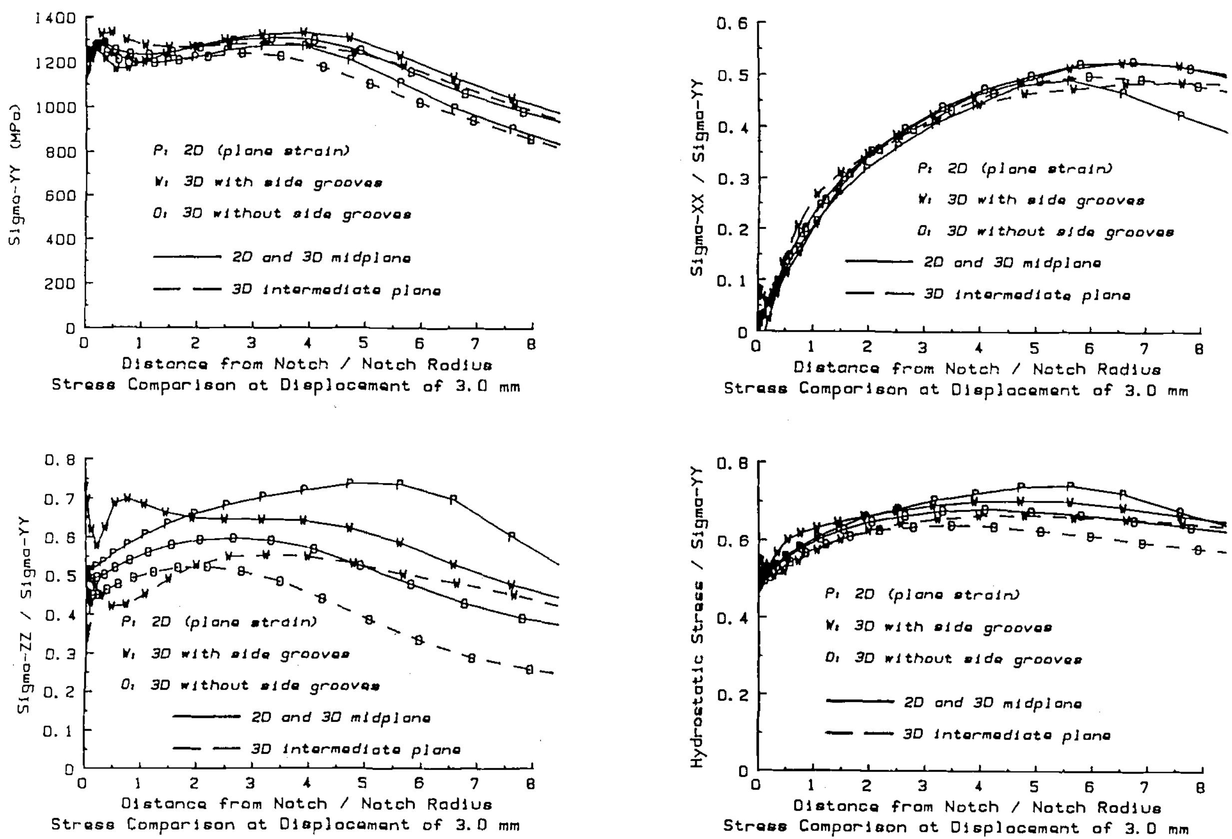

FIG. 5--2D and 3D model notch region stress behavior at an applied displacement level of 3.0 mm (near peak load conditions)

3D side groove solution behavior at small distances from the notch seen for the σ_{zz} stress is believed to be the result of the relatively coarse side groove modeling contributing to the above noted element distortion effects.

In summary, it can be concluded from the finite element solutions that the center-half portions of the notch fronts for side grooved and non-side grooved specimens exhibit plane strain behavior for applied displacement levels up to those representative of general yield. Beyond general yield load, the through thickness stresses are much closer to plane strain when the specimen is side grooved. Further comparisons using stress contours on the fracture plane will be made below. The beneficial effect of the side grooves will become more apparent during that discussion.

Central Notch Region Stress Behavior

The relevance of the 2D plane strain idealization to the central notch front region stress states has been demonstrated. In this section stress behavior from a refined 2D plane strain model are presented. Contours of the $\sigma_{yy}(=\sigma_{11})$ stress in the notch tip region for an applied displacement of 3 mm showed that this stress component peaks on the notch symmetry plane at a point that is about 2.5 times the initial notch radius or about 1 times the deformed notch radius. Severe distortion of the elements at the notch tip was observed. The σ_{xx} $(=\sigma_{22})$ stress component is zero at the notch tip and peaks at about 4 times the initial notch tip radius from the notch tip. The $\sigma_{zz}(=\sigma_{33})$ also peaks ahead of the notch tip. Contours of equivalent plastic strain, unlike the stress contours, show that the peak plastic strain occurs at the notch tip surface. The plastic strain gradient is very large near the notch tip. The hydrostatic stress peaks at about 4 times the initial notch root radius for this load level.

Stresses at the notch symmetry plane as functions of distance from the notch tip were analyzed at four load levels. The lowest load level is 0.63 of the Green & Hundy (G&H) [18] general yield load (P_o) and therefore has very limited plasticity effects. The highest load level that was analyzed is for a load ratio of 1.56. The (σ_{yy}) stresses tend to peak at 1 to 3 initial notch tip radii from the notch tip surface. Also, the distance to the peak stress increases with load level as is predicted by the G&H model. Since these results are from a large deformation finite element formulation, this shift is probably amplified due to the fact that the notch tip radius is increasing as the load increases. As with σ_{yy}, the location of the peak values of the σ_{xx} and σ_{zz} stresses is shifted further from the notch tip with increasing load, and again there is an apparent change in the near tip stress behavior between the 1.27 and 1.56 load levels which is probably due to severe finite element distortion at the notch tip. Figure 6 shows the hydrostatic stress behavior using two normalizations. It can be seen that the hydrostatic stress behavior changes in going from a largely elastic notch tip field (P/P_o = 0.63) to a largely plastic field (P/P_o = 1.02). Considering that higher hydrostatic stresses indicate higher constraint, it can be seen that plasticity initially increases constraint near the notch tip while lowering it at locations farther from the notch tip. Then further plasticity causes the location of the highest constraint to move farther from the notch tip. Using the σ_{yy} normalization, it can be seen that once the yield load is exceeded, the magnitude of the peak constraint increases, but only by a small amount.

Side Groove Effects on Notch Region Stress Behavior

Putting side grooves in the MNT specimens has two fundamental effects. By reducing the fracture plane area, the load required to achieve a critical stress state is reduced. At the same time, the

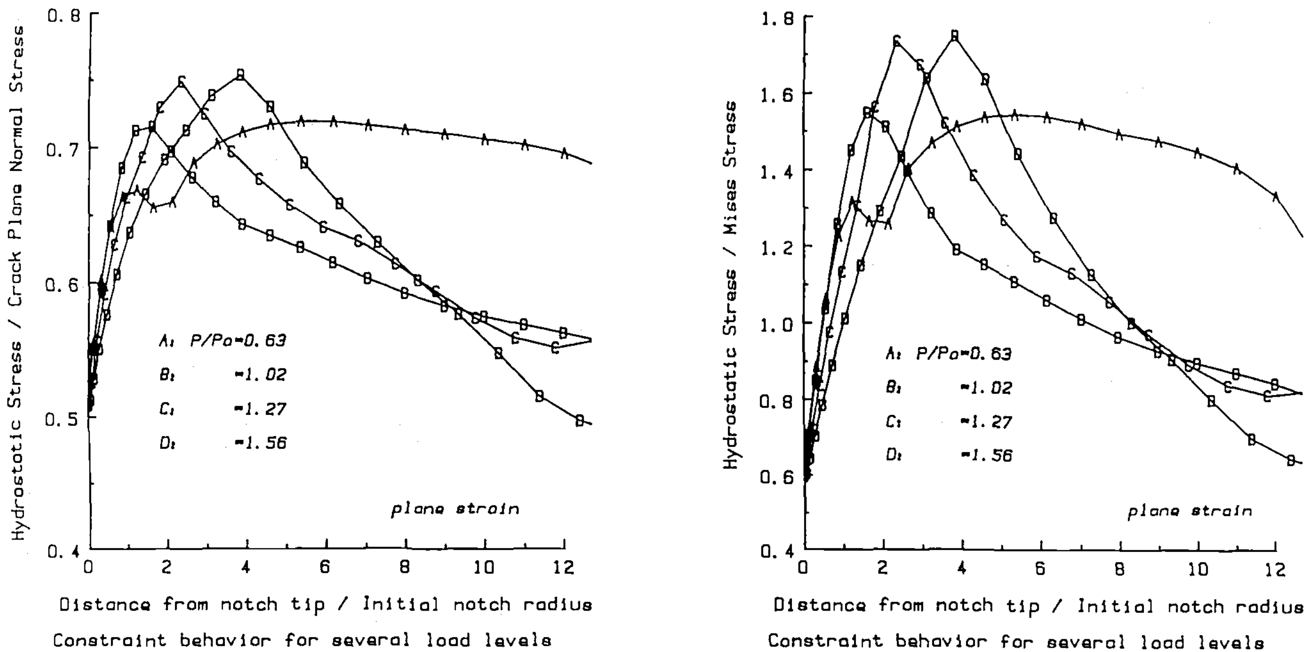

FIG. 6--Notch tip region behavior of hydrostatic stress at four load levels
(refined 2D plane strain model of the standard Charpy specimen)

cross-section at the region where plastic collapse can occur in the non-side grooved specimens is not reduced. Therefore, the shear stress in the plastic zone to either side of the fracture plane is significantly reduced by the addition of side grooves. This results in an increase in the plastic collapse load relative to the fracture load. The second fundamental effect, as will be demonstrated in the following discussion, is that a larger portion of the notch front has plane strain fields.

In the following, crack plane stress fields from the 3D models of a standard Charpy specimen and a standard specimen with 20% side-grooves are compared. The purpose of the comparison is to show how the introduction of side grooves affects the variation in stress field behavior in going from the specimen midplane to the external specimen surface. Since the crack plane normal stress (σ_{yy}) and the hydrostatic stress are considered to be the most important stress quantities for illustrating plane strain behavior, only these stresses are compared.

Figures 7 through 10 compare the crack plane σ_{yy} and hydrostatic pressure contours for the refined 3D model with side grooves and the refined 3D model without side grooves. Figures 7 and 8 show the behavior at a displacement of 0.2 mm (approximately at general yield), and Figures 9 and 10 show the behavior at 1.5 mm of displacement. The left side plots in these figures are the results without side grooves and those on the right are with 20% side grooves. The notch front is the right edge of each contour plot while the left edge is at the tup contact region. The bottom edge of these plots corresponds to the specimen midplane. For the model without side grooves, the top edge of the plot is the external surface of the specimen. For the model with side grooves, the top edge of the plot corresponds to the root of the side groove.

In Figures 7 and 8 it can be seen that there is a significant reduction in the σ_{yy} and hydrostatic stress between the quarter thickness plane (intermediate plane of Figures 3, 4, and 5) and the external surface of the specimen. For the side grooved specimen, the stresses near the notch show little variation between the midplane and the side groove root. Since Figure 3 shows that both 3D models have plane strain behavior at the midplane, it can be concluded, that adding side grooves resulted in an increase in the portion of the notch exhibiting plane strain behavior. In Figures 9 and 10, it can be seen that the loss of plane strain behavior over the outer quarter thickness of the model without side grooves is greater than it was for the smaller displacement level. Although there is some reduction in the hydrostatic stress for the side grooved specimen near the side groove, the loss is much less significant than for the model without side grooves. Calculations at 3 mm of displacement showed that the loss in plane strain behavior in the outer quarter thickness of the side grooved and non-side grooved models is not substantially different than at the displacement level of 1.5 mm. This strongly suggests that further displacement increases would not result in substantially different plane strain behavior than observed at 1.5 and 3 mm of displacement.

The observation that the loss of plane strain behavior does not appear to continue after a displacement of about 8 times the general yield displacement is important. This is because dimensional analysis shows that miniature specimens will require relatively larger displacements than full scale specimens to achieve comparable crack tip field intensities. Further, the use of side grooves results in a larger volume of material being sampled at near plane strain conditions. We estimate that for the miniature specimen with side grooves the peak hydrostatic stress field extends along the notch to 80% of the distance calculated in the conventional specimen. Whereas, the peak hydrostatic

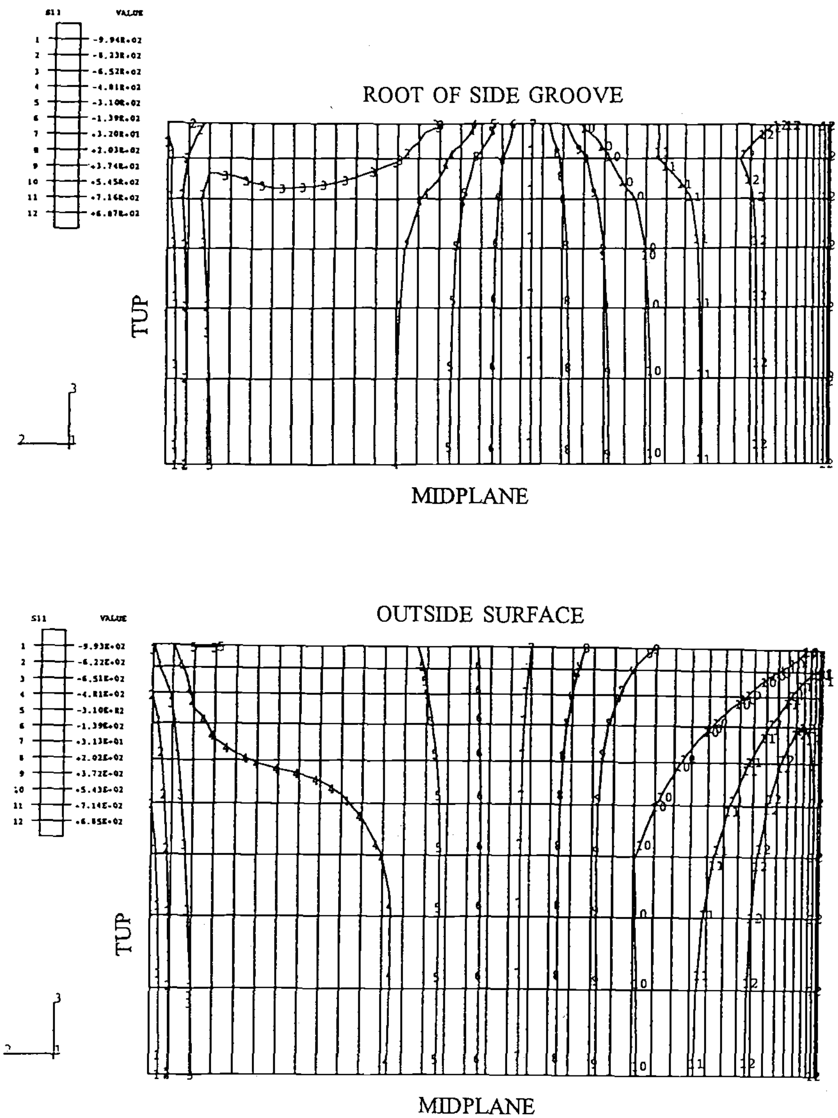

FIG. 7--Comparison of fracture plane σ_{yy} contours at a displacement of 0.2 mm for notched specimens both with (top) and without (bottom) side grooves

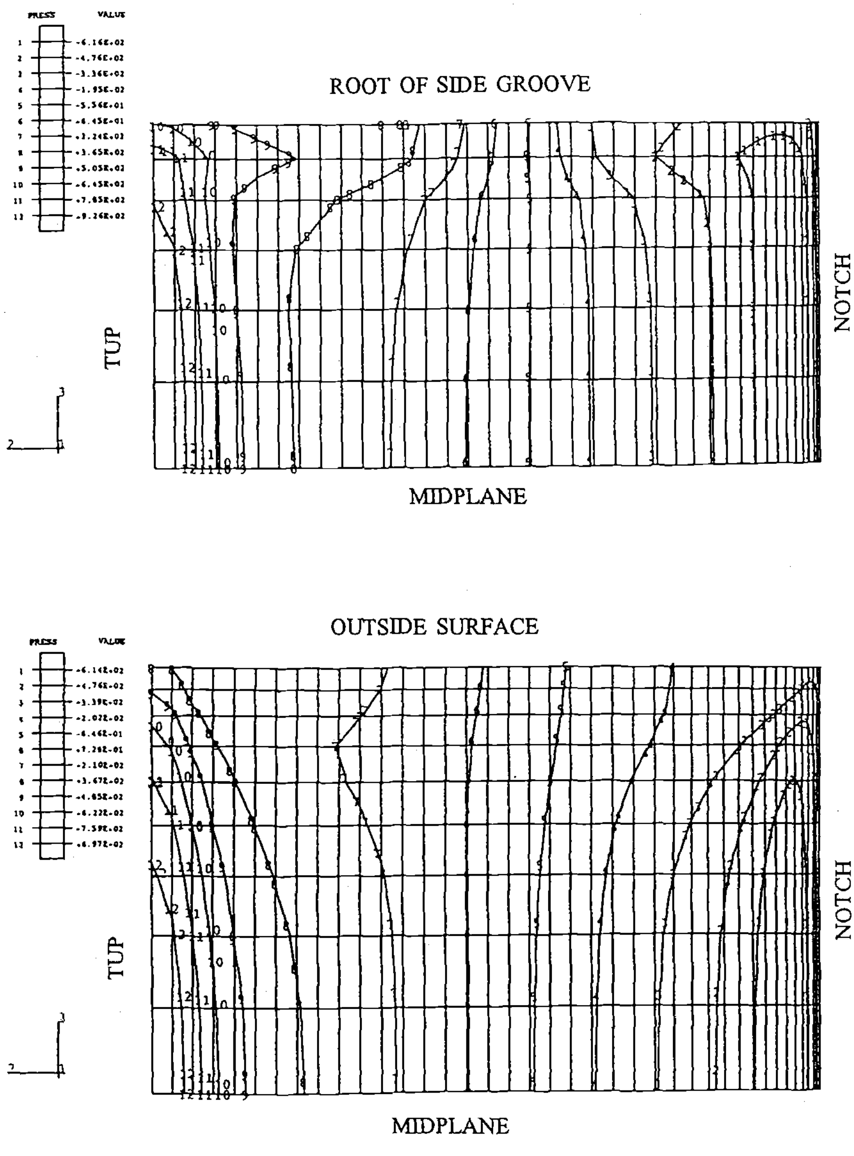

FIG. 8--Comparison of fracture plane hydrostatic pressure contours at a displacement of 0.2 mm for notched specimens both with (top) and without (bottom) side grooves

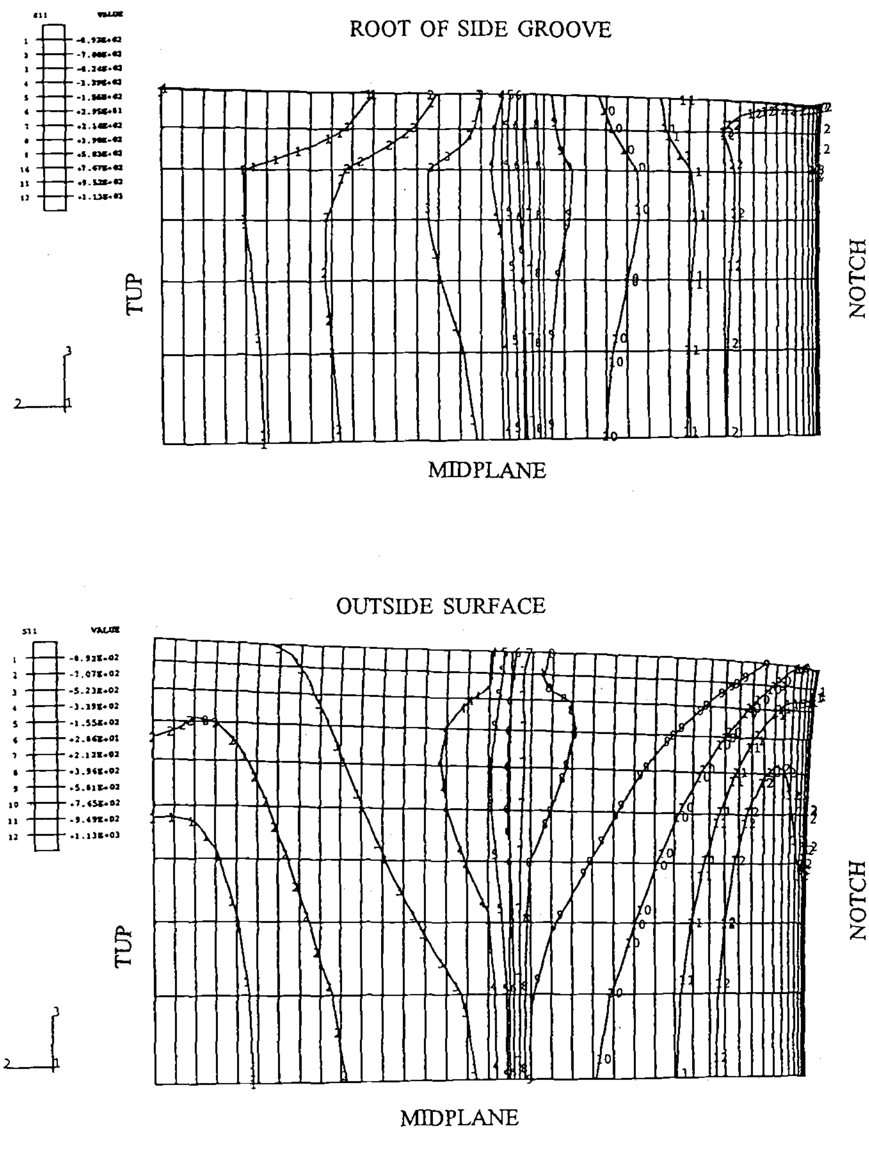

FIG. 9--Comparison of fracture plane σ_{yy} contours at a displacement of 1.5 mm for notched specimens both with (top) and without (bottom) side grooves

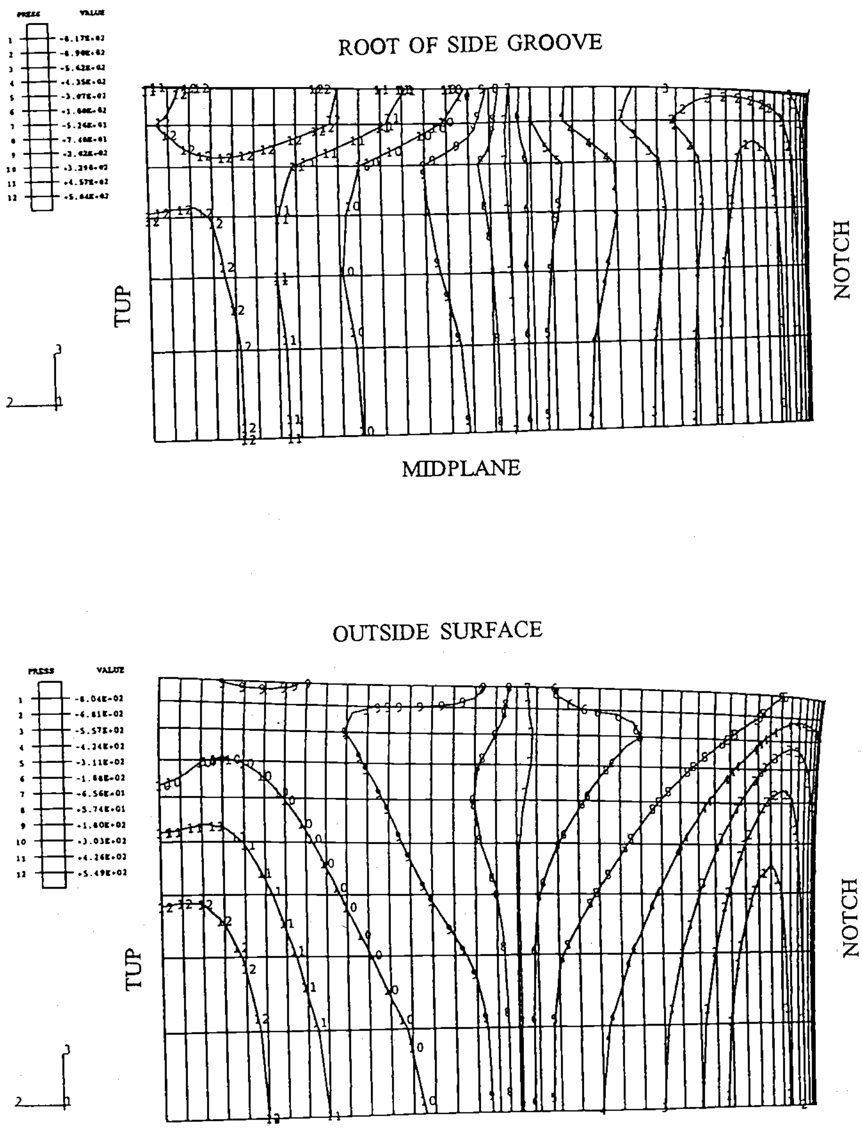

FIG. 10--Comparison of fracture plane hydrostatic pressure contours at a displacement of 1.5 mm for notched specimens both with (top) and without (bottom) side grooves

stress field in the miniature specimen without side grooves extends along the notch to half the distance of the conventional specimen. This relative increase in the peak stress region size due to size grooves is expected to reduce scatter (and therefore less specimens will be needed) for specimens tested in the transition region where the trigger particle mechanism dominates brittle fracture initiation.

Striker Design and Contact Conditions

In our recent finite element study, which was focused on non-linear response prior to crack initiation, two sensitivity studies related to tup design were performed. The first study compared the load versus deflection behavior from the ISO and ASTM tup designs. For loading up to displacements representative of peak Charpy test loads, the ISO tup was found to result in load levels that were about 5% below those of the ASTM tup. This load decrease was attributed to the fact that the relatively flat contact region of the ASTM tup is about 10% of the support span width. This flat contact region results in the contact forces being significantly concentrated near the ends of the contact region. This concentration, in effect, results in a four point bending condition. If the contact forces were exactly concentrated at the corners, the applied moment for a given load level would be 10% less than for the three point bending condition. The smaller 5% effect that was observed in the finite element simulation is easily accounted for by the fact that contact forces, while peaked at the corners, do exist all along the contact region.

In the second finite element sensitivity study, the ASTM tup design was used with two levels of friction. In one case, the friction coefficient was zero while in the other, the coefficient was 0.5. In the latter case, the maximum friction force was further limited by the shear yield strength of the specimen material. Since the frictional forces were observed to be largely limited by this yield stress value, the assumed coefficient had little effect on the results. The calculations showed that the addition of frictional forces increased the applied load levels by about 10%. This load increase was attributed to frictional forces at the support points restraining the longitudinal expansion of the notched side of the specimen.

Both of these results are consistent with several experimental observations that have appeared in the literature for which the sum of the Charpy energies for the two tup geometries have been compared. Tower [19] showed that different Charpy energies can result from using the ISO and the ASTM tups when testing highly ductile materials. While for energy levels below 60 J, differences were negligible, for energies in the 100 to 200 J range, energies were as much as 25% larger for the ASTM tup. The explanation given for this increase in energy was the intense localized deformation caused by the corners of the ASTM tup design. These corners allowed the tup to essentially gouge the contact surface as the result of the contacted surface of the specimen wanting to contract under the bending induced compression at this surface. This gouging action results in significant plastic deformation and energy dissipation. While the higher Charpy energy levels of the Tower study were for materials other than vessel steels, similar behavior with energy differences in the 10 to 15% range have been observed for nuclear pressure vessel steels on the upper shelf [11].

By restricting the contraction of the specimen's contacted surface, the ASTM tup results in a net tensile stress being superimposed on the fracture plane bending stress distribution. This additional tension might be expected to decrease the chance that a specimen will wrap around the tup rather than break into two pieces. This behavior has been observed by researchers at the Belgian Nuclear Research Center [20]. It is not clear how this superimposed tensile stress would be reflected in the Charpy energy differences since the higher loads of the ASTM design would be truncated at the time of separation while the lower load levels of the ISO design would continue until the specimen slips off the supports.

Some direct evidence exists for the contact surface gouging being the primary cause of the higher energies for the ASTM tup design. In their specimen reconstitution work, Belgian Nuclear Research Center researchers have found that localized hardening due to welding near the tup contact region can reduce the degree of gouging [21]. When the gouging is avoided, the ISO and ASTM tups result in esentially the same Charpy energies. To further confirm this conclusion that the gouging and higher energies are linked, tests were done in which a hard tungsten foil was placed between the ASTM tup and the specimen. Again the gouging was avoided, and the Charpy energies were essentially the same as those from using the ISO tup design.

With the above observations, it was decided that our miniature specimen testing program would focus on using the ISO tup design. One reason for this choice is that the energy that one obtains from a Charpy test is intended to be indicative of the fracture resistance of the material. The fact that a part of the energy obtained from some tests using the ASTM tup design is totally unrelated to the fracture process is seen as an unattractive feature. Perhaps the more compelling reason is that miniature specimens will tend to behave in a more ductile manner than full scale specimens therefore tending to exaggerate this undesireable gouging behavior in the miniature specimens. If there is a negative side to using the ISO tup in the miniature specimen testing, it is probably that there may be a greater chance that the specimen will not fracture to the point of becoming two pieces. This behavior would be expected to be more likely for the miniature specimens than full size specimens due to the relatively more ductile behavior of the smaller specimen.

<u>Inertial Effects</u>

Figures 11 and 12 show the results of two dynamic analyses. Both analyses assume plane strain conditions. Quasi-static stress-strain properties were used for these simulations. The data presented in Figure 11 is for a constant tup velocity of 3 m/sec which is the low end of the tup velocity range stipulated by the ASTM standard E23. Figure 12 resulted from assuming a constant tup velocity of 6 m/s, the upper end of the stipulated velocity range. The load-deflection curves from the static analyses are included in these plots for comparison with the dynamic curves. For the static loading case, the tup and anvil loads are equal (but in opposite directions). This is not generally the case for the dynamic analysis due to the inertial effects and therefore both loads are plotted. It can be seen that the tup and anvil loads tend to be out of phase with respect to each other. For earlier times (small deflections), the oscillation of the loads is very large. However, once plastic deformation becomes significant, the high frequency oscillations are quickly damped out. Another factor which contributes to the dynamic behavior approaching quasi-static loading behavior is that the loading rate is relatively slow compared to the stress wave speeds. Elastic stress wave speeds are between 3×10^6 mm/sec and 6×10^6 mm/sec depending on the type of wave (compressive, shear, or surface). At this speed, stress waves can propagate to the end of the specimen and return to the notch region 25 to 55 times by the time the tup displaces the specimen 3 mm.

Examining the right side plots of Figures 11 and 12, it can be seen that the anvil does not exert a reaction until a tup displacement of about 0.04 or 0.08 mm. This reflects the time that it takes for the stress wave from initial contact to propagate to the anvil contact

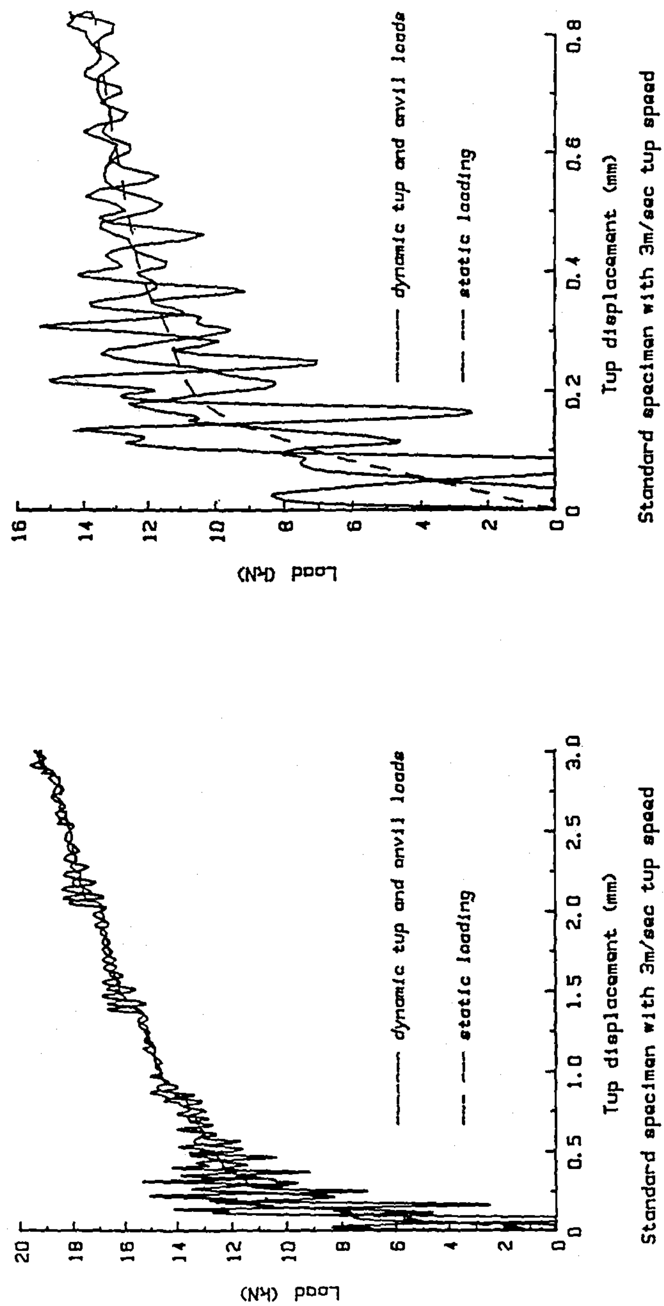

FIG. 11--Dynamic load versus tup displacement behavior for the standard specimen being struck with a tup speed of 3 m/sec

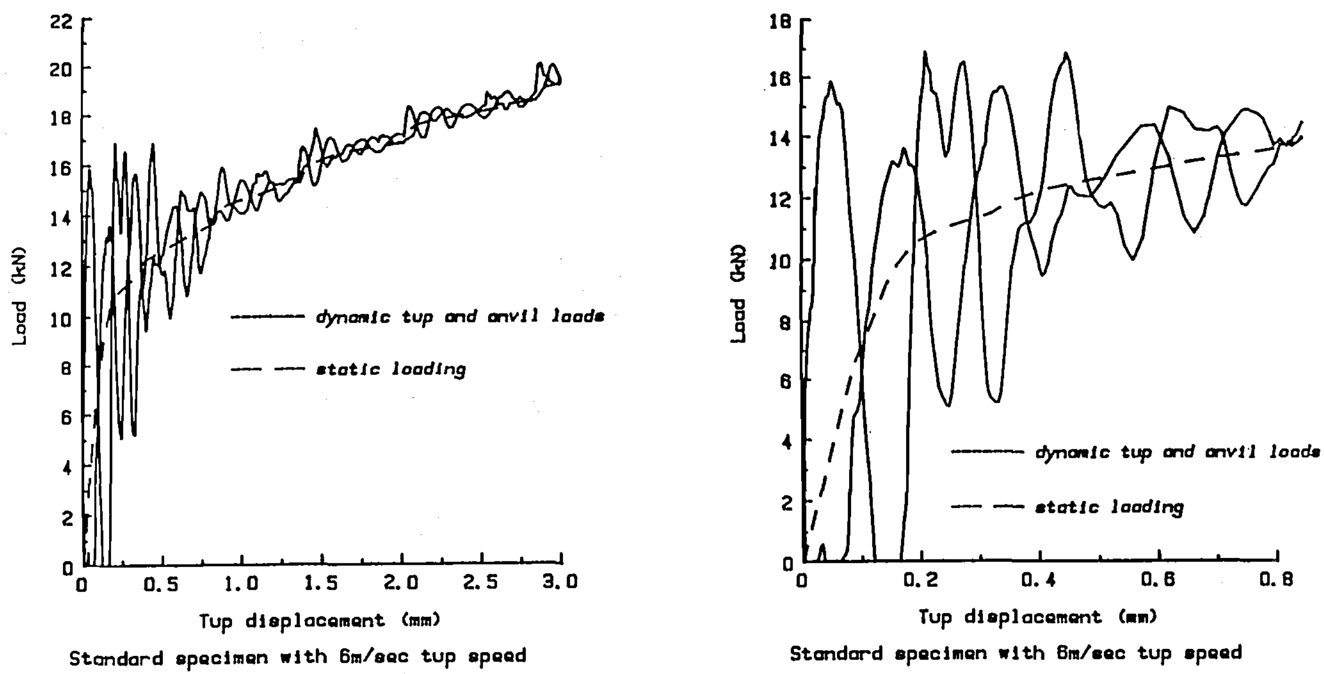

FIG. 12--Dynamic load versus tup displacement behavior for the standard specimen being struck with a tup speed of 6 m/sec

location. These plots also show that the first oscillation in the tup load results in the tup load going to zero for a period of time. This is the result of the specimen springing away from the tup shortly after initial contact. This springing away is the result of the first stress wave returning to the tup contact region after having reflected from the end of the specimen.

It is worth noting that the size of the tup load oscillations found in these dynamic simulations are larger than typically measured during instrumented Charpy testing. The fact that the size of the oscillations obtained experimentally seem to depend to some extend on the group doing the work suggests that perhaps "electrical damping" in the measurement systems may be a partial explanation. In fact, many researchers have used signal conditioners which operate in the few tens of kHz range. Our calculations show that the load transducer signal is in the 20 to 40 kHz range. Therefore, a system capable of at least 100 kHz, with a 1 MHZ sampling rate, is needed to accurately determine the general yield load.

To verify scalability of the full size dynamic Charpy solution to a half size specimen, a half scale version of the coarse 2D grid was generated. All dimensions, including those of the tup and anvil, were halved. For static loading, the stress and strain solution scaled exactly with that of the full scale model. The dynamic simulation, run with a tup velocity of 6 m/sec, verified that the dynamic solution also scales exactly if both specimen sizes are impacted with tups having the same velocity. The principal conclusion to be drawn from this analysis is that the tendency for inertial effects to become negligible after general yield also occurs for the half scale specimen.

Weld Reconstitution

The effect of weld reconstitution was simulated using a refined 2D plane strain model of a standard Charpy in which the weld and heat affected zones were given a yield stress 20% above the base metal value. The elevated yield stress was applied to a region that extended from 4 mm to 6 mm from the specimen's fracture plane. The model was then loaded to a deflection representative of peak load values for upper shelf behavior. It was found that the plastic zones emanating from the notch and the tup contact region reached the high yield region even before general yield. This interaction resulted in a strain increase at the notch relative to that in an unwelded specimen. This strain increase was nearly 15% for displacements representative of peak load conditions. If crack growth behavior is strain controlled, this suggests that Charpy energies in the reconstituted specimen could be reduced by about 15%.

Figure 13 shows the extent of the plastic zones in a Charpy specimen as a function of applied load and as a function of applied displacement. Normalizing the load by general yield load makes the results applicable to other yield stress levels. Normalizing plastic zone size and applied deflection by the specimen height allows the results to be applied to specimens of nonstandard size. It can be seen that the plastic zone extent tends to peak at about one specimen height. This strongly suggests that the minimum distance that a weld should be from the fracture plane is about one specimen height. With half scale specimens, this would enable a change of material orientation in the reconstituted specimens.

TEST GEOMETRY RECOMMENDATIONS FOR RPV STEELS

Microstructural considerations resulted in the proposed specimen cross-sectional dimensions being set at half of the standard Charpy

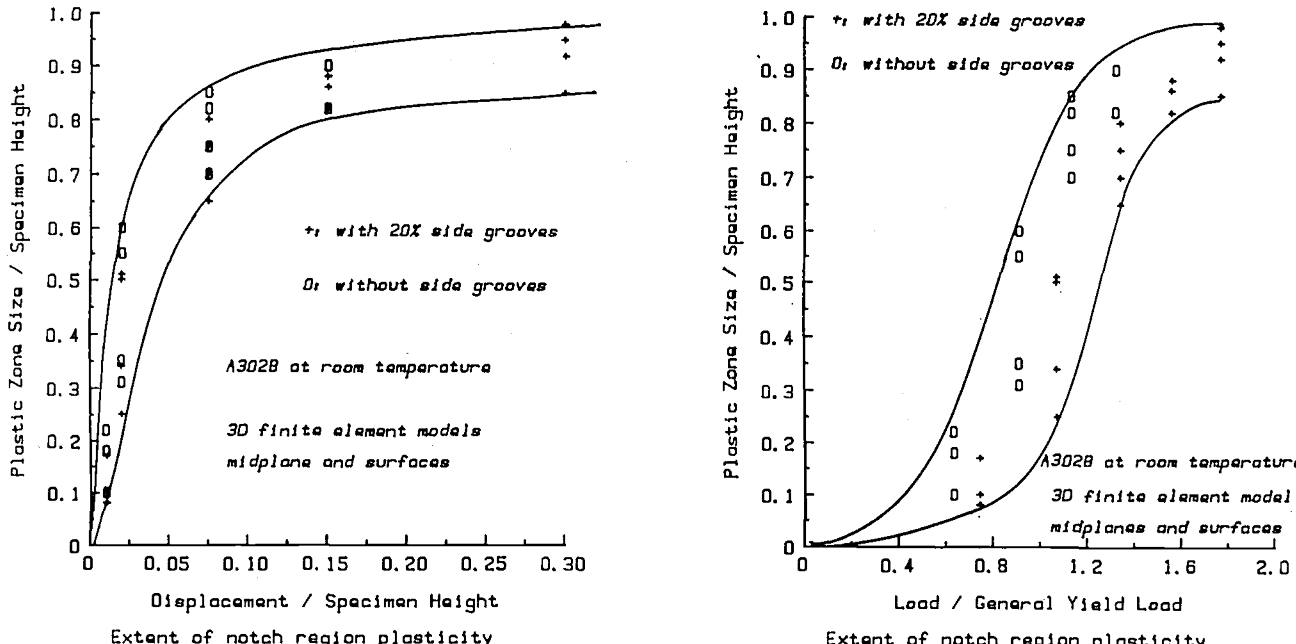

FIG. 13--Summary of plastic zone size results from 3D finite element simulations of Charpy specimens

specimen dimensions. Therefore the miniature specimen cross-section is 5 mm by 5 mm. It was determined that scaling the length of the miniature specimen so as to maintain the same bending-to-shear ratio as the standard specimen would be best. This decision was based in part on the fact that miniature specimens will require relatively higher load levels than full scale specimens which could have adverse effects if a shortened design were selected. The only disadvantage of not using a shorter design is that fewer specimens can be made from a single broken Charpy specimen. However, it is believed that this can be overcome by the use of weld reconstitution. To the extent that it is the spacing between the support points which determined the bending-to-shear stress ratio, the miniature specimens can be slightly shorter than half scale provided that the half scale of the support spacing is maintained.

Although it is possible that keeping the same bending-to-shear ratio as for the full size specimen (i.e., span-to-depth ratio) could have prevented the plastic collapse type miniature specimen failures observed in previous work, the use of side grooves is still highly advantageous. Although both full size and miniature specimens have plane strain fields over a significant portion of their notch or crack fronts, the portion of the front with plane strain behavior tends to decrease with increasing plasticity. The use of side grooves greatly increases the percentage of the notch or crack front that exhibits plane strain behavior. This is particularly important for small specimens since fracture behavior is known to depend on the size of the region that is subjected to critical stress levels. By maximizing the plane strain zone of the miniature specimen, the fracture behavior should be more like that of a larger specimen. This relatively larger plane strain zone size should therefore also tend to reduce experimental scatter such as might be expected for a smaller specimen size.

It was concluded that relatively standard side grooves are appropriate (20% of thickness, 0.2 to 0.4 mm radius, 45° angle). Using deeper side grooves than 20% would be expected to result in a net decrease in the absolute size of the notch or crack region with plane strain behavior as the result of reducing the total notch front length. Using shallower side grooves would be expected to provide less satisfactory stress field improvement at the higher load levels. Using a larger groove angle would tend to reduce the side groove effectiveness by reducing the intensity of the stress field induced by the side groove. Decreasing the side groove angle would tend to increase the intensity of the side groove stress field and possibly provide slightly better performance in terms of the notch tip fields, but could lead to side groove closure on the compression side of the specimen which would result in discontinuous specimen stiffness behavior.

The use of side grooves is likely to decrease or eliminate the tendency for ductile fracture (shear lips) near the surfaces of the specimen. This might be expected to shift the Fracture Appearance Transition Temperature (FATT) to higher temperatures by reducing the percent shear at a given temperature. This reduction in shear lip formation would also seem to result in less resistance to a dynamically propagating crack; thus again tending to promote a decrease in the percent ductile fracture evaluation. (It seems likely that tunneling associated with cleavage crack growth in specimens without side grooves results in plastic dissipation of energy that would otherwise be available for cleavage.) These effects would tend to increase the FATT, making results more conservative, and would therefore be expected to reduce any correction needed to relate the miniature specimen results to full scale specimen results.

The above described 2D and 3D, large deformation, finite element analyses have shown that plane strain conditions exist over a significant portion of the standard specimen notch for loads up to those representative of upper shelf behavior. For loads below general yield (lower shelf), about 3/4 of the notch tip is reasonably close to the 2D plane strain solution. As loads approaching those for upper shelf fracture behavior are applied, the portion of the notch exhibiting plane strain behavior decreases to about 1/4 of the total notch length. Adding 20% side grooves greatly reduces the loss of plane strain at the higher load levels. At load levels representative of upper shelf behavior, the side grooved geometry retains plane strain behavior over about 1/2 of the notch front. For a half scale specimen, the absolute length of plane strain along the notch is then 1/2 x 80% x 5 mm = 2 mm. For the full scale specimen, the plane strain region is 1/4 x 10 mm = 2.5 mm. Therefore the side grooves significantly offset the absolute reduction in the plane strain notch front region.

A 2D simulation of a weld reconstituted specimen showed that if the weld is too close to the fracture plane, the presence of the weld can induce larger plastic strains in the fracture process zone for a given applied displacement level. This increase in the fracture process zone strain intensity for a given applied displacement can be expected to reduce Charpy energy levels. This is consistent with available experimental results [22][23]. This weld reconstitution simulation, when combined with plastic zone size information from the 3D simulations of this study, allow a smallest weld insert size to be determined. The plastic zones in the 3D models were observed to extend as far as one specimen height from the fracture plane. Since any interaction between the weld heat affected zone and the fracture region plastic zone could result in the weld affecting the specimen behavior, this means that the weld and its heat affected zone should be no closer to the fracture plane than one specimen height.

A study of tup design effects on measured Charpy energies showed that the difference between the ASTM standard tup geometry and the ISO tup geometry is negligible except when very ductile materials are being tested [19]. This increase in energy is mainly associated with the corners of the ASTM tup gouging the contact surface of the specimens when large deformations are required to break the specimens. Since the miniature specimens will tend to require relatively larger deflections than the full scale specimens, it is judged that the ISO tup design is preferable.

Scaling the ASTM anvil (support) radius and spacing appears most appropriate for the miniature specimen testing. Scaling the spacing will result in equal bending-to-shear load ratios for full scale and mini specimens. Scaling the support radius should result in similar behavior for both size specimens.

Inertial effects (i.e., stress wave effects) tend to become insignificant after general yield load is reached due to the damping associated with plastic deformation. Experimental results show that general yield conditions are attained prior to crack growth throughout the transition temperature range [4, 16]. General yield occurs at an energy level of about 3 or 4 J (standard Charpy). The tendency for higher load levels in mini specimens relative to the general yield load should make inertial effects even less significant.

Strain rate effects associated with impact testing (as opposed to quasi-static testing) are significant for both full scale and mini specimens. Though strain rates in a half scale miniature specimen will be twice those of a full scale specimen if equal impact speeds are used, this change in strain rate is expected to have negligible effects on specimen behavior. This is because strain rate effects enter primarily though the elevation of yield stress and a doubling of strain rate increases the yield stress by only a couple percent.

Finite element analysis as well as dimensional analysis has shown that stress and strain states in the miniature specimen can simulate those in a full scale specimen provided proper scaling is applied. However, it has also been shown that load and displacement levels required to induce fracture will be relatively higher in the miniature specimen (e.g., compared to those at general yield). Before correcting for the load reduction associated with the use of side grooves, load levels would be expected to be about 5 to 10% larger in the half scale miniature specimen. Displacement levels could be 80 to 90% larger. Energies can be expected to be between 1/8 and 1/4 of those for full scale specimens.

SUMMARY AND CONCLUSIONS

Design of all miniature specimens should begin with a thorough examination of the material microstructure to determine the minimum specimen dimension. In the case of the MNT, the proposed minimum cross section dimension is 5 mm x 5 mm for RPV materials to ensure that chemical bands and inclusion stringers within the steel are adequately represented. In order to simulate the stress state of the conventional specimen, a 1/2 scale factor has been proposed. The 1/2 scale factor applies to the specimen dimensions as well as to the span and tup radius. In addition to scaling the key test parameters, 20% side grooving is recommended to substantially increase the volume of material which is exposed to plane strain conditions. Miniature specimens tested on the upper shelf which are side grooved will produce an absolute length of plane strain along the notch which is about 80% of that experienced in conventional 10 mm x 10 mm x 55 mm specimens. Therefore, side grooves will significantly offset the reduction in plane strain at the notch/crack tip for miniature specimens.

Generally, it is expected that a smaller specimen will tend to behave as though the material is tougher. This is the fundamental result of the nonscalability of the material microstructure and the mathematics associated with singular crack tip fields. In terms of transition temperature behavior, this means that the transition temperature measured with a smaller specimen will tend to be lower than the transition temperature measured with a larger specimen. The design of the miniature specimen has focussed on minimizing this shift. The most significant design aspects in terms of reducing this shift are the side grooves, and the use of proportional scaling. Basically, the side grooves will make the smaller specimens behave as though the material is less tough, as compared to the behavior that would be obtained if a perfectly scaled Charpy geometry were used.

Although the feasibility preparing 16 miniature specimens from the broken halves of one conventional specimen has been experimentally demonstrated, detailed analysis of the miniature specimen stress fields has shown that the conventional specimen aspect ratio results in a favorable bending-to-shear ratio. The larger aspect ratio limits the number of specimens which can be machined from a conventional specimen to 8 (4 from each broken half). However, the larger miniature specimens have the significant advantage that they can be weld reconstituted since the requirement of providing an insert of 4 times the width (W) can be satisfied. Therefore, it is now possible to produce 24 miniature specimens (as opposed to 16 earlier) from one conventional specimen using the weld reconstitution procedure. This strategy is particularly effective in nuclear reactor pressure vessel surveillance in cases where a limited fixed volume of material is available. A surveillance capsule can be withdrawn, the specimens tested, and 8 miniature specimens can then be machined from the broken halves of each specimen. Then, after further irradiation, the specimens can be tested and weld reconstituted to produce an additional 24 specimens for re-irradiation and testing.

Thus, using this strategy, it will be possible to produce sufficient data for accurate trend curve development on a plant-specific basis.

ACKNOWLEDGMENT

The authors are grateful to the Empire State Electric Energy Research Corporation (ESEERCO) and the New York state utilities for their sponsorship of this work. We are also grateful to Dr. L.J. Cuddy (Metallurgical Consultants) for his technical assistance with the microstructural work. We also wish to thank Mr. A.J. Peterson for his recognition of the importance of this work and his efforts in championing the technology.

REFERENCES

[1] Lucas, G.E., Odette, G.R., Sheckherd, J.W., McConnell, P., and Perrin, J., "Subsized Bend and Charpy V-Notch Specimens for Irradiated Testing", The Use of Small-Scale Specimens for Testing Irradiated Material, ASTM STP 888, W.R. Corwin and G.E. Lucas, Eds., American Society for Testing and Materials, Philadelphia, 1986, pp. 305-324.

[2] Corwin, W.R. and Hougland, A.M., "Effect of Specimen Size and Material Condition on the Charpy Impact Properties of 9Cr-1Mo-V-Nb Steel", The Use of Small-Scale Specimens for Testing Irradiated Material, ASTM STP 888, W.R. Corwin and G.E. Lucas, Eds., American Society for Testing and Materials, Philadelphia, 1986, pp. 325-338.

[3] Harling, O.K., Lee, M., Sohn, D-S., Kohse, G., and Lau, C.W., "The MIT Miniaturized Disk Bend Test", The Use of Small-Scale Specimens for Testing Irradiated Mateiral, ASTM STP 888, W.R. Corwin and G.E. Lucas, Eds., American Society for Testing and Materials, Philadelphia, 1986, pp. 50-65.

[4] Manahan, M.P. and Charles, C., "A Generalized Methodology for Obtaining Quantitative Charpy Data From Test Specimens of Nonstandard Dimensions", Nuclear Technology, Vol. 90, May 1990.

[5] "Small Specimen Test Techniques Applied to Nuclear Reactor Vessel Thermal Annealing and Plant Life Extension", American Society for Testing and Materials, ASTM STP 1204, October, 1993.

[6] Rosinski, S.T., Kumar, A.S., Cannon, N.S., and Hamilton, M.L., "Application of Subsize Specimens in Nuclear Plant Life Extension", Small Specimen Test Techniques Applied to Nuclear Reactor Vessel Thermal Annealing and Plant Life Extension, ASTM STP 1204, W.R. Corwin, F.M. Haggag, and W.L. Server, Eds., American Society for Testing and Materials, Philadelphia, 1993, pp. 405-416.

[7] Kumar, A.S., Louden, B.S., Garner, F.A., and Hamilton, M.L., "Recent Improvements in Size Effects Correlations for DBTT and Upper Shelf Energy of Ferritic Steels", Small Specimen Test Techniques Applied to Nuclear Reactor Vessel Thermal Annealing and Plant Life Extension, ASTM STP 1204, W.R. Corwin, F.M. Haggag, and W.L. Server, Eds., American Society for Testing and Materials, Philadelphia, 193, pp. 47-61.

[8] Hamada, J., Sato, S., and Kohyama, A., "Fracture Toughness Evaluation of Neutron-Irradiated Composites by a Miniaturized Charpy Test", Small Specimen Test Techniques Applied to Nuclear Reactor Vessel Thermal Annealing and Plant Life Extension, ASTM STP 1204, W.R. Corwin, F.M. Haggag, and W.L. Server, Eds., American Society for Testing and Materials, Philadelphia, 1993, pp. 77-89.

[9] Kryukov, A.M. and Sokolov, M.A., "Investigation of Material Behavior Under Reirradiation After Annealing Using Subsize Specimens", Small Specimen Test Techniques Applied to Nuclear Reactor Vessel Thermal Annealing and Plant Life Extension, ASTM STP 1204, W.R. Corwin, F.M. Haggag, and W.L. Server, Eds., American Society for Testing and Materials, Philadelphia, 1993, pp. 417-423.

[10] Amayev, A.D., Badanin, V.I., Kryukov, A.M., Nikolayev, V.A., Rogov, M.F., and Sokolov, M.A., "Use of Subsize Specimens for Determination of Radiation Embrittlement of Operating Reactor Pressure Vessels", Small Specimen Techniques Applied to Nuclear Reactor Vessel Thermal Annealing and Plant Life Extension, ASTM STP 1204, W.R. Corwin, F.M. Haggag, and W.L. server, Eds., American Society for Testing and Materials, Philadelphia, 1993, pp. 424-439.

[11] van Walle, E., Fabry, A., Van de Velde, J., Chaouadi, R., Puzzolante, J.L., Van Ransbeeck, T., "Pressure Vessel Steel Programme at the Belgian Nuclear Research Centre", March 8, 1993.

[12] Manahan, M.P., Williams, J., and Martukanitz, R.P., "Laser Weld Reconstitution of Conventional Charpy and Miniaturized Notch Test (MNT) Specimens", Small Specimen Test Techniques Applied to Nuclear Reactor Vessel Thermal Annealing and Plant Life Extension, ASTM STP 1204, W.R. Corwin, F.M. Haggag, and W.L. Server, Eds., American Society for Testing and Materials, Philadelphia, 1993, pp. 62-76.

[13] Manahan, M.P., "Determination of Charpy Transition Temperature of Ferritic Steels Using Miniaturized Specimens", Journal of Materials Science 25 (1990) 3429-3438.

[14] Manahan, M.P., "Determination of Fracture Behavior of Ferritic Steels Using Miniaturized Specimens", Journal of Nuclear Materials 166 (1989) 321-330.

[15] Cheverton, R.D., Bolt, S.E., Ball, D.G., Iskander, S.K., Nanstad, R.K., "Pressure Vessel Fracture Studies Pertaining to the PWR Thermal-Shock Issue: Experiments TSE-5, TSE-5A, and TSE-6", NUREG/CR-4249, June, 1985.

[16] Rolfe, S.T. and Barsom, J.M., Fracture and Fatigue Control in Structure, Prentice-Hall, Englewood Cliffs, NJ, 1977.

[17] Flemings, M.C., Solidifcation Processing, McGraw-Hill, 1974, p. 149.

[18] Green, A.P. and Hundy, B.B., "Initial Plastic Yielding in Notched Bend Tests", Journal of the Mechanics and Physics of Solids, Vol. 4, No. 2, March 1956, pp. 128-144.

[19] Towers, O.L., "Effects of Striker Geometry on Charpy Results", Metal Construction, 1983, 15(11).

[20] Private communication, M.P. Manahan, MPM Research & Consulting, and E. van Walle, SCK/CEN, 1994.

[21] van Walle, E., Fabry, A., Van Ransbeeck, T., Puzzolante, J-L., Vandermeulen, W., Van de Velde, J., "The Reconstitution of Small Remnant Parts of Charpy-V Specimens", presented at SMIRT 11, PCS II, Taipei, Taiwan, August 1991.

[22] van Walle, E., Van Ransbeeck, T., Chaouadi, R., A. Fabry, Puzzolante, J.L., Vandermeulen, W., and Van de Velde, J., "The Reconstitution Effort at SCK/CEN", SCK/CEN Research Group Materials, 1993.

[23] Fabry, A., Puzzolante, J.L., Van Walle, E., Vandermeulen, W., Vandevelde, J., and Van Ransbeek, T., "Changing the Notch Orientation of Charpy-V Specimens by Stud Welding of Broken Remnants", Work performed on Request of Yankee Atomic Electric Company.

James F. Williams[a]
Regis P. Shogan[b]
Leo Albertin[a]

THE OPTIMIZATION OF INSERT SIZE FOR RECONSTITUTING PREVIOUSLY TESTED CHARPY SPECIMENS

REFERENCE: Williams, J. F., Shogan R. P., Albertin, L., "**The Optimization of Insert Size for Reconstituting Previously Tested Charpy Specimens**," Pendulum Impact Machine: Procedures and Specimens for Verification, ASTM STP 1248, Thomas A. Siewert and A. Karl Schmeider, Eds., American Society for Testing and Materials, Philadelphia, 1995.

ABSTRACT: The reconstitution of previously tested Charpy impact specimens via projection welding can be used to obtain additional data for nuclear reactor surveillance programs. Typically, a broken Charpy half contains a large portion of untested material. This untested material can be machined from a broken Charpy half to obtain an "insert." "Endtabs" of similar material can then be welded to the insert. After the welded sample is machined to ASTM E23 specifications, it is then retested to obtain additional toughness data. The materials in this study show that 14 mm inserts can be successfully reconstituted and 10 mm inserts can be reconstituted with limited success.

KEYWORDS: Charpy V-Notch, reconstitution, projection welding, upper shelf energy, pressure vessel, steel, A302B, A533B, modified A302B

BACKGROUND

The Charpy impact test is used as the primary method of monitoring the effects of irradiation on the fracture toughness properties of nuclear reactor pressure vessels. Prior to initial start-up, most utilities placed surveillance material in the downcomer region of the pressure vessel. This material is used to monitor the degrading effects of neutron irradiation on the fracture properties of the pressure vessel. However, in some cases, the limited number of surveillance specimens does not provide sufficient data to thoroughly assess the effects of

[a]Engineer/Scientist, Nuclear Services and Materials Testing, Westinghouse Science and Technology Center, Pittsburgh, PA.

[b]Manager, Nuclear Services and Materials Testing, Westinghouse Science and Technology Center, Pittsburgh, PA.

irradiation. If enhanced assessment of irradiation embrittlement is required, methods to obtain more surveillance data must be employed.

There are a number of parameters that affect the Charpy data obtained from a reconstituted sample. First, the length of the insert must be large enough to accommodate the plastic zone resulting from the impact test. Second, the welding process has to provide for high integrity welds without resulting in high temperatures that change material properties in the central portion of the insert. Weld heat input is a function of weld parameters, material geometry, and material properties. In this study, variations in the weld insert size have been used to try to minimize the amount of material needed to obtain valid test values. It has been shown that relatively small inserts can be welded without large heat inputs, and these inserts are able to accommodate the plastic zone which occurs at upper shelf test temperatures.

INTRODUCTION

Since the beginning of reactor surveillance, the Charpy impact test has been used as the primary method of monitoring the effects of irradiation on the fracture toughness properties of nuclear reactor pressure vessels. The standard Charpy specimen used in reactor surveillance is a 10 mm X 10 mm Type A, notched bend bar as described by the American Society for Testing and Materials (ASTM) E23-91.[1] The impact specimen is tested by being struck with a heavy swinging pendulum. From the results of this test, it is possible to determine the ductile-to-brittle failure mode transition temperature (DBTT) in ferritic steels. Also, the absorbed energy to failure at service temperature is measured as a value of fracture resistance. In addition, the Charpy test provides the energy to fracture, the crystallinity of the fracture face, and the extent of shear lip formation as a function of temperature.

As a result of neutron irradiation, the impact properties of a pressure vessel steel can change. The two important changes are a decrease in the upper-shelf energy, and an increase in DBTT. Prior to initial start-up, most nuclear utilities placed surveillance material designed in accordance with ASTM E185 in the form of Charpy, tensile, and dosimetry specimens in the downcomer region of the pressure vessels.[2] This surveillance material is used to monitor the degrading effects of neutron irradiation on the fracture properties of the pressure vessel. However, in some cases, the limited number of surveillance specimens does not provide sufficient data to thoroughly assess the effects of irradiation. Furthermore, some utilities have begun to investigate the possibility of extending their arbitrarily set forty year operating license. With the advent of license extension, there is an increasing probability that pressure vessels may be annealed to recover damage accrued by neutron embrittlement. If complete assessment of irradiation embrittlement were to be conducted, or if license extensions were to be granted, or if recovery of annealed vessels were to be measured, methods to obtain more surveillance data must be implemented. One such developed method is the weld reconstitution of previously tested Charpy impact specimens.

Through reconstitution and testing of previously fractured Charpy specimens, more data is available to measure the increases in the transition temperature and the decreases in the upper shelf energy. In addition, continued surveillance of the reactor pressure vessel can occur by re-encapsulating and re-inserting previously tested material for reconstitution. Both of these applications would provide valuable information to the nuclear utilities, particularly for plant life extension and plant availability considerations.

THE WELD RECONSTITUTION PROCESS

The primary goal of Charpy weld reconstitution is to obtain additional Charpy toughness data from previously tested material. The American Society for Testing and Materials has developed a recommendation guide for reconstituted Charpy specimens, "Reconstitution of Irradiated Charpy Specimens," E1253.[3] This recommendation provides guidelines for Charpy insert size, heat input, reconstitution technique qualification, and dimensional requirements. E1253 was used where it was applicable in this reconstitution program.

Typically, broken Charpy halves contain a large portion of untested material. This untested material can be machined from a broken half of a sample to obtain an "insert." "Endtabs" of similar material can then be welded to the "insert." The weld sample is machined to obtain a Charpy V-notch specimen as described in ASTM E23-91. This reconstituted sample is then tested to obtain additional data. A schematic diagram of this process is shown in Figure 1.

Although the process is a simple idea, arriving at the final product requires knowledge and experience in remote handling, welding, heat transfer, irradiation effects on materials, and fracture mechanics. The majority of Charpy samples tested for utilities are radioactive, and hence, require remote handling, machining, and testing. This can only be accomplished by use of hot cell capabilities. There have been a number of weld processes studied to date. Among these processes are arc-stud, laser, electron beam, and projection welding. Westinghouse's Nuclear Services and Materials Testing (NSMT) has developed and implemented a process using projection welding. This process ensures that heat input to the central portion of the insert does not change the material's properties. Heat input is monitored through thermocouple attachments, and heat transfer is increased by using materials with high thermal conductivity, such as copper, as supports or clamps in the welding process. Finally, the fracture mechanics of Charpy testing must be understood in order to have accurate interpretation of the collected data.

Although the primary concentration of this paper is on irradiated surveillance material, it should be noted that the reconstitution process can be applicable to any impact test where the material available is less than that required for a standard specimen.

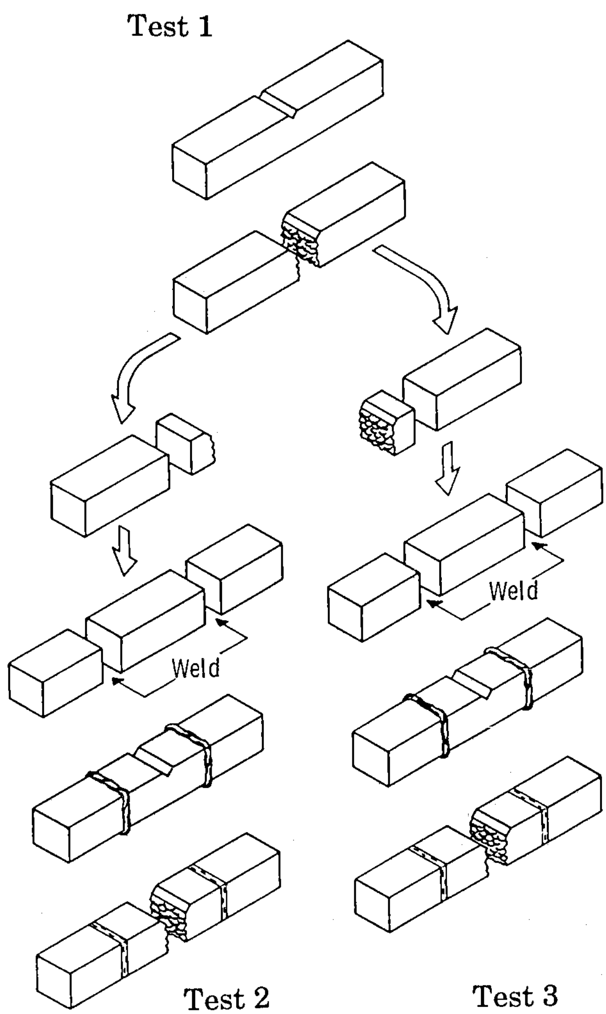

Figure 1. Charpy weld reconstitution schematic showing process from start to finish. Drawing is not to scale.

RECONSTITUTION TECHNIQUE - PROJECTION WELDING

The broken halves of a Charpy specimen are machined to remove the fracture face and the plastically disturbed material that results from the impact test. Since melting will occur at both ends of the insert during welding, no specimen preparations are needed. The ends need only be reasonably flat, smooth, clean, and perpendicular to the specimen axis. In view of remote handling, this ease of specimen preparation is an advantage of the projection welding technique. Endtabs used in reconstitution should have elastic properties similar to the weld insert.

The welding machine is a spot/projection welder, with a 50-kVA transformer, a bottom platen type electrode, and a pneumatically operated 454 kg maximum force system. The welding system is fully automated and is initiated with a foot switch. A welding cycle consists of several phases: application of the force, a "squeeze" period, current flow for a selected time, a force hold period, and finally, release of the force. Each of the weld phases is adjustable with respect to time. The force and the current flow can also be regulated.

A copper jig was designed to hold the pieces during welding. As mentioned previously, the copper also serves as a chill block. This increases conductivity (heat flow) and results in minimization of temperatures within the insert. The weld insert is clamped securely in the jig to eliminate movement. The endtabs, on the other hand, are more lightly clamped because they must move more readily under the applied force during welding. In operation, a current passes through the top electrode into the top endtab, through the projection to the weld insert, then through the clamp into the bottom platen. This fuses the insert to the top endtab (Figures 2 and 3). After the top weld is made, the clamped section is flipped over in the welding jig, and the second endtab is welded onto the insert.[4]

After welding, some misalignment along the finished specimen is inevitable due to weld insert and endtab tolerances, weld cooling deformation, fixture misalignment, and magnetic force fields during current applications. This generally results in approximately 0.025 mm to 0.075 mm of misalignment along the length of the specimen. There is also considerable metal expulsion at the weld interface. The endtabs that are welded to the specimen inserts are made 0.25 mm thicker than the specimen insert. This larger cross-sectional size allows for post-weld machining of the specimen resulting in finished dimensions which meet ASTM E23 requirements. Welds made with this system are sound and porosity free. The extent of fusion is near 100 percent.

WELD INSERT CONSIDERATIONS

The insert size determination is based on the meeting of several requirements. The insert must be of a size to accommodate the plastic deformation that occurs as the result of impact testing. This minimum size is determined by the knowledge of the strength and toughness of

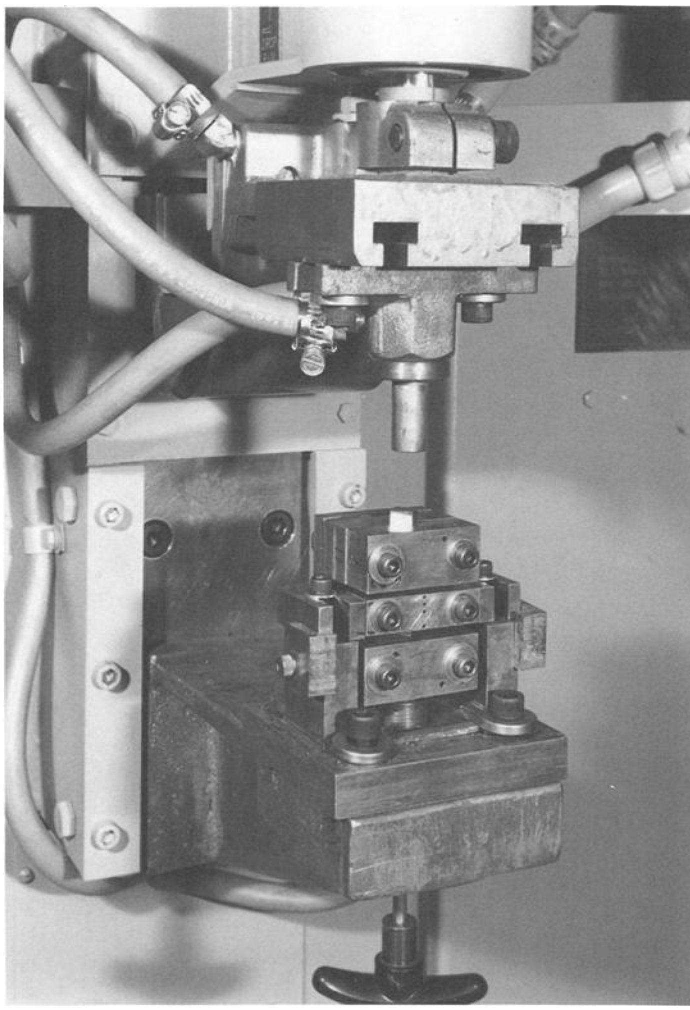

Figure 2. Set-up of projection weld system prior to welding the endtab to the insert.

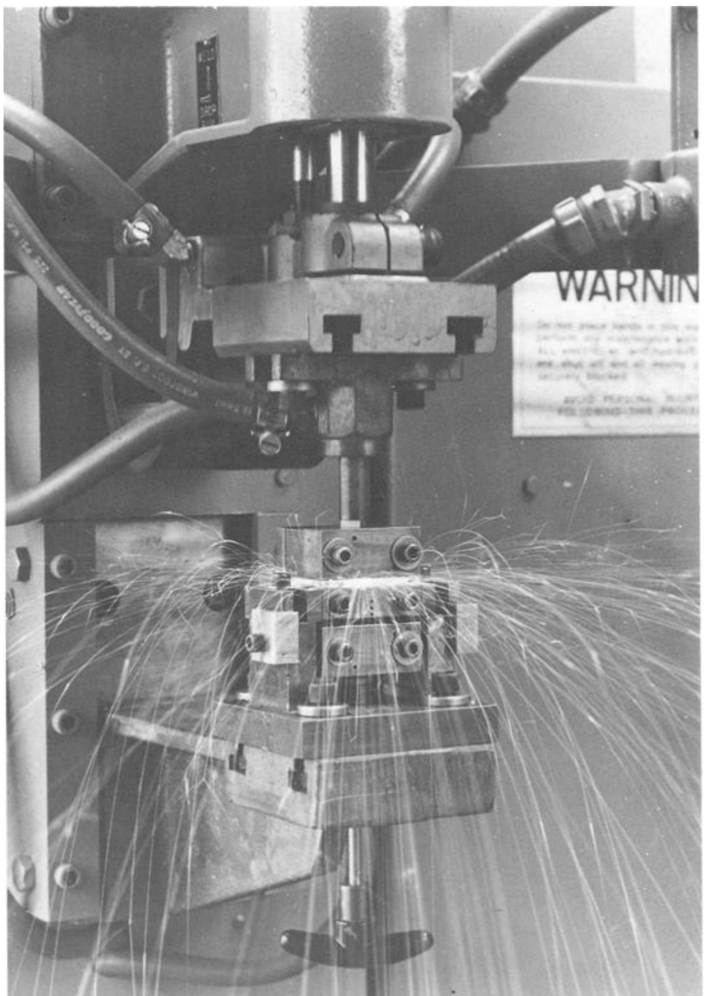

Figure 3. Projection welding process.

the material as well as the temperature at which the specimen is tested. It is well established that pressure vessel steels become brittle at sufficiently low temperatures. A measure of this brittleness is the fracture appearance of the broken face on a Charpy specimen. The lower the percentage of shear fracture, the lower is the toughness of the material. Low toughness materials tend to exhibit small amounts of plastic deformation, and hence, would require smaller reconstitution inserts. As expected, a higher percentage of shear fracture or a higher toughness material (or a material tested at a sufficiently high temperature where it is tough) requires a larger volume of material to encompass the plastic deformation involved in the fracture process. Studies have been conducted to verify this phenomenon. Shogan et al performed profiled hardness test on an unirradiated steel that had an upper shelf energy of 169 J (125 ft-lbs).[4] This material was Charpy tested at a range of temperatures which resulted in a range of fracture appearances from 2% to 100% shear. The 100% shear specimen showed that a minimum insert size required for this material would be approximately 13.6 mm, whereas the 2% shear specimen required approximately 5 mm of material. The results of this study are shown in Figure 4. [4] In terms of irradiated pressure vessel steels, upper shelf Charpy energies (for the most part) tend to be less tough than the material used to establish the limit shown here, and therefore, it would be expected that less material would be required to reconstitute previously tested, irradiated specimens.

Another parameter that dictates the limiting size of the Charpy insert is the temperature profile that results from the welding process. The temperature at the crack tip notch root should be maintained at less than the reactor operating temperature of the material being tested. This requirement becomes increasingly difficult as the size of insert is reduced. Thermal profile studies were conducted on a typical pressure vessel steel to show that the temperature in the specimen at the crack tip notch root was maintained below the normal operating temperature of most reactors of 288°C (550°F). This study was conducted on two sizes of inserts, 10 mm and 14 mm, respectively. Thermal profiles were taken at 1 mm off the notch root in the direction of the weld. The results of this study concluded that for the weld parameters used in the program, the 14 mm inserts would not reach temperatures greater than 193.3°C (380°F). However, the 10 mm inserts showed variations in temperatures. Temperatures were normally observed at values below the set limit. Occasionally, however, temperatures above the limit were also observed. This increased temperature occurred as the result of the clamping mechanism. If the central insert is not securely clamped in the copper fixturing, conduction from the insert into the copper jig is limited resulting in higher temperatures in the inserts. Figures 5 and 6 show characteristic thermal profiles for the 14 mm inserts and 10 mm inserts, respectively. Figure 6 shows the profile obtained from improper clamping. Note that the duration of time above 288°C was less than 2.0 seconds. Further study would need to be conducted to determine if this small duration of time is really long enough to affect the material properties.

The width of the weld and the heat affected zone are also parameters

(a)

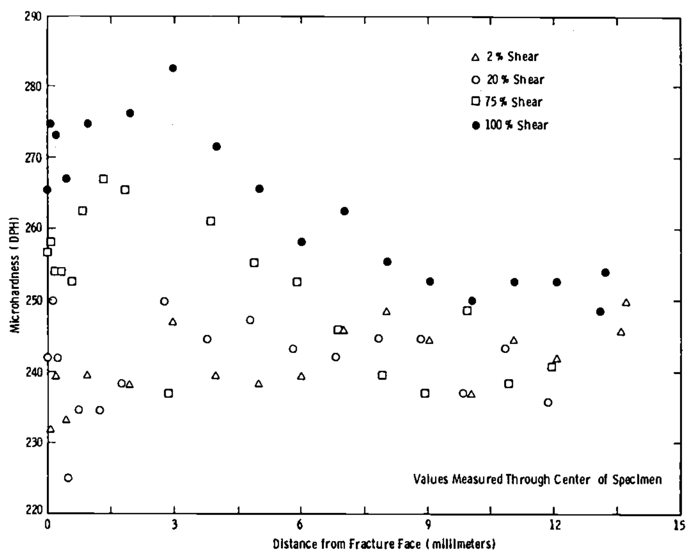

(b)

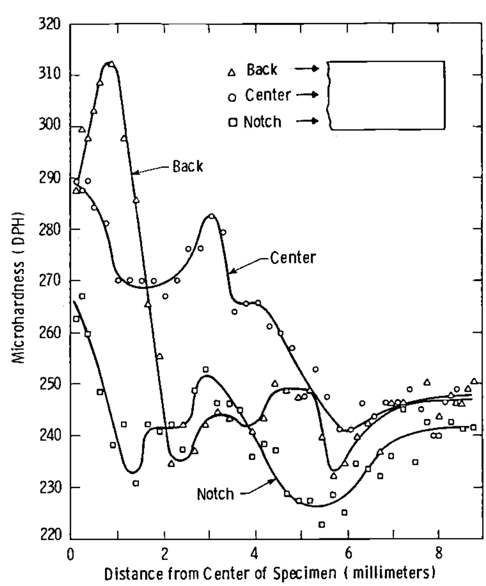

Figure 4. Microhardness versus distance from fracture face for broken Charpy specimens. Results show extent of plastic zone measured (a) through the center of the specimen for various shear values and (b) for 100% shear specimen at various planes on the specimen.

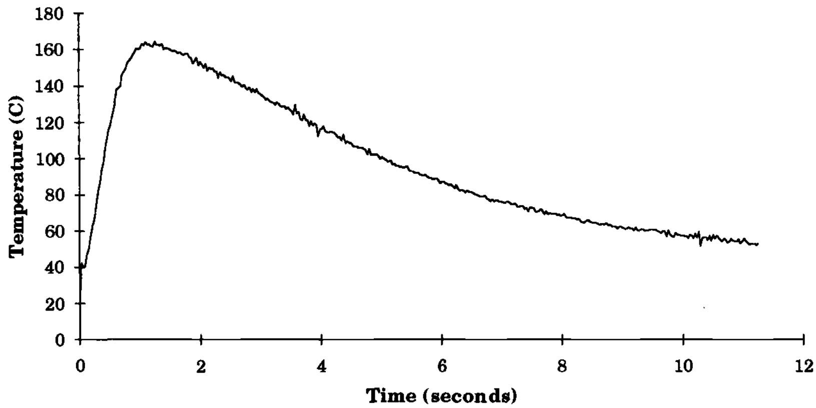

Figure 5. Characteristic thermal profiles for 14 mm insert using the projection welding reconstitution technique. Measurements taken 1 mm off the notch root in the direction of the weld face.

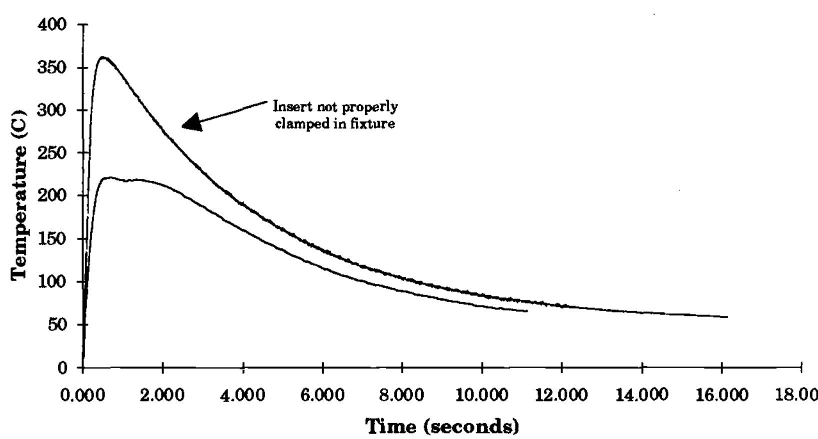

Figure 6. Characteristic thermal profiles for 10 mm insert using the projection welding reconstitution technique. Measurements taken 1 mm off the notch root in the direction of the weld face. Higher temperature curve is result of improper clamping in the copper fixturing.

that need to be considered when reconstituting Charpy specimens. Hardness measurements have been taken across the weld area to determine the extent of disturbed material as the result of welding. This result is summarized in Figure 7. This profile is in agreement with other profiles taken for this weld process with the total disturbed material approximately equal to 2.8 mm. [4]

Of all the requirements discussed in the previous paragraphs, the plastic deformation provides the greatest variability. The temperature profiles tend to be constant (provided clamping is consistent) in the insert as is the extent of disturbed weld material. A benefit to the variability in the plastic deformation is the possibility of using smaller inserts for reconstituting low toughness samples. This will be discussed in a later section.

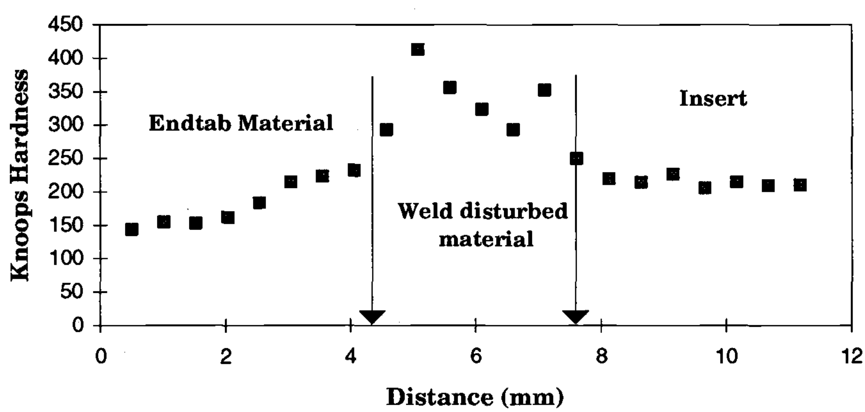

Figure 7. Characteristic hardness profile for a reconstituted Charpy using the projection welding. Center of weld area is approximate location of interface.

TESTING OF UNIRRADIATED MATERIAL

A study was conducted on an unirradiated steel which had a very high upper shelf energy (average USE = 192.3 J). This approach determined the minimum insert size applicable for all test temperatures, because it maximized the amount of plastic deformation in the Charpy test. Three specimens were tested at an upper shelf temperature of 93.3 ^{0}C (200^{0}F). The broken halves from these specimens were machined and reconstituted. Two were machined for 14 mm insert lengths, and two were machined for 10 mm inserts. All four inserts were reconstituted and tested. The results of these tests are summarized in Table 1. The 14 mm samples produced results in agreement with the whole specimens.

Table 1

Unirradiated Reconstituted Charpy Impact Testing at 93.3 ^{0}C for Projection Welding Reconstitution

	Energy (J)	**Lateral Expansion (mm)**	**Percent Shear (%)**
Whole Specimen			
RR1	195	2.2	100
RR2	183	2.0	100
RR3	199	2.2	100
14 mm Recon			
RR1-1	194	2.2	100
RR3-1	195	2.2	100
10 mm Recon			
1	137	--*	100
3	140	--*	100

* - These measurements were not taken. Specimens were not available to perform these measurements.

The 10 mm samples showed results that were lower in energy than the whole specimens. This is due to the plastic constraints as the result of the plastic zone interacting with the weld affected material. Based on these data, it is concluded that for pressure vessel steels, the minimum amount of reconstituted material needed for a valid Charpy test is a 14 mm insert. This is further supported when neutron embrittlement is considered. Other studies have been conducted to show that the 14 mm insert is a valid insert size for Charpy reconstitution. A laser welding reconstitution program conducted on an unirradiated modified A302B steel resulted in similar conclusions for a valid insert size.[5] Results of this program are summarized in Table 2. Data for this program were obtained at a temperature of 43.3^{0}C which was on the upper shelf for this material.

From the unirradiated studies that have been conducted, it has been concluded that provided a 14 mm insert can be obtained prior to welding, a reconstituted Charpy specimen can be machined which yields valid impact data. Of course, it should always be a goal to maximize the insert size when reconstitution is being used. Neutron irradiation of pressure vessel steel normally results in materials with lower fracture energy (due to a lower toughness) for the same test temperature. This implies that the irradiated insert requires less volume to accommodate the plastic zone, and that 14 mm inserts, provided all other requirements are met, are also good for reconstituted irradiated samples.

Table 2

Unirradiated Reconstituted Charpy Impact Testing at 43.3°C for Laser Weld Reconstitution Using a Modified A302B Pressure Vessel Steel - Longitudinal Oriented

Specimen ID	Energy (J)	Lateral Expansion (mm)	Percent Shear (%)
Whole Specimen			
108	116	1.8	100
310	112	1.9	100
20 mm Recon			
AH	111	1.7	100
CI	115	1.6	100
14 mm Recon			
NH	105	1.6	100
NK	113	1.7	100
NA	99	1.5	100
NQ	115	1.6	100
NG	121	1.7	100
3	108	1.5	100
10 mm Recon			
JE	96	1.6	100
JO	97	1.3	100

RECONSTITUTION OF IRRADIATED MATERIAL

An annealing study was conducted on an irradiated pressure vessel steel (A302, Grade B plate with fluence = $3.30X10^{19}$ n/cm^2) to determine how much temperature shift could be recovered at the 41 J energy level of the steel. The limited amount of available material to perform this annealing study resulted in reconstitution as the viable option to obtain toughness recovery data.

Inserts were obtained from two whole bend bars which were 56.1 mm long, 15.7 mm wide, and 10 mm thick (Specimens S-33 and S-35) and two bend bar halves which were previously tested and were 10.7 mm wide (Specimens S-37 and S-39). The specimens were originally oriented to obtain fracture toughness data in the transverse direction. However, longitudinal data were required by the program. Two as-irradiated inserts were taken: one from S-33 which was 15.7 mm in length and one from S-37 which was 10.7 mm in length. One of the whole bend bars, S-35, was annealed at a temperature of 341°C for 168 hours in a split tube furnace . Part of the whole bend bar, S-33, and one of the previously tested halves, S-39, were annealed at 341°C for 336 hours. Thermocouples, associated potentiometers, and digital thermometers were used for measuring and monitoring the temperature. The final thermal conditions for the bend bars and the number of inserts obtained are shown in Table 3.

Table 3

Thermal Conditions of Bend Bar Inserts
for the A302B Steel Irradiated to $3.30X10^{19}$ n/cm^2

Specimen #	**Anneal Temp (C)**	**Anneal Time (hrs)**	**Number of Inserts**	**Length of Insert (mm)**
S-33	NA	NA	2	15.7
S-33	341	336	2	15.7
S-35	341	168	4	15.7
S-37	NA	NA	1	10.7
S-39	341	336	1	10.7

NA = not applicable/ not performed

All of the inserts were reconstituted into Type A full-sized Charpy specimens as described by ASTM E23. Qualification tests were also conducted on an unirradiated, standard pressure vessel steel (A533B) using 15.7 mm length inserts. Hot rolled AISI 1020 carbon steel was used as endtab material for all of the reconstituted specimens. The reconstitution technique was performed in accordance with ASTM E1253-88, where applicable, and techniques described by Shogan et al. [3,4]

Since the length of the irradiated inserts were smaller than recommended in ASTM E1253-88, the validity of the reconstitution technique was demonstrated using impact data from a known reactor pressure vessel material (A533B). These results are summarized in Table 4. As seen in Table 4, the results were in agreement for conventional and reconstituted specimens. In addition to the standard, reconstituted specimens of known impact properties, temperature measurements were taken during welding to show that the central segment of the insert (8.9 mm of the 15.7 mm insert in this case) did not exceed the predetermined critical temperature of 260°C.

Table 4

Charpy V-Notch Data for an Unirradiated A533B Pressure Vessel Steel

Impact Energy (J)	**Lateral Expansion (mm)**	**Percent Shear (%)**
Before Recon		
92.1	1.4	75
96.2	1.4	75
94.9	1.4	65
15.7 mm Insert		
88.1	1.3	75
93.5	1.3	75
88.1	1.1	70
104.3	1.4	75
101.6	1.4	75

Once it was determined from the standard specimens that valid results can be obtained from the 15.7 mm inserts, the irradiated material was reconstituted. Results of the irradiated reconstituted specimens are summarized in Table 5. Two of the ten specimens failed in the welds; one in the irradiated condition (S-33-1) and one in the irradiated/annealed (336 hours) condition (S-33-4). Failure occurred in the weld because the fracture resistance of the weld was low in comparison to the notched area of the specimen. This is attributed to the martensite formation in the weld which occurs from rapid cooling of the weld zone. These specimens are not listed in the table.

Table 5

Reconstituted Charpy V-Notch Data for the A302B Reactor Vessel Material for the Irradiated Condition (Fluence of $3.30X10^{19}$ n/cm^2, E > 1.0 MeV) and After 168 hrs and 336 hrs of Low Temperature Annealing at 341^{0}C

Specimen #	**Condition***	**Temp. (°C)**	**Impact Energy (J)**	**Lateral Expansion (mm)**	**Percent Shear (%)**
S-33-2	I	79.4	24.4	.33	30
S-37-1**	I	79.4	56.9	.97	60
S-35-1	IA (168)	51.7	32.5	.43	30
S-35-2	IA (168)	60.0	51.5	.56	50
S-35-3	IA (168)	54.4	65.0	.91	60
S-35-4	IA (168)	51.7	46.1	.58	50
S-33-3	IA (336)	51.7	50.1	.76	50
S-39-2**	IA (336)	43.3	43.4	.18	40

* - I = Irradiated Only ; IA (168) = Irradiated/Annealed for 168 hours
IA (336) = Irradiated/Annealed for 336 hours

** - Insert Size of 10.7 mm

DISCUSSION OF IRRADIATED RESULTS

Original unirradiated baseline data were obtained from records for the A302B used in the irradiated reconstitution program. This data is plotted in Figure 8. Reg. Guide 1.99 was used to estimate the shift in temperature for the irradiated steel.[6] The shift is plotted along with the reconstituted data. The annealed data are also plotted on this curve. The curve shows an estimated recovery of 28^{0}C for the low temperature anneal. Based on all of the unirradiated data studies, the 15.7 mm data is considered valid. However, there are questions in regards to the validity of the 10.7 mm insert data. This is primarily due to the scarcity of the available data produced for this size insert using the ASTM tup. The laser welding study mentioned earlier in this report attempted to quantify this effect for the modified A302B used in its program.[5] Reconstituted 10 mm insert specimens were tested for a number of temperatures to determine the energy level (or temperature) for which the 10 mm insert would be valid. This study is summarized in Table 6 and Figure 9. From Figure 9, it can be concluded that the energy curves begin to merge at energy values approaching 40 J.

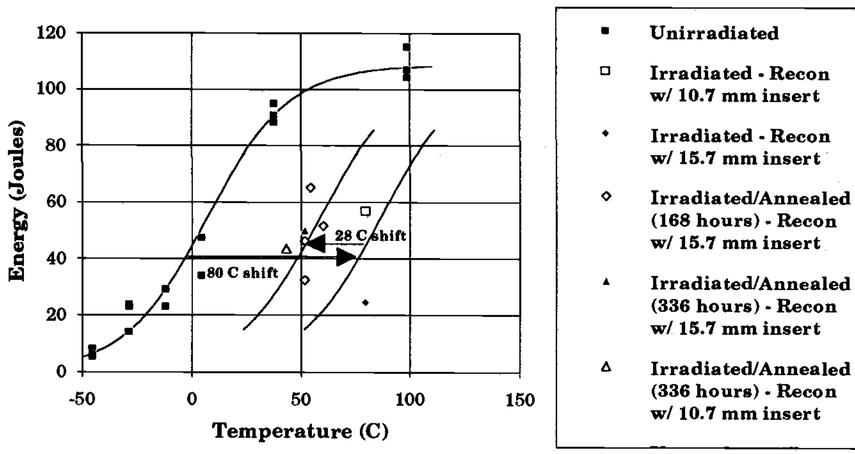

Figure 8. Reconstituted Charpy V-Notch properties of an irradiated A302B reactor vessel plate material (Fluence =3.30X10^{19} n/cm^2 with longitudinal orientation) before and after irradiation and before and after post-irradiation anneal.

Table 6

Unirradiated Reconstituted Charpy Impact Testing for Laser Weld Reconstitution Using a 10 mm Insert of a Modified A302B Pressure Vessel Steel Longitudinal Oriented

Specimen ID	Test Temp (°C)	Energy (J)	Lateral Expansion (mm)	Percent Shear (%)
JE	43.3	96.2	1.6	100
JO	43.3	96.5	1.3	100
JF	13.7	73.2	1.0	68.5
7	13.7	85.1	1.2	72.0
JP	-12.3	40.7	.53	26.0
8	-12.3	44.1	.71	31.5

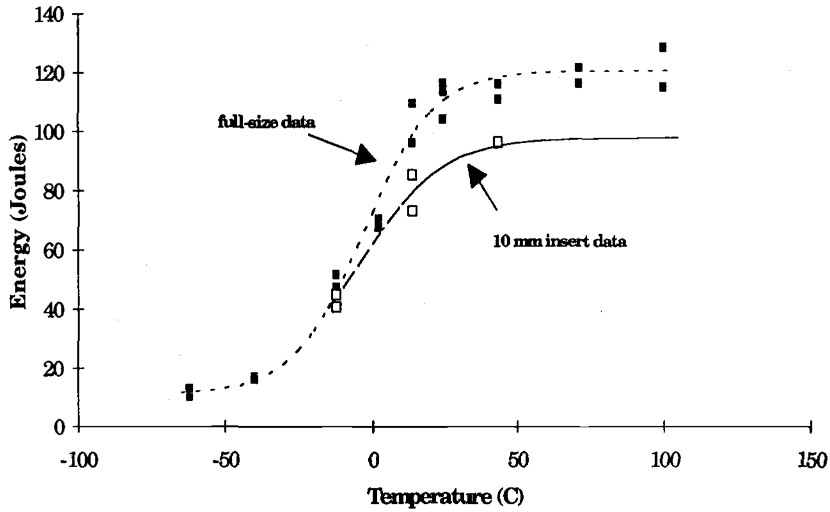

Figure 9. Comparison of full-size Charpy data with 10 mm insert data for an unirradiated A302B steel which was reconstituted using laser welding. The energies for the 10 mm data tend to merge with the full-size data at lower energies.

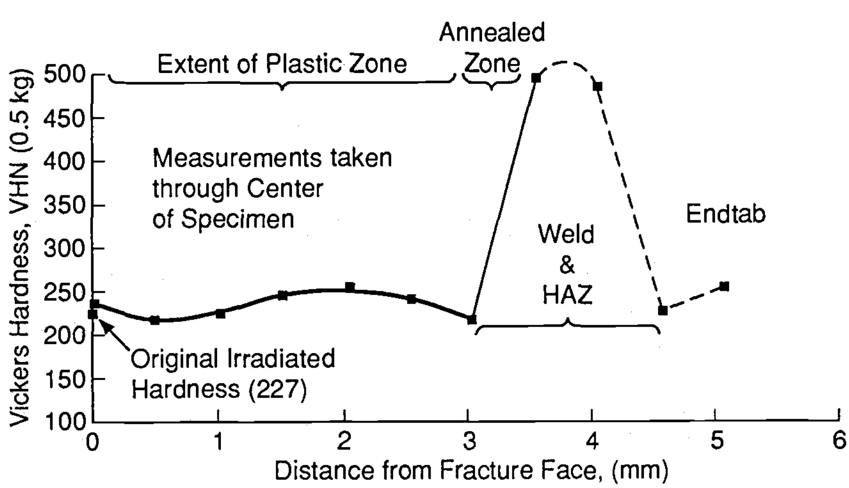

Figure 10. Microhardness versus distance from the fracture face for broken reconstituted Charpy specimen S37-1 (10.7 mm insert) indicating the extent of the plastic zone, weld, and the heat-affected zone.

Because of the limited amount of specimens tested in this program, it can only be used to show the tendency.

To validate the 10.7 mm irradiated data, Vickers hardness was performed on one of the 10.7 mm, reconstituted samples. Figure 10 shows the results of this study. No change in microstructure can be observed to a distance of 2.8 mm from the fracture face. Within this distance, the Vicker's hardness was affected by the plastic zone which raised the Vicker's hardness from the specimens average of 227 to 256 at a distance of 2.0 mm from the fracture. The hardness then dropped to 218 at a soft heat affected zone 3.0 mm from the fracture. This hardness profile suggests that reconstitution of the 10.7 mm inserts was achieved without changing the original irradiated properties of the test section containing the V-notch. In addition to providing validation to the 10.7 mm inserts, the hardness profile also reinforces the values obtained for the 15.7 mm inserts.

CONCLUSIONS

The results of the materials in this study have successfully demonstrated that inserts equal to or larger than 14 mm for Type A specimens can be used to obtain valid data for all Charpy tests performed using the ASTM tup.

Preliminary studies suggest that for low Charpy energies (or for small amounts of plastic deformation) 10 mm inserts can be used. For higher energy levels, plastic constraints result in lower Charpy energy values for the reconstituted specimens. For the same weld process, this loss may be constant. However, more studies need to be done to verify or disprove this hypothesis.

This and other reconstitution programs have verified the validity of obtaining additional data from previously tested material. For embrittled pressure vessels for which the material to perform required testing is limited, reconstitution can provide and has provided accurate and reliable data. For continued surveillance of reactors beyond the license period, this testing method is a viable and proven option.

ACKNOWLEDGMENTS: The authors would like to thank Greg Kustra, Chris Deflitch, Bob Rees, Ken Galbraith, Dennis Yeager, and Lin Thomas of the Westinghouse's Nuclear Services and Materials Testing hot cell team for providing their assistance in this program. The authors would also like to extend their gratitude to Tom Mager of Westinghouse's Nuclear Technology Division for his support on this program and other pressure vessel related work.

REFERENCES

[1] "Notched Bar Impact Testing of Metallic Materials," Standard Method E23-91, American Society for Testing and Materials (1991).
[2] "Standard Practice for Conducting Surveillance Test for Light-Water Cooled Nuclear Power Reactor Vessels," Standard Method E185-82, American Society for Testing and Materials (1982).
[3] "Standard Guide for Reconstitution of Irradiated Charpy Specimens," Standard Guide E1253-88, American Society for Testing and Materials (1988).
[4] R.P. Shogan, S.E. Yanichko, W.S. Galloway,"The Use of Reconstituted Charpy Specimens to Extend R.E. Ginna Reactor Pressure Surveillance Data," Westinghouse Science & Technology Center, May 29, 1985.
[5] J.F. Williams, M.P. Manahan,"Reconstitution of Pressure Vessel Steel Charpy Specimens Using Laser Welding," unpublished data taken from graduate thesis work performed at the Pennsylvania State University, Radiation Science and Engineering, Nuclear Engineering Department, August 1992.
[6] Regulatory Guide 1.99, Revision 2, "Radiation Embrittlement of Reactor Vessel Materials", U.S. Nuclear Regulatory Commision, May, 1988.

The Anvils and the Striker

Earl A. Ruth,[1] Daniel P. Vigliotti,[2] Thomas A. Siewert[2]

EFFECT OF SURFACE FINISH OF CHARPY ANVILS AND STRIKING BITS ON ABSORBED ENERGY[3]

REFERENCE: Ruth, E. A., Vigliotti, D. P., and Siewert, T. A., "**Effect of Surface Finish of Charpy Anvils and Striking Bits on Absorbed Energy**", Pendulum Impact Machines: Procedures and Specimens for Verification, ASTM STP 1248, Thomas A. Siewert and A. Karl Schmieder, Eds., American Society for Testing and Materials, Philadelphia, 1995.

ABSTRACT: Some new Charpy impact testing machines often report higher energy values than machines which have been in service for a period of time. An investigation into the cause of this phenomenon revealed that a major contributing factor was the surface finish of the Charpy anvils and the striking bit. Depending on the trajectory of the Charpy specimen halves after impact and the configuration of the testing machine, a considerable amount of friction may occur between the specimen and the anvils as the specimen is broken. Friction may also occur between the specimen and the striking bit as the specimen exits the machine. Polishing the anvils and the striking bit minimizes the friction between these parts. As a Charpy impact testing machine tests many samples, the striking bit and anvils become burnished and energy absorption due to friction is reduced. If new parts are highly polished prior to installation, the burnishing, normally caused by testing many samples, is simulated. In this way energy absorption associated with friction during the wear-in period is minimized and remains more constant during the life of the anvils and striking bit. ASTM Standard Test Methods for Notched Bar Impact Testing of Metallic Materials (E 23) requires the surface finish of the anvil and striking bit to be better than 4 μm

---

[1]Manager, Engineering & Systems, Tinius Olsen Testing Machine Co., Inc., Willow Grove, Pennsylvania 19090

[2]Technician and Supervisory Metallurgist, respectively, Materials Reliability Division, National Institute of Standards and Technology, Boulder, Colorado 80303

(125 μin.). Specifying a 0.1 μm (4 μin.) surface finish as a requirement in E 23 will not only eliminate the wear-in period, but will minimize shifts in test results when anvils and/or striking bits are replaced in Charpy impact testing machines.

KEYWORDS: anvils, Charpy impact test, energy loss, friction, impact test, striker, surface finish

---

BACKGROUND

In the fall of 1991, several new Charpy impact testing machines were verified using National Institute of Standards and Technology (NIST) Low-Energy Samples for Charpy V-Notch Machines (SRM 2092). The test results indicated absorbed energies which exceeded the average by more than 1.4 J. An extensive investigation into the cause of the discrepancy was initiated.

All dimensional aspects of the machines were evaluated and were found to be well within the ranges permitted by ASTM E 23. Measurements were made by three different investigators, all of whom developed similar results.

The structural integrities of the machines' frames and foundations were investigated. Experiments were conducted that stiffened the frame. Other experiments that stiffened the pendulum were conducted. No improvements due to these procedures were noted.

One observation made at the time was that the NIST reference specimens (SRM 2092) were tending to exit the testing machine in the direction of swing of the pendulum. In the past, it was typical for these specimens to exit the testing machine in a direction opposite to the direction of swing of the pendulum. Further, the striking bits and anvils on the NIST reference Charpy impact testing machines used to develop the reference value for the SRM's, were burnished to a high polish as a result of having been used to test many specimens. We hypothesized that perhaps the relatively rough surfaces on the new striking bits and anvils were causing additional friction with the specimens as they were being broken. The friction would add to the energy absorbed during a test.

In order to test this hypothesis, new anvils and striking bits were polished to a mirror-like surface and installed on a machine which had previously been unable to pass the NIST requirements on low-energy specimens. A dramatic decrease in energy absorbed was observed at that time. The average energy obtained on the NIST specimens tested on that machine dropped approximately 0.7 J. The tests conducted at that time were not well structured or documented, due to the expediency and shipping schedule demands for the new impact testing machines. As a result, the data from those tests are not included in this paper. A more structured experiment was designed and the results are offered here.

EXPERIMENTAL METHOD

Charpy V-notch tests were performed in accordance with ASTM Standard Test Methods for Notched Bar Impact Testing of Metallic Materials (E 23). The test temperature in all cases was -40°C. The tests were performed on a 400 J capacity, pendulum Charpy impact testing machine having a "U" type pendulum. The standard size Type A specimen was used. Some of the tests were performed with a 2 mm radius striking bit instead of the standard 8 mm radius striking bit. This machine had been evaluated for repeatability when the strikers were interchanged. The repeatability was found to be better than the uncertainty in the test data.[1] These tests conformed to E 23 in all other ways.

Three types of specimens were tested. The three types of specimens were:

Lot LL-1: Nominal 16 J energy specimens which exited the testing machine opposite the direction of swing of the pendulum.

Lot LL-44 & 33: Nominal 16 J energy specimens which exited the testing machine in the direction of swing of the pendulum (note: the material used for the tests employing the 2 mm striker were not from the same lot of material as the tests employing the 8 mm striker).

Lot HH-1: Nominal 100 J energy specimens which exited the machine in the direction of swing of the pendulum.

Five different test conditions were used. The five conditions were:

Condition 1: Rough anvils and a rough 8 mm radius striker.

Condition 2: Smooth anvils and a rough 8 mm radius striker.

Condition 3: Smooth anvils and a smooth 8 mm radius striker.

Condition 4: Smooth anvils and a rough 2 mm radius striker.

Condition 5: Smooth anvils and a smooth 2 mm radius striker.

Under Condition 1, five LL-1 specimens, five LL-44 specimens, and five HH-

1 specimens were broken. The anvils had an rms surface finish of approximately 0.25 μm (10 μin.). The 8 mm striking bit had an rms surface finish of approximately 0.25 μm (10 μin.) on the nose and the 30° sides. On the parallel sides the rms surface finish was approximately 0.625 μm (25 μin.) (Fig. 1).

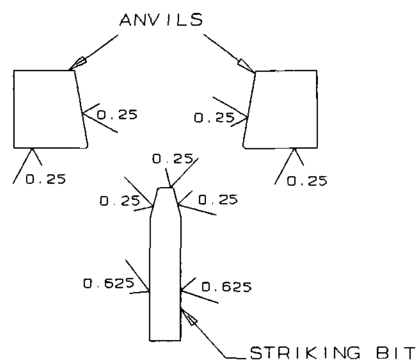

FIG. 1--Surface Finish (μm) of Unpolished Anvils and Striking Bit

After the first tests, the anvils were removed and polished to a mirror finish. The rms surface finish measured 0.05 μm (2 μin.) after polishing. The anvils were reinstalled in the impact testing machine. Five LL-1 specimens, five LL-44 specimens, and five HH-1 specimens were then broken. This was Condition 2.

The striking bit was then removed and polished to a mirror finish. The nose, the 30° sides and the parallel sides were all polished to the same rms finish, approximately 0.05 μm (2 μin.). Five LL-1 specimens, five LL-44 specimens, and five HH-1 specimens were again broken. This was Condition 3.

The striking bit was again removed and a striking bit with a 2 mm radius nose was installed. The 2 mm striking bit had a rms surface finish of approximately 0.25 μm (10 μin.) on the nose and the 30° sides. On the parallel sides the rms surface finish was approximately 0.625 μm (25 μin.). Five LL-1 specimens, five LL-33 specimens, and five HH-1 specimens were broken. This was Condition 4.

The 2 mm striking bit was then removed and the nose, the 30° sides and the parallel sides were all polished to an rms finish of approximately 0.05 μm (2 μin.). Five LL-1 specimens, five LL-33 specimens, and five HH-1 specimens were again broken. This was Condition 5.

After a quick examination of the data, we decided to test five more LL-44 specimens which had been reserved. We removed the 2 mm striker and reinstalled the polished 8 mm striker. The five specimens were then tested under Condition 3.

RESULTS

Twenty-five specimens were tested from lot LL-1 (Table 1). These specimens tended to exit the testing machine in a direction opposite the direction of swing of the pendulum. As seen in Table 1, there was very little difference in the average of the five different test conditions.

TABLE 1--Results of tests on specimens (lot LL-1) with a nominal energy of 16 J which exit the testing machine opposite the direction of swing of the pendulum. Test results are in joules.

Condition	1	2	3	4	5
	16.3	16.6	16.9	15.9	16.9
	16.9	16.6	16.6	16.6	16.9
	16.9	16.9	16.3	16.9	16.6
	16.5	15.9	15.6	18.0	16.3
	16.0	16.3	16.6	16.6	15.9
Average	16.52	16.46	16.40	16.80	16.52
Standard Deviation	0.35	0.34	0.44	0.68	0.38

TABLE 1A--Results of tests on specimens (lot LL-1) with a nominal energy of 16 J which exit the testing machine opposite the direction of swing of the pendulum. Test results are in joules. Outlier removed.

Condition	1	2	3	4	5
	16.3	16.6	16.9	15.9	16.9
	16.9	16.6	16.6	16.6	16.9
	16.9	16.9	16.3	16.9	16.6
	16.5	15.9	15.6	...	16.3
	16.0	16.3	16.6	16.6	15.9
Average	16.52	16.46	16.40	16.50	16.52
Standard Deviation	0.35	0.34	0.44	0.37	0.38

The condition with the highest variation was Condition 4 (smooth anvils and a rough 2 mm radius striking bit). An examination of the data for that group of tests indicated that the fourth specimen tested under Condition 4 was almost two standard deviations higher than the average. If this specimen is eliminated as an outlier, Table 1A is the result.

An examination of the averages and standard deviations listed in Table 1A yields very close agreement between the various conditions. The differences in the averages are much less than the standard deviations.

Twenty specimens were tested from lot LL-44 with an 8 mm striking bit (Table 2). These specimens tended to exit the testing machine in the direction of swing of the pendulum. Originally, five specimens were tested for each of the first three Conditions. After we noticed a substantial drop in the absorbed energy between Conditions 2 and 3, five additional specimens were tested under Condition 3 so a greater population could be analyzed. There is a difference of approximately a 0.4 J (0.3 ft-lb) between the tests that were run before and after polishing the striking bit. This difference amounts to about 1 standard deviation.

TABLE 2--Results of tests with an 8 mm striker on specimens (lot LL-44) with a nominal energy of 16 J which exit the testing machine in the direction of swing of the pendulum. Test results are in joules.

Condition	1	2	3	3
	17.5	17.6	17.3	16.3
	18.0	18.8	17.6	17.6
	17.3	17.4	16.9	17.3
	16.9	17.6	16.6	17.3
	18.0	17.4	17.3	17.6
Average	17.54	17.76	17.14	17.22
Standard Deviation	0.42	0.53	0.35	0.48
Average of 10	17.65		17.18	
Standard Deviation of 10	0.49		0.42	

There is a difference of approximately a 0.2 J (0.15 ft-lb) between the tests done before and after polishing the anvils. The tests done with the polished anvils show a higher average absorbed energy than the average for tests done with unpolished anvils.

Two specimens in Table 2 are almost two standard deviations from the average for their condition. Table 2A is a presentation of the results with these two specimens removed. Using this data, there is virtually no change between the results for polished and those for unpolished anvils. The difference between the polished and unpolished striking bit, although not as notable, is still evident.

TABLE 2A--Results of tests with an 8 mm striker on specimens (lot LL-44) with a nominal energy of 16 J which exit the testing machine in the direction of swing of the pendulum. Test results are in joules. Outliers removed.

Condition	1	2	3	3
	17.5	17.6	17.3	...
	18.0	...	17.6	17.6
	17.3	17.4	16.9	17.3
	16.9	17.6	16.6	17.3
	18.0	17.4	17.3	17.6
Average	17.54	17.50	17.14	17.45
Standard Deviation	0.42	0.12	0.35	0.17
Average of 9	17.52		17.28	
Standard Deviation of 9	0.32		0.34	

Ten specimens were tested from lot LL-33 with a 2 mm striking bit (Table 3). We expected these specimens to exit the testing machine in the direction of swing of the pendulum. Many of the specimens exited in the opposite direction or did not exit the area of the anvils at all. Testing performed with an 8 mm striking bit led us to think that these specimens would exit the testing machine in the direction of swing of the pendulum. Perhaps it was a higher stress concentration due to the smaller radius striker used in these tests that caused the specimens in most cases to exit the machine in the direction opposite that of the pendulum or to not exit at all. Even though the specimens did not exit the machine in the direction of swing of the pendulum, a reduction in absorbed energy was observed when the striking bit was polished.

TABLE 3--Results of tests with a 2 mm striker on specimens (lot LL-33) with a nominal energy of 16 J which exit the testing machine in the direction of swing of the pendulum. Test results are in joules.

Condition	4	5
	17.3**	16.6*
	16.9*	17.4**
	16.9**	16.9**
	16.9**	16.9
	17.3*	16.6**
Average	17.06	16.88
Standard Deviation	0.20	0.29

** Specimens which exited opposite to the direction of swing
* Specimens which remained in the area of the anvils

TABLE 4--Results of tests on specimens (lot HH-1) with a nominal energy of 100 J which exit the testing machine in the direction of swing of the pendulum. Test results are in joules.

Condition	1	2	3	4	5
	86.8	89.2	96.6	95.6	92.5
	91.9	92.9	93.6	90.5	88.1
	92.2	85.8	87.1	85.1	91.9
	94.2	89.8	89.2	89.5	90.2
	92.2	89.8	86.1	94.2	91.2
Average	91.46	89.50	90.52	90.98	90.78
Standard Deviation	2.47	2.26	3.99	3.71	1.54

Twenty-five specimens were tested from lot HH-1 (Table 4). These specimens tended to exit the testing machine in the direction of swing of the pendulum. While the differences in the average absorbed energies are substantial by comparison with the energies for the low-energy specimens, with the exception of Condition 1 the difference between the test results is insignificant. The tests performed under Condition 1 with the unpolished anvils may have significantly higher energies than the other four cases with polished anvils.

CONCLUSION

For low-energy specimens which exit the testing machine in the direction opposite to the direction of swing of the pendulum, there seems to be very little difference between polished and unpolished anvils and strikers. There is only a slight downward trend in the average absorbed energies as the tooling is polished.

For low-energy specimens which exit the testing machine in the direction of swing of the pendulum, the average absorbed energy dropped as much as 0.4 J (0.3 ft-lb) when the striking bit was polished. When a low-energy specimen is broken, the broken halves spin at high velocity and strike the anvils a second time (Fig. 2). Specimens which exit the machine in the direction of swing of the pendulum rebound off the anvils and may continue to rotate in such a way as to scrape between the anvil support and the sides of the passing striking bit. We think that when we polish the striking bit, the friction is reduced between the striking bit and the specimen after the specimen breaks.

While the differences reported here may not seem large, 0.4 J can be important when compared to the $\pm$ 1.4 J range permitted by ASTM E-23 when verification specimens are tested. A machine that may pass with an old striker that has been burnished by testing many specimens may fail when a new striker that is not highly polished is installed.

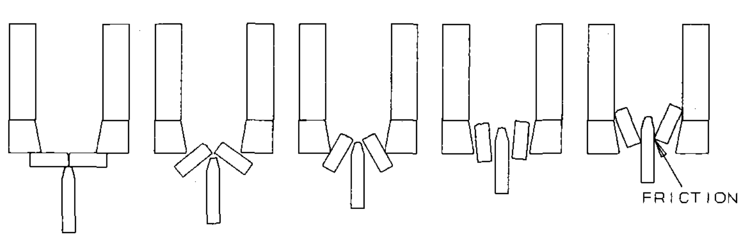

FIG. 2--Proposed Trajectories of Low-energy Specimens which cause Lost Energy due to Friction with the Striking Bit

For high-energy specimens, we found that the absorbed energy dropped as much as 2 J (1.5 ft-lb) when the anvils were polished. Again a 1 or 2 J reduction in energy when attempting to qualify a machine can determine whether a machine passes or fails verification tests.

High-energy specimens are dragged across the anvils as they are broken (Fig. 3). Higher friction between the anvils and the specimen causes the testing machine to indicate higher absorbed energy values.

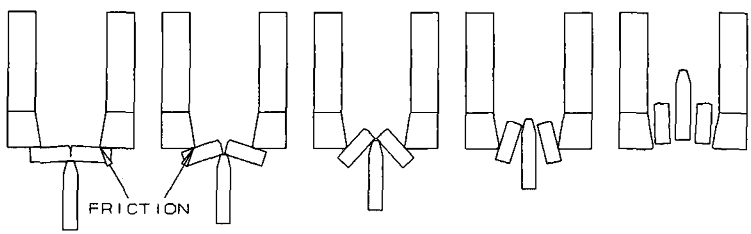

FIG. 3--Proposed Trajectories of High-energy Specimens Which Cause Lost Energy due to Friction with the Anvils

ASTM Standard Test Methods for Notched Bar Impact Testing of Metallic Materials (E 23) requires a 4 μm (125 μin.) rms finish on the anvils and the striker. Through use, these parts are burnished to a high polish. In order to reduce the shift in results that may result from a change in the striker or anvils, ASTM E 23 should require that these parts be highly polished. We suggest that ASTM E 23 be changed to require that the anvil and striking bit have rms finishes of 0.1 μm (4 μin.) or better.

REFERENCES

[1] Siewert, T. A. and Vigliotti, D. P., "The Effect of Charpy V-notch Striker Radii on the Absorbed Energy," Pendulum Impact Machines: Procedures and Specimens for Verification, ASTM STP 1248.

Earl A. Ruth,[1]

STRIKER GEOMETRY AND ITS EFFECT ON ABSORBED ENERGY

REFERENCE: Ruth, E. A., "**Striker Geometry and its Effect on Absorbed Energy**", Pendulum Impact Machines: Procedures and Specimens for Verification, ASTM STP 1248, Thomas A. Siewert and A. Karl Schmieder, Eds., American Society for Testing and Materials, Philadelphia, 1995.

ABSTRACT: ASTM Standard Test Methods for Notched Bar Impact Testing of Metallic Materials (E 23) requires the face of the striker to have an 8 mm radius and to be 4 mm wide. At the corners where the 8 mm radius meets the sides of the striker, E 23 calls for a radius of 0.25 mm ± 0.05 mm. This 0.25 mm radius causes a problem, as it can be worn out of tolerance quickly during normal testing. This paper presents data which exhibits the effects on absorbed energy when the corner radius is enlarged. Data is also presented which compares absorbed energy obtained using an ASTM E 23, 8 mm striker with absorbed energy obtained using an ISO 2 mm striker.

KEYWORDS: Charpy impact test, impact test, striker, striker geometry

BACKGROUND

In the 1960's, a 0.25 mm radius was added to the corners of the striking bit in ASTM Standard Test Methods for Notched Bar Impact Testing of Metallic Materials (E 23). This 0.25 mm radius is specified where the 8 mm nose radius meets the 30° sides of the striker. To conform to ASTM E 23 now, one must maintain that corner radius at 0.25 mm ± 0.05 mm. During routine testing, these corners can be worn out

[1]Manager, Engineering & Systems, Tinius Olsen Testing Machine Co., Inc., Willow Grove, Pennsylvania 19090

of tolerance in a short period of time. In 1989 this problem was presented to the ASTM Task Group (E28.07.02) which has oversight of ASTM E 23. An ad hoc committee was formed to learn if the tolerance of the radius of the corner of the striker could be relaxed.

EXPERIMENTAL METHOD

Standard Charpy V-notch specimens (ASTM E 23 Type A) were supplied by the U. S. Army, Watertown Arsenal who were supplying reference specimens at that time. The specimens supplied were made from three different lots of steel, each lot having a different nominal absorbed energy value. The three absorbed energy values were 16 J, 100 J, and 200 J.

All of the tests were performed on one 400 J capacity machine at -40° C. Tests were performed using five different striker geometries. The same striking bit was used for all tests. Between each set of tests the striker was removed and ground to the new geometry. The striker was then reinstalled in accordance with the manufacturer's specifications. A thin layer of machinist bluing was applied to the mating surface of the striker each time the striker was installed. This was done so that the fit of the striker could be evaluated upon removal by looking at the mounting surface on the pendulum of the impact testing machine. In every case, blueing had been transferred to more than 80% of the mounting surface.

Twenty specimens of each of the three energy levels were tested using the standard ASTM E 23, 8 mm striker geometry with the 0.25 mm corner radius (see Fig. 1). The corner radius was then increased to 0.50 mm and ten specimens of each energy level were tested. The corner radius was increased again, this time to 1.00 mm and ten specimens of each energy level were tested. The next geometry tested was an attempt at a compromise between the ASTM E 23, 8 mm geometry and ISO 2 mm geometry. The nose of the striker had an 8 mm radius and the corners were 1.50 mm in radius. The width was the same as an ISO 2 mm striker. Ten specimens of each energy level were tested with this geometry. The final geometry to be tested was an ISO 2 mm striker. Twenty specimens of each energy level were tested with this striker.

Tables 1 through 3 include all of the test results. Table 4 is a summary of the test results. Table 5 is a summary of the test results with a couple of probable outliers removed. Figure 2 is a graphical representation of the results for each of the materials with the outliers removed.

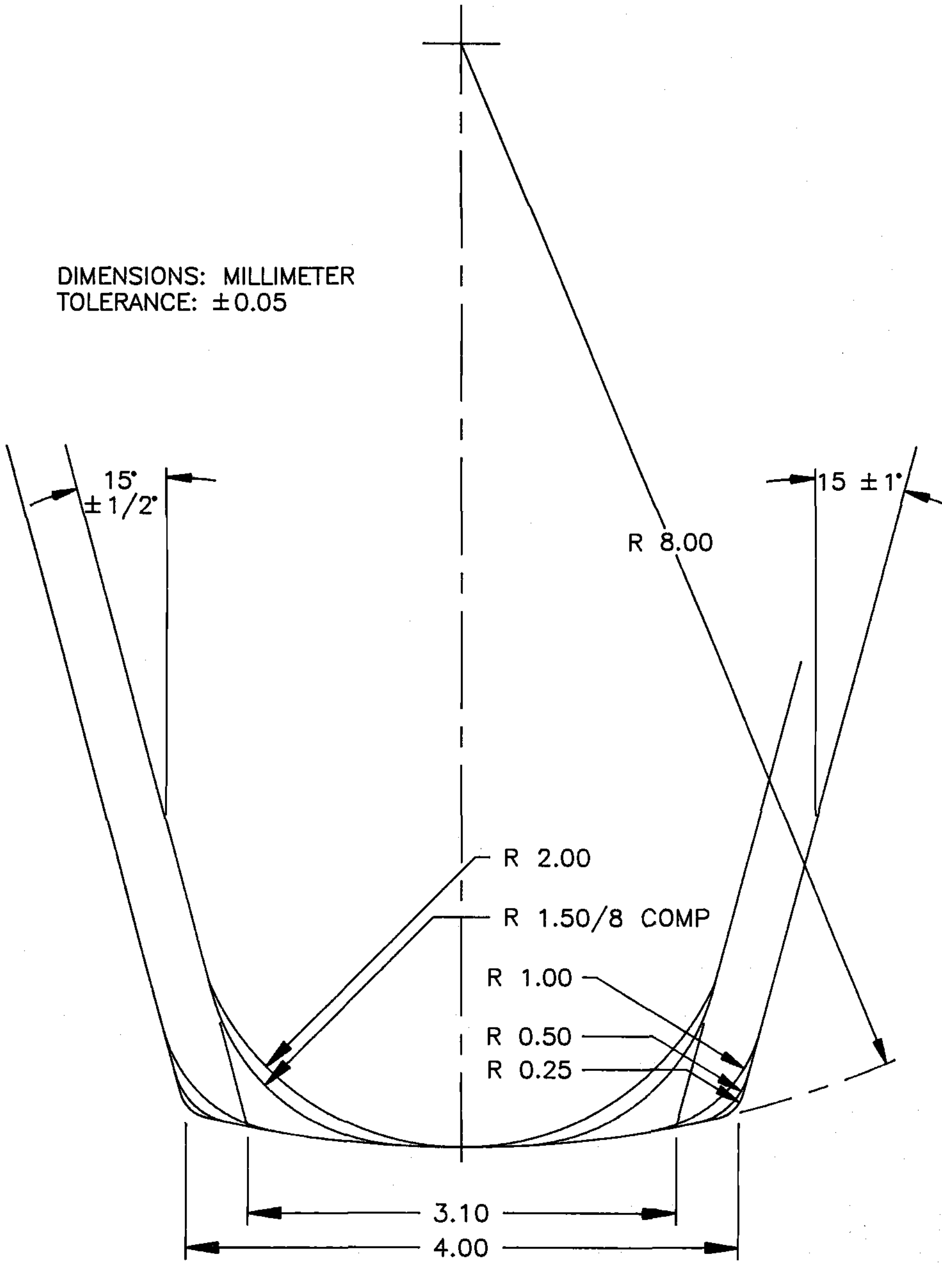

FIG. 1 -- Striker Geometries

TABLE 1--Low Energy Test Results

Low Energy Test Results, J				
ASTM 8 mm with 0.25 mm Radius Corners.	ASTM 8 mm with 0.50 mm Radius Corners.	ASTM 8 mm with 1.00 mm Radius Corners.	ASTM/ISO Compromise 8 mm nose with 1.5 mm Corners.	ISO 2 mm Radius.
14.0	16.2	16.9	16.7	15.1
17.3	15.4	15.3	17.0	15.9
16.9	15.3	16.4	17.1	16.2
17.4	16.7	15.9	16.9	17.0
16.0	17.5	16.9	17.1	17.2
16.0	16.0	16.2	16.6	18.1
15.2	17.3	15.0	17.1	19.0
16.0	15.2	15.2	15.0	15.9
16.1	15.1	16.3	15.0	18.3
15.7	15.9	15.8	16.2	17.8
15.0				16.6
16.4				17.5
16.3				17.1
16.4				17.1
16.7				17.0
16.1				15.0
17.9				16.9
15.5				16.0
17.0				16.9
15.5				17.0

TABLE 2--Medium Energy Test Results

Medium Energy Test Results, J				
ASTM 8 mm with 0.25 mm Radius Corners.	ASTM 8 mm with 0.50 mm Radius Corners.	ASTM 8 mm with 1.00 mm Radius Corners.	ASTM/ISO Compromise 8 mm nose with 1.5 mm Corners.	ISO 2 mm Radius.
93.2	93.8	96.0	92.0	97.2
98.0	96.5	100.4	99.0	97.0
97.0	103.0	95.0	93.3	90.0*
96.0	100.4	97.0	93.7	98.0
100.8	98.2	103.0	94.3	97.5
99.8	96.8	102.5	98.0	99.8
94.1	99.0	98.3	96.0	95.3
103.3	89.4	99.7	95.5	100.0
95.3	93.0	99.7	97.0	98.1
89.3	93.9	96.9	95.0	98.2
92.2				98.8
92.9				97.9
96.3				94.9
96.2				100.0
95.4				96.2
96.7				98.2
101.6				91.0*
99.0				99.8
97.1				97.9
100.5				100.0

Values marked with an * are possible outliers

TABLE 3--High Energy Test Results

High Energy Test Results, J				
ASTM 8 mm with 0.25 mm Radius Corners.	ASTM 8 mm with 0.50 mm Radius Corners.	ASTM 8 mm with 1.00 mm Radius Corners.	ASTM/ISO Compromise 8 mm nose with 1.5 mm Corners.	ISO 2 mm Radius.
199.4	188.2	216.5	192.0	204.0
197.5	190.5	213.5	203.5	174.0
201.0	194.3	196.5	206.8	180.5
197.5	185.3	207.5	201.8	186.5
202.3	197.0	206.0	199.2	194.5
217.5*	205.8	211.0	205.5	181.0
192.0	200.5	196.8	225.0*	176.0
200.5	206.3	212.5	206.0	196.2
191.5	190.0	203.5	197.5	207.7
201.4	203.8	203.1	188.5	182.0
194.0				193.5
195.5				188.0
200.0				199.2
207.3				184.5
205.0				183.0
194.0				217.2
203.0				202.2
199.0				195.3
217.7*				182.0
199.7				192.8

Values marked with an * are possible outliers

TABLE 4--Summary of all Test Results

	Low Energy J		Medium Energy J		High Energy J	
	Avg.	S.D.	Avg.	S.D.	Avg.	S.D.
ASTM 8 mm with 0.25 mm Radius Corners. n=20	16.17	0.91	96.7	3.47	200.8	7.05
8 mm with 0.50 mm Radius Corners. n=10	16.06	0.87	96.4	3.99	196.2	7.66
8 mm with 1.00 mm Radius Corners. n=10	15.99	0.67	98.8	2.68	206.7	6.84
ASTM/ISO Compromise 8 mm with 1.5 mm Corners. n=10	16.47	0.82	95.4	2.18	202.6	9.94
ISO 2 mm Radius n=20	16.88	1.01	97.3	2.75	191.0	11.28

TABLE 5--Summary of Test Results with Probable Outliers Removed

	Low Energy J		Medium Energy J		High Energy J	
	Avg.	S.D.	Avg.	S.D.	Avg.	S.D.
ASTM 8 mm with 0.25 mm Radius Corners. n=20	16.17	0.91	96.7	3.47	198.9 n=18	4.32 n=18
8 mm with 0.50 mm Radius Corners. n=10	16.06	0.87	96.4	3.99	196.2	7.66
8 mm with 1.00 mm Radius Corners. n=10	15.99	0.67	98.8	2.68	206.7	6.84
ASTM/ISO Compromise 8 mm with 1.5 mm Corners. n=10	16.47	0.82	95.4	2.18	200.1 n=9	6.43 n=9
ISO 2 mm Radius n=20	16.88	1.01	98.0 n=18	1.56 n=18	191.0	11.28

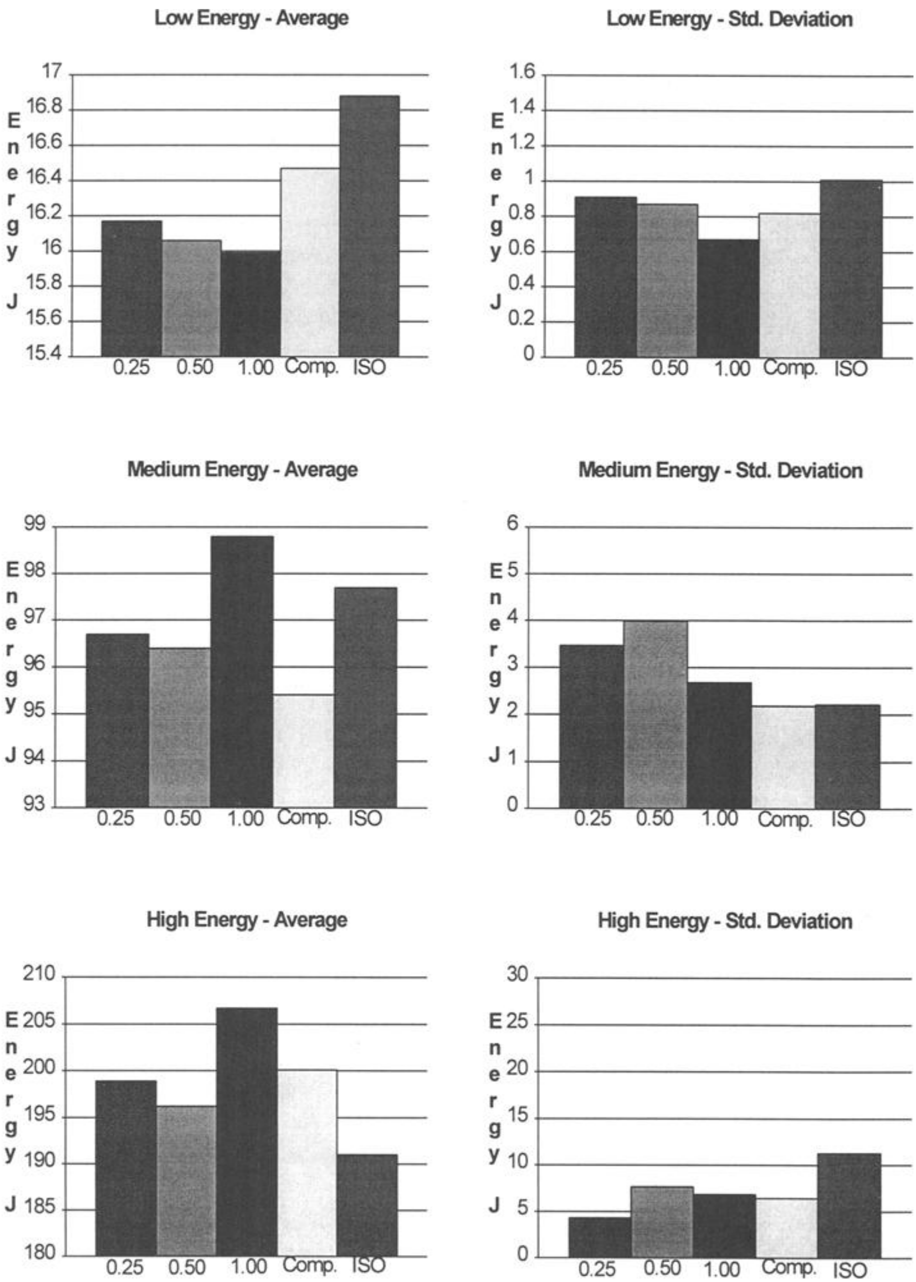

FIG. 2 -- Graphs of Test Results with Outliers Removed

DISCUSSION

There was little or no difference in absorbed energy between tests using the standard ASTM E 23, 8 mm striker with a 0.25 mm corner radius and tests using a striker with a corner radius of 0.50 mm. When the corner radius was increased to 1.00 mm the absorbed energy in tests at the 100 J and 200 J level increased significantly.

The striker which we had hoped would be a compromise between the ASTM E 23, 8 mm striker and the ISO 2 mm striker gave disappointing results. It had been speculated that it would agree with the ASTM E 23, 8 mm striker at low absorbed energies and with the ISO 2 mm striker at high absorbed energies. Unfortunately that was not the case.

The energy absorbed by the tests using the ISO 2 mm striker was considerably higher than the energy absorbed in tests using the ASTM E 23, 8 mm striker at the 16 J level. The material used in these tests was a high strength 4340 steel. A possible reason for the higher absorbed energy by the ISO 2 mm striker is greater plastic deformation of the steel due to the higher contact stresses at the point of impact. Compressive contact stresses due to the smaller radius could be twice as high as those with the ASTM E 23, 8 mm striker.

The energy absorbed by the tests using the ASTM E 23, 8 mm striker was considerably higher than the energy absorbed in tests using the ISO 2 mm striker at the 200 J level. The wider width of the ASTM E 23, 8 mm striker required that the specimen be bent around the corners of the striker. While one can argue that this additional bending process is absorbing more energy, the specimens broken with the ASTM E 23, 8 mm striker were completely fractured. This was not the case with the ISO 2 mm striker.

CONCLUSION

The tolerance on the corner radius of the striker given in ASTM Standard Test Methods for Notched Bar Impact Testing of Metallic Materials (E 23) could be relaxed to a range of 0.25 mm to 0.50 mm with little or no effect on absorbed energy.

There seem to be advantages and disadvantages for both the ASTM E 23, 8 mm and the ISO 2 mm strikers. Additional work is needed to fully understand why there are differences in absorbed energy between the two strikers.

Acknowledgment

The author wishes to acknowledge Walter Roy, Tim Holt, and Karl Schmieder as members of the ASTM E28.07.02 ad hoc committee which initiated this work.

Randy K. Nanstad[1] and Mikhail A. Sokolov[1]

CHARPY IMPACT TEST RESULTS ON FIVE MATERIALS AND NIST VERIFICATION SPECIMENS USING INSTRUMENTED 2-mm AND 8-mm STRIKERS

REFERENCE: Nanstad, R. K., and Sokolov, M. A., **"Charpy Impact Test Results on Five Materials and NIST Verification Specimens Using Instrumented 2-mm and 8-mm Strikers,"** *Pendulum Impact Machines: Procedures and Specimens for Verification, ASTM STP 1248*, Thomas A. Siewert and A. Karl Schmieder, Eds., American Society for Testing and Materials, Philadelphia, 1995.

ABSTRACT: The Heavy-Section Steel Irradiation Program at Oak Ridge National Laboratory is involved in two cooperative projects, with international participants, both of which involve Charpy V-notch impact tests with instrumented strikers of 2-mm and 8-mm radii. Two heats of A 533 grade B class 1 pressure vessel steel and a low upper-shelf (LUS) submerged-arc (SA) weld were tested on the same Charpy machine, while one heat of a Russian Cr-Mo-V forging steel and a high upper-shelf (HUS) SA weld were tested on two different machines. The number of replicate tests at any one temperature ranged from 2 to 46 specimens. Prior to testing with each striker, verification specimens at the low, high, and super high energy levels from the National Institute of Standards and Technology (NIST) were tested. In the two series of verification tests, the tests with the 2-mm striker met the requirements at the low and high energy levels but not at the super high energy. For one plate, the 2-mm striker showed somewhat higher average absorbed energies than those for the 8-mm striker at all three test temperatures. For the second plate and the LUS weld, however, the 2-mm striker showed somewhat lower energies at both test temperatures. For the Russian forging steel and the HUS weld, tests were conducted over a range of temperatures with tests at one laboratory using the 8-mm striker and tests at a second laboratory using the 2-mm striker. Lateral expansion was also measured for all specimens and the results are compared with the absorbed energy results. The overall results showed generally good agreement (within one standard deviation) in energy measurements by the two strikers. Load-time traces from the instrumented strikers were also compared and used to estimate shear fracture percentage. Four different formulas from the European Structural Integrity Society draft standard for instrumented Charpy test are compared and a new formula is proposed for estimation of percent shear from the force-time trace.

[1]Metals and Ceramics Division, Oak Ridge National Laboratory, P.O. Box 2008, Oak Ridge, TN 37831-6151.

KEYWORDS: Charpy impact testing, verification, 2-mm striker, 8-mm striker, lateral expansion, instrumented striker, energy, percent shear, standard deviation, plate, weld, forging

---

Charpy V-notch (CVN) impact testing is performed by hundreds of organizations around the world using very similar procedures, usually either that of the American Society for Testing and Materials (ASTM) [1] or that of the International Organization for Standardization (ISO) [2]. Unfortunately, two different specimen striker designs are described and are sufficiently different so that the equivalence of the test results is questionable. Figure 1 shows that the 2-mm striker described in the ISO standard is thinner and has a 2-mm radius compared to the 8-mm radius of the striker described in the ASTM standard. Recently, the ISO incorporated the 8-mm striker into the standards in addition to the 2-mm striker. This situation can present difficulties for manufacturers of materials and structures which are required to meet minimum specified CVN impact toughnesses according to, for example, the ASTM (which allows only the 8-mm striker), but they have data available from tests conducted with the 2-mm striker. Likewise, for codes and standards organizations, adoption of materials based on data obtained with the 2-mm striker into a code which references the ASTM specification presents a dilemma. Towers [3] tested verification specimens from the Army Mechanics and Materials Research Center (AMMRC) and nine other materials (e.g., aluminum alloys, aluminum-bronze, stainless steels, carbon steel, 5% Ni and 9% Ni steels) with the two different strikers. For the verification specimens, which ranged in nominal absorbed energies up to 107 J, the two strikers gave equivalent energies. For the nine other materials, he observed equivalent results up to about 60 J, as shown in Fig. 2. Above that energy, however, although the 8-mm striker showed generally higher energies, the energies at which the differences were observed and the magnitudes of the differences were material dependent. Naniwa [4] tested carbon and low-alloy steels and, as shown in Fig. 3(a), observed general equivalence up to about 200 J; above that level, the 8-mm striker gave higher energies with the differences increasing with increasing energy. Naniwa stated no differences were observed in lateral expansion, percent shear, or transition temperature. The data from Ref. 4, however, shown in Fig. 3(b), appear to show a general deviation from equivalence with the 2-mm striker showing a tendency for greater expansion. Revise [5] tested "metallic samples" at a few different energy levels and observed equivalence up to about 100 J; at the level of 160 J for the 2-mm striker, however, the 8-mm striker gave about 165 J. The Heavy-Section Steel Irradiation (HSSI) Program at Oak Ridge National Laboratory (ORNL) is involved in two cooperative projects that include international participants. For both projects, CVN impact tests were performed with both the 2-mm and 8-mm strikers; one objective of both projects was to compare the results from the two strikers with different materials and, where practicable, with enough tests for statistical evaluations.

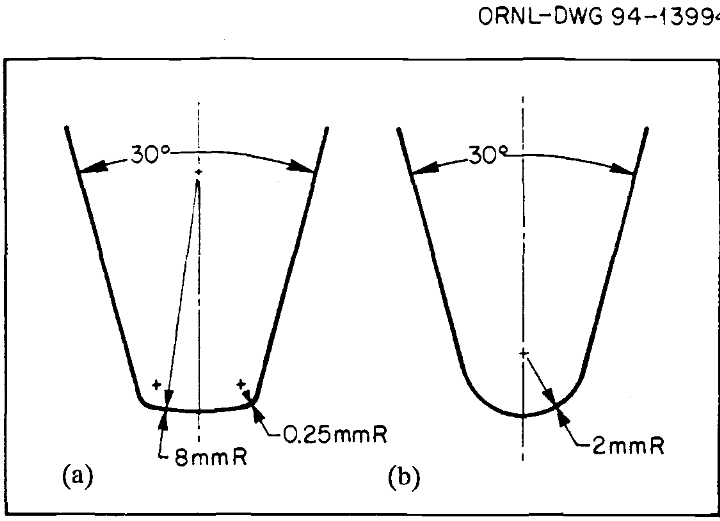

FIG. 1. Schematic drawing showing the differences in the striking ends of the (a) 8-mm and (b) 2-mm radius Charpy impact strikers. The 8-mm striker is thicker and has a substantially larger radius of curvature and relatively sharp edges.

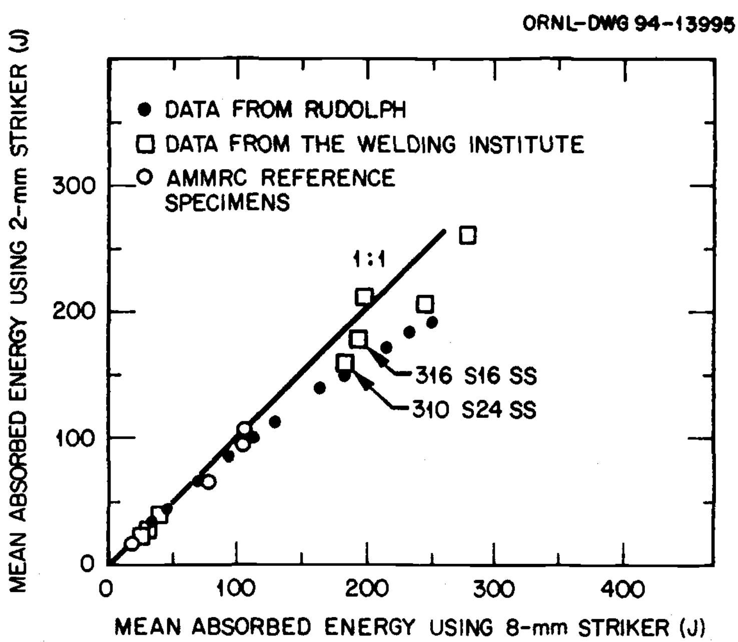

FIG. 2. Plot of data from Tower showing effect of striker shape on absorbed energy in Charpy impact test for different materials.

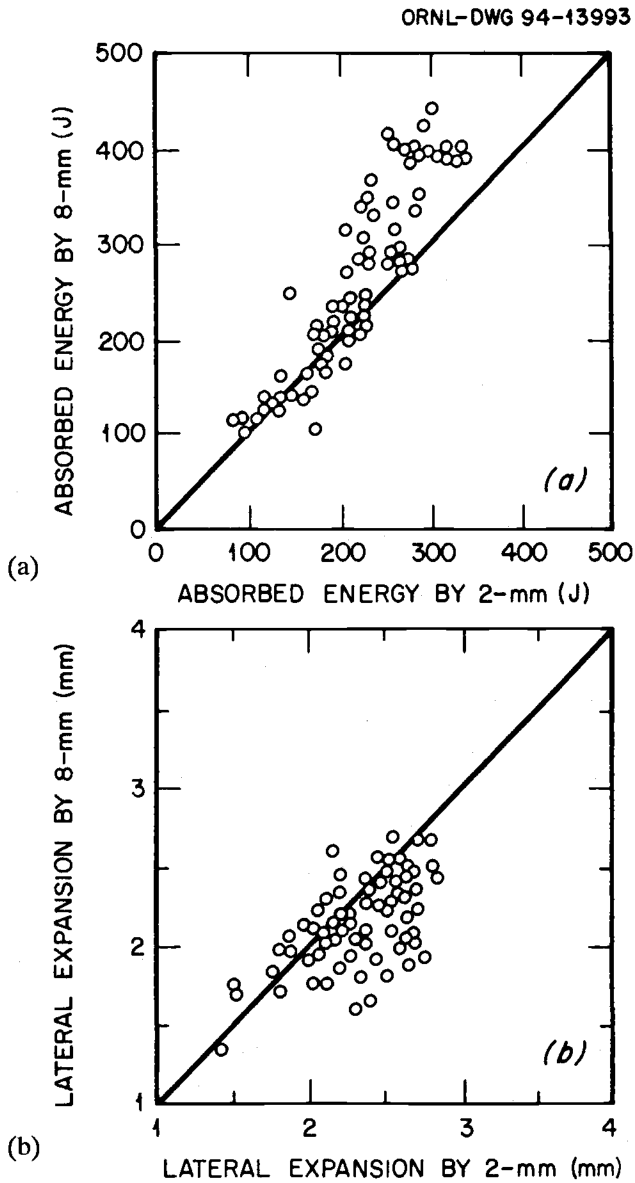

FIG. 3. Plot of data from Naniwa for carbon and low-alloy steel: (a) general equivalence of energy values for the two strikers was observed to about 200 Nm (J) with the 8-mm striker measuring higher energies than the 2-mm striker above that level, and (b) tests with the 2-mm striker appear to exhibit a tendency for greater expansion values.

MATERIALS AND PROCEDURES

Table 1 summarizes the test matrix for the various materials. Verification of 4340 high-strength steel from the National Institute of Standards and Technology (NIST) were tested at ORNL on the same machine using the 2-mm and 8-mm strikers. Two different heats of A 533 grade B class 1 low-alloy (Mn-Mo-Ni) pressure vessel steel plate and a low upper-shelf (LUS) submerged-arc (SA) weld (Mn-Mo-Ni) were tested on the same Charpy machine, while one heat of a Russian forging steel (Cr-Mo-V) and a high upper-shelf (HUS) SA weld (Mn-Mo-Ni) were tested on three different machines, one at ORNL with the 8-mm striker and two in Russia with the 2-mm striker. One of the heats of A 533 grade B (HSST Plate 13) was also tested on two machines in Russia with the 2-mm striker. Tests were conducted at four temperatures for one plate, while two test temperatures were used for the other plate and the LUS weld. Table 2 provides the room temperature tensile properties of the five steels tested, respectively. The number of replicate tests were quite variable and were dependent on the specific program of testing. In some of the cases, the number of tests were relatively high, (e.g., 23 and 46) which provides for reasonable credibility from a statistical basis.

In most of the cases shown in Table 1 for ORNL, tests were conducted to provide direct comparison of results with the two strikers on the same Charpy machine. Prior to testing of these materials with each striker, verification specimens at the low, high, and super high energy levels from NIST were tested. These specimens are designed to be applicable to the verification of a pendulum impact machine with the 8-mm striker. The energy levels are specified in English units and are nominally about 12, 75, and 160 ft-lb (about 16, 102, and 217 J), respectively, with the actual values dependent on the particular heat of steel used to produce the supply of specimens. For the verification testing, five specimens from each energy level are tested. For each level, the average energy of the five tests must be within a specified deviation from a specified mean value supplied by NIST for the heat of material used. The general procedure followed in this series of experiments was, (1) verification with the 8-mm striker, (2) verification with the 2-mm striker, (3) testing of test materials with the 2-mm striker, (4) verification with the 8-mm striker, and (5) testing of test materials with the 8-mm striker. This procedure was designed to provide assurance that the machine stayed in calibration throughout the series of tests and striker changes.

For the testing at ORNL, a 326-J (240-ft-lb) capacity pendulum-type impact machine, Baldwin Model SI1C, was used. Both the 8-mm and 2-mm strikers are instrumented with strain gages to provide a load-time record, but all energy values reported herein were obtained from the dial energy. The machine is equipped with a semiautomated specimen thermal conditioning and transfer system. The transfer system places the specimen in the thermal conditioning system which heats the specimen by contact with graphite electrodes, cools the specimen with cold nitrogen gas, and includes a calibrated contact thermocouple for temperature measurement. The transfer system allows for transfer of the specimen to the anvils for testing in less

TABLE 1--Number of test temperatures, machines, and replicate tests for the tested materials

Material	Number of temperatures	Test laboratories	Replicates
A533B (HSST-03)	2	ORNL	2-mm: 23/46 8-mm: 23/46
A533B (HSST-13)	3	ORNL	2-mm: 10/20 8-mm: 10/20
A533B (HSST-13)	4 4	RUSSIA ORNL	2-mm: 2-5 8-mm: 2-5
HUS weld 72W	4	ORNL	8-mm: 6-10
HUS weld 72W	4	RUSSIA	2-mm: 2-5
LUS weld	2	ORNL	2-mm: 23/46 8-mm: 23/46
15Kh2MFA forging	7	ORNL	8-mm: 4-6
15Kh2MFA forging	7	RUSSIA	2-mm: 4-6
15Kh2MFA forging	2	ORNL	8-mm: 10
15Kh2MFA forging	2	RUSSIA	2-mm: 10
NIST verification (3 energy levels)	1	ORNL	2-mm: 3 sets 8-mm: 5 sets

TABLE 2--Tensile properties of tested materials at room temperature

Material	Yield strength (MPa)	Ultimate strength (MPa)
A533B (HSST-03)	460	618
A533B (HSST-13)	424	600
SAW, Linde 80	500	603
SAW HSSI weld 72W	500	609
15Kh2MFA forging 103672	630	680

than 5 s following removal from the conditioning chamber. Figure 4 shows a composite photograph of the system (photo shows a different Charpy machine). The percent shear fracture was visually measured and the lateral expansion was measured with a device similar to that described in ASTM E-23. For the testing in Russia, a 300-J (221-ft-lb) capacity pendulum-type machine, Amsler Model RKP-300 was used; only the 2-mm striker was used for those tests. Calibration of that machine was performed by direct methods of alignment, etc. by the official state standardization committee of Russia.

RESULTS

Verification Specimens

Figure 5 summarizes the results of NIST verification specimen tests for both the 8-mm and 2-mm strikers in terms of deviation from the NIST supplied nominal mean values for each particular set of specimens tested. The 8-mm striker met the specified requirements at all three energy levels in all cases. The 2-mm striker met the requirements in all cases for the low and high energy levels but not at the super high level, with the average energies being about 25 J (about 11%) below the nominal mean values. The nominal mean values for verification are supplied for the 8-mm striker only.

Low-Alloy Steels

For tests conducted with HSST Plate 13 to directly compare the two strikers, 10 tests with each striker were conducted at -60°C and 150°C, while 20 tests with each were conducted at 0°C. Figure 6(a) shows the average energies, as well as the minimum and maximum values, and two standard deviations for each case. Somewhat surprisingly, tests with the 2-mm striker showed generally higher energies at all three temperatures. The differences, however, are within one standard deviation in each case. The lateral expansion results exhibit a similar comparison, Fig. 6(b). The percent shear fracture results are the same for the two studies, Fig. 6(c). Figure 6(d) shows the definite trend for the 2-mm striker to result in somewhat higher lateral expansion per unit of absorbed energy. Tests with HSST Plate 13 were also conducted in a separate study on different machines, one at ORNL and two in Russia. Figure 7 shows the same trend as obtained with a large number of tests on the ORNL machine (Fig. 6); the tests with the 2-mm striker exhibited somewhat higher average energies, although these results also revealed overlap within one standard deviation. Thus, all the results with that material show consistent comparisons.

In two other similar studies to compare results on different machines in the United States (8-mm striker) and Russia (2-mm striker), Figs. 8 and 9 show somewhat mixed results. Although the results in Fig. 9 would appear to indicate that the 2-mm striker gives much higher results, the data were highly scattered for this Russian Cr-Mo-V forging steel, and the average values did overlap within one

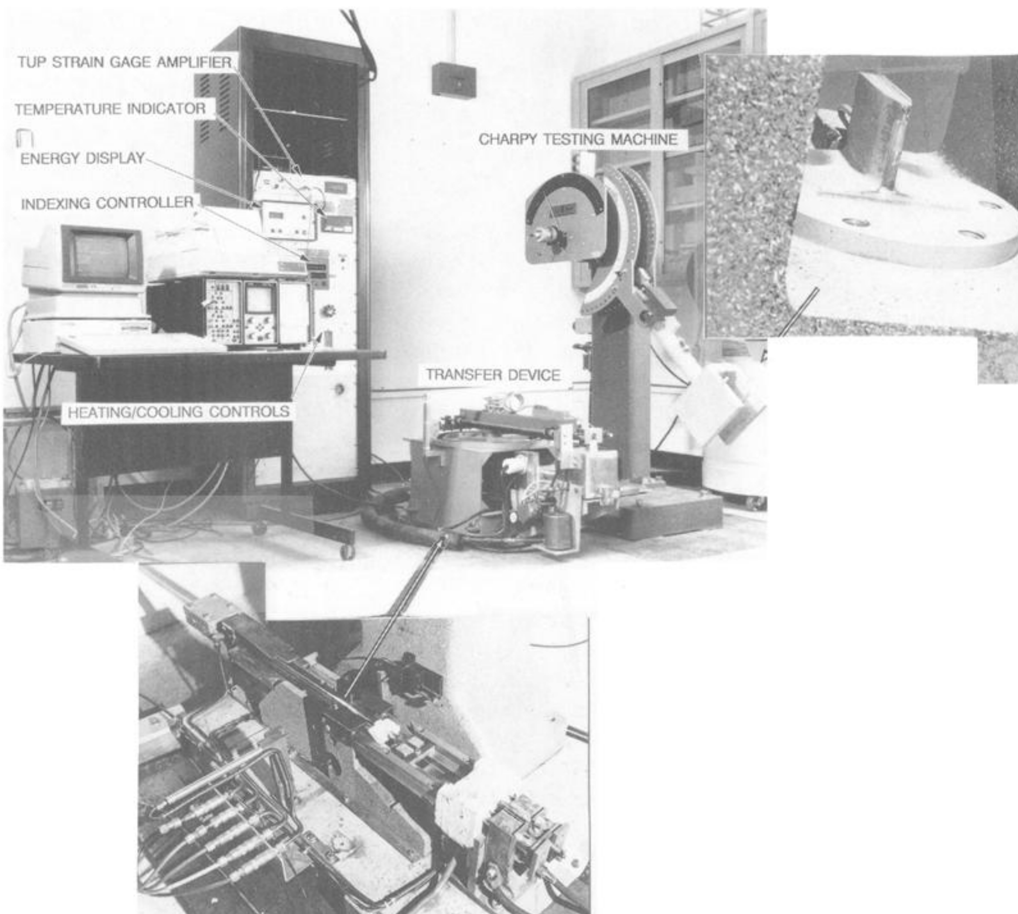

FIG. 4. Composite photograph of the ORNL Charpy impact system used to conduct the striker comparisons.

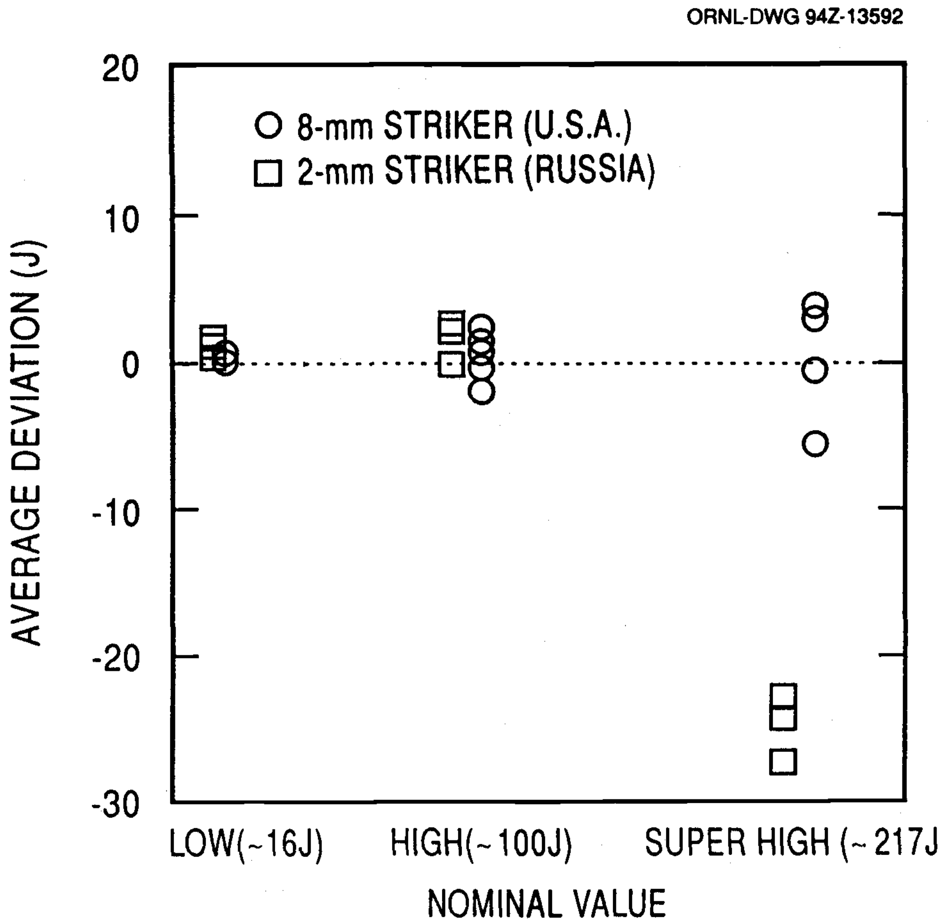

FIG. 5. Plot of average deviation from nominal values for 2-mm and 8-mm strikers at three nominal energy levels supplied by NIST for the 8-mm striker.

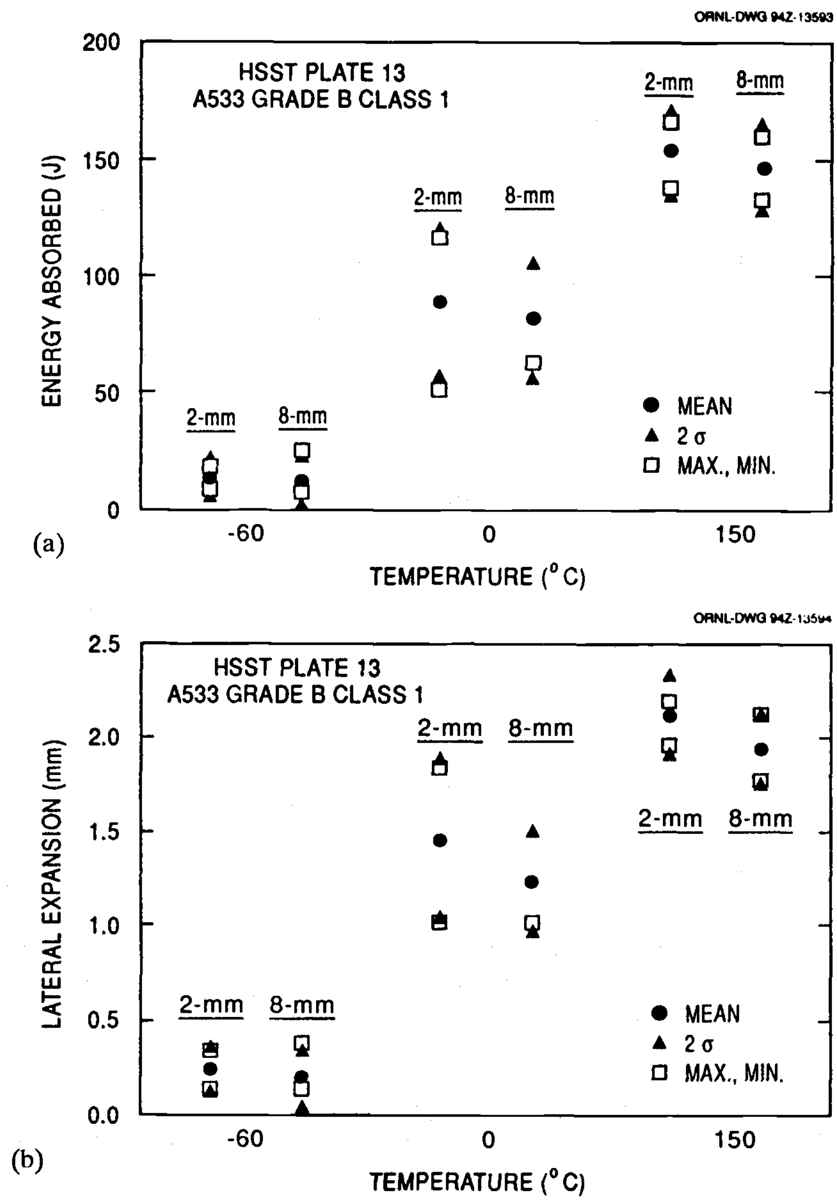

FIG. 6. Plots of ORNL data for Charpy impact tests at three temperatures for A 533 grade B class 1 steel (HSST Plate 13) conducted with both 2-mm and 8-mm strikers: (a) average absorbed energy, (b) average lateral expansion, (c) average percent shear, and (d) absorbed energy versus lateral expansion.

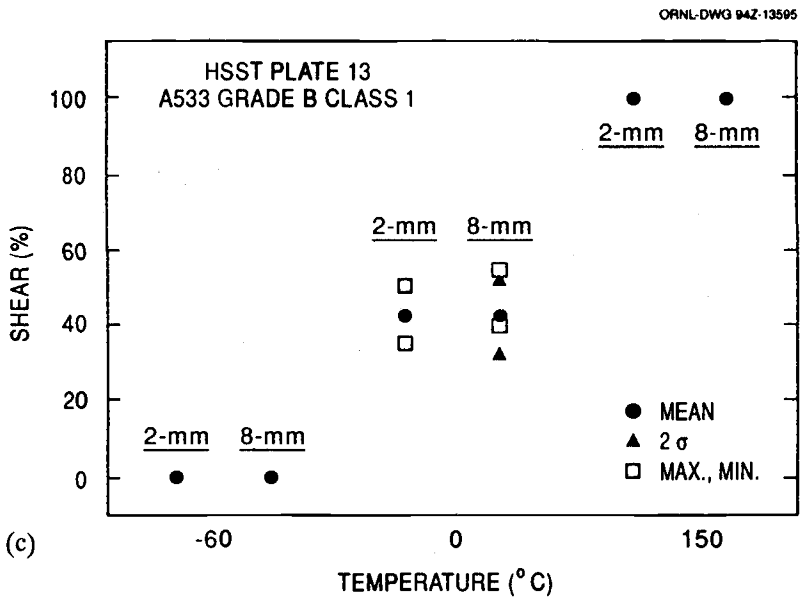

(c)

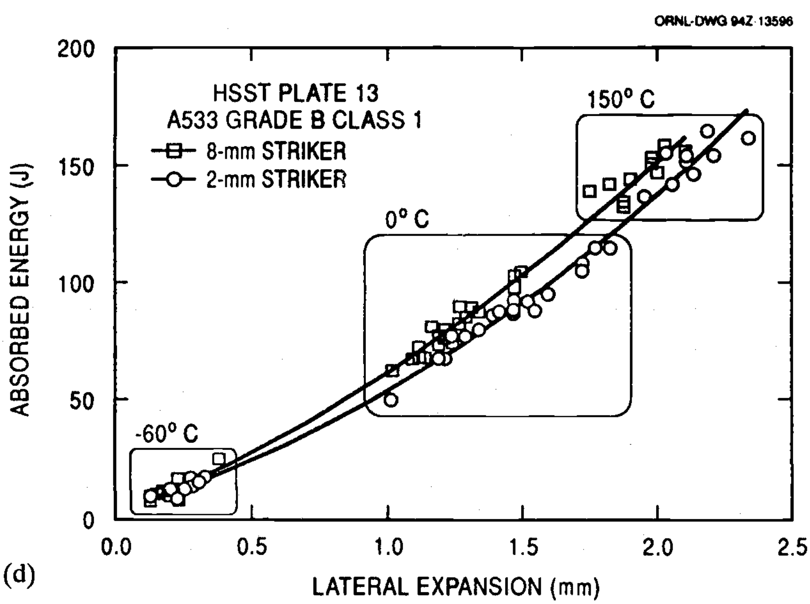

(d)

FIG. 6. (Continued)

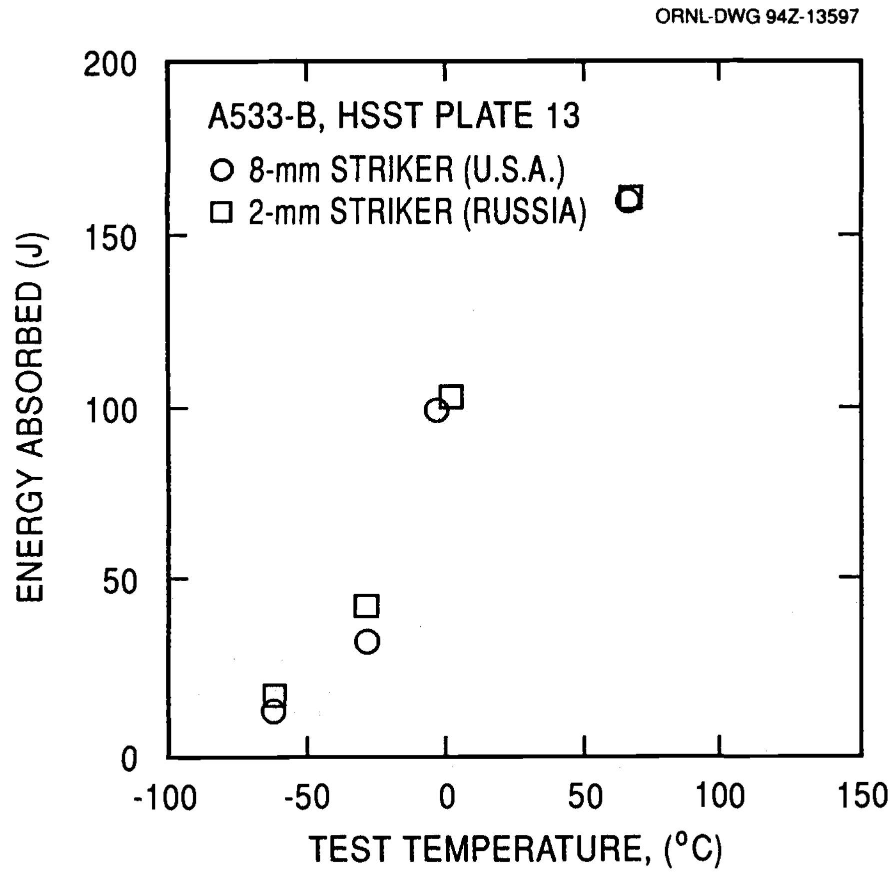

FIG. 7. Plot of average Charpy impact absorbed energy versus temperature for A 533 grade B class 1 steel (HSST Plate 13) tested on different machines in the United States (8-mm striker, one machine) and Russia (2-mm striker, two machines).

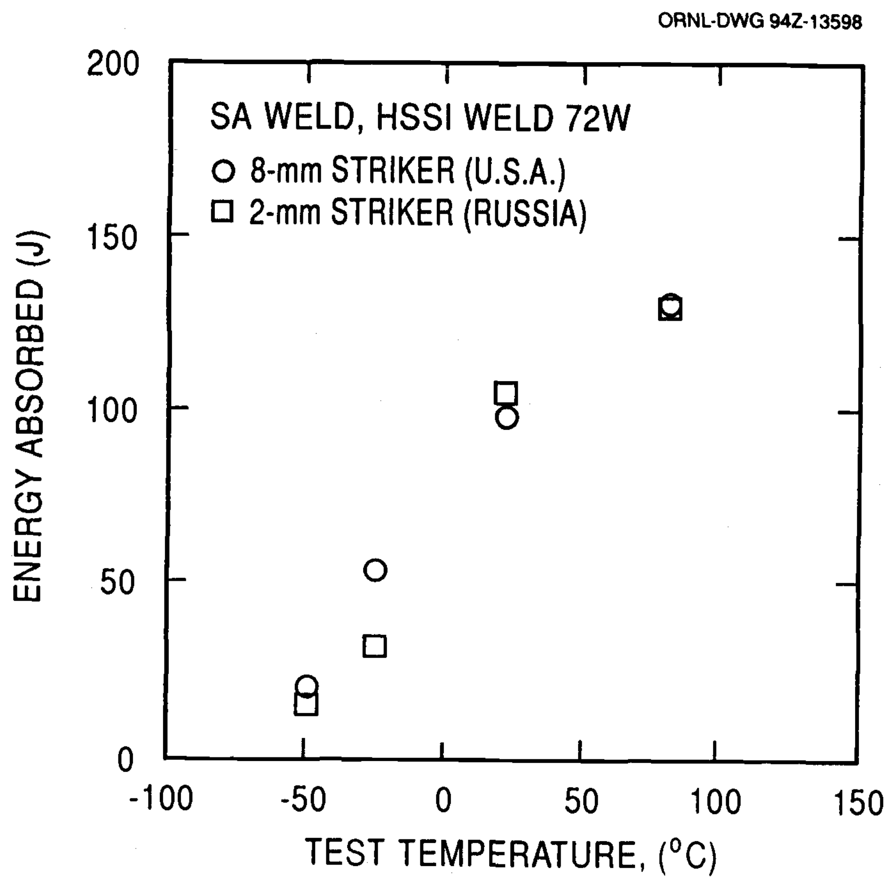

FIG. 8. Plot of average Charpy impact absorbed energy versus temperature for high-copper, high upper-shelf SA weld tested on different machines in the United States (8-mm striker) and Russia (2-mm striker).

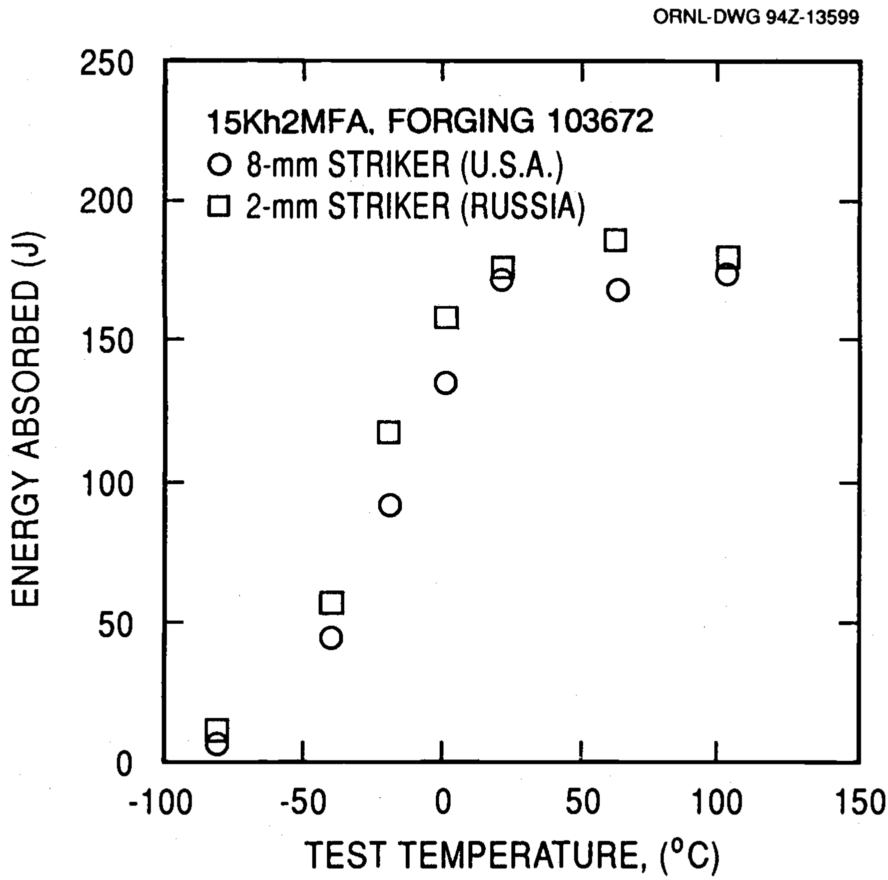

FIG. 9. Plot of average Charpy impact absorbed energy versus temperature for a Russian forging steel (Cr-Mo-V) tested on different machines in the United States (8-mm striker) and Russia (2-mm striker).

standard deviation. Even so, the tendency in that case is, as with HSST Plate 13, for the 2-mm striker to measure somewhat higher energies.

In a separate study on the same ORNL test machine, a relatively large number of specimens were tested with each striker, 46 at the low temperature and 23 at the high temperature for a plate steel and a SA weld. The A 533 grade B steel (HSST Plate 03) was tested at −12 and 93°C (10 and 200°F), while the high-copper low upper-shelf SA weld was tested at 2 and 93°C (35 and 200°F). Figures 10(a) and 10(b) show the average absorbed energies and lateral expansions. The results from the two strikers are very comparable at the three lower energy levels. At the ≈160-J level, the 8-mm striker results are somewhat higher but, again, they are within one standard deviation. The lateral expansion results are similar except the 2-mm striker has a tendency for the higher value at the higher temperature.

DISCUSSION OF TEST RESULTS

Prior to conducting the testing described above, it was anticipated that, for the steels included in the testing programs, the 8-mm striker would be observed to measure higher energies, especially at temperatures where the specimen bending and plastic deformation were relatively high. Figure 11, however, shows general equivalence of the absorbed energy results up to almost 200 J. There is scatter about the 1:1 equivalence, but all the results are within two standard deviations of the equivalence line. For the lateral expansion measurements, a linear fit to the overall data shows that tests with the 2-mm striker tend to give about 8% higher values.

The expectation of higher energy measurements with the 8-mm striker was based not only on previous results (e.g., Ref. 4) and the rationale that higher energy would be measured by a striker with a large radius when the specimen bending is sufficient, but also on observations from load-time record comparisons. Figure 12 shows the original load-time records at two temperatures for A 533 grade B steel (HSST Plate 13) for both the instrumented 2-mm and 8-mm strikers. For this comparison, the specific specimen records were chosen because the two strikers measured the same absorbed energy in each case. In Figs. 12(a) and (b), the records are comparable, although the 8-mm striker appears to have a somewhat greater increase in load from the point of general yielding to maximum load. Other comparisons have not yet been conducted to ascertain if that is a general observation. At the higher temperature, however, a comparison of Figs. 12(c) and (d) show that the 8-mm striker load-time record includes a region near the end of the test whereby the rate of load decrease is substantially reduced for about 1.5 ms. If the absorbed energy were obtained from the load-time record, that feature would result in a higher energy determination due to the additional area under the curve. This feature is associated with increased loading on the striker from the specimen "wrapping around" the striking edge and/or, if the bending angle is very high, the specimen being forced through the anvils with a resultant side loading. The load-time record for the 2-mm striker does not indicate such a change in the loading of the striker. It is assumed that all interactions between the specimen, striker, and/or anvils would undoubtedly

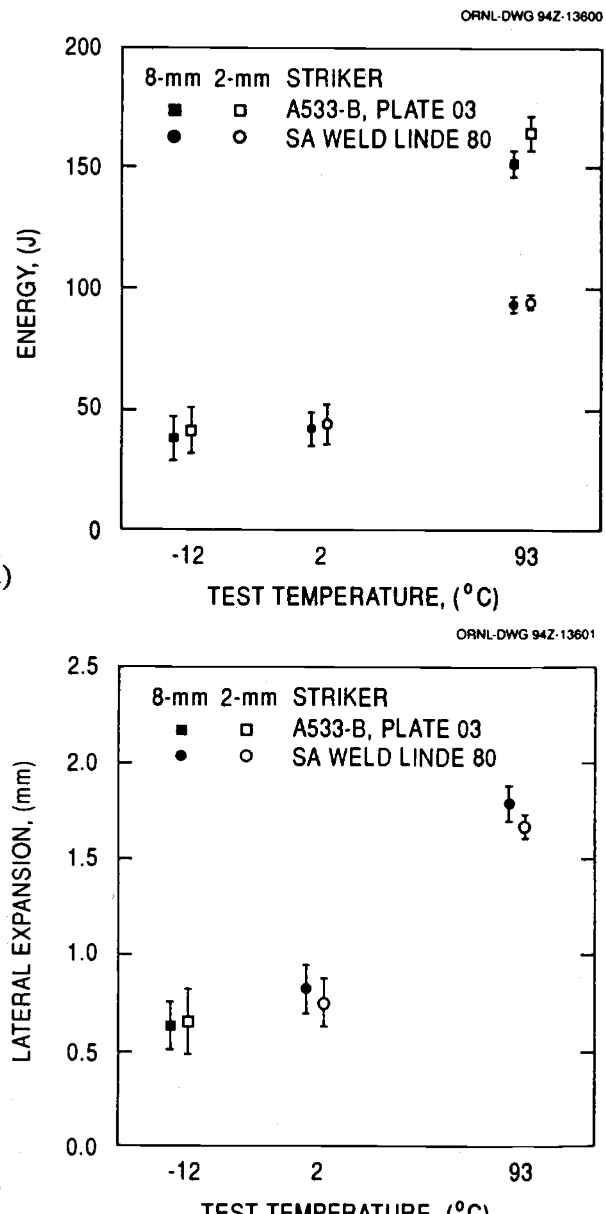

(a)

(b)

FIG. 10. Plot of average Charpy impact (a) absorbed energy, and (b) lateral expansion, versus temperature for A 533 grade B class 1 steel (HSST Plate 03) and a high-copper, low upper-shelf SA weld conducted with both 8-mm and 2-mm strikers. For each striker and each material, 46 tests were conducted at the low temperature and 23 tests at the high temperature.

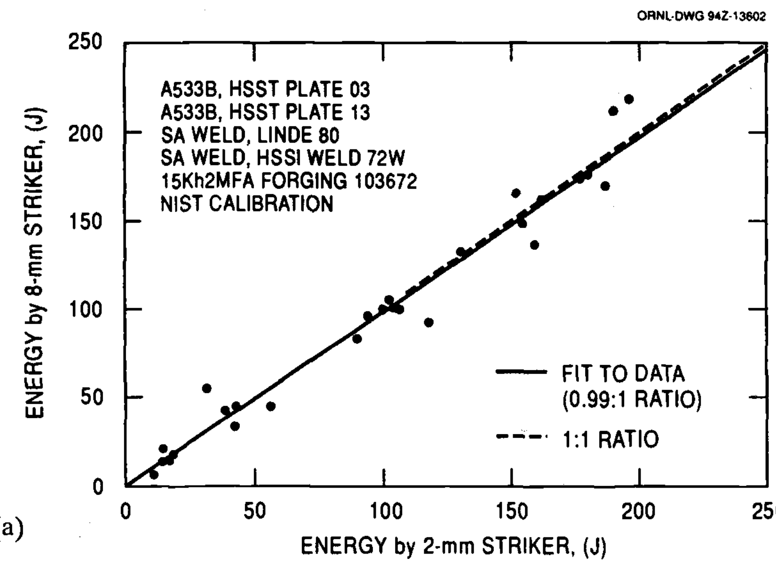

(a)

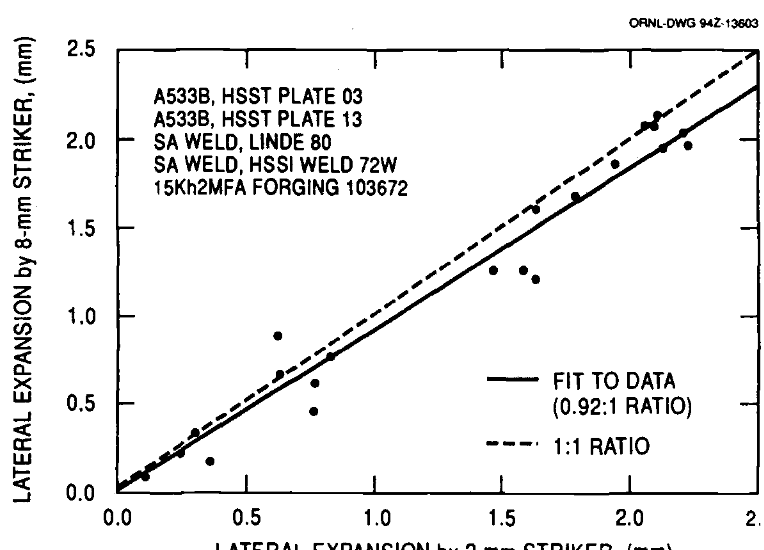

(b)

FIG. 11. Plot of average Charpy impact (a) absorbed energy, and (b) lateral expansion, versus temperature for all the steels tested. Some of the results represent direct comparisons of the two strikers on the same machine while others are based on comparisons from different machines in the United States (8-mm striker) and Russia (2-mm striker).

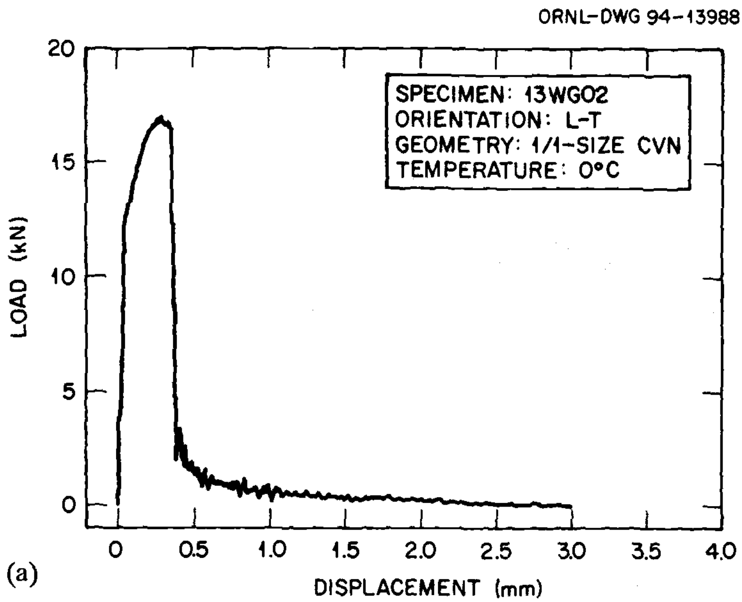

(a)

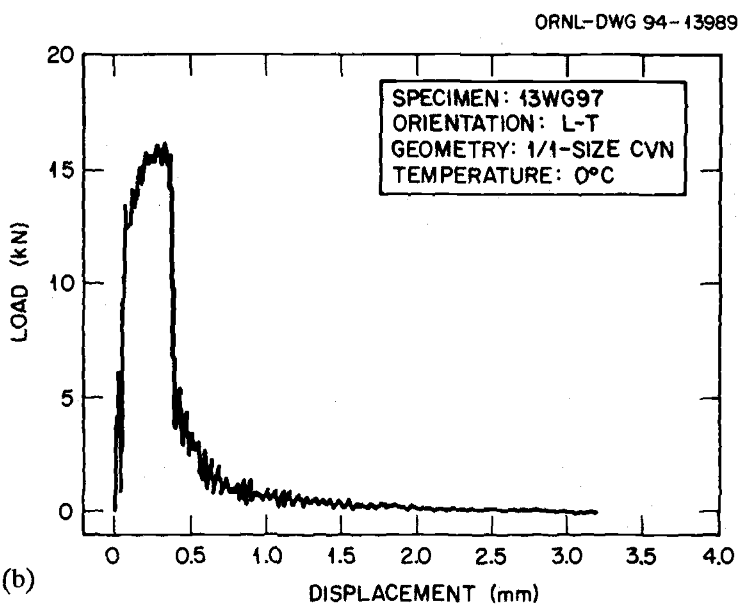

(b)

FIG. 12. Load-time records from Charpy impact tests with A 533 grade B class 1 steel (HSST Plate 13) at two temperatures with both the 8-mm and 2-mm strikers: (a) 8-mm at 0°C, (b) 2-mm at 0°C, (c) 8-mm at 150°C, (d) 2-mm at 150°C. At 0°C, both tests showed 78-J energy, while at 150°C, both tests showed 157 J.

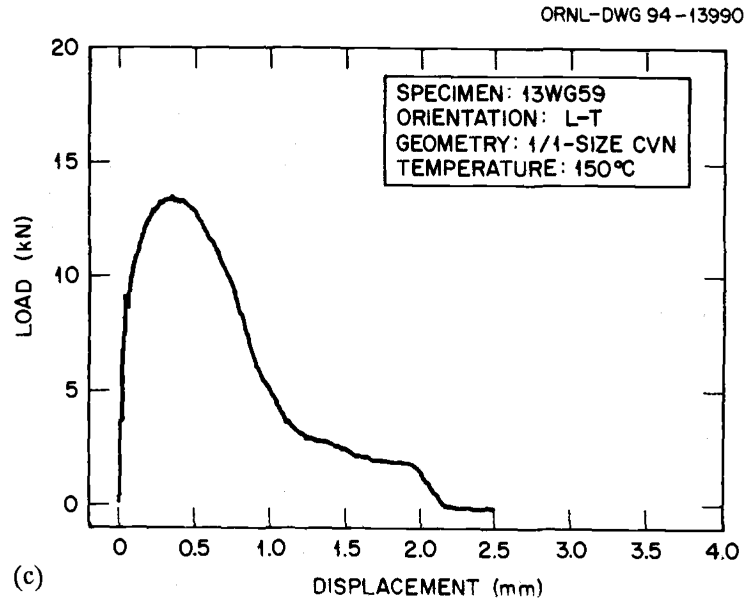

(c)

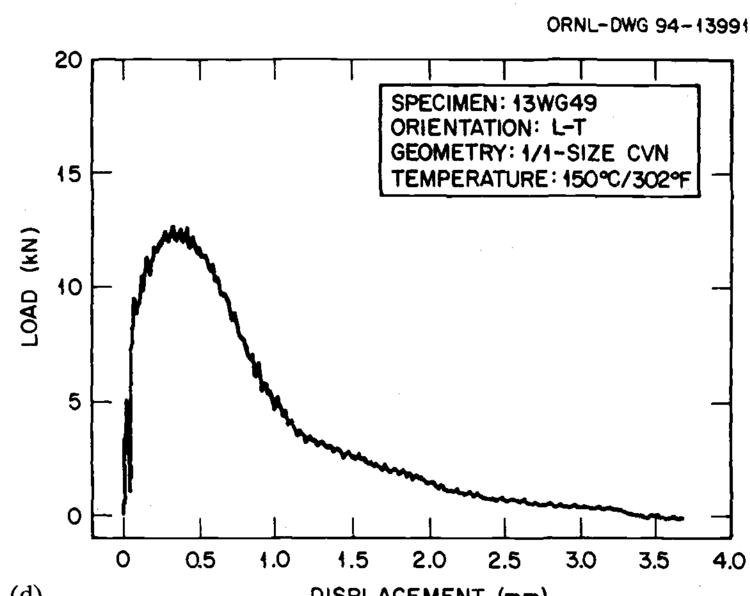

(d)

FIG. 12. (Continued)

result in additional energy reflected by the machine dial. This observation does not explain the case presented earlier where the 2-mm striker showed a tendency to measure higher energy. Other factors, such as deeper penetration of the smaller striker into the test material and effects of more localized plastic deformation, may contribute to these observations. Differences in tensile properties, strength, and strain hardening, for example, likely contribute to a material-specific rationale for some of the observed results. This also applies to the lateral expansion observations. An analysis of all the test results regarding the load-time records, bending analyses, etc., has not yet been performed.

ESTIMATION OF SHEAR FRACTURE PERCENTAGE

Determination of the percentage of shear fracture is based on the measurement of the cleavage portion of the fracture surface of broken Charpy V-notch (CVN) specimens and comparison with the full fracture surface by any of four methods given in E-23 [1]. The disadvantage of such a procedure is the dependence of the measured percentage of shear on interpretation of the cleavage portion of the fracture surface which can vary from person to person. For example, the fracture surfaces of CVN specimens representing weld metal of reactor pressure vessels can be particularly difficult to interpret. In-service surveillance programs require the performance of tests remotely. Thus, the remote measurement of the percentage of shear on the fracture surface of irradiated specimens can be even more complicated. As a result, some researchers have attempted to develop a more objective and simple procedure by analyzing the instrumented CVN impact trace [6,7]. The main idea of that approach is based on association of the cleavage part of the fracture with the fast load drop observed on the load-time diagram of an instrumented CVN test. Moreover, the European Structural Integrity Society (ESIS) has prepared a draft of a standard method for the instrumented CVN test on metallic materials [8], which allows one to estimate an approximate value of the proportion of ductile fracture surface by using one of the following formulae:

$$\%\ \text{shear} = [1 - (P_{iu} - P_a)/P_m] \times 100\%\ , \tag{1}$$

$$\%\ \text{shear} = [1 - (P_{iu} - P_a)/(P_m - P_{gy})] \times 100\%\ , \tag{2}$$

$$\%\ \text{shear} = \{1 - (P_{iu} - P_a)/[P_m + 0.5\ (P_m - P_{gy})]\} \times 100\%\ , \tag{3}$$

$$\%\ \text{shear} = \{1 - \surd[P_{gy}/P_m) + 2]/3 \times [\surd P_{iu}/P_m - \surd P_a/P_m\} \times 100\%\ , \tag{4}$$

where P_{gy}, P_m, P_{iu} and P_a are characteristic points on the load-time diagram which will be described later.

This portion of the paper discusses the correlation between visually measured shear fracture percentages and those estimated from the load-time traces of the instrumented 8-mm and 2-mm design strikers. A typical load-time trace from an instrumented CVN test is presented in Fig. 13. The load at the point of general

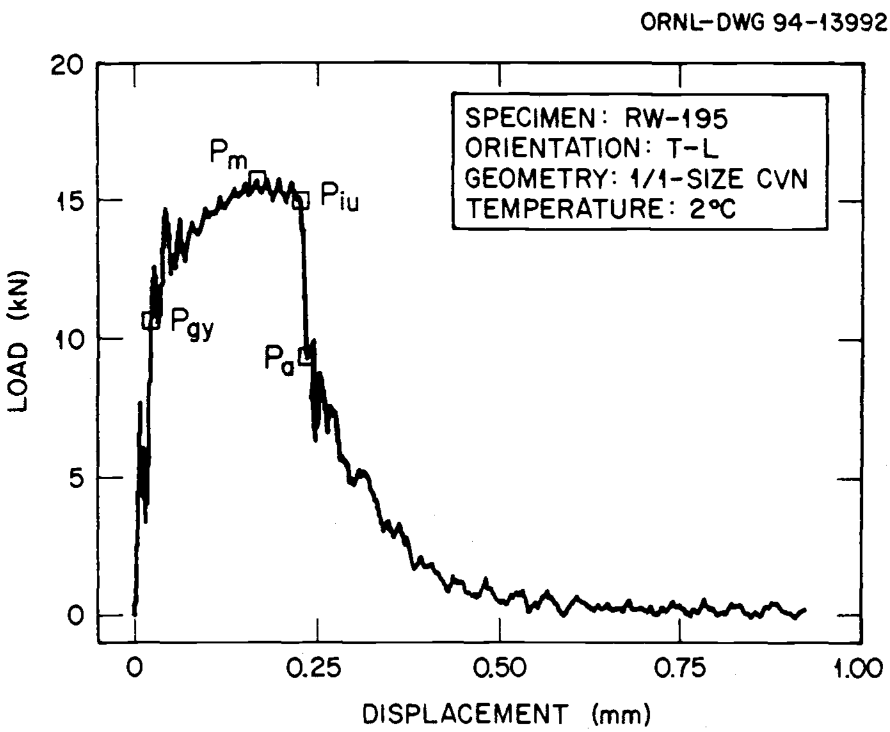

FIG. 13. Load versus time record showing the definitions of the various load points used in various models to estimate the percent shear fracture.

yield, P_{gy}, is a characteristic value of the onset of plastic deformation and it was determined as the load at the intersection of the linear rising portion of the load-time trace and the fitted curve through the oscillations of the load-time trace following the onset of the plastic strain part to maximum load. The maximum load, P_m, is the largest load in the course of the load-time trace and was determined as the maximum value on the fitted curve through the oscillations of the load-time trace in the area of the maximum load. The load at the initiation of unstable crack propagation, P_{iu}, characterizes the start point of the unstable crack propagation and was determined as the load at the beginning of the rapid drop-in-load in the load-time trace. The load at the end of unstable crack propagation, P_a, characterizes the point of crack arrest and was determined as the load at the end of the drop-in-load in the load-time trace.

The load-time traces of HSST Plate 03 and the LUS weld specimens, tested by 8-mm and 2-mm strikers, were analyzed using Eqs. (1) through (4) to calculate the value of percent shear fracture. The calculated values were then compared with the visually measured percent shear fracture (see Figs. 14 through 17). No significant differences were observed between values of shear calculated from instrumented 8-mm or 2-mm striker traces for all four models. Thus, the same approach can be used for both striker geometries. Furthermore, each of the four models provides an overestimation of percent shear compared with the visually measured value. Of the four models (i.e., equations), the relatively simple model 1 showed closer correlation with visually measured percent shear. The more complicated model 4 showed the worst correlation. This overestimation can be explained by closer consideration of the proposed models. The main approach is based on association of the cleavage portion of the fracture with the ratio of the drop-in-load value ($P_{iu} - P_a$) to the maximum load P_m in model 1, with some variations in models 2, 3, and 4. The maximum load P_m is considered the point at the beginning of crack extension. However, the ductile portion of the fracture can be formed also during flow of the material (plastic deformation), which begins at the point of general yield. Taking that into account, then, we consider an equation:

$$\%\ \text{shear} = [1 - (P_{iu} - P_a)/0.5\,(P_{gy} + P_m)] \times 100\%\ , \tag{5}$$

as a more reasonable formula for estimation of the percentage of shear fracture from the instrumented CVN specimen test, where $0.5(P_{gy} + P_m)$ can be assumed to be the load at the point of material flow. Comparison of visually measured and calculated percent shear by the proposed Eq. (5) shows good correlation (see Fig. 18). In the range of small percentages of shear calculation, Eq. (5) can provide negative values which should be assumed equal to zero. Determination of percent shear fracture based on calculation from the instrumented striker provides a more objective value and can be especially worthwhile for testing of irradiated specimens or any specimens where interpretation of the fracture surfaces could be difficult.

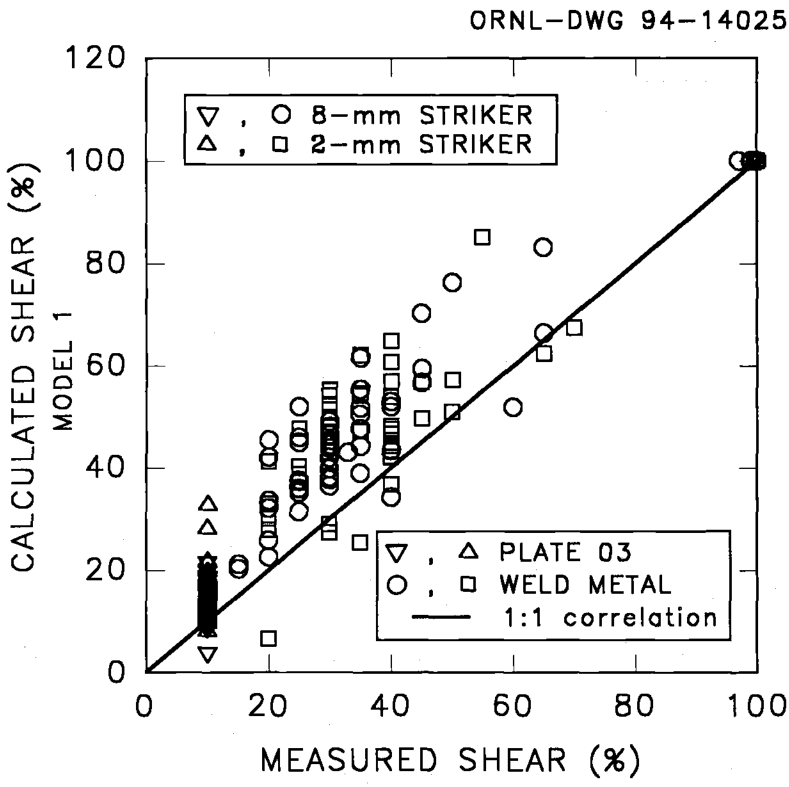

FIG. 14. Calculated shear from instrumented strikers using Model 1 (see text) versus visual measurements for A 533 grade B class 1 steel (HSST Plate 03) and a high-copper, low upper-shelf submerged-arc weld metal.

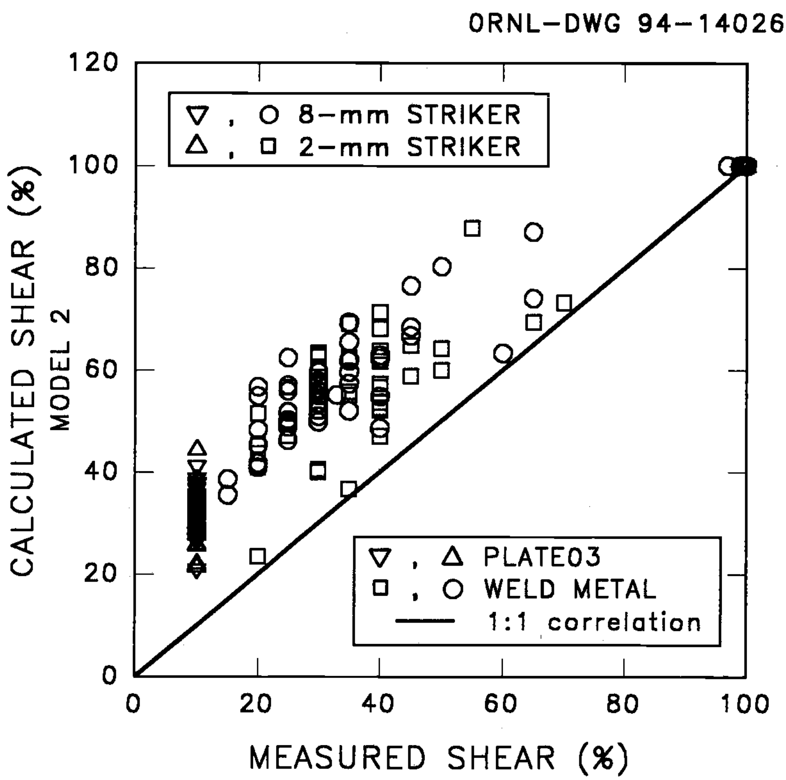

FIG. 15. Calculated shear from instrumented strikers using Model 2 (see text) versus visual measurements for A 533 grade B class 1 steel (HSST Plate 03) and a high-copper, low upper-shelf submerged-arc weld metal.

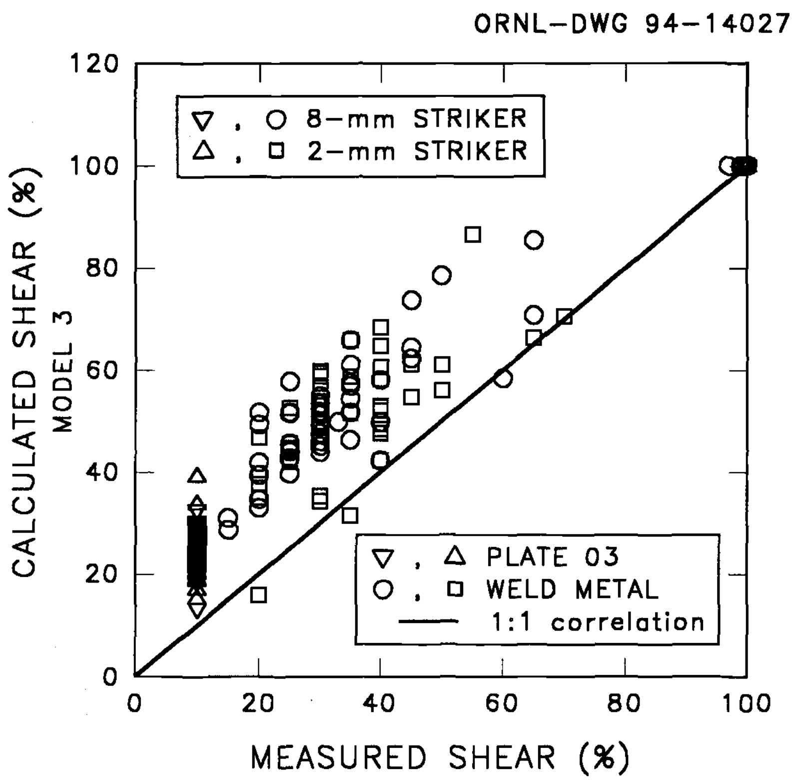

FIG. 16. Calculated shear from instrumented strikers using Model 3 (see text) versus visual measurements for A 533 grade B class 1 steel (HSST Plate 03) and a high-copper, low upper-shelf submerged-arc weld metal.

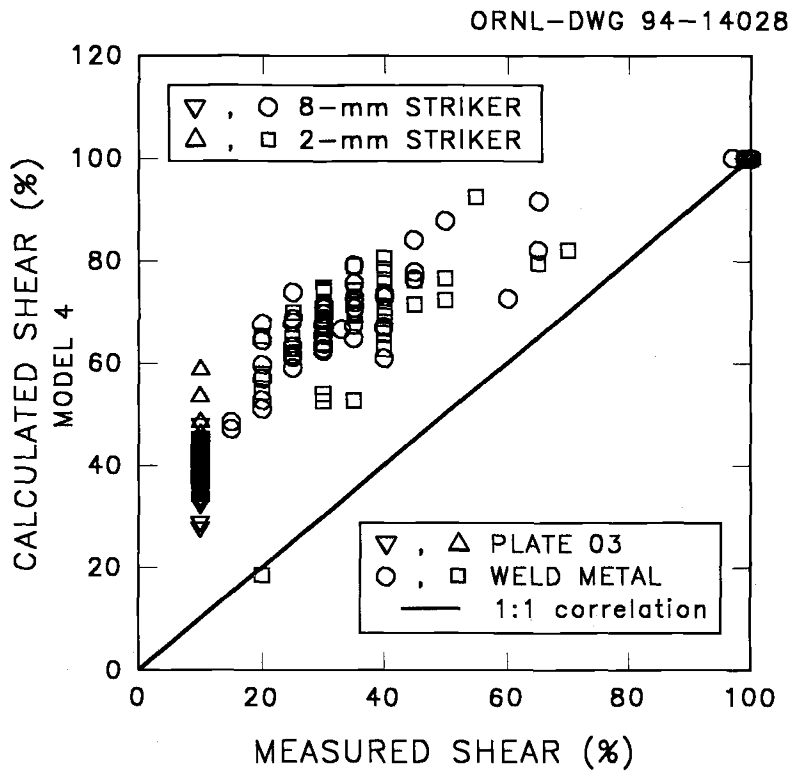

FIG. 17. Calculated shear from instrumented strikers using Model 4 (see text) versus visual measurements for A 533 grade B class 1 steel (HSST Plate 03) and a high-copper, low upper-shelf submerged-arc weld metal.

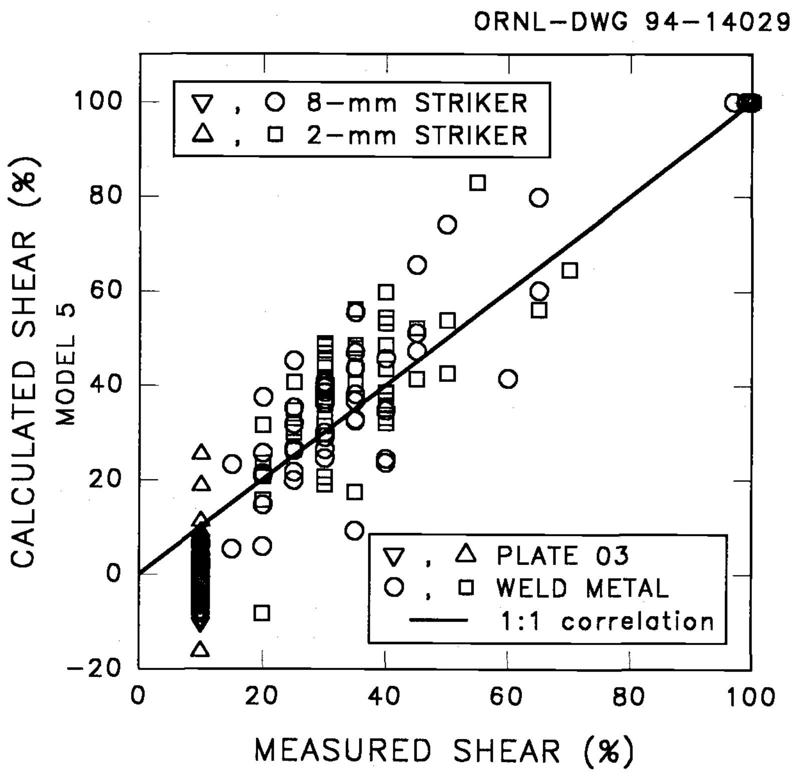

FIG. 18. Calculated shear from instrumented strikers using ORNL proposed model (see text) versus visual measurements for A 533 grade B class 1 steel (HSST Plate 03) and a high-copper, low upper-shelf submerged-arc weld metal.

CONCLUSIONS

Five different low-alloy pressure vessel steels, a U.S. plate, a Russian forging, and two U.S. submerged-arc welds, were tested in various programs to evaluate differences in test results between the instrumented 8-mm and 2-mm strikers. The number of replicate tests ranged from as low as 2 to as high as 46. Although most of the testing was performed on the same machine, comparisons were also made with results from other machines. Testing with each striker was also conducted with the high-strength 4340 steel verification specimens supplied by NIST. Additional analyses of the test results, especially the force-time traces, remain to be performed, but the following observations and conclusions can be stated:

1. The results of tests of the NIST verification specimens with 2-mm and 8-mm strikers show close agreement at the "low" (16-J) and "high" (~102-J) energy levels, but the 2-mm striker measured about 11% lower energy at the "super high" (~217-J) level.

2. For energy measurements, the overall results for the low-alloy steels showed good agreement, within one standard deviation, up to about 175 J.

3. For lateral expansion measurements, the overall results for the low-alloy steels showed somewhat greater values, up to about 8%, for the 2-mm striker tests.

4. The load-time record from the instrumented 8-mm striker sometimes shows an effect of loading not associated with fracture of the specimen.

5. The instrumented striker load-time record can be used to estimate the percent shear fracture and a proposed model shows good agreement with visual measurements. In this regard, no differences were observed between the 2-mm and 8-mm strikers.

ACKNOWLEDGMENTS

The authors acknowledge the programmatic support of the Heavy-Section Steel Irradiation Program at ORNL, managed by Bill Corwin; conduct of the Charpy impact tests by Eric Manneschmidt and John Henry at ORNL and Yuri Korolyev at Kurchatov Institute; supply of Charpy data from Prometey Institute by Dr. Vladimir Nikolayev; and preparation of the technical manuscript by Julia Bishop.

REFERENCES

[1] Standard Method for Notched Bar Impact Testing of Metallic Materials. ASTM Standard E-23, *Annual Book of ASTM Standards*, Vol. 03.01, American Society for Testing and Materials, Philadelphia, 1994.

[2] International Standard ISO 148, Steel - Charpy Impact Test (V-Notch), International Organization for Standardization, Switzerland, 1983.

[3] O. L. Towers, "Effects of Striker Geometry on Charpy Results," *Metal Construction*, 15(11), 682-686 (1983).

[4] T. Naniwa, M. Shibaike, M. Tanaki, H. Tani, K. Shiota, N. Hanawa, and T. Shiraishi, "Effects of the Striking Edge Radius on the Charpy Impact Test," *Charpy Impact Test: Factors and Variables, ASTM STP 1072*, John M. Holt, Ed., American Society for Testing and Materials, Philadelphia, 1990.

[5] G. Revise, "Influence of Dimensional Parameter of an Impact Test Machine on the Results of a Test," *Charpy Impact Test: Factors and Variables, ASTM STP 1072*, John M. Holt, Ed., American Society for Testing and Materials, Philadelphia, 1990.

[6] D. A. Canonico, W. J. Stelzman, R. G. Berggren, and R. K. Nanstad, "Use of Instrumented Charpy Tests to Determine Onset of Upper-Shelf Energy," *Weld. J. (Miami)* 60(5), 85-91 (May 1981).

[7] R. K. Nanstad and R. G. Berggren, *Irradiation Effects on Charpy Impact and Tensile Properties of Low Upper-Shelf Welds, HSSI Series 2 and 3*, NUREG/CR-5696 (ORNL/TM-11804), August 1991.

[8] ESIS Instrumented Charpy-V Standard, *Proposed Standard Method for the Instrumented Charpy-V Impact Test on Metallic Materials*, Draft 10, European Structural Integrity Society, January 14, 1994.

Thomas A. Siewert[1] and Daniel P. Vigliotti[1]

THE EFFECT OF CHARPY V-NOTCH STRIKER RADII ON THE ABSORBED ENERGY[2]

REFERENCE: Siewert, T.A. and Vigliotti, D.P., "**The Effect of Charpy V-notch Striker Radii on the Absorbed Energy,**" Pendulum Impact Machines: Procedures and Specimens for Verification, ASTM STP 1248, Thomas A. Siewert and A. Karl Schmieder, Eds., American Society for Testing and Materials, Philadelphia, 1995.

ABSTRACT: The two most common Charpy V-notch striker designs (8-mm and 2-mm radii on the striking edge) were compared using verification (reference-grade) impact specimens. Other variables in the test matrix included two different brands of U-type pendulum machines and four different specimen energy ranges (near 18, 45, 100, and 200 J). In this comparative study, we found a very small difference between the two striker designs and an even smaller difference between the two brands of machines. At 200 J, the difference between the two striker designs was about 10 J. This difference might not be important in most production testing, but must be considered in verification testing where the acceptable range may be 5 %. The standard deviations of absorbed energy for the two strikers were similar, except at 200 J where the 2-mm striker produced standard deviations about 3 times higher than the 8-mm striker.

KEYWORDS: absorbed energy, Charpy V-notch, impact test, striker radius, verification specimens

Two different striker designs are commonly found on Charpy V-notch (CVN) machines. These two common designs are described in ASTM E23 and ISO Standard R442-1965 (presently being revised by ISO TC 164/SC 4) and are distinguished primarily by the radii of the leading edge that strikes the specimen, prompting their common identification as the 8-mm and 2-mm strikers, respectively [1]. Figure 1 compares the specified profiles near the nose of the two striker designs. The 8-mm striker is more common in the U.S. and is required for the CVN testing procedure described in ASTM Standard E 23 [2]. The 2-mm striker is more

[1]Supervisory Metallurgist and Technician, respectively, Materials Reliability Division, National Institute of Standards and Technology, Boulder, Colorado 80303

common in Europe and Asia. A few machines with the less common strikers are also found in each country, since some companies have contracts with organizations in other countries that require impact data with the other striker design. The difference in the dimensions between the two strikers is many times greater than the tolerances, so there is no possibility of producing a striker that can meet the requirements of both designs.

Interchanging strikers (of the two designs) on a single impact machine is not a simple solution for obtaining data with the two strikers. One reason for not interchanging strikers is that replacing a striker can be very difficult for certain machine designs. Further, ASTM Standard E 23 requires recertification of the machine performance when the striker is changed [2]. The generally accepted justification for this requirement is that improper mounting of a striker could have such an effect on the machine performance that the machine would fall outside the certification limits.

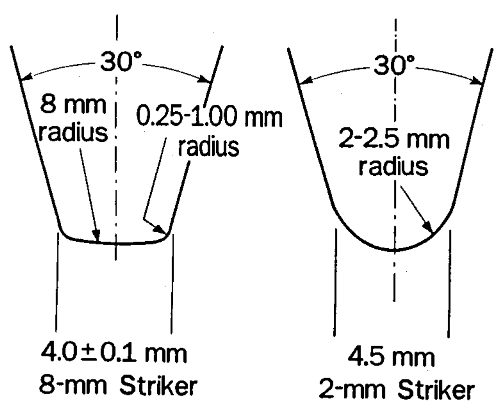

Figure 1. Comparison of the 8- and 2-mm striker dimensions.

Recent comparisons of the two striker designs have reported differences in the energies. A study by Fink describes the effects of striker radius (8 mm versus 2 mm) and notching procedure on the energy [3]. He reported a linear correlation between the energies (in ft-lb) produced with the two strikers,

$$(E_{2\text{-mm}}) = 1.0420\ (E_{8\text{-mm}}) + 0.5160,$$

with a coefficient of determination (r^2) of 0.9987 and a standard error of estimate of

1.36 ft-lb. In metric units, (with the number of significant digits reduced to reflect the standard error), this equation is

$$(E_{2\text{-mm}}) = 1.042\ (E_{8\text{-mm}}) + 0.70,$$

where E is expressed in joules. The coefficient of determination (r^2) is 0.9987 and the standard error of estimate is 1.84 J. The study included three steels (AISI 4340, ASTM A 537, and HY-80) covering the range of 15 to 200 J.

A study by Naniwa et al. also compares the effect of the two striker designs [4]. They compared steels over a range in strengths to produce a range in CVN energies (well distributed within the range of 100 to 400 J when tested with the 8-mm striker). They did not report any difference between the two striker designs for energies below 200 J, but found that the absorbed energy with the 8-mm striker was greater than that with the 2-mm striker for energies above 200 J. The difference in absorbed energies was as great as 100 J when the 2-mm striker indicated 300 J. This conclusion is in opposition to the relationship reported by Fink, who indicated that the 2-mm striker developed the higher energies.

The conflicting conclusions in these two reports indicated a need to further investigate the effects of striker design. Ideally, a relationship might be developed between the data generated with the two strikers, so that data for either striker could be calculated from the other. At least, there is a need to understand the reason for the different conclusions in these two studies. In this report, we compare the results when high-precision verification specimens were tested on two different brands of CVN machines using both striker designs.

EXPERIMENTAL PROCEDURE

The primary purpose of our program was to evaluate the effects of striker design (8 mm versus 2 mm) over a range in absorbed energy, but we broadened the test matrix to include machine-specific effects. The machine-specific effects were evaluated with two brands of U-type pendulum machines.

We produced specimens with mean energies near the verification ranges currently used in the United States (18, 100, and 200 J) and additional specimens near 45 J. We used the same steel from which we manufacture the verification specimens (NIST Standard Reference Materials - SRM 2092, 2096, and 2098). We used a heat-treatable low-alloy steel for absorbed energies up to 100 J and a maraging steel for the 200 J energy. We obtained mean energies from 18 to 100 J in the low-alloy steel by varying the heat treatment (tempering temperature), with the lowest energies being produced by the treatments with the highest hardnesses. A wide range of energies was considered important because we wanted to span the ranges of the Fink and the Naniwa studies. We were most interested in the effect at 18 J because this is the energy that is most commonly the cause of a machine failing the verification test using the NIST specimens. It is also the energy closest to the requirements of many fabrication standards that require a minimum CVN energy. We do not yet have a reference grade material with energies near 400 J, so we were unable to reevaluate the upper end of the trend noted by Naniwa et al.

Each CVN test is destructive; an individual specimen cannot be evaluated again (without complex reconstitution techniques). To allow us to compare machines, we produced our specimens in conveniently sized batches (also called series), each identified by one or two letters followed by one or two numbers. The specimens in each batch were kept together through the machining and heat treating operations to minimize the effect of processing variables. Each batch was divided into fourths at random, providing between 5 and 11 specimens from each batch for testing on each machine at each combination of energy range and striker. These data were analyzed to obtain an estimate of the standard deviation in the absorbed energy for each combination.

The use of reference-grade specimens (meeting all the requirements of E 23, but with stricter controls on their manufacturing procedures) was the most important part of our procedure. These steels and heat treatments are characterized by a narrow spread in the energy, which permits very small effects to be resolved. Verification specimens consistently have standard deviations of 5% or less of the mean energy, standard deviations smaller than those for most commercial steels. ASTM Research Report E28-1014 lists 2.4 J as the 95% Repeatability Limit for these 18-J absorbed-energy verification specimens when evaluated by the ASTM E 691 interlaboratory test procedure [5,6].

We purchased two new CVN machines (from different manufacturers), each with both the 8-mm and 2-mm strikers. We selected new machines so they would reflect the latest in machine design and construction techniques. Each was of the U-pendulum design (see Ref. 2), and had a maximum capacity of 405 J (300 ft-lb). On both machines the strikers were held in place by only four bolts and could be removed and replaced easily.

The machines were carefully mounted according to the requirements of ASTM E 23. Both machines were evaluated with NIST verification specimens and were certified to the requirements of E 23. We also checked the machine's performance with NIST-certified reference materials for CVN machines (5 specimens at 18-J nominal energy and 5 specimens at 100-J nominal energy) after removing and remounting the strikers. We could detect no differences in the mean or standard deviation of the specimen energies after striker replacement. Apparently these two machines have very tight striker mounting tolerances and have mounting designs that permit accurate realignment of the striker.

We used a single operator to perform the tests and to record the data, to further reduce the variation in the data. The strikers were changed after testing each series, a total of 8 changes on each machine. A machine's performance was not checked after each change in the strikers. Our initial tests of striker replacement with NIST-certified specimens convinced us that changing the strikers on these machines had an effect smaller than we could measure. The specimens with mean energies near 18, 45 and 100 J were tested at -40°C, and the specimens with mean energies near 200 J were tested at room temperature.

RESULTS AND DISCUSSION

Table 1 lists the mean energies obtained for each combination of energy range, machine, and striker. Figure 2 shows the data from Table 1 as an X-Y plot with the 8-mm data along the Y axis and the 2-mm data along the X-axis. The data fall very close to the solid line, which represents a one-to-one relationship between the two strikers, so close that it is difficult to determine the fine structure on this scale. To reveal the small differences between the two strikers, we have replotted the data in Figure 3 as the difference in the energy (2-mm minus 8-mm) for the various combinations of the test matrix. Either the 2-mm or 8-mm data could have been selected for the horizontal scale: we arbitrarily selected the 8-mm data for this axis. Figure 3 shows that the 2-mm striker gives higher energies than the 8-mm striker at 45 J, and vice-versa at 200 J. It also indicates that the two brands of machines have similar behavior.

Table 2 lists the standard deviation for each combination of energy range, machine, and striker, together with the number of specimens tested. We have plotted the standard deviation as a vertical bar extending one standard deviation both above and below the mean data from Figure 3. Figure 4 is intended only to show how the standard deviation compares to the bias in the means as a function of energy. A detailed comparison of the standard deviations for the two strikers is included near the end of this section. Figure 4 reveals that the standard deviation is roughly proportional to the energy, increasing with increasing energy. The means for the two different machines differ by less than one standard deviation, according to the data from Table 2, suggesting that the machine effect is small. However, Figure 4 shows the difference between the two strikers is sometimes greater than one standard deviation in the 8-mm data, at least for certain energies. The difference between the two strikers is less than one standard deviation at 18 J, slightly more than one standard deviation at 45 J, nearly 0 at 100 J, and about two standard deviations at 200 J. We interpret this to indicate that the radius of the striker nose can be an important parameter, varying in importance as a function of energy.

Table 1. Averages (Mean) Energy from CVN Testing of Reference-Grade Specimens

Specimen Series	CVN Machine Brand	8-mm Striker, J	2-mm Striker, J	Difference,* J
LL-39	A	18.3	18.6	0.3
	B	18.1	18.4	0.3
LL-40	A	18.5	18.8	0.3
	B	18.4	18.2	- 0.2
M-6	A	43.3	45.2	1.9
	B	44.0	45.8	1.8
HH-37	A	112.5	115.1	2.6
	B	116.7	114.0	- 2.7
HH-39	A	99.8	102.0	2.2
	B	104.7	103.2	- 1.5
HH-40	A	100.5	99.8	- 0.7
	B	100.9	101.7	0.6
SH-1	A	215.9	204.1	- 11.8
	B	216.5	200.9	- 15.6
SS-1	A	225.2	215.6	- 9.6
	B	223.8	215.3	- 8.5

* Derived by subtracting the 8-mm absorbed energy from the 2-mm absorbed energy.

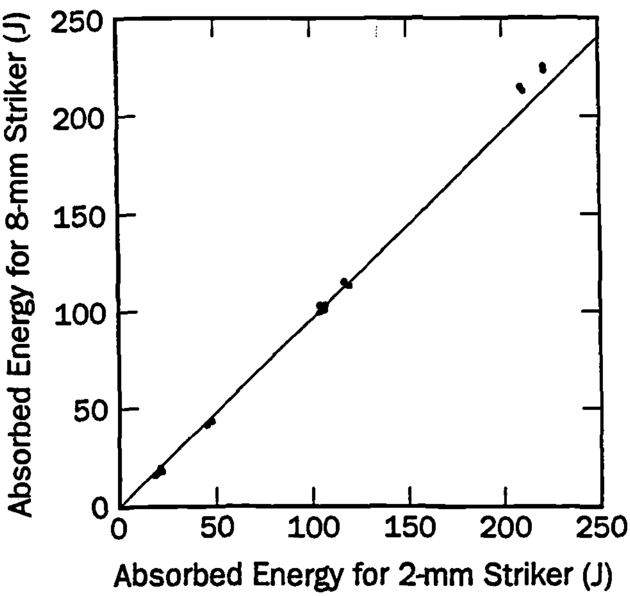

Figure 2. Energy means when tested by the two striker designs. Each point represents data from a single batch tested by the two strikers.

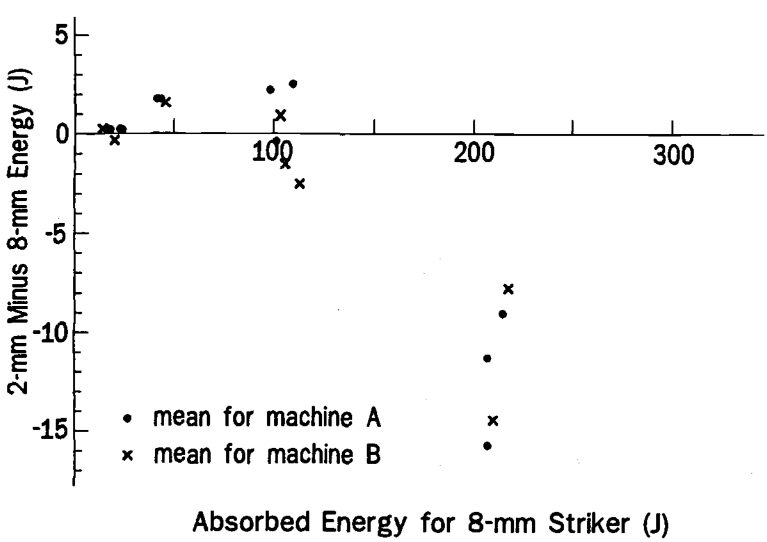

Figure 3. Graphical representation of the differences in the means for the data in Table 1 (2-mm minus 8-mm striker data for each series and each machine).

Table 2. Standard Deviations of the Energy from CVN Testing of Reference-Grade Specimens

Specimen Series	Number of Specimens in Series*	CVN Machine Brand	8-mm Striker, J	2-mm Striker, J
LL-39	40	A	0.48	0.36
		B	0.60	0.35
LL-40	40	A	0.43	0.58
		B	0.86	0.44
M-6	20	A	2.25	2.02
		B	1.81	2.21
HH-37	44	A	3.61	3.85
		B	3.36	3.48
HH-39	44	A	1.81	2.88
		B	3.64	3.32
HH-40	36	A	2.77	2.29
		B	3.38	2.35
SH-1	20	A	4.70	11.60
		B	2.51	11.67
SS-1	20	A	5.41	16.56
		B	2.57	12.97

* Number of specimens in a series which was split between two machines and two strikers, so each standard deviation is based on one-fourth of this number.

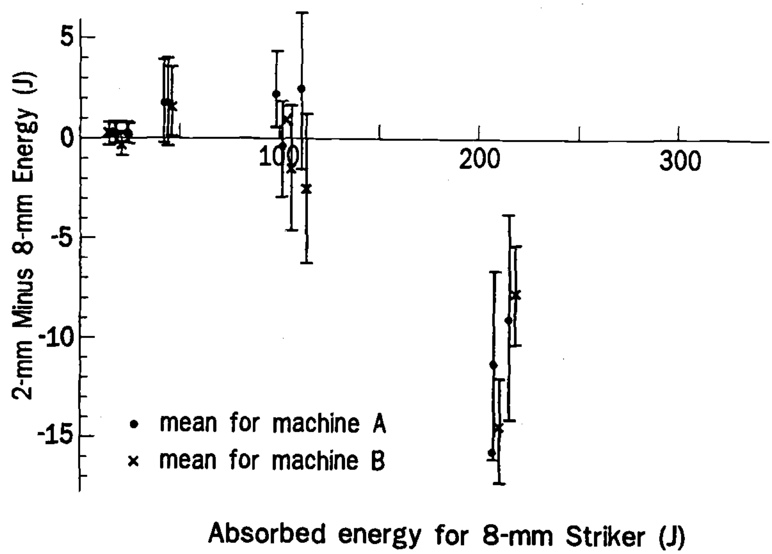

Figure 4. Graphical representation of the standard deviations for the 8-mm striker data in Tables 1 and 2.

The data in the Naniwa report were only graphical and the uncertainties in recovering the correct energies have precluded us from attempting to develop statistical measures of the scatter. Their report suggests that they performed a comparison similar to ours, splitting batches for testing by the two striker designs. Figure 5, which we have reproduced from their report, shows their data as the open circles on a plot with the two energies on the two axes [4]. We have added our data as solid circles, Fink's data as X's, and a line which represents our best estimate of the mean of the Naniwa data. The apparent scatter in their data suggests a standard deviation near 40 J. Unfortunately, the scale necessary to contain the Naniwa data is so coarse that the fine structure in the data below 100 J (the Fink data and our data) can not be resolved.

To show the small differences between the two strikers, we have replotted in Figure 6 our standard deviation data, the Fink data, and the mean for the Naniwa data in this energy range, as difference between the two strikers versus the mean. We have drawn smooth lines through both the upper and lower bounds of our standard-deviation data from Figure 4 and shaded the band between them. Although we have data gaps with our energy range that could affect the shape of the band in between our data, the band shows the general trend of our data and emphasizes that the differences between the two striker designs are nonlinear. Figure 6 indicates that the 2-mm striker (relative to the 8-mm striker) has a small positive bias that grows as the mean energy increases from 18 to 45 J, then decreases and goes negative.

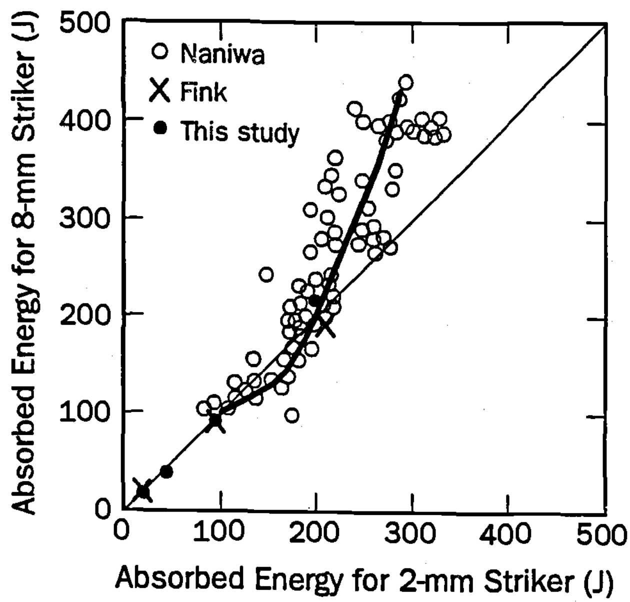

Figure 5. Data from the Naniwa study as open circles (Figure 3a in their report) to which we have added a line indicating the approximate mean, the Fink data, and our data.

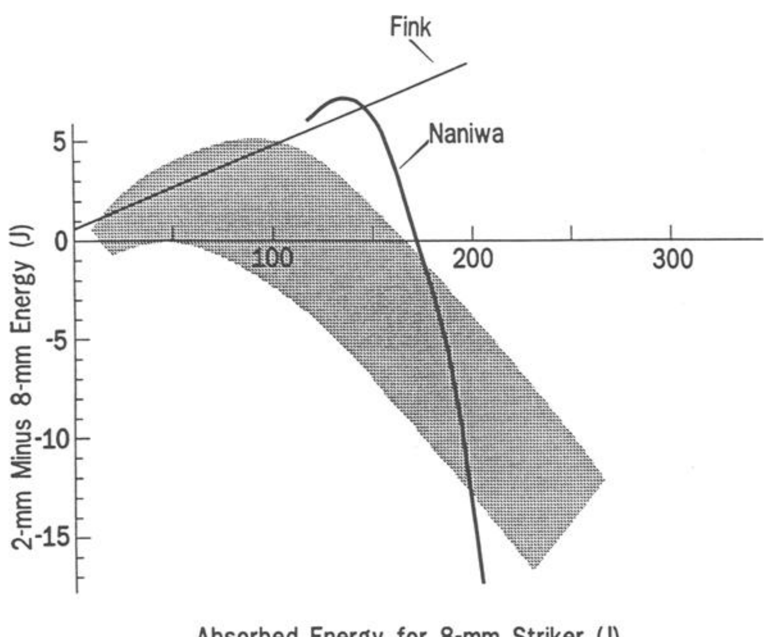

Figure 6. Comparison of our standard deviation scatter band to the mean of the data reported by Fink and Naniwa et al.

The Naniwa data appear to support the negative trend that we observed above 100 J. It is not surprising that steels with this large a standard deviation in absorbed energy would not resolve the trend noted by Fink between 100 and 200 J.

Our band follows the relationship reported by Fink [Equation (2)] up to about 100 J. In this range, Fink used materials that were very similar to ours, and this may help to explain the good fit with our data. Beyond this, our data indicate a significant negative deviation from his prediction. Fink's report included all his data in tabular format, so we were able to calculate standard deviations for his data [3]. Although his data near 200 J show a positive bias, the standard deviation (15 J) is sufficiently large that our mean is within one standard deviation of his mean. However, the HY-80 material that he used for his 200 J specimens has a composition and microstructure significantly different than those for the martempering steel that we used in this range, so there might be a material effect, perhaps hardness or strain hardening.

These results indicate that great caution should be used when comparing the data developed on two different striker designs. Data generated with the wrong striker (a striker other than the striker specified in a standard or testing protocol) should be used only to obtain a rough estimate of material performance. Conversion of data generated with one striker to the other type of striker is subject to the uncertainty of our scatterband and additional uncertainty if the material properties are different from those used in our study. While the difference above 200 J is most dramatic, the bias between the two strikers appears to be about 0.3 J for an energy near 18 J. This bias seems small but can be important when material is very near a specification requirement. The 1.8 J bias at 45 J makes comparison of data developed with the two different strikers even more difficult in this range.

We noticed one other difference between the two designs of striker. Figure 7 shows the standard deviation in our data by striker. Both strikers had similar standard deviations (following a linear trend) up to 100 J, but at 200 J we found a significant difference. For both machines and with two different batches of specimens, we found the same result: the 2-mm striker produced standard deviations at 200 J about 3 times as great as those with the 8-mm striker. We have not yet found the reason for the difference, but it does suggest that the 8-mm striker produces more reproducible results when testing materials with absorbed energies of 200 J. Perhaps this is due to the fact that there is a greater tendency for specimens to wrap around the 2-mm striker in this energy range, rather than completely separate into two pieces.

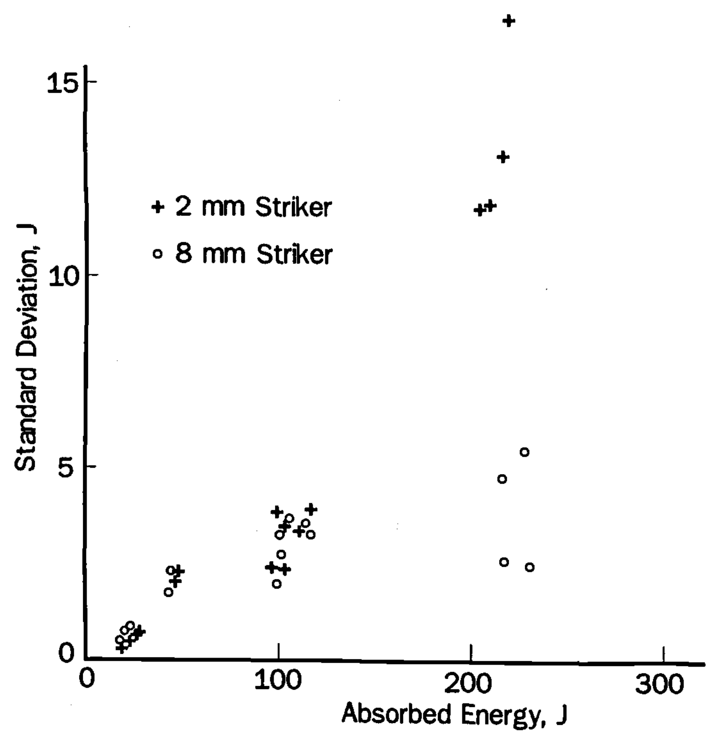

Figure 7. Comparison of the standard deviation in the energies for the two strikers.

CONCLUSIONS

1. Up to 100 J, the two striker designs produce very similar data, differing by less than one standard deviation (2 to 5%) of the energies when measured with verification specimens. The practical effect of this difference is small, based on the qualitative nature of CVN impact testing.

2. At 200 J, the differences exceed one standard deviation, being about 10 J.

3. Although the differences between the two strikers are small they must be considered in a verification program, where the acceptable range may be near 5 %.

4. The difference between energies measured using 2-mm and 8-mm strikers is complex. It is unlikely that a general relationship can be developed that will allow one machine to be certified for both strikers from a test with only one

striker (except perhaps for low energies, where the difference is least).

5. The 8-mm striker produces a 3-times-smaller standard deviation that the 2-mm striker near 200 J, but no explanation for this effect is yet apparent.

REFERENCES

1. ISO Standard R442, "Verification of Pendulum Impact Testing Machines for Testing Metallic Materials," International Organization for Standards, 1965.

2. ASTM Standard E 23-92, "Standard Test Method for Notched Bar Impact Testing of Metallic Materials", Annual Book of ASTM Standards, American Society for Testing and Materials, Philadelphia, Pennsylvania, 1992.

3. D.A. Fink, "Quantitative Comparison and Evaluation of Various Notch Machining Methods and how They Affect ASTM E 23 and ISO R442 Testing Equipment Results," Charpy Impact Test: Factors and Variables, ASTM STP 1072, ed. J.M. Holt, American Society for Testing and Materials, Philadelphia, 1990.

4. T. Naniwa, M. Shibaike, M. Tanaka, H. Tani, K. Shiota, N. Hanawa, and T. Shiraishi, "Effects of the Striking Edge Radius on the Charpy Impact Test," Charpy Impact Test: Factors and Variables, ASTM STP 1072, ed. J.M. Holt, American Society for Testing and Materials, Philadelphia, 1990.

5. Research Report: E28-1014, "Interlaboratory Test Study for the Determination of Precision and Bias in Charpy V-notch Impact Testing," D.A. Shepherd and T.A. Siewert, available from American Society for Testing and Materials, Philadelphia, 1991.

6. ASTM Standard E 691-87, "Practice for Conducting an Interlaboratory Test Program to Determine the Precision of Test Methods," Annual Book of ASTM Standards, American Society for Testing and Materials, Philadelphia, 1987.

Megumu Tanaka, Yoshinobu Ohno, Hidekazu Horigome, Hiroshi Tani, Kenichiro Shiota, and Akinori Misawa

EFFECTS OF THE STRIKING EDGE RADIUS AND ASYMMETRICAL STRIKES ON CHARPY IMPACT TEST RESULTS

REFERENCE: Tanaka, M., Ohno, Y., Horigome, H., Tani, H., Shiota, K., and Misawa, A., "Effects of the Striking Edge Radius and Asymmetrical Strikes on Charpy Impact Test Results," Pendulum Impact Machines: Procedures and Specimens for Verification,, ASTM STP 1248, Thomas A. Siewert and A. Karl Schmieder, Eds., American Society for Testing and Materials, Philadelphia, 1995.

ABSTRACT: The effects of the striking edge radius of the Charpy impact test on the absorbed energy and lateral expansion were investigated. The effects of the changes of the length of test specimens and effects of symmetry of test specimens was also investigated. The absorbed energy of the 8mmR's was higher than the 2mmR's as in the study by Naniwa et al.[1]. For every machine tested, the absorbed energy was higher when the striking point did not contact the specimen opposite the notch. The effects of the length of test specimens were larger when the asymmetric test specimens were tested.

KEYWORDS: Charpy impact test, pendulum striking edge,absorbed energy, lateral expansion, striking point, location of notch

INTRODUCTION

Two different types of strikers are found in Charpy impact tests. The radius of ISO and JIS type Charpy impact testing machines is 2mm (2mmR's), and the radius of ASTM type Charpy impact testing machines is 8mm (8mmR's). So,the ironworks in Japan must have both two types of machines in order to keep both of these standards. Maintaining two types of machines interferes with attempts to establish intensive and automated facilities in the near future. During the establishment of the ISO standard for Charpy impact testing machines, there were discussions to standardize the test around the 2mmR's, however the 8mmR's was also standardized. If the ASTM standard accepts the 2mmR's, many companies can avoid maintaining both types of Charpy impact

Y. Ohno is with Nippon Steel Corp., M.Tanaka and H.Horigome are with NKK Corp., H.Tani is with Sumitomo Metal Industries,Ltd., K.Shiota is with Kobe Steel,Ltd., A.Misawa is with Kawasaki Steel Corp.. All the members belong to The Mechanical Testing Subcommitee, The Joint Research Society of The Iron and Steel Institute of Japan, 9-4, Otemachi-1-Chome,Chiyoda-Ku, Tokyo,Japan.

testing machines.

It is commonly understood in Japan, that the absorbed energy obtained from the 8mmR's is higher than that of 2mmR's when the absorbed energy is above 200J. There were two reports in the last (1989) ASTM symposium concerning this point[1],[2].

The verification of the specifications for JIS type Charpy impact testing machines is now performed in the same manner as ASTM type Charpy impact testing machines by Class NK (Nippon Kaiji Kyoukai). The verification uses the total error factor taken from the test results.

On the other hand, National Institute of Standards and Technology (NIST) has supplied the standardized test specimens for the verification of 8mmR's on the level of absorbed energy L (about 20J),M (about 50J),and H (about 100J). Recently NIST began supplying SH (about 200J) test specimens for the demand from the users in the U.S.A..

In Japan, 400J class absorbed energy appears in the ful-curve test of Charpy impact tests, when the line pipe is for North Europe or the U.S.A.. It is a matter of strong concern whether the test results of absorbed energy are correct or not.

EXPERIMENTS

Material

Table 1 Materials Tested

No.	Material tested	YP (N/mm2)	TS (N/mm2)	El (%)
A	JIS SM570Q	579	662	26
B	JIS SM400C	315	450	36
C	JIS SM400B	289	444	42
D	API 5L X56	408	517	36

A,B,C : Rolled steels for welded structure
D : Line Pipe

YP:yield point
TS:ultimate tensile strength
El:total elongation

Determination of the temperature for experiments

Depending on the results of the full-curve tests performed by the ASTM type and ISO type Charpy impact testing machines, the temperature for experiments are determined by the lowest temperature when the absorbed energy becomes stable in the upper shelf side.

Checking of the capabilities of the machines

Nine test specimens sampled from the same lot are tested by each of 8 machines (ASTM 4,ISO 4) which are used for the experiments.

Investigation of the effects of the accuracy in manufacturing the test specimens

The experiments and the dimension of test specimens (TSP) prepared are shown in Table 2.

Procedure of experiments

The experiments were performed using the test specimens sampled from the same lot of the materials listed in Table 1.

Nine test specimens were tested in each case listed in Table2. The absorbed energy, the percent brittle fracture, and the lateral expansion were measured. The average,standard deviation, and each value of the test results were evaluated. Experiments were performed by the material test centers of four ironworks, and 36 test specimens sampled from the same lot were tested in each case listed in Table2.

Table 2 The Experiments

Radius of striker	Location of V-notch	Method of setting TP	Length of TSP mm				
			52.5	53.8	54.4	55.0	55.6
8mmR	center of TP	tongs	○	○		○	
		end-centering		○	○	○	
	end-oriented	tongs	○	○		○	
		end-centering		○	○	○	
2mmR	center of TP	tongs					
		end-centering		○	○	○	○
	end-oriented	tongs					
		end-centering		○	○	○	○

RESULTS

Determination of the temperature for experiments

The temperatures for experiments of materials were determined by the full-curve tests. There were no substantive difference in the transition temperature between two types of testing machines.

Table 3 Temperature for experiments (°C)

No.	Materials tested	Test Machine type	Transition temperature	temperature for experiment
A	JIS SM570Q	ASTM	-90	-20
		JIS	-96	
B	JIS SM400C	ASTM	-50	+20
		JIS	-50	
C	JIS SM400B	ASTM	-40	+30
		JIS	-39	
D	API 5L X56	ASTM	-129	-80
		JIS	-108	

Checking of the capabilities of the machines

The average and the standard deviations(1) of the absorbed energy were plotted in Figure 1. The horizontal axis shows the average of the absorbed energy obtained from the tests using 2mmR striker. The vertical axis shows the absorbed energy of 8mmR and the standard deviation between them.

(1)There were no remarkable difference among machines in the absorbed energy. The absorbed energy differs 20-45J in the case of 2mmR's, and 15-48J in the case of 8mmR's depending on materials. But no testing machines showed substantive difference in the test results with the same material.

(2)The standard deviation of the absorbed energy did not change so much while the level of absorbed energy differed in the range above 200J.

(3)The standard deviation of the absorbed energy is smaller and

stable in the case of 8mmR's than the case of 2mmR's.
Figure 2 shows the standard deviation in absorbed energy for specimens tested with 2mm and 8mm strikers. The results show the result of the difference of curvature of 2mm and 8mm strikers. In the case of 8mmR's, the fracture energy is combined with additional plastic deformation as the specimen is bent around the corners of striker. In the case of 2mmR's, the test specimens fractured instantaneously because of the small curvature. It is clear from the Photo 1 of the study by Naniwa et al[1]. And so, the results of 2mmR's seems to be more sensitive to the fracture characteristics of materials than 8mmR's.

(4)The absorbed energy and the lateral expansion are evaluated in Figure 3. The horizontal axis shows the average of the absorbed energy obtained from four 2mmR machines. The vertical axis shows the average of the lateral expansion and the absorbed energy of each machine.

Table 4 Angle of test specimens after tests (deg)

Test Machine type	Angle of test specimens
8mmR	52-54
2mmR	56-57

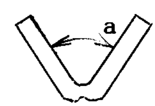

The test specimens halves did not separate in three of materials tested. The test results of these materials showed that the absorbed energy of 8mmR's were higher than 2mmR's. The absorbed energy of 8mmR's and 2mmR's were about the same, only in the case of the test specimens which indicated an absorbed energy about 260J, and these which separated after the tests.
Table 4 shows the fine angle between specimen ends for test specimens which did not separate after strike. In the case of 8mmR's, the angle of 52-54 deg was necessary for the test specimens to pass through the anvil, while the angle was 56-57 deg in the case of 2mmR's. These results may come from the behavior at the critical condition where the test specimens have the possibility of separation. In the case of 260J material, it was likely that the absorbed energy related to the friction did not appear when tested by 8mmR's and so the absorbed energy level was same as the case of 2mmR's.
In the cases that the test specimens did not separate, it is likely that the absorbed energy increases depending on the bending deformation of test specimens and the friction between the anvil and the test specimens like a study of Naniwa et al..

<u>Difference of the absorbed energy between 2mmR striker and 8mmR striker when the absorbed energy is above 200J</u>

The average(n=9) of the absorbed energy of test specimens which were used for the check of the capabilities of the machines for experiments are plotted in Figure 4, including the test results of the study of Naniwa et al.. The distribution of the

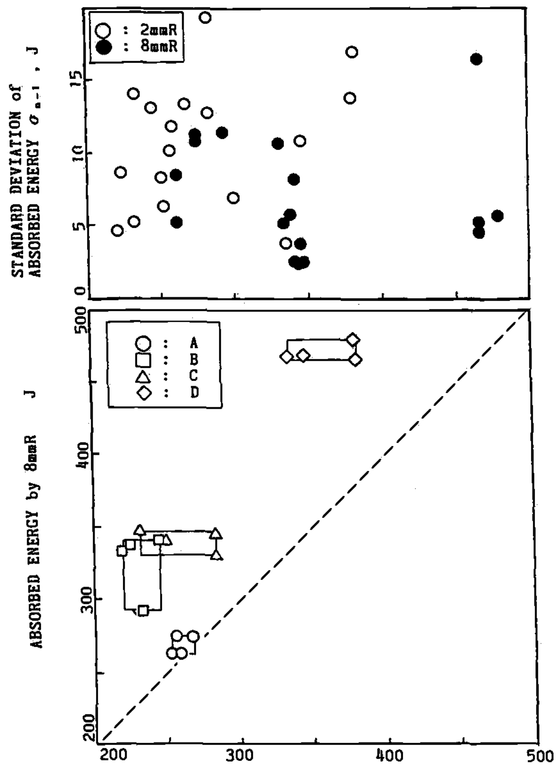

Figure 1 COMPARISION of AVERAGE and STANDARD DEVIATION of ABSORBED ENERGY

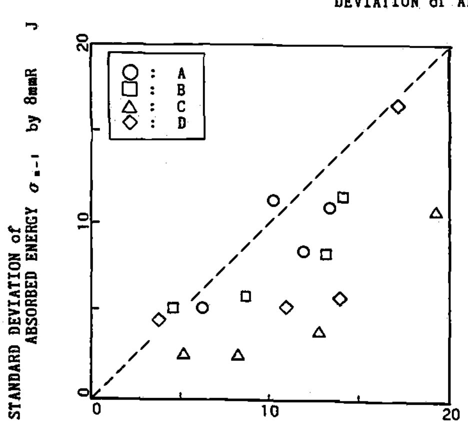

Figure 2 COMPARISION of STANDARD DEVIATION between 2mmR and 8mmR of ABSORBED ENERGY

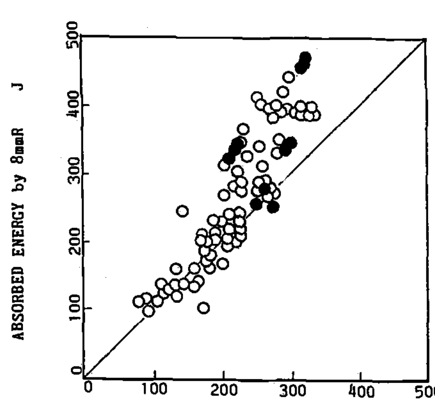

Figure 4 COMPARISION of ABSORBED ENERGY between 2mmR and 8mmR

○ : a study of Naniwa et al.
● : additional data (this report)

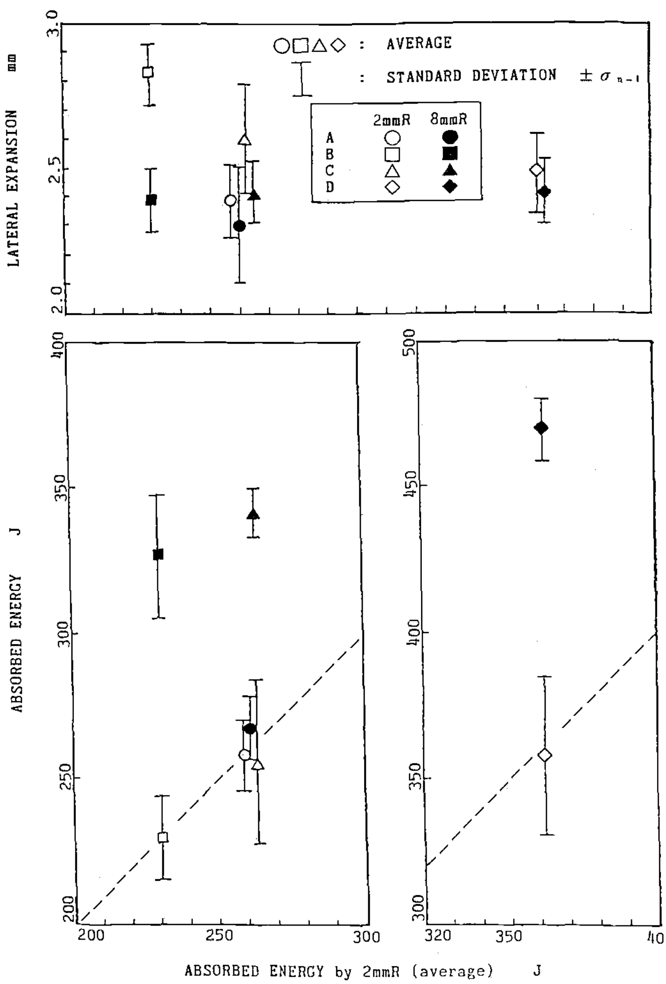

Figure 3 COMPARISION of LATERAL EXPANSION and ABSORBED ENERGY

plots may be mainly influenced by the characteristics of the materials prepared for the tests,because the area of distribution spreads more than three times of the standard deviation (2mmR: 4-17J,8mmR:5-15J) shown in Table 5.

Table 5 Check of the capabilities of the machines

No.	supllier	ASTM type machines				ISO type machines				temp. for tests
		absorbed energy		lateral expansion		absorbed energy		lateral expansion		
		ave.	S.D.	ave.	S.D.	ave.	S.D.	ave.	S.D.	
A	①	262	5.2	2.46	0.04	252	6.3	2.30	0.12	-20
	2	269	8.2	2.35	0.18	268	13.4	2.50	0.11	
	3	261	8.5	2.41	0.04	259	11.9	2.34	0.10	
	4	274	11.3	2.33	0.11	255	10.2	2.41	0.11	
B	1	342	8.3	2.40	0.11	245	13.2	2.76	0.12	+20
	②	338	5.8	2.41	0.06	223	8.7	2.95	0.03	
	3	334	5.2	2.30	0.12	220	4.6	2.82	0.05	
	4	293	11.5	2.44	0.11	233	14.1	2.77	0.06	
C	1	345	3.8	2.47	0.06	284	12.8	2.50	0.12	+30
	2	342	2.5	2.43	0.05	251	8.3	2.85	0.10	
	3	347	2.5	2.47	0.04	232	5.2	2.68	0.03	
	④	331	10.8	2.56	0.10	284	19.4	2.45	0.10	
D	1	479	5.7	2.43	0.07	380	14.0	2.34	0.11	-80
	2	465	16.6	2.35	0.06	381	17.1	2.46	0.08	
	③	467	4.5	2.34	0.05	335	3.8	2.64	0.02	
	4	467	5.2	2.24	0.06	346	10.9	2.42	0.09	

Effects of the changes of the length of test specimens within the tolerance and effects of the displacement between the strike point and the location of notch

For the investigation of the effects of the changes of the length of test specimens, test specimens whose length were distributed within the tolerance of ASTM standard and ISO standard were prepared as shown in Table 2. And for the investigation of the effects of the displacement between the strike point and the location of notches, one group of the test specimens were manufactured with the V-notches at the center of the test specimens,and another group of them were manufactured with the notches a certain location from one end of the test specimens. The placement of test specimens are establishe by tongs or a end stop.

Figure 5 shows the dimensions of test specimens and the location of V-notches and the striking points.

(1)Comparison of the test results between ASTM type machines (8mmR's) and ISO type machines(2mmR's) is shown in Figure 6. Figure 6 shows the test results in the case when the striking points met the location of the notches.
The absorbed energy of the 8mmR's was higher than the 2mmR's as in the study of Naniwa et al., while the lateral expansion indicated different behavior depending on materials. Lateral expansion of 8mmR's was higher in the case of SM570Q and SM400C, and lower in the case of API5L X56 and SM400B compared with 2mmR's.
Now, the commercial based specifications deal with only the lower level of absorbed energy. But in the near future, if

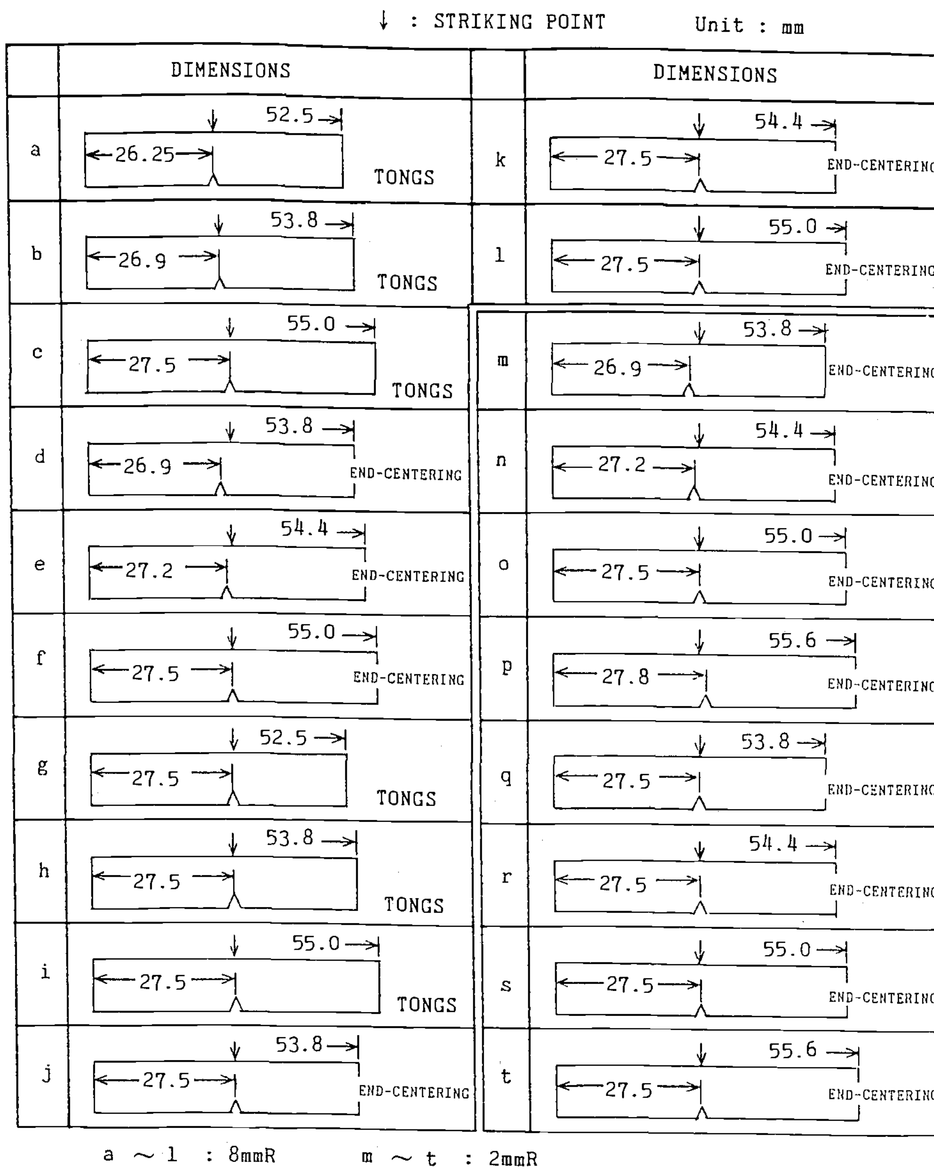

Figure 5 DIMENSIONS of TEST SPECIMENS and the location of STRIKING POINT

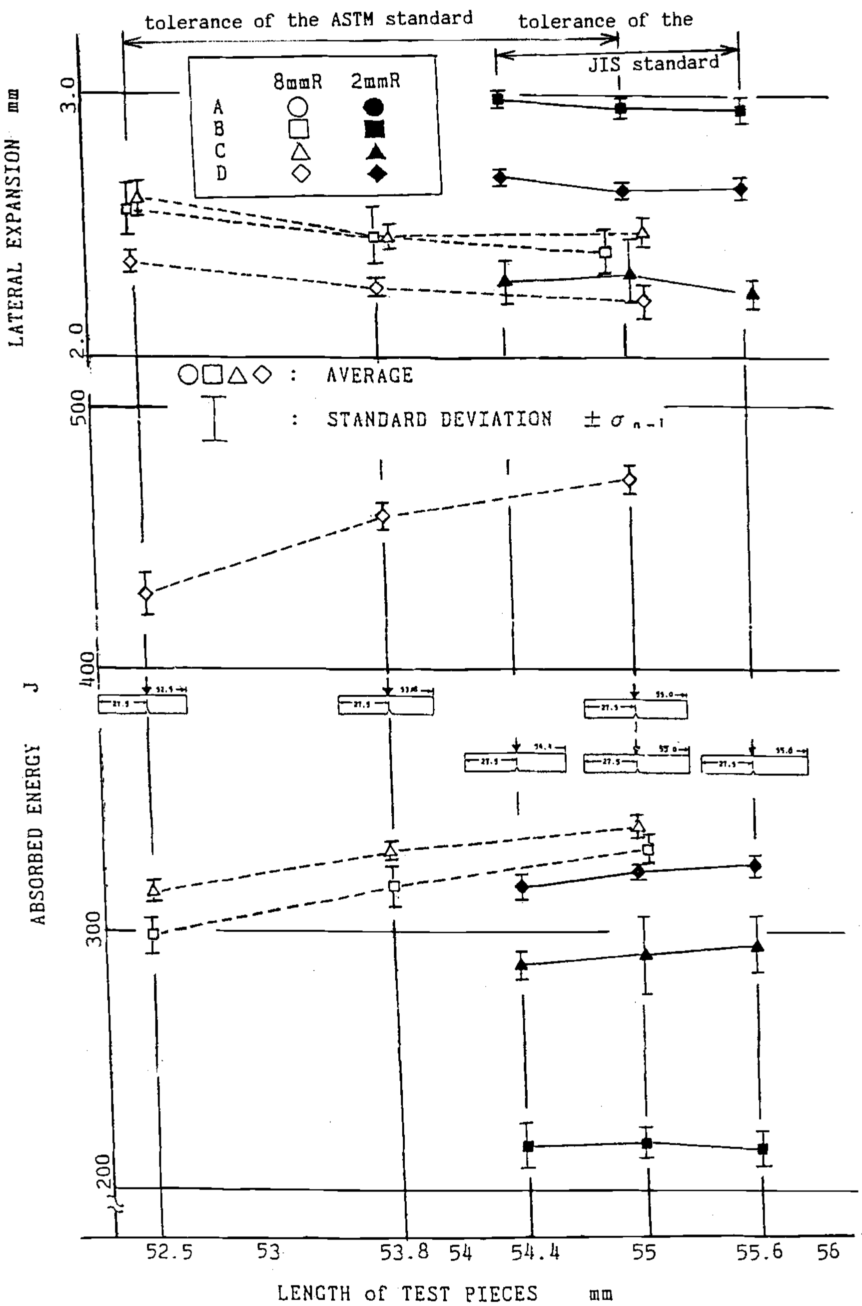

Figure 6 COMPARISION of LATERAL EXPANSION and ABSORBED ENERGY between 2mmR STRIKER and 8mmR STRIKER

the materials with absorbed energy above 400J like the line pipes for North Europe and the U.S.A. are in demand, the test results of 2mmR's may become the most valuable information. The lateral expansion of 2mmR's seems to be larger than that of 8mmR's in many cases because of its smaller curvature. In the case that the lateral expansion of 8mmR's was larger, the authors have conjectured that a rupture might appear, caused by the difference of malleability.
The effects of the changes of the length of test specimens appeared larger in the case of 8mmR's. Moreover, the tolerance of ASTM standard (2.5mm) test specimens is larger than that of the ISO standard (1.2mm), so the effect of the change of length may appear to be more in the test results of 8mmR's. (A complete summary of the effects of the tolerances can be seen in Figure 10.)

(2)Figure 7 and Figure 8 show the effects of the displacement between the strike point and the location of the notch. Figure 7 is for ISO type machines, and Figure 8 is for ASTM type machines. Figure 9 shows the comparison of the standard deviation. In this case, the V-notch was manufactured at the center of the test specimens and the striking point met the location of the notch, when the length of test specimens was 55mm.
The absorbed energy was higher when the striking point did not meet the location of the notch in every machine, while the test results on lateral expansion were about the same. The standard deviation of the absorbed energy had a tendency to become the lowest value when the length of test specimens was 55mm. And the standard deviation seemed to be higher when the test specimens were longer or shorter than 55mm. The test specimens whose striking point does not meet the location of the notch may show complex behavior when passing through the anvil.
It may be important for obtaining stable results in Charpy impact tests that the striking point meet the location of V-notches of the test specimens.

(3)Figure 10 shows the effects of symmetry of test specimens. In these cases the striking points met the location of notches. The absorbed energy was higher in the case of symmetric test specimens compared with asymmetric test specimens, while the lateral expansion was about the same. The effects of the changes of the length of test specimens seemed to be larger when the asymmetric test specimens were tested. There was no surprising tendencies in the standard deviation of the absorbed energy and the lateral expansion.
From the observation of the symmetric test specimens, it was clear that the deformation of the edge of test specimens grew larger when the test specimens became longer. From the observation of the asymmetric test specimens, it was clear that the deformation at the shorter side of test specimens were larger than that of the longer side. Asymetric test specimens may slide to the shorter side when passing through the anvil. For ASTM type machines, it may be important for obtaining stable results in Charpy impact tests, that the test specimen is to be manufactured symmetric like the ISO

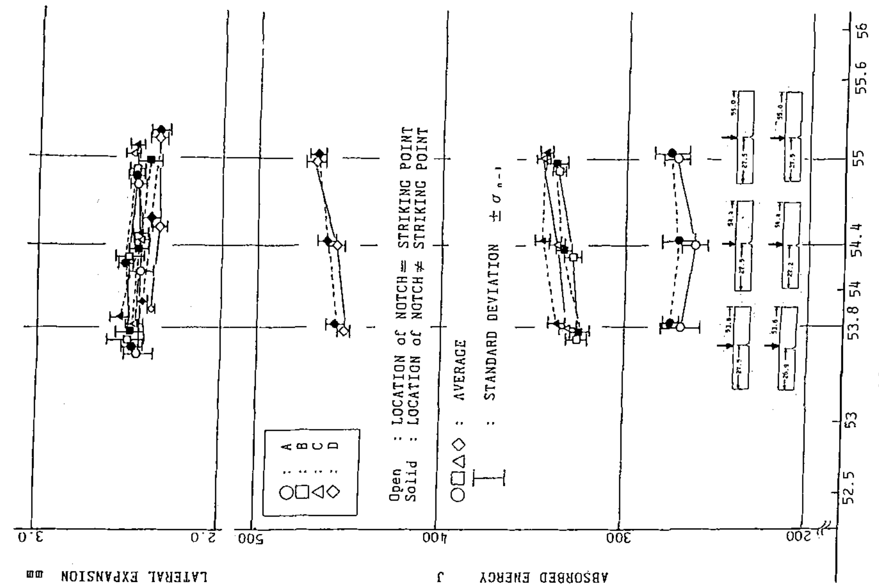

Figure 8 EFFECTS of DISPLACEMENT between STRIKING POINT and LOCATION of NOTCH (8mmR STRIKER)

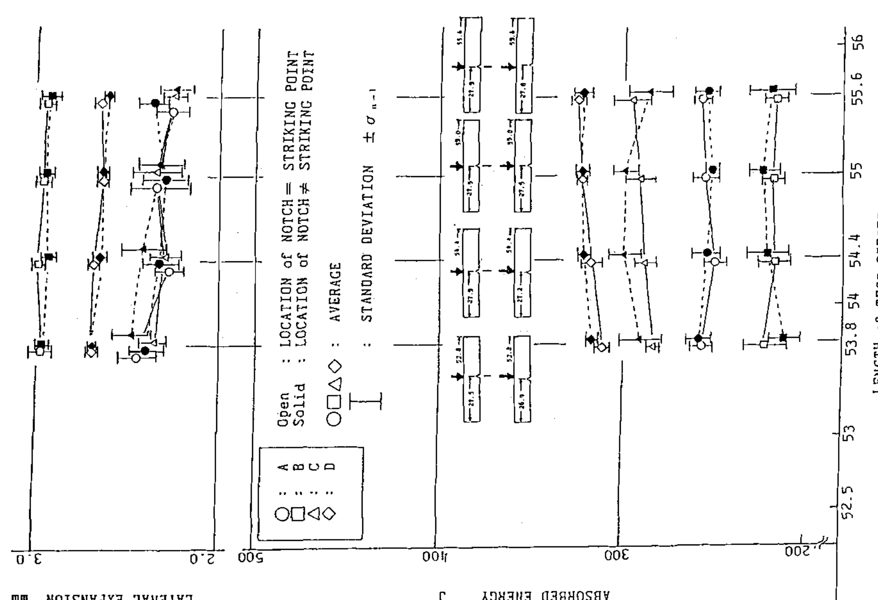

Figure 7 EFFECTS of DISPLACEMENT between STRIKING POINT and LOCATION of NOTCH (2mmR STRIKER)

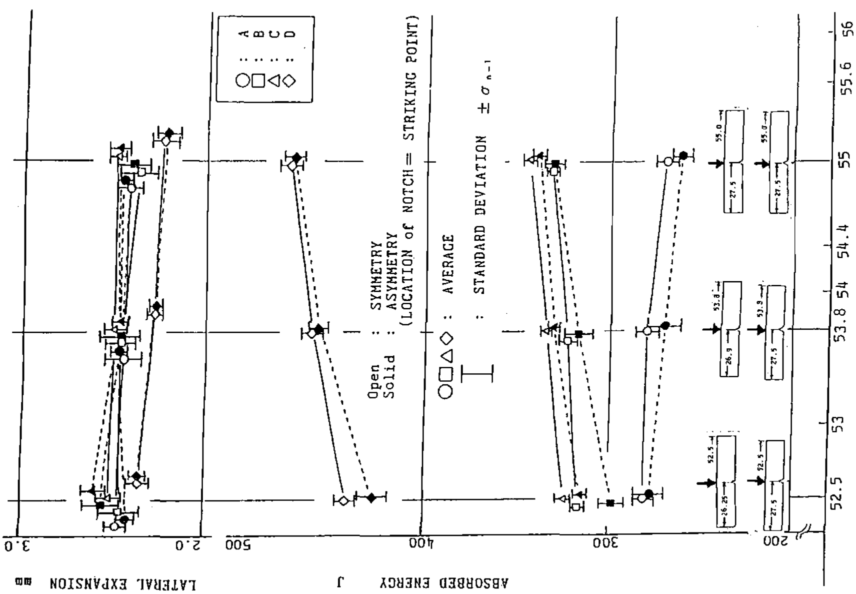

Figure 10 EFFECTS of SYMMETRICITY of TEST SPECIMENS (8mmR STRIKER)

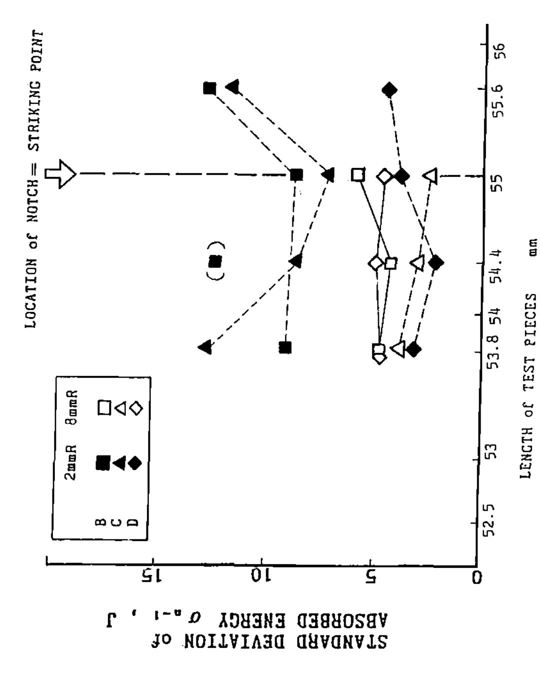

Figure 9 CONPARISON of STANDARD DEVIATION of ABSORBD ENERGY

standard.

(4)Figure 11 shows a simulation result using FEM, Finite Element Method. This is one of our trials of further investigations on the reason why there exist some differences in the test results between 2mmR's and 8mmR's. The program used for the simulation is named DYNA3D which is developed at the Lawrence Livermore National Laboratry by Dr.J.O.Hallquist.
These figures show the change of strain energy. The strain energy is the integration of products of the equivalent stress and the equivalent plastic strain.
In the case of 8mmR's, the high absorbed strain energy area near the V-notch separates into two parts, and the bending or stretching deformation seemed to appear from the stage number 3 to 5. As a result of such a deformation, in the case of 8mmR's there remained the shape of the head of striker at the striking point of the test specimen.
In the case of 2mmR's, the large strain energy area did not separate.
The test specimens after the test had two cracks in the case of 8mmR's and only one crack in the case of 2mmR's.
We can not tell the reason why the difference between 8mmR's and 2mmR's appears clearly at this stage. But the results of experiments and FEM simulations are talking to us someting.

CONCLUSIONS

Investigations with test specimens sampled from the same lot of materials, SM570Q, SM400C, SM400B, and API5L X56, have been performed. Some imporant suggestions for charpy impact test are obtained. The summary of the test results is as follows.

(1)The absorbed energy of the 8mmR's was higher than the 2mmR's as in the study of Naniwa et al.. In the near future, if the materials with absorbed energy above 200J grow in demand, the test results of 2mmR's may become the most important information.

(2)The tolerance of test specimens of the ASTM standard (2.5mm) is larger than that of the ISO standard (1.2mm), so the effect of the change of length may appear more in the test results of 8mmR's.

(3)The absorbed energy had a tendency to become higher when the striking point did not meet the location of notch in every machine. The standard deviation almostly became the smallest when the striking piont met the location of notch. It may be important for obtaining stable results in Charpy impact tests that the striking point meet the location of notches on the test specimens.

(4)The effects of the changes of the length of test specimens seemed to be larger when the asymmetric test specimens were tested.
It may be important for obtaining stable results in Charpy

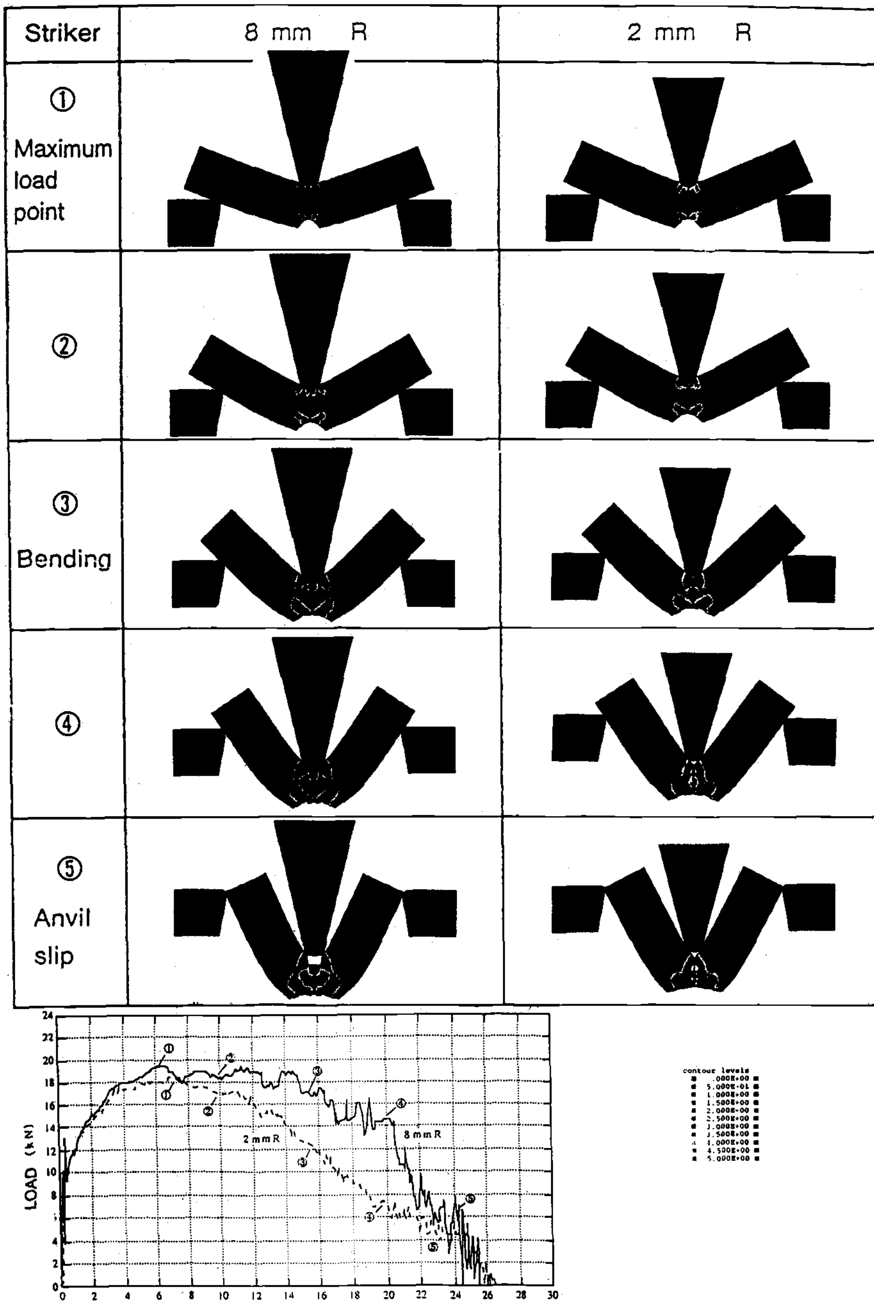

Figure 11 A result of FEM simulation

impact tests that the test specimen should manufactured symmetric like the ISO standard.

ACKNOWLEDGMENT

The authors would like to acknowledge the cooperation and the assistance of the others in The Mechanical Testing Subcommittee, The Joint Research Society of The Iron and Steel Institute of Japan.

REFERENCE

[1] T. Naniwa, M. Shibaike, M. Tanaka, H. Tani, K. Shiota, N. Hanawa, and T. Shiraishi, "Effects of the Striking Edge Radius on the Charpy Impact Test,"Charpy Impact Test:Factors and Variables, ASTM STP 1072, ed.J.M.Holt,American Society for Testing and Materials, Philadelphia,1990.

[2] M. Etoh et al.,"Investigation of the Effects on Charpy Impact Characteristics by Shape of Pendulum Striking Edge,"ASTM A10, 13 Subcommittee on testing (seminar), Louisvill K.Y.May 10, 1983.

Establishing Reference Energies

Namiteru Hida[1,2]

PRODUCTION OF CHARPY IMPACT VERIFICATION SPECIMENS AND VERIFICATION OF MACHINE PERFORMANCE

REFERENCE: Hida, N., "**Production of Charpy Impact Verification Specimens and Verification of Machine Performance,**" Pendulum Impact Machines: Procedures and Specimens for Verification, ASTM STP 1248, T.A. Siewert and A.K. Schmieder, Ed., American Society for Testing and Materials, Philadelphia, 1995.

ABSTRACT: In 1990, Japan established the industrial standard "Standard Specimens for Charpy Impact Testing Machines" and revised "Charpy Impact Testing Machines". Before establishing these standards, the Iron and Steel Institute of Japan had studied the standardization of the reference test pieces and the reference testing machines. Reference test pieces for two energy levels (30 J and 100 J) are available, with a coefficient of variation within a lot of less than 4%.

Furthermore, the effect of non-uniformity of reference test pieces within a lot in the indirect verification have been examined. The verification test accuracy (estimation of the error and repeatability) is limited by the non-uniformity of test pieces within a lot.

KEYWORDS: reference test piece, uniformity, reference testing machine, indirect verification, error, repeatability, reproducibility

---

To improve the reliability of Charpy impact testing, the Iron and Steel Institute of Japan considered introducing indirect verification into the procedures for verification of impact testing machines as early as 1970. To assure that the technical requirements could be met, studies on standardized specimens (test pieces) of domestic product were performed in a joint research program under the Iron and Steel Institute of Japan (JISI) from the end of 1970's to the early of 1980's.

---

[1] Technical Adviser, Mitutoyo Corporation, Kawasaki, Japan

[2] A member of the National Committee for "Mechanical Testing of Metallic Materials" under The Iron and Steel Institute of Japan.

Subsequently, the National Research Laboratory of Metrology evaluated methods for testing the uniformity of the standardized test pieces.

At the end of the 1980's, we introduced a system to supply reference test pieces, after discussions with the affected parties. In 1990, we established a new Japanese Industrial Standard (JIS) for reference test pieces [1] and revised the related standard for the verification of testing machines [2].

This paper describes the current situation of impact testing and the machines, the accuracy requirement of the test, the quality of reference test pieces, and the problems associated with evaluation of a testing machine by using the reference test pieces.

ACCURACY REQUIREMENT OF CHARPY IMPACT TEST

a. Survey of industrial impact test machines

Table 1 shows the results of a survey of existing test machines, including the capacity of the machines and the kinds of standards applied to the machines. Notice that among iron and steel makers, machines with a capacity of 500 J are almost as common as 300 J machines.

The survey indicates that the JIS standard is the most common. However, the ASTM standard [3] is also quite common, being applied to the machines which are used for inspection of materials to be exported. In these cases, the users are obliged to maintain both types of machines.

Accuracy of impact test

The survey also asked about the accuracy requirements for the impact test data. Of those who responded, most said that they did not know the accuracy requirements for their impact data, but half of the questionnaires did not include an answer to this question. This fact shows that the accuracy of the impact test is difficult to separate into its two components: the uniformity of the test material and the fluctuation of the testing machine.

Table 1 Survey of testing machines (capacity of machine and applicable standard). The data are in percent of the responses.

Capacity	Standard	All industries	Steel industry
300	JIS	64.5	46.7
	ASTM	2.4	2.5
	other	10.1	5.8
	total	77.0	55.0
500	JIS	9.2	20.3
	ASTM	2.4	7.8
	other	0.9	1.7
	total	12.5	29.8
other	JIS	4.1	5.8
	ASTM	5.6	8.6
	other	0.8	0.8
	total	10.5	15.2

In the steel industry, the most common requirement for the accuracy (precision) of the impact test is ±5%. The distribution of the answers for the accuracy are shown in Table 2.

Table 2 Accuracy requirement of impact test (units of %)

accuracy requirement	5%	10%	other	no answer
all industries	43.4	11.3	7.6	37.7
steel industry	45.5	9.0	27.3	18.2

Table 3 shows the responses to a question about the interest in introducing indirect verification by the use of reference test pieces for the verification of test machines. These results indicate that those users who do the most testing also have the strongest interest in the accuracy of test and in the introduction of the reference test piece into a program for verification for testing machines.

Table 3 Introduction of indirect verification method (units of %)

yes or no	yes	no	no answer
all industries	39.2	15.2	45.6
steel industry	55.6	13.0	31.4

PRODUCTION OF REFERENCE TEST PIECES AND THEIR PERFORMANCE

Production of reference test pieces

In order to introduce the verification method for the testing machine using reference test pieces, it was necessary that a large quantity of high quality reference test pieces be available. In the joint research on the reference test piece produced by JISI, the manufacturing method was established in 1984.

The material of the test piece is SNCM 439 (nickel-chromium-molybdenum steel) [4], nearly the same as SAE 4340. To produce the test pieces, we carefully melted, rolled, and heat treated the material. Special care was put into machining the V notches. As a result, we produced test pieces (at 30 J and 100 J absorbed energy) of high enough quality to be used for verification. In another trial, 150 J material was obtained.

Uniformity within a lot

As mentioned above, the test pieces produced by JISI are examined for their performance. The uniformity within a lot is expressed in standard deviation (σ) or coefficient of variation ($CV = \sigma / \bar{x} \times 100\%$).

The test results are shown in Figure 1. This figure indicates that the variation of the test pieces within a lot is expected to be smaller than 4% (in CV) above 30 J and 1.5 J (in σ) under 30 J. The quality of these test pieces is satisfactory, and compares well with the 5% in CV which are required by the major standards in foreign countries. Furthermore, a high quality of the test pieces at the 150 J energy level was also obtained under the trial production. In a small size lot, we have obtained 1 ~ 2% in CV with a carefully controlled heat treatment.

SYSTEM FOR DETERMINING STANDARDIZED VALUES

Supply system for reference test pieces

A supply system for the reference test pieces in Japan, has been formed as a result of long discussions with the concerned parties. The system consists with the following three major procedures.

(1) The manufacturer of the test pieces assures the uniformity of test pieces within a lot by means of dimensional measurements and hardness tests after heat treatment and machining. The regulations require that the manufacturer

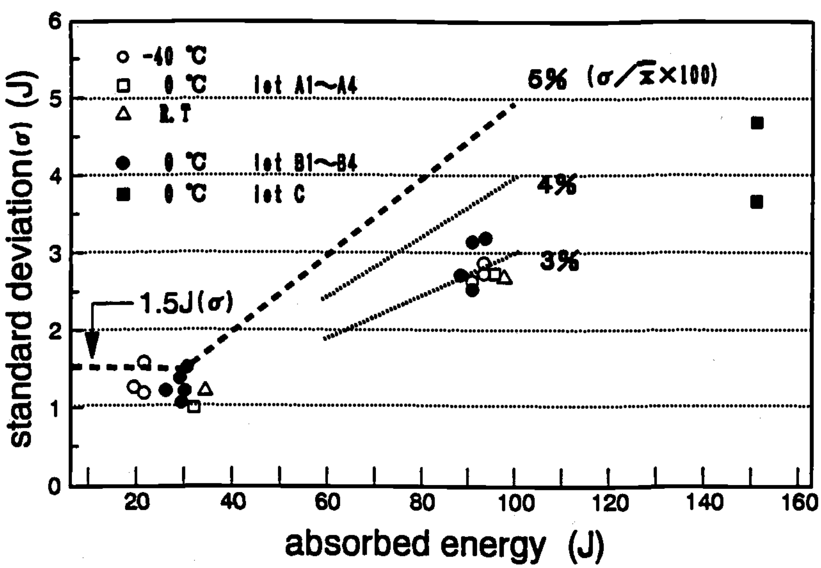

Figure 1 Uniformity of reference test pieces within a lot, with standard deviations

select representative sample test pieces from each lot manufactured, and send them to a public inspection office. The sampling rate is 1/10 of each lot, but the number of samples should be at least 20 pieces.

(2) The inspection office carries out impact test on the requested samples using a reference testing machine, and determines the reference value and the uniformity of the lot. After the test, the office issues the certificate of test results on each lot to the manufacturer.

(3) The manufacturer or its selling agent sells the verification set with the corresponding certificate to a customer.

Standard testing machine and reference testing machine

Two Japanese standard machines are situated at the National Research Laboratory of Metrology in Tsukuba. These machines are recognized as national standard machines under the following conditions. The dimensions of these machines are strictly adjusted to within a half of the allowance for industrial test machines. The foundation and installation of the machines comply with the strictest requirements of the standards, so long-term stability of the machines is confirmed. The reference testing machine used for calibration of the reference test piece in the inspection office must be traceable to the national standard. The reference testing machine is compared with national standard machines every two years. Furthermore, the long-term stability of the machine must be confirmed by means of a $\bar{x}$ control chart.

VERIFICATION OF THE TESTING MACHINE

Indirect verification of the testing machine

Each testing machine should be evaluated by direct verification. However, direct verification can not evaluate the dynamic characteristics of the machine, especially the rigidity of the machine and its foundation. Accordingly, indirect verification using the reference test pieces should also be used to evaluate the performance of the testing machine.

However, the dispersion of test results from any impact machine is a combination of not only the variation of machine itself, but also the non-uniformity of the reference test pieces within a lot. Moreover, that non-uniformity of the test pieces is not necessarily small compared with the variation of the test machine itself. Therefore, the effect of non-uniformity of the reference test piece within a lot in the indirect verification is examined in next section.

Error of industrial testing machines

A series of impact tests using a set of reference test pieces is carried out for the indirect verification of a testing machine. The error of the machine is given by the following Equation,

$$E = \overline{A_V} - A_R \tag{1}$$

where

$$\overline{A_V} = \frac{A_{V_1} + A_{V_2} + \cdots + A_{V_n}}{n}$$

E : error (difference from the reference machine)
A_{Vi} : each test result in absorbed energy
$\overline{A_V}$: mean of the test result
A_R : reference value of the test pieces using a reference machine
n : number of reference test pieces

The variation of error for Equation 1 can be obtained as follows.

$$\sigma(E) = \sqrt{\frac{\sigma_{AV}^2}{n} + \sigma_{AR}^2} \tag{2}$$

$$= \sqrt{\frac{\sigma_{AR}^2 + \sigma_{Me}^2}{n} + \frac{\sigma_{AR}^2}{n}} \tag{3}$$

where σ_{AV}^2 : variance of test result of verification
σ_{AR}^2 : uniformity of reference test piece within a lot, expressed in variance
σ_{Me}^2 : variance of dispersion of the testing machine during the test

As shown in Equation 3, the variance σ_{AV}^2 is the sum of the variances of non-uniformity σ_{AR}^2 and of the testing machine σ_{Me}^2. It is impossible to separate the variance σ_{Me}^2 from the variance σ_{AV}^2. Assuming that the variance σ_{Me}^2 is nearly equal to zero, Equation 3 can be rewritten as follows.

$$\sigma(E)=\sqrt{\frac{2\sigma_{AR}^{2}}{n}} \tag{4}$$

Equation 4 indicates that, even when $\sigma_{Me}^{2}=0$, the limitation of the power of the calibration test is the variation caused by nonuniformity of the reference test pieces. The values calculated from Equation 4 are shown in Table 4.

Table 4 Confidence interval for the difference ($\overline{A_V}$ - A_R) at a confidence coefficient of 95%

uniformity		CV (unit: %)			σ (unit: J)		
		5	4	3	2	1.5	1
n	5	8.8	7.0	5.3	3.5	2.6	1.8
	10	5.1	4.0	3.0	2.0	1.5	1.0
	25	2.9	2.3	1.8	1.2	0.9	0.6

In Table 4, for example, the confidence interval for the difference with a confidence coefficient of 95% is ±8.8 % at n=5, when the CV of uniformity is 5%. So, if an error is larger than 8.8%, the difference between the reference machine and the inspected machine is significant. In other words, the maximum permissible error for the machine to be verified should be larger than the value in Table 4. If a smaller difference is detected in the verification, we must chose between higher quality reference test pieces or a larger number of the test pieces.

Repeatability of industrial testing machine

In general, the repeatability obtained in verification tests are adopted for the evaluation of test machines during testing. The repeatability is defined by the following equation.

$$R = A_V \max - A_V \min \tag{5}$$

where R : range between the maximum and the minimum data obtained in the verification test

A_V max : maximum data in the verification test

A_V min : minimum data in the verification test

By this method, the range obtained from Equation 5 includes not only the fluctuation of testing machine during tests but also the non-uniformity of the reference test pieces within a lot. Moreover, the non-uniformity of the reference test piece within a lot is larger than the fluctuation of the testing machine.

The uniformity of the reference test pieces within a lot can be expressed as the standard deviation σ_{AR}. When n samples are taken from reference test pieces in a lot having the uniformity of σ_{AR}, the range R has a statistical distribution. The mean value and variation of range can be estimated from the uniformity of σ_{AR} as follows.

$$\bar{R} \pm k\sigma(R) = (d_2 \pm kd_3)\ \sigma_{AR} \tag{6}$$

where $\bar{R}$: mean value of the range

$\sigma(R)$: variation of the range in standard deviation

σ_{AR} : uniformity of the reference test piece within a lot

d_2 , d_3 : coefficient for the control chart

k : coverage factor

The calculated values by Equation 6 are shown in Table 5.

Table 5 Estimated range (repeatability) at a confidence coefficient of 95%

uniformity		CV (unit: %)			σ (unit: J)		
		3	4	5	1.0	1.5	2.0
n	5	12.2	16.2	20.3	4.1	6.1	8.1
	10	14.0	18.7	23.4	4.7	7.0	9.4

As indicated in Table 5, the repeatability of the test machines due to the non-uniformity of the test pieces is about 20% of A_R, under the conditions of $n = 5$, $\sigma_{AR} = 5\%$ of A_R at confidence coefficient of 95%. Therefore, it seems meaningless to evaluate the testing machine by means of the repeatability during the test. For this reason, in JIS, the repeatability is not a criterion for the performance of testing machines.

Error and reproducibility of reference testing machine

For reference testing machines, it is important that the machine should be traceable to the national standard and here reproducibility is important. To confirm the traceability, periodic comparison tests are carried out between the machine to be verified and the standard machine. The differences between the two machines are examined by the following equation:

$$E = A_R - A_S \tag{7}$$

where E : error (the difference between two machines)
A_R : reference value by the reference machine
A_S : standard value by the standard machine

In this case, the machine must also meet the requirements of equation 4 and Table 4. For example, the limiting values are 3% of A_R and 1.2 J in σ under σ_{AR}=5%, n=25, and a confidence coefficient of 95%. We can assure traceability to the national standard within above mentioned values. Another important item is that the long-term reproducibility of the reference machine should be examined in routine checks and the periodic inspection using the reference test pieces.

The reproducibility of the test machine is expressed by the following equation.

$$\sigma_{\overline{AR}} = \sqrt{\frac{\sigma_{AR}^2}{n} + \sigma_{Mr}^2} \tag{8}$$

$$= \sqrt{\frac{\sigma_{AR}^2 + \sigma_{Me}^2}{n} + \sigma_{Mr}^2} \tag{9}$$

where $\sigma_{\overline{AR}}$: variation of the mean, in standard deviation
σ_{Mr}^2 : variance of the machine in the long term.

If the variance is $\sigma_{Me}^2 \fallingdotseq 0$, $\sigma_{Mr}^2 \fallingdotseq 0$, Equation 9 can be rewritten as Equation 10.

$$\sigma_{\overline{AR}} = \sqrt{\frac{\sigma_{AR}^2}{n}} \tag{10}$$

Consequently, if the conditions of the machine to be controlled are maintained within the limiting interval given by Equation 10, the reproducibility of machines are certified as acceptable. This evaluation system is similar to the $\bar{x}$ control chart method.

CONCLUSIONS

For improved reliability of Charpy impact testing, we have established a production technique for high quality reference test pieces, and a system for the standardization and for the supply of the reference test pieces. In 1990, the Japanese Industrial Standards for reference test pieces was established and the associated standards were revised to correspond with this new standard.

The quality of the reference test piece has satisfied the customer requirements. The uniformity within a lot is about 3~4% of the reference value A_R, in coefficient of variation.

However, in indirect verification using these reference test pieces, the value of the test for industrial machines is limited by the non-uniformity of the test pieces within a lot, in the estimation of the error and the repeatability of the test machine.

For reference test machines, the reproducibility is important in the evaluation of performance.

REFERENCES

[1] JIS B 7740 Standard Specimens for Charpy Impact Testing Machine
[2] JIS B 7722 Charpy Impact Testing Machines
[3] ASTM E 23 Test Methods for Notched Bar Impact Testing of Metallic Materials
[4] JIS G 4103 Nickel Chromium Molybdenum Steels

Jolene D. Splett[1] and Jack C.-M. Wang[1]

PROPOSED CHANGES TO CHARPY V-NOTCH MACHINE CERTIFICATION REQUIREMENTS

REFERENCE: Splett, J. D., and Wang, J. C.-M., "**Proposed Changes to Charpy V-Notch Machine Certification Requirements**," Pendulum Impact Machines: Procedures and Specimens for Verification, ASTM STP 1248, Thomas A. Siewert and A. Karl Schmieder, Eds., American Society for Testing and Materials, Philadelphia, 1995.

ABSTRACT: In 1989 the administration of the Charpy V-Notch Certification Program was assumed by the National Institute of Standards and Technology. The United States Army originated the program to insure the measurement integrity of Charpy V-notch machines across the country. The program has been operated for many years using candidate machine acceptance limits which can possibly be traced to a 1955 paper by Driscoll, however, the original statistical justification for using these acceptance criteria has been lost or never existed. A statistical analysis of recent certification program data indicates that the existing candidate machine acceptance limits should be modified. In this paper, we will discuss and justify potential changes to candidate machine acceptance limits.

KEYWORDS: notched-bar testing, reference specimens, Charpy V-notch machine certification program, pendulum impact machines, impact testing

---

The Charpy V-Notch Machine Certification Program has been operating for many years to ensure the measurement quality of Charpy machines across the country. Basically, the program works as follows. The National Institute of Standards and Technology (NIST) obtains a pilot lot of 100 specimens from a supplier and measures the

[1]Mathematical Statistician, Statistical Engineering Division, Computing and Applied Mathematics Laboratory, National Institute of Standards and Technology, Boulder, CO 80303.

impact toughness of the specimens using three reference machines. Impact toughness is measured as absorbed energy in the test. If the 100 measurements meet certain criteria, then the remainder of the lot is machined and sent to NIST where an additional 30 specimens, called the confirm lot, are randomly selected and broken. If the absorbed energy of the confirm lot is in agreement with the absorbed energy of the pilot lot, the lot is certified as a reference material by NIST. Sets of five reference specimens are then sold to companies that want to certify their candidate Charpy machine. The specimens are broken using the candidate machine and the broken specimens, along with their observed absorbed energies, are sent to NIST for analysis. If the specimens and measurements are satisfactory, then the candidate Charpy machine can be certified. NIST currently certifies candidate Charpy machines for both "Low" and "High" absorbed energy ranges. The reference value for the Low energy range is between 15.4 and 21.0 Joules (J), while the High energy reference value is between 92.4 and 109.2J.

The origins of the current Charpy V-Notch Machine Certification Program can be traced to a 1955 paper by Driscoll [1]. Evidently, the reliability of Charpy measurements was in question and people were reluctant to use Charpy machines for acceptance testing, so Driscoll conducted a large-scale study to prove that Charpy machines were reliable. Driscoll realized that the key to demonstrating reliability and reproducibility for this type of destructive testing was in the homogeneity of the material used in the study, so he was able to show that the Charpy machines were in fact reliable by carefully selecting homogeneous specimens. Driscoll's contribution to the certification program is observed in the general limits which encompass the majority of absorbed energy averages from samples of size five for the Low and High energy ranges. Specifically, most of the Low energy samples had an average absorbed energy within 1.4J of the lot average, while the average absorbed energy of five High energy specimens was usually within 5% of the lot average. These limits are identical to those used in the current certification program to pass or fail a company's Charpy machine.

Various aspects of the current program merit careful study if we are to understand and improve the performance of the certification process. For instance, the number of specimens in both the pilot lot and the candidate machine's verification set, and the definition of a single reference value from measurements on two or more "standard" machines, ultimately affect the error rates associated with classifying machines as conforming or nonconforming. In this article, however, we limit our attention to the properties of the current criteria by which machines are judged acceptable.

The main concern regarding the present certification criteria is the arbitrary nature of the acceptance limits. The justification for using these limits is unknown and does not appear to be linked to any statistical reasoning or evaluation of their performance. We intend to demonstrate the statistical properties of the existing limits as well as illustrate potential new candidate machine certification limits which are more objective and statistically defensible.

ASSUMPTIONS AND DEFINITIONS

Several assumptions regarding the certification program in general are necessary to simplify the discussion in this paper. While somewhat artificial, these assumptions nevertheless serve to illustrate and explain the potential shortcomings in current evaluation procedures.

For demonstration purposes, we will assume that the three reference machines used to determine the reference value of the lot are basically identical. Under this assumption, the process of determining a reference value can be simplified, hypothetically, by assuming that all 100 pilot lot specimens are measured on one "standard" machine. Furthermore, we assume that the pilot lot is a representative sample of the machined lot of specimens. Thus the unknown average absorbed energy of all specimens in a lot can be estimated by breaking the random sample of 100 specimens known as the pilot lot. The computed average absorbed energy of the pilot lot serves as our estimate of the true absorbed energy of the lot.

Because of the destructive nature of the Charpy test, we are unable to separate the sources of variation inherent in testing. Specifically, the inherent variation among specimens in a lot cannot be distinguished from measurement error variation associated with operators, ambient conditions, and other noise sources. We will define the sum of these two sources of variation as the *system variation*, σ^2, which can be written as

$$\sigma^2 = \sigma_s^2 + \sigma_e^2 \tag{1}$$

where σ_s^2 is the true specimen variation and σ_e^2 is the true variation associated with measurement errors. Since specimen inhomogeneity is a critical component of the system variation, it is clear that one way to minimize σ^2 is to reduce the specimen variation.

Under our simplifying assumptions, the NIST system variance would be estimated by computing the sample variance of the pilot lot, S_p^2, while the candidate machine's system variation would be estimated by the sample variance of five reference specimens, S_c^2, measured on the machine under test. Since the pilot lot and the five reference specimens, or *verification set*, come from the same lot, the specimen variance, σ_s^2, is the same for every machine tested on a single lot. In addition, we will assume that both the absorbed energy and measurement error distributions can be well-approximated by Gaussian distributions, and that the variance of the candidate machine's measurement errors is the same as that of the NIST measurement system.

Finally, we make no provision for the occurrence of outliers in the calculations and results presented below. (In actual practice, a value is considered an outlier if there is physical evidence to indicate that a test result is "bad".) While outliers are an important issue, and their detection and treatment deserves more consideration, the only effect of generating outliers in our hypothetical situation would be to reduce the size of the verification set.

EXISTING LOW ENERGY CERTIFICATION LIMITS

Since the existing certification acceptance criterion are different for the Low and High energy ranges, we will discuss the two cases separately, starting with the Low energy specifications. A candidate Charpy machine is certified in the Low energy range if the measured values of five reference specimens meet two conditions: (i) the average of the five measurements is within $1.4J$ of the reference value, and (ii) the range of the five measurements is not greater than $2.8J$. (The range of a sample is the difference between the largest and smallest measurements.) If the five measurements from the Charpy machine under test are denoted by C_1, C_2, C_3, C_4, C_5, then the Low energy certification criteria can be expressed as:

$$-1.4J \leq \overline{P} - \overline{C} \leq 1.4J \quad \text{and} \quad \max\{C_i\} - \min\{C_i\} \leq 2.8J \tag{2}$$

where $\overline{P}$ denotes the average of the 100 pilot lot specimens, and $\overline{C}$ is the average of the five reference specimens measured on the Charpy machine under test.

To understand the implications of the current Low energy certification criteria, we computed the probability of certifying a candidate machine based on the limits in (2) under the assumptions outlined in the previous section. The probability of certification depends on three parameters: the unknown average absorbed energy of the lot as defined by the NIST system, μ_p, the unknown average absorbed energy of the lot according to the candidate machine, μ_c, and the system standard deviation, σ, which is assumed to be the same for both NIST and the candidate machine. In other words, we calculated the probability that a machine will be certified (that is, the probability of observing $|\overline{P} - \overline{C}| \leq 1.4J$ and range$\{C_i\} \leq 2.8J$) for specified values of the parameters μ_p, μ_c, and σ. By specifying the parameters, we know a priori if the "simulated" candidate machine is behaving properly or not, but random variation makes it impossible to correctly classify a candidate machine as "good" or "bad" all the time. The probability of certification is given by

$$\Pr\left[-1.4J \leq \overline{P} - \overline{C} \leq 1.4J, \quad \text{range}\{C_i\} \leq 2.8J\right] =$$
$$5\left\{\Phi\left(\frac{1.4-\delta}{\sigma\sqrt{0.21}}\right) - \Phi\left(\frac{-1.4-\delta}{\sigma\sqrt{0.21}}\right)\right\} \cdot \int_{-\infty}^{\infty}\left\{\Phi\left(x + \frac{2.8}{\sigma}\right) - \Phi(x)\right\}^4 \phi(x)\, dx$$

where $\delta = \mu_p - \mu_c$, $\phi(x) = (2\pi)^{-1/2}e^{-x^2/2}$ is the standard Gaussian probability distribution, and $\Phi(x) = \int_{\infty}^{x} \phi(z)\, dz$. The probability of certification, calculated using numerical integration routines in IMSL [2], is shown in Fig. 1 as a function of $|\delta| = |\mu_p - \mu_c|$ and σ. (The probability is a symmetric function of δ.)

The horizontal axis in Fig. 1 represents the magnitude of the difference between the *true* average absorbed energy of specimens measured on a single candidate machine and specimens measured on the NIST reference machine. The vertical line at $1.4J$ in Fig. 1 is added as a point of reference; it denotes the point at which the difference between NIST and candidate machine *sample* average absorbed energies separates "good" and "bad" candidate machines according to the current certification criteria. Because of system variation, a "good" machine may fail, or a "bad" machine may pass purely by chance, and the probability of either type of error can be read from Fig. 1. For example, if $|\mu_p - \mu_c| = 0$ and the system standard deviation is high ($\sigma = 1.0J$), then the chance of correctly certifying a candidate machine is only about 72%, even though the candidate machine is in agreement with the NIST system.

If the current criterion $|\overline{P} - \overline{C}| \leq 1.4J$ is interpreted to mean that we would like to correctly certify candidate machines 100% of the time if $|\mu_p - \mu_c| \leq 1.4J$ while correctly failing candidate machines 100% of the time if $|\mu_p - \mu_c| > 1.4J$, then the ideal probability curve for certification limits would be a step function. Of course, perfect certification is possible only in the unrealistic circumstance that $\sigma = 0$. The curves displayed in Fig. 1 show the chance of making an error, either by certifying a "bad" machine or not certifying a "good" machine, for three realistic values of the system standard deviation σ. The increasing frequency of misclassification as the system standard deviation increases from the smallest value, $\sigma = 0.6J$, to the largest standard deviation, $\sigma = 1.0J$, demonstrates that the performance of the certification criteria is very sensitive to random variation. We will return to this point shortly.

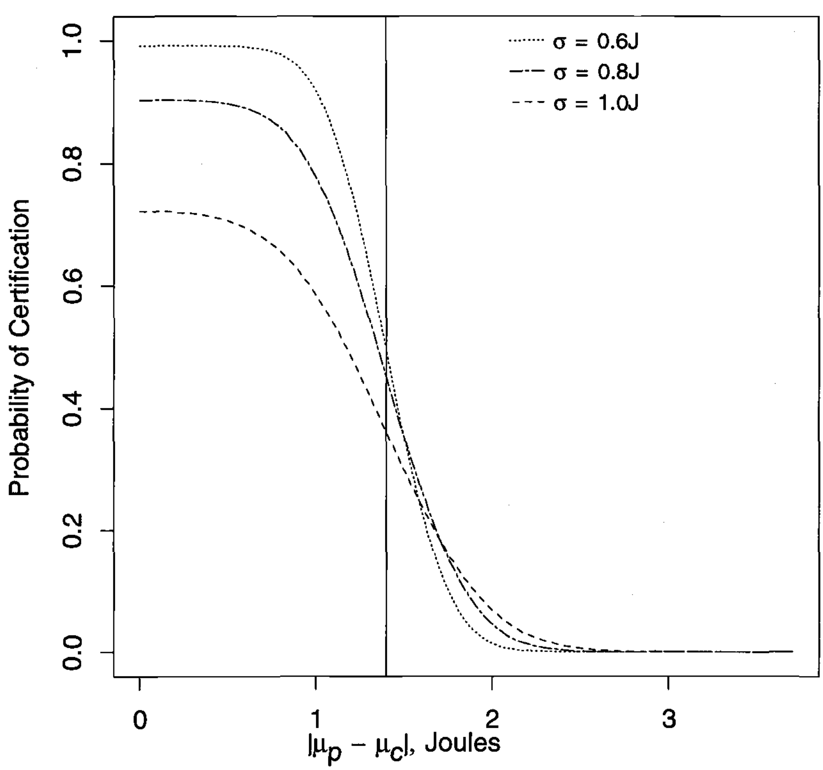

FIG. 1–Probability of certifying a candidate machine under the existing Low energy certification criteria.

EXISTING HIGH ENERGY CERTIFICATION LIMITS

To certify a candidate Charpy machine in the High energy range, the average of the five reference specimens measured on the candidate machine must be within 5% of the pilot lot average, or reference value; that is, we require $0.95\overline{P} \leq \overline{C} \leq 1.05\overline{P}$. In other words, there is only one certification limit which we may write as:

$$0.95 \leq \frac{\overline{C}}{\overline{P}} \leq 1.05 \tag{3}$$

where $\overline{P}$ and $\overline{C}$ are defined as in the Low energy case.

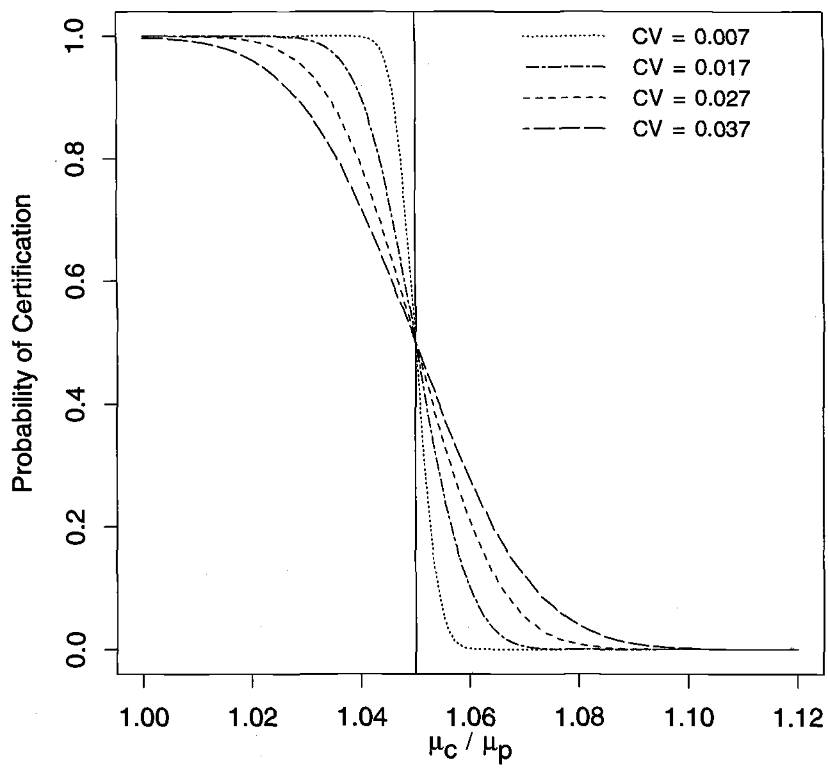

FIG. 2–Probability of certifying a candidate machine based on the existing High energy certification criterion.

To illustrate the properties of the current High energy certification criterion (3), we calculated the probability of certification for given values of the parameters μ_p, μ_c, and σ. The parameters are defined as in the Low energy case. The probability of certification for the High energy criterion is given by

$$\Pr\left[0.95\overline{P} \leq \overline{C} \leq 1.05\overline{P}\right] =$$

$$\int_{-\infty}^{\infty} \left\{ \Phi\left(\frac{1.05\sqrt{5}x}{10} - \frac{\mu_c/\mu_p - 1.05}{\mathrm{CV}/\sqrt{5}} \right) - \Phi\left(\frac{0.95\sqrt{5}x}{10} - \frac{\mu_c/\mu_p - 0.95}{\mathrm{CV}/\sqrt{5}} \right) \right\} \phi(x)\, dx$$

where $\Phi(\cdot)$ and $\phi(\cdot)$ were defined in the previous section. While there are three parameters, the certification probability only depends on the ratio, μ_c/μ_p, and the coefficient of variation, $CV = \sigma/\mu_p$, of the NIST reference machine. CV is a unitless measure of relative variation which may as well be called the noise–to–signal ratio. Fig. 2 displays the probability of certification for the High energy range as a function of μ_c/μ_p for various values of CV that are acceptable according to the specimen manufacturer's contract. Since the probability of certification is symmetric about the value $\mu_c/\mu_p = 1$, it is sufficient to show the curves for ratios greater than or equal to 1.

The horizontal axis in Fig. 2 denotes the ratio of true averages, so machines having a ratio smaller than 1.05 could be called "good" while a "bad" machine would have a ratio larger than 1.05. From the figure, we see that the probability of certifying a candidate machine is roughly 0.5 when $\mu_c/\mu_p = 1.05$, regardless of the value of CV. In other words, if the average absorbed energy of the machine under test exceeds the NIST system average by 5%, the candidate machine essentially has a 50% chance of being certified.

As in the Low energy case, the probability of making an error deteriorates rapidly with increasing system variation. Fig. 2 shows how the probability of making an error, either by certifying a "bad" machine or not certifying a "good" machine, increases with CV. For example, if $\mu_c/\mu_p = 1.06$ the probability of incorrectly certifying a candidate machine is roughly 0.1 when $CV = 0.017$; however, if $CV = 0.037$ (i.e., a greater noise–to–signal ratio), the probability of incorrect certification rises to about 0.3.

ALTERNATE CERTIFICATION LIMITS

The results illustrated in Figs. 1 and 2 show that system variation, which comprises both inherent specimen–to–specimen differences as well as laboratory measurement errors, is the critical determinant of misclassification rates in the Charpy testing program. Yet, estimates of system variation (both for NIST and the candidate machine) are not assigned a prominent role in the existing certification procedure. Currently, the only part of the procedure which addresses system variation explicitly is the Low energy bound on the range of the candidate machine's verification set measurements. The range–test is designed to detect excessive candidate machine system variance, but does not actually incorporate any of the information from the pilot lot. Similarly, neither the Low or High energy criteria for comparing the average of the verification set to the reference value presently depend on the estimated NIST system variance, our best indicator of variability in the *current lot* of specimens.

An alternative to the current practice is to replace the existing Low and High energy certification procedures by a single protocol that incorporates system variation into the test procedure in two ways. First, the candidate machine's system variation would be compared to the NIST system variation by conducting a standard statistical test based on the sample variance of the verification set and the sample variance of the pilot lot. Because specimens come from the same lot, candidate machine variance which exceeds the lot variance can only be attributed to excessive measurement error variability in the candidate machine. The second way of accounting for system variation in the test criteria is to evaluate the difference between the reference value and the candidate machine's verification set average based on an acceptance limit which implicitly depends on the actual specimen–to–specimen variation of the current lot, so the computed limit would fluctuate with an estimated system variation based on the pilot lot and candidate machine data. A test for excessive candidate machine system variability and alternate limits on the average of the verification set measurements are discussed below.

The standard test to compare NIST and candidate machine system variation is the ratio of the sample variance of the five reference specimens to the sample variance of the pilot lot. In this application we will only be concerned if the variance of the five reference specimens is large compared to the variance of the pilot lot. Regardless of the energy level, the sample variance of the five reference specimens will be considered too large if the ratio

$$F = \frac{S_c^2}{S_p^2} \tag{4}$$

is greater than the $100(1-\alpha)$th percentile of the F distribution, denoted by $F_{1-\alpha:4,99}$. Here S_c^2 and S_p^2 denote, respectively, the sample variance of the five reference specimens broken on the candidate machine and the sample variance of the pilot lot. The values 4 and 99 appearing in (4) are the respective degrees of freedom for S_c^2 and S_p^2, and α is the probability of *erroneously* concluding that the system variation of the candidate machine exceeds that of the NIST system when it does not. Usually α is small; for example, if $\alpha = 0.05$ we would claim that the system variation associated with a candidate machine is excessive if the F–ratio is greater than the the threshold value $F_{0.95:4,99} = 2.46$. See [3] for more information about statistical tests for comparing variances.

If the candidate machine passes the variability test, we would assume the system variation of the candidate machine does not exceed that of NIST, and the second test would be applied. The procedure we have developed is similar to the current Low energy criterion, but is based on an explicit statistical test of the hypothesis that $|\mu_p - \mu_c| \leq d$. By the new test, we will conclude that the candidate machine may be certified if $\overline{P} - \overline{C}$ is in some interval, say (L, U). The acceptable deviation d, which represents the amount by which the conceptual lot average of the candidate machine is permitted to differ from the NIST lot average, can be adjusted according to program requirements. The acceptance limits L and U, derived in the Appendix, are given by

$$U = -L = (d + 0.4583 \cdot S \cdot t_{1-\alpha:103})J \tag{5}$$

where $S^2 = (99S_p^2 + 4S_c^2)/103$, $t_{1-\alpha:103}$ is the $100(1-\alpha)$th percentile of Student's t distribution with 103 degrees of freedom, and α is the probability of failing a "good" candidate machine.

The particular value of the allowable deviation, d, between the true reference average and that of the machine under test at a given energy level is a choice that is based on engineering judgement. For illustration, we will choose $d = 1.4J$ to coincide with the current Low energy acceptance criterion. (No value of d is defined under the current program for High energy.) The particular value $d = 1.4J$ is not necessarily the best Low energy limit for actual use in the certification program. Driscoll [1] implies that system variation is already accounted for by the value $1.4J$.

Having specified d, the certification limits in (5) are quite easy to calculate; all that is required is a t-table. Under the current program, for example, the Low energy limit is $d = 1.4J$. Supposing that a machine under test has passed the variability test in (4), and that the pooled standard deviation is $S = 0.5J$, then the final certification criterion when $\alpha = 0.05$ would require that $|\overline{P} - \overline{C}| \leq 1.7803J$. The acceptance limit was calculated by substituting d, S and the tabled value $t_{0.95:103} = 1.6598$ in (5).

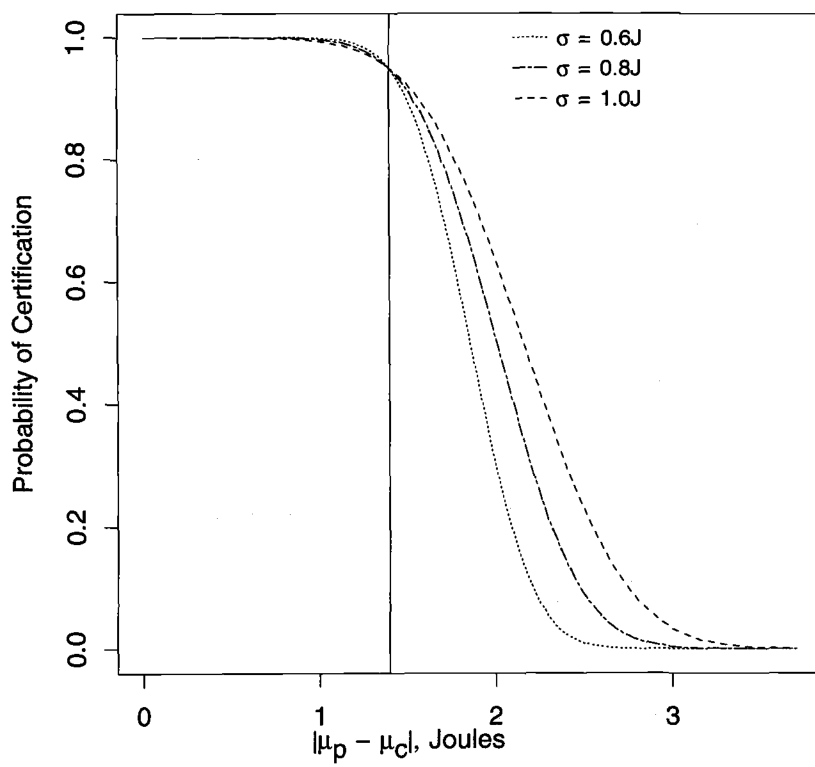

FIG. 3–Probability of certifying a candidate machine at the Low energy level versus the theoretical difference between the reference value and the true candidate machine average absorbed energy when $\alpha = 0.05$.

By contrast to the fixed limits on $\overline{P} - \overline{C}$ in (2), the new criterion based on (5) takes the variation of the specimens into consideration when computing the acceptance limits; the more variable the specimens, the wider the acceptance interval. The current Low energy acceptance interval $(-1.4J, 1.4J)$ is believed to be too stringent, resulting in unsatisfactorily low probabilities of certifying a "good" machine (see Fig. 1). The probability of certifying a candidate machine using the interval (L, U) based on $d = 1.4J$ is displayed in Fig. 3.

In Fig. 3, the probability of certification is quite close to 1.0 regardless of variation for values of $|\mu_p - \mu_c|$ less than $1.4J$; that is, a "good" machine will almost always be certified. While the probability of certification is still dependent on σ, the main influence of increasing variability occurs when $|\mu_p - \mu_c| \geq 1.4J$, where the effect of increasing σ is to make it more likely that we will certify a "bad" machine. Again, a step function would be ideal, but progress toward the ideal could only be achieved by accepting lots with very small specimen variation.

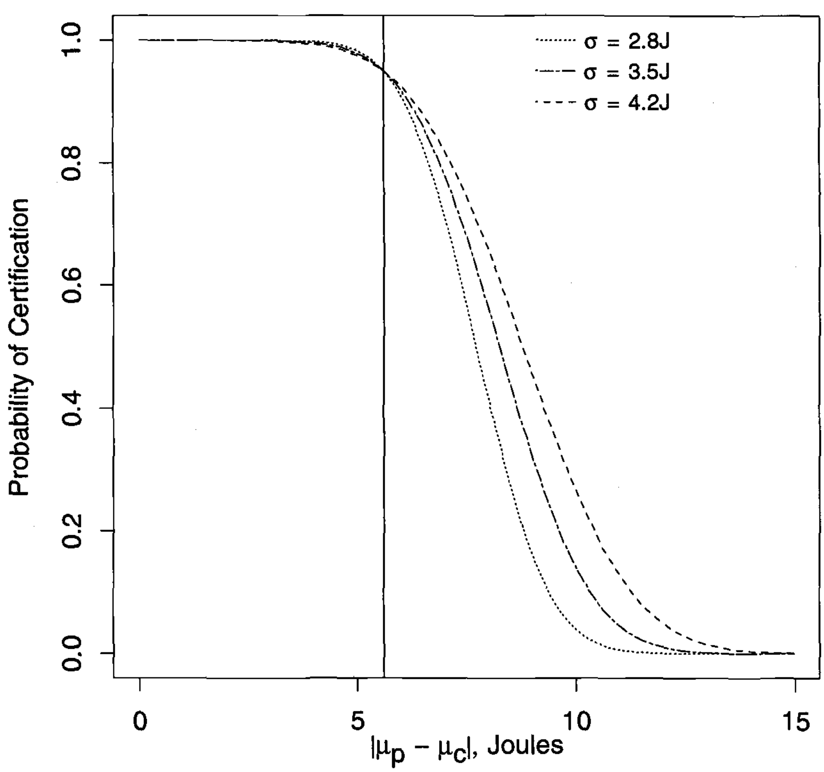

FIG. 4–Probability of certifying a candidate machine at the High energy level versus the theoretical difference between the reference value and the true candidate machine average absorbed energy when $\alpha = 0.05$.

The procedure described above can be applied to the High energy case as well. Assuming that the F–test has been passed, the acceptance limits for the High energy case would be calculated exactly as they were for the Low energy test, but substituting any appropriate value of d in (5). For illustrative purposes, we have used $d = 5.6J$ in (5) and computed the probability of certifying a candidate machine for realistic values of the variance for High-energy specimens. Fig. 4 displays the probability of certifying a candidate machine for the High energy case, assuming that the system variation for the candidate machine is the same as for NIST.

The probabilities shown in Fig. 4 are similar in structure to those observed for the Low energy case. The probability of certification is nearly 1.0 for "good" machines, $|\mu_p - \mu_c| \leq 5.6J$, while the probability of certifying "bad" machines, $|\mu_p - \mu_c| > 5.6J$, drops off gradually depending on σ.

CONCLUSIONS

We have shown that the current limits for certifying candidate Charpy machines need to be reconsidered, since they are not adjusted for lot-to-lot system variation. A crucial step in revising the certification limits is to select an appropriate value of d, the amount of allowable deviation between the conceptual lot averages for the candidate machine and the NIST reference machines. Perhaps the chosen value of d could be listed in section 10 of ASTM E 23–88, Standard Test Methods for Notched Bar Impact Testing of Metallic Materials, rather than the fixed certification limits currently documented.

We have made some assumptions regarding the reference value and the system variation of the reference machines that may not be appropriate in the practical application of the certification program. Therefore, other aspects of the program should be adressed before changing the certification limits. Specifically, the development of a method for calculating appropriate estimates of the reference value and the NIST system standard deviation when there are differences among the three reference machines is critical. The verification set sample size and the pilot-lot sample size also merit further investigation.

This paper introduced one alternate certification procedure that accounts for system variation and is more rigorous in its statistical validity than the existing procedure. A general destructive testing procedure has not been developed as yet, but is an important area for future statistical research.

ACKNOWLEDGMENT

The authors thank Dom Vecchia, Chris McCowan, Dan Vigliotti and Tom Siewert of the National Institute of Standards and Technology for their input during the preparation of this document. This work is a contribution of the U. S. government, not subject to copyright in the United States.

APPENDIX

For the Lower energy, the hypothesis we want to test is $H_0: |\mu_p - \mu_c| < 1.4J$. The decision rule is to reject H_0 if $\overline{P} - \overline{C}$ is not in (L, U), where L and U are chosen so that the test has size α. The size of the test is defined as the probability of rejecting H_0

when H_0 is true, or the probability of not certifying a "good" machine. Notationally, we write

$$\Pr\left[\overline{P} - \overline{C} \notin (L,\, U) \mid -1.4J \le \mu_p - \mu_c \le 1.4J\right] = \alpha.$$

Common values of α used in practice are 0.05 and 0.01.

With a pre-determined α, acceptance limits L and U can then be determined from

$$\begin{aligned} 1-\alpha &= \Pr\left[L \le \overline{P} - \overline{C} \le U \mid \mu_p - \mu_c = -1.4J\right] \\ &= \Pr\left[L \le \overline{P} - \overline{C} \le U \mid \mu_p - \mu_c = 1.4J\right] \end{aligned} \tag{6}$$

(e.g., see [4], p. 427). Equation (6) can be depicted in Fig. 5 if we assume that $\overline{P} - \overline{C}$ is normally distributed with average $\mu_p - \mu_c$ and variance $\sigma^2(1/100 + 1/5) = 0.21\sigma^2$.

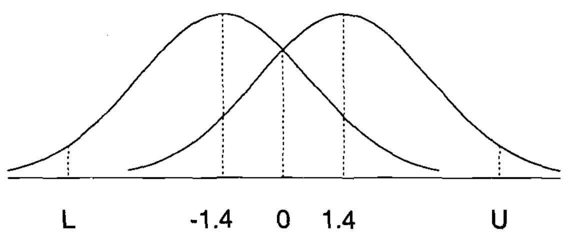

FIG. 5–Acceptance limits L and U with respect to two normal distributions.

From Fig. 5, it is easily seen that $U = -L$. Furthermore, by making use of the result that

$$\frac{\overline{P} - \overline{C} - (\mu_p - \mu_c)}{\sqrt{0.21}S}$$

is distributed as a Student's t with 103 degrees of freedom, the value of U satisfies

$$T_{103}\left(\frac{U + 1.4}{0.4583\,S}\right) - T_{103}\left(\frac{1.4 - U}{0.4583\,S}\right) = 1 - \alpha \tag{7}$$

where $S^2 = (99S_p^2 + 4S_c^2)/103$ is the pooled estimate for σ^2, and $T_n(\cdot)$ is the distribution function of Student's t with n degrees of freedom. If S is not too large, say $S \le 4$, which should be the case in our problem, a simple solution for (7) is

$$U = 1.4 + 0.4583\,S\,t_{1-\alpha:103} \tag{8}$$

where $t_{1-\alpha:103}$ is the $1-\alpha$ quantile of Student's t with 103 degrees of freedom. The solution can be verified as follows. With the solution in (8), the left-hand side of (7) reduces to

$$T_{103}\left(\frac{2.8}{0.4583\,S} + t_{1-\alpha:103}\right) - T_{103}(-t_{1-\alpha:103}) = T_{103}\left(\frac{2.8}{0.4583\,S} + t_{1-\alpha:103}\right) - \alpha.$$

With $S \le 4$ and commonly used values of α,

$$T_{103}\left(\frac{2.8}{0.4583\,S} + t_{1-\alpha:103}\right)$$

is very close to 1, and (7) is satisfied.

REFERENCES

[1] Driscoll, D. E., "Reproducibility of Charpy Impact Test," Symposium on Impact Testing, ASTM STP 176, American Society for Testing and Materials, 1955, pp 70–74.

[2] IMSL Inc., The IMSL Math/Library, Houston, Texas, 1987.

[3] Walpole, R. E. Introduction to Statistics, Third Edition, Macmillan Publishing Company, New York, 1982.

[4] Mood, A. M., Graybill, F. A, and Boes, D. C. Introduction to the theory of Statistics, Third Edition, McGraw-Hill Inc., New York, 1974.

[5] Fahey, N. H., "Effects of Variables in Charpy Impact Testing," Materials Research and Standards, Vol. 1, No. 11, November 1961, pp 872–876.

[6] ASTM E 1236-91, "Standard Practice for Qualifying Charpy Impact Machines as Reference Machines," pp 1–6.

[7] ASTM E 23-88, "Standard Test Methods for Notched Bar Impact Testing of Metallic Materials," pp 198–213.

Gérard Galban,[1] Ivan Le Muet,[2] Denis Mougin,[3] Gilbert Revise,[1] Roger Roche,[4] and Louis Roesch[5]

PRESENTATION OF THE FRENCH SUPPLY OF CHARPY V REFERENCE TEST PIECES

REFERENCE: Galban, G., Le Muet, I., Mougin, D., Revise, G., Roche, R., and Roesch, L., **"Presentation of the French Supply of Charpy V Reference Test Pieces,"** Pendulum Impact Machine : Procedures and Specimens for Verification, ASTM STP 1248, Thomas A. Siewert and A. Karl Schmieder, Ed., American Society for Testing and Materials, Philadelphia, 1995.

ABSTRACT: Charpy V reference test pieces are required by standards EN 10045-2 and ISO DIS 442 for the indirect verification of pendulum impact testing machines. Based on an agreement between Aubert & Duval, LNE, ETCA and FFA, production of such test pieces has begun in France. A preliminary study, made with an experimental batch, has shown that these test pieces are equivalent to the BCR test pieces. This trial production allowed us to define the manufacturing and calibration conditions for the industrial production of Charpy V reference test pieces. Three levels of impact energy are available. The main features of this production are presented.

For verification of the pendulum impact testing machines used in industry, indirect verification by the use of reference test pieces is generally sufficient. Furthermore,

[1]National Testing Laboratory (LNE), Zone Industrielle Trappes Elancourt, 5, rue Enrico Fermi, 78190 TRAPPES.

[2]Aubert & Duval, 41, rue de Villiers, 92200 NEUILLY-sur-SEINE.

[3]Technical Central Army Laboratory (ETCA), 16bis, Avenue Prieur de la Côte d'Or, 94114 ARCUEIL CEDEX.

[4]Iron and Steel Standardization Office (BNS), Immeuble Ile de France, 4, Place de la Pyramide, Cédex 33, 92070 PARIS LA DEFENSE.

[5]French Iron and Steel Research Institute (IRSID), 34, rue de la Croix de Fer, 78105 SAINT-GERMAIN-EN-LAYE CEDEX.

it is easier to carry out and more economical than detailed direct verification. In France, indirect verification has traditionally been performed with unnotched beam impact specimens [1]. Prismatic test pieces of the same length and width as the notched impact test pieces were machined to different heights, and tested at room temperature with the pendulum impact testing machine to be verified. With this method, it was easy to obtain a range of values for the absorbed energy. The test pieces were easier to prepare than notched bars and the results had less scatter. Nevertheless, the repeatability and error of the data were a good measure of the metrological quality of the machine. At the national level, a procedure for the production and certification of Charpy V-notch reference test pieces was established. A detailed study has been made on the factors affecting the accuracy of the results of such tests [2] and reduced tolerances were fixed for the reference machines.

After several years of tests, we discovered that machines that produced identical results with unnotched reference test pieces, could produce significantly different results (between machines) when testing Charpy V test pieces from the same material. This difference was commercially important, when values from one machine met the material specification and values from the other machine did not. In the case of notched bars, additional factors influence the accuracy of test results [3, 4]. This explains why some countries have based their indirect verification method on the use of notched reference test pieces [3]. At the international level, it was agreed to standardize on the use of Charpy V reference test pieces [6, 7]. The scatter of the results is greater than in the case of unnotched bars, but the machines are verified under conditions representative of their industrial usage.

In North America, verification specimens of heat-treated steel are available for machines with 8 mm strikers. In Europe, Charpy V reference test pieces for both 2 and 8 mm strikers, have only become available recently and in limited quantities [8]. In view of the large number of reference test pieces now required in France, it was considered necessary to create a French supply of such test pieces, produced and qualified according to the specifications of EN 10045-2. The BCR specimens, tested with the French reference machines (ETCA and LNE), allow the national specimens to be traced to the European reference. A preliminary study made with a small scale trial production, showed that specimens of the quality required for reference test pieces could indeed be produced at the national level. A program leading to the production of commercial batches of such test pieces has therefore been defined and successfully completed.

PRELIMINARY TRIAL

a. Test program

An interlaboratory test program including 14 impact testing machines (2 reference machines and 12 industrial machines) was defined. Each machine tested three types of test pieces: a verification set of unnotched bars (UNB), a verification set of BCR Charpy V reference test pieces (KV-BCR), and a verification set of the

French experimental reference test pieces (KV-FR). Each verification set consisted of 15 test pieces (5 test pieces per energy level): a low-energy level (20-30 J), a medium energy level (70-85 J) and a high-energy level (120-180 J). All tests were done at room temperature with the 2 mm striker.

b. Experimental batch of French reference test pieces

As for the ASTM and BCR reference specimens, a type AISI 4340 steel was used. Preliminary tests allowed the determination of the heat treatment conditions leading to energy levels similar to those of the BCR reference specimens. The detailed specifications of the material are given in the Materials Section. For the trial production, the heat treatments were carried out on small blocks (20 test pieces per block), all taken from a selected billet of a single heat. For each energy level, 120 test pieces were machined to the dimensions and tolerances shown in Table 1. Special precautions have been taken and a careful machining procedure was followed. Three test pieces from 5 blocks, randomly selected, were tested with a reference machine for the assessment of the homogeneity of the batch.

c. Statistical parameters of the verification sets

1. Unnotched impact bars

The verification sets consist of 5 specimens each of 3, 5, and 7 mm heights. The sets used for each energy level came from a single production batch (10 blocks as identical as possible). Five testpieces per block are tested with the national reference machine (Code R1). The statistical analysis of the results (Fig. 1) shows that test pieces coming from different lots belong to a common statistical population with a Gaussian type of distribution. The average value of this distribution is taken as the certified value for the batch (E_c).

For a verification set of 5 test pieces, the standard deviation s_5 of the average can be estimated by $s/\sqrt{5}$, where s is the standard deviation of the distribution. For the three energy levels considered in the present program, Table 2 indicates the values of E_c, s and s_5.

2. BCR reference test pieces

The verification sets consist of 5 test pieces of respectively 30, 80 and 120 J nominal impact energies. The production and certification procedures are described in [8]. The test pieces corresponding to a given energy level all came from the same batch. The certificate delivered by BCR indicates the reference value for the impact energy of the batch (E_c) and the uncertainty corresponding to a set of 5 test pieces ($\pm$ 2 s_5). These parameters are given in Table 2.

TABLE 1--Designation, dimensions and tolerances of the reference test pieces

Designation	Dimensions	Tolerances		
		Trial production test pieces	French reference test pieces	EN 10045-2
Length of test piece	55 mm	± 0,1 mm	+ 0 - 0,25 mm	+ 0 - 0,25 mm
Height of test piece	10 mm	± 0,01 mm	± 0,04 mm	± 0,06 mm
Width of test piece	10 mm	± 0,01 mm	± 0,04 mm	± 0,06 mm
Angle of notch	45°	± 2°	± 1°	± 1°
Ligament length	8 mm	± 0,02 mm	± 0,04 mm	± 0,08 mm
Radius of curvature of base of notch	0,25 mm	± 0,03 mm	± 0,025 mm	± 0,025 mm
Distance between the symetry plane of the notch and one of the endfaces of the test piece	27,5 mm	± 0,1 mm	± 0,10 mm	± 0,10 mm
Angle between the symetry plane of the notch and the longitudinal axis of the test piece	90°	± 2°	± 2°	± 2°
Angle between adjacent faces	90°	± 0,10°	± 0,10°	± 0,10°

TABLE 2--Parameters of the statistical distribution of the impact energy determined with reference machines (2 mm striker)

Verification set	Batch	Certified or reference value E_c (J)	Standard deviation batch s (J)	Standard deviation for 5 tests	
				s_5 (J)	% E_c
UNB	P 30	26,780	0,193	0,086	0,32
	P 80	83,605	0,370	0,165	0,20
	P 180	181,126	0,911	0,407	0,22
KV-BCR	30 A	25,5	2,01	0,9	3,53
	80 A	74,1	2,46	1,1	1,48
	120 B	123,3	5,92	2,65	2,15
KV-FR	F 25	21,60	1,685	0,753	3,49
	F 75	71,66	2,250	1,006	1,40
	F 120	124,81	3,950	1,766	1,41

UNB : french reference machine R1

KV-BCR : BCR certificate

KV-FR : french reference machine R2

s_5 : standard deviation of the average value of 5 tests.

3. Experimental batch of French reference test pieces

Only 15 specimens per energy level were available for the statistical evaluation of the homogeneity of the batches, 3 specimens from 5 different lots tested with the national reference machine (Code R2). The procedure described in ISO 5725 [9] has nevertheless been applied in order to estimate the within-lot and between-lot standard deviations. The following trends are shown:

- the scatter of results is statistically comparable in all blocks corresponding to a given impact energy,
- there is no statistically significant difference between the scatter in the lots of the 70 and 120 J batches,
- there is a small difference between lots for the 20 J batch: for this energy level, room temperature is close to the FATT of the steel and the increased scatter of the results is related to the transition in fracture mode.

Keeping in mind the preceding reservations, the cumulative frequency curves have nevertheless been drawn (Fig. 2). As a good approximation, the 15 test results can be considered as a single statistical population with a normal distribution of impact energy. The statistical parameters of this distribution are listed in Table 2.

4. Comparison of the homogeneity of the three types of verification sets

The self induced scatter of the impact energy within a given batch of reference test pieces can be described by s or s_5 (Table 2). The characterization is made with reference machines for all the batches considered. Table 2 confirms that the uncertainty of the reference energy is much greater in the case of Charpy V reference test pieces than in the case of unnotched bars. The experimental KV-FR reference test pieces and the BCR verification sets have quite similar uncertainties for the average impact energy.

d. Results of the interlaboratory test program

1. Charpy V reference test pieces of medium impact energy

In the 70 to 80 J energy range, 14 machines have been verified with BCR reference test pieces (Batch 80 A) and with the experimental French reference test pieces (Batch F 75). The total spread of values is similar in both sets, but the histograms are slightly different (Fig. 3 and 4). The machine averages for impact energy are compared on Fig. 5. The KV-FR results are closely correlated with the KV-BCR results: the scatter around the regression line is small and both types of test pieces rank all machines in the same order. The correlation between UNB results and KV-BCR is much looser: machines which are found quite similar with UNB test pieces give quite a range of results with the Charpy V test pieces (spread of about 6 J). The detailed results (not presented here) show further that both types

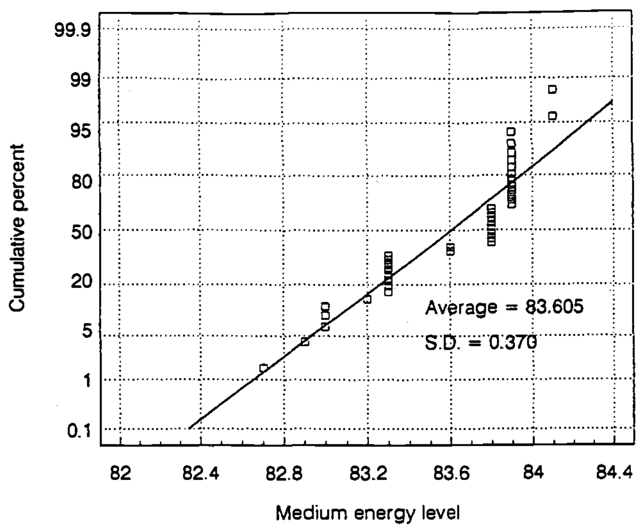

FIG. 1--Normal probability plot of the absorbed energy values measured with reference machine R1 for the certification of the batch of unnotched reference test pieces

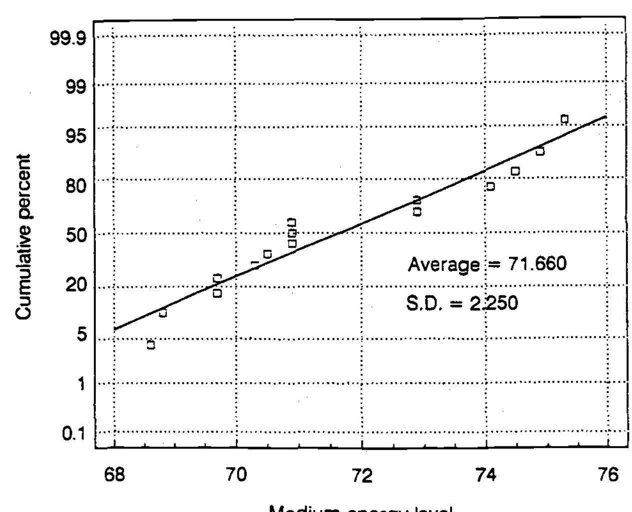

FIG. 2--Normal probability plot of the absorbed energy values measured with reference machine R2 for the certification of the experimental batch of Charpy V reference test pieces

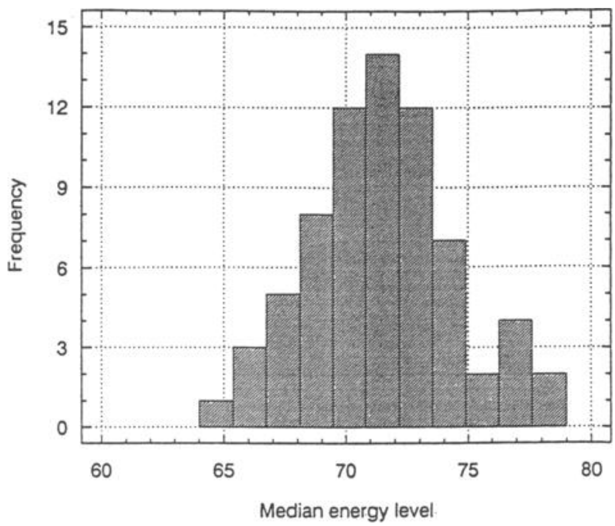

FIG. 3--Frequency histogram of values KV-BCR

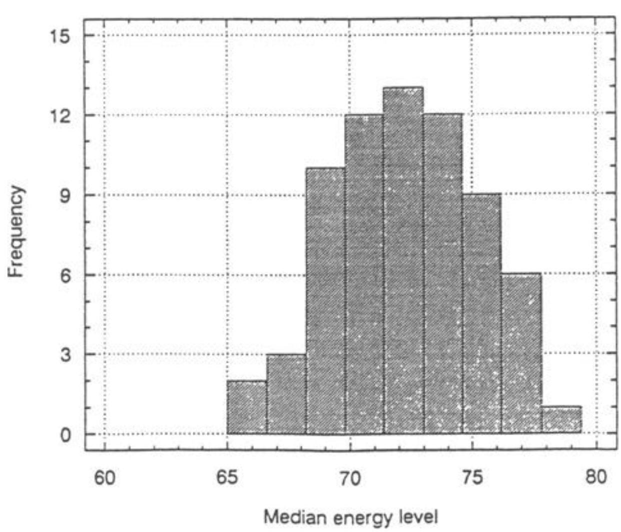

FIG. 4--Frequency histogram of values KV-France

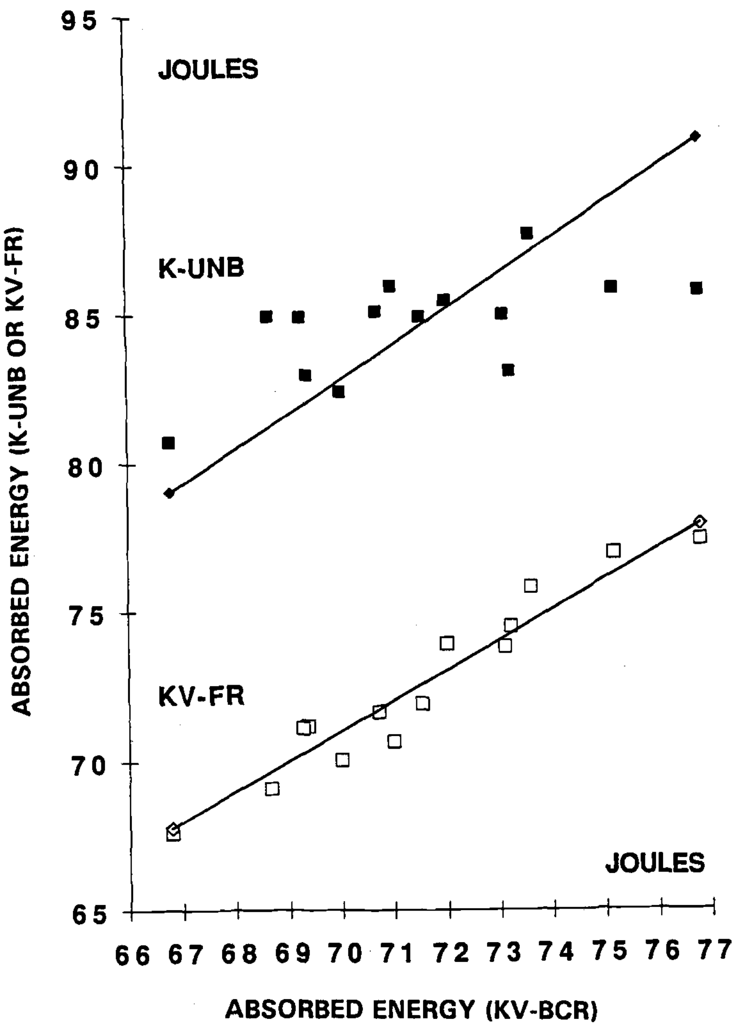

FIG. 5--Correlation between the results obtained with BCR reference test pieces, and unnotched bend test pieces (K-UNB) and French Charpy V reference test pieces (KV-FR), respectively. The slope of the solid lines corresponds to the ratio of the reference energies of the corresponding batches.

of Charpy verification sets lead to similar repeatability errors: intralaboratory standard deviation of 1.51 J for KV-BCR and 1.50 J for KV-FR.

2. *Statistical analysis of all data*

From the type of data, the following statistical parameters were calculated, according to ISO 5725 [8]:

- the general average of the impact energy $\bar{\bar{E}}$,
- the estimated repeatability standard deviation within laboratories, s_r,
- the estimated between laboratories standard deviation, s_L,
- the estimated reproducibility standard deviation,
  $s_r = \sqrt{(s_r^2 + s_L^2)}$,
- the estimated standard deviation of the average of five tests,
  $s_5 = \sqrt{(s_r^2 / 5 + s_L^2)}$.

The results are shown in Table 3. The following comments can be made :

- the repeatability and reproducibility are always better with unnotched test pieces than with Charpy V test pieces,
- the figures for s_r, s_L, and s_R are very similar for KV-BCR and KV-FR reference test pieces,
- in the case of unnotched test pieces, s_L is the predominant factor of scatter and the small s_r value facilitates the discrimination between machines (this was the principal reason for the choice of this type of test pieces for the indirect verification of impact machines),
- in the case of Charpy V test pieces, s_r and s_L both contribute significantly to the overall scatter of the results.

A more detailed analysis of the results, not presented here, confirms that KV-BCR and KV-FR reference test pieces give equivalent results when used for the indirect verification of industrial impact machines.

c. Application of the criteria for indirect verification of impact machines

For both unnotched and KV test pieces, the verification standards specify maximum values for repeatability and error. These values have been calculated from the 9 reference sets used in the present interlaboratory program (Table 4). The average results for the 14 machines considered (including the reference machines) are always within the tolerance. Individual machines may be outside of tolerance, sometimes because of excessive error, but mostly because of excessive scatter (Table 4). Even in those cases, the criteria are only exceeded by a small amount. The few cases of violation of the tolerance limits are probably not significant and may be attributed to random factors. In cases where the tests have been repeated (not shown in this report), the violations were not confirmed.

TABLE 3--Results of the indirect verification of 14 machines using three types of reference test pieces

Range of impact energy	20-30J			70-85 J			110-180 J		
Type of specimens	UNB	KV-BCR	KV-FR	UNB	KV-BCR	KV-FR	UNB	KV-BCR	KV-FR
BatchP 30	30 A	F 25	P 80	80 A	F 75	P 180	120 B	F 120	
E_c (J)	26,8	25,5	21,60	83,6	74,1	71,7	181,1	123,3	124,8
s_5 (J)	0,1	0,9	0,75	0,2	1,1	1,0	0,4	2,65	1,8
E (J)	27,07	24,63	20,87	84,64	71,52	72,55	183,00	118,28	128,42
s_r (J)	0,162	1,401	1,772	0,405	1,567	1,602	1,003	3,564	4,107
s_L (J)	0,895	2,064	1,327	1,778	2,606	2,842	2,945	4,328	4,719
s_R (J)	0,909	2,494	2,214	1,823	3,041	3,262	3,111	5,606	6,256
s_R/E (%)	3,34	10,1	10,6	2,15	4,25	4,97	1,70	4,74	5,01
s_5 (J)0,8982,157	1,546	1,787	2,698	2,931	2,979	4,612	5,064		
s_5/E_c (%)	3,35	8,46	7,15	2,14	3,64	4,09	1,64	3,74	4,06

TABLE 4--Application of the repeatability and error criteria of EN 10045-2 (all values in J)

Range of impact energy	20-30J			70-85 J			110-180 J		
Type of specimens	UNB	KV-BCR	KV-FR	UNB	KV-BCR	KV-FR	UNB	KV-BCR	KV-FR
Reference energy	26,8	25,5	21,6	83,6	74,1	71,7	181,1	123,3	124,8
Maximum repeatability	2	6	6	4,18	11,11	10,75	9,05	18,5	18,7
Maximum error	2	4	4	4,18	7,41	7,17	9,05	12,3	12,5
Average results for 14 machines	27,07	24,63	20,87	84,64	71,52	72,55	183,0	118,28	128,42
Repeatability	0,386	3,507	3,886	0,862	3,600	3,521	2,48	8,63	10,1
Error	0,27	-0,87	-0,73	1,04	-2,68	0,85	1,90	-5,02	3,62
Greatest values found for									
$E - E_C$	2,1	5,3	2,6	4,1	7,3	5,7	8,5	10,2	12,0
Repeatability	1,0	6,5	6,7	2,4	5,6	5,0	6,9	15,0	21,0
Number of machines out of tolerance	1	2	1	0	0	0	0	0	1
Cause	$E - E_C$	r, $E - E_C$	r						r

e. Qualification of the French reference machines for the characterization of Charpy V reference test pieces

On different occasions, including the present interlaboratory program, BCR reference test specimens were tested on reference machines R1 and R2. This procedure establishes traceability to the BCR system. Appendix B of EN 10045 Part 2 specifies the repeatability and error requirements.

Tests have been made at the four energy levels for which BCR reference test pieces were available. The results are given in Table 5. Machine R1 meets the requirements in all cases. Machine R2 violates the error requirement in 2 cases (out of 9). These batches were retested after a verification of the machine, but the new values were still out of tolerance. No explanation could be found. In later tests with this machine, the results were always satisfactory. It may be concluded that the requirements of Appendix B are not easy to meet, keeping in mind the rather large scatter within each batch of BCR reference test pieces. Table 5 nevertheless shows that both reference machines R1 and R2 can be used to characterize reference Charpy V test pieces from other sources than BCR.

f. Conclusion of the preliminary program

Three batches of about 120 Charpy V reference test pieces have been produced in France. Tests with the national reference machines have shown that these test pieces are equivalent to BCR certified reference batches, with similar energies and similar uncertainty for the certified energy. In an interlaboratory program of indirect verification of industrial impact testing machines, the test pieces gave results for repeatability and error very similar to those obtained with BCR reference test pieces. The French reference machines meet the requirements for machines certifying Charpy V reference test pieces traceable to BCR. These encouraging results lead to the decision to go on with a larger scale national production of Charpy V reference test pieces.

MATERIAL SPECIFICATION

a. Basic needs

An important aim was to allow the indirect verification of impact testing machines over a range of energy matching the critical applications of structural steels, i.e. 10 to 180 J.

On the other hand, the manufacturing process has to guarantee the lowest scatter of impact energy value compatible with industrial manufacturing conditions, for every batch of around 1,000 test pieces.

TABLE 5--Results obtained with the french reference machine for different sets of BCR reference test pieces

Reference batch	30 A	30 C	60 B	60 C	80 A	80 D	120 B	120 C	120 D
Values certified by BCR									
Energy (J)	25,5	25,5	56,3	56,9	74,1	77,6	123,3	122,9	118,3
Uncertainty (J)	1,8	1,4	1,8	1,7	2,2	2,4	5,3	5,5	4,4
95 % confidence interval	23,7-27,3	24,1-26,9	54,5-58,1	55,2-58,6	71,9-76,3	75,2-80,0	118-128,6	117,4-128,4	113,9-122,7
Ec ± 0,04E_c(J)	24,5-2,65	24,5-26,5	54,0-58,5	54,6-59,2	71,1-77,2	74,5-80,7	118,4-128,2	118,0-127,8	113,6-123,0
Values obtained with reference machines R1									
Energy	26,06	26,22	56,34	58,32	73,22	77,34	123,4	122,8	118,98
Standard deviation for 5 test pieces	1,496	0,725	1,65	0,902	1,539	1,101	2,699	1,138	3,802
% difference with specified value	2,20	5,18	0,07	2,49	1,19	0,33	0,08	0,08	0,57
Values obtained with reference machine R2									
Energy	24,58/25,34	25,12	56,14	57,19	70,0/71,06	76,68	113,8/115,7	121,64	117,24
Standard deviation for 5 test pieces	1,465/1,236	0,92	0,72	0,963	1,483/1,033	2,095	5,455/3,862	1,913	3,119
% difference with specified value	3,61/0,063	1,49	0,28	0,51	5,53/4,10	1,18	7,7/6,2	1,02	0,90

b. Grade and process selection

Considering recent work on the same topic (U.S. Army Watertown Laboratory and BCR activities), and the need for cost optimization, we selected an E-4340-H type of steel (AUBERT & DUVAL's NC 40 MW grade equivalent to ASTM A 540 grade B 23), which is able to cover the whole range 15 to 150 J by adjusting the tempering temperature.

In order to minimize the variation of the energy level from one batch to another, different production schemes were tried. For each scheme, test pieces of about 25, 70 and 115 J were prepared and impact tested. These trials allowed to define the following three requirements:

- high quality primary melting (air melt) followed by vacuum degassing, in order to obtain a very low sulphur content (S $\leq$ 0,003 %) and a high cleanliness,
- vacuum arc remelting in order to guarantee a high chemical homogeneity by reducing the segregation level, and a very high purity. Another characteristic of the V.A.R. process is the low porosity in the ingots, which reduces the risk of internal defects (after transformation the material is able to meet the requirements of the MIL-STD 2154 - AAA class), and
- processing of the steel ingot into an intermediate shape which allows a very homogeneous heat treatment to be performed.

c. Heat treatment and testing of the material

After a stringent ultrasonic inspection, the intermediate steel products are quenched in a way which allows the actual cooling rate to be the same at every location in the material where test pieces will be machined.

The tempering temperature is selected to produce the appropriate toughness level in the steel (See Fig. 6). It should be noted that the ductile-to-brittle transition temperature is near room temperature for this high-strength steel, when the test pieces are treated for an impact energy of 15-20 J. This may be responsible for a relatively large scatter of the impact energy, unless the tempering conditions are strictly controlled. The risk of this scatter in energies is reduced for the target level of 20-25 J that was finally chosen, and is kept under control with strict procedures. All furnaces used for the heat treatment have an temperature homogeneity better than 5°C. Tempering conditions leading to impact energy levels of 20-25 J, 70-75 J, and 110-120 J have been accurately defined.

A first validation was performed on a preproduction batch of 900 test pieces (300 per energy level). The present procedures and equipment allow the production of batches of about 1,100 test pieces, limited by the heat treatment processing equipment, and traceable to a specific ingot from a well defined heat.

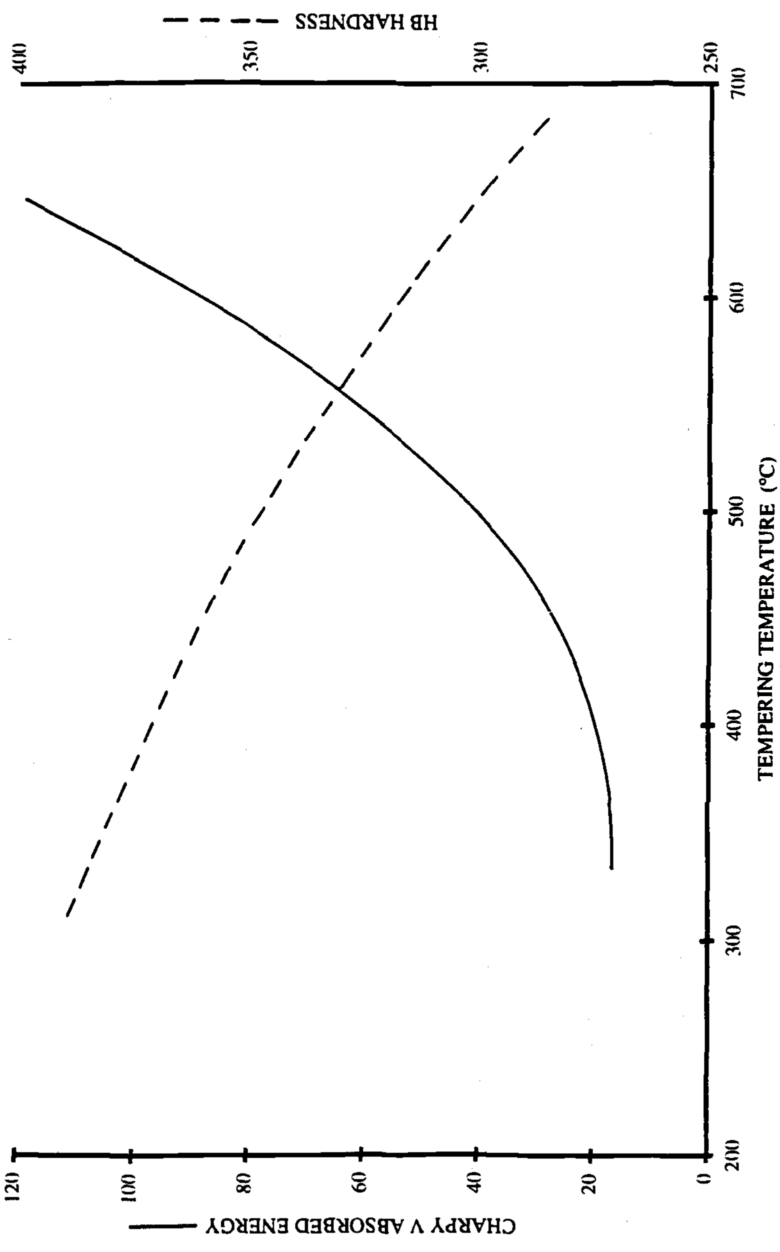

E - 4340 - N type steel

FIG. 6--Evolution of the Charpy V impact energy level with the tempering temperature

After heat treatment, an initial sample of 5 pieces is tested at the steelmaker's laboratory in order to check the homogeneity of the batch before machining, and the batch is marked with a unique batch serial number which is maintained at every subsequent stage in manufacturing.

MANUFACTURING AND INSPECTION OF THE REFERENCE CHARPY V TEST PIECES

The manufacturing of the French Charpy V reference test pieces is under the responsibility of the LNE. The inspection of these test pieces is carried out by the two laboratories LNE and ETCA. The LNE is also in charge of the shipment of the French reference test pieces to the customers. The principal requirements concerning the manufacture of the test pieces have also been fixed by the LNE and ETCA.

Some of the dimensional characteristics of the test pieces are stricter than those defined in the EN 10045-2. Table 1 gives these characteristics.

To obtain satisfactory homogeneity in a batch, special care has been taken during the machining process, specifically:

- to minimize the dimensional variations, all the machining operations are carried out on the same machines with the same adjustments and the tool wear is checked regularly, and
- to avoid the effects of heating and cold working which can produce structural modifications of the steel, a high-quality lubricant is applied and the cutting speeds are controlled.

The cutting processes have been carefully chosen so as not to alter the metallurgical properties of the test pieces.

The following conditions have been retained:

- the normal cutting process by milling,
- wire electrical discharge machining (EDM), after confirming that there was no problem with decarburization, and
- final preparation by grinding.

The operating sequence consists of the following operations:

- identification of the intermediate product,
- cutting of the intermediate product and machining of the blanks, leaving an excess thickness of 0,1 to 0,2 mm,
- marking of the number of the batch and of the orientation of the notch,
- machining of the test pieces to the dimensions given in Table 7,

- final check of the dimensions of the test pieces. This is carried out with a three dimensional measuring device for: the principal dimensions, the angle between adjacent faces, and the included angle of the V notch (with a profile projector) at a magnification of 50. This check was carried out on test pieces which are taken at random, taking into account that intermediate inspections are carried out on the first and last test pieces of the grinding plate,
- demagnetization of the test pieces, and
- protection of the test pieces by a lubricant.

When the test pieces are delivered to the LNE, a visual inspection is carried out to confirm that the surface finish and the identification requirements were met. For each batch, 50 test pieces are selected at random and are evaluated by the two laboratories (25 by LNE and 25 by ETCA). The evaluation includes the dimensions of the test pieces and the quality of the machining of the V notch (radius of curvature of base of notch and uniformity of the notch profile).

The test pieces are packed and stored in a room with a controlled temperature.

Calibration of the batches of test pieces

a. Principle

The calibration of the batches of test pieces is carried out with the two national reference impact testing machines (at LNE and ETCA) in accordance with the NF EN 10045-2 standard. These 2 laboratories are accredited by the national accrediting body, BNM-Fretac [1].

Two series of 25 test pieces are selected at random in each batch. One series is used by LNE (n_L) and the other one is used by ETCA (n_E). In each laboratory, the test pieces are broken in accordance with the NF EN 10045-1 standard at a test temperature of 20 °C ± 2 °C.

The impact energy values are used to verify the homogeneity of the batch and to determine the energy reference value (E).

b. Tests results - Reference value

Each laboratory determines the mean value and the experimental standard deviation for the 25 results :

[1] BNM : Bureau National de Métrologie - France Etalonnage Accréditation

ETCA: $\bar{X}_E$, s_E

LNE: $\bar{X}_L$, s_L .

<u>First step</u> : Comparison of the experimental standard deviations

The following condition must be satisfied in order to state the identity of the experimental standard deviations :

Condition (1) Table 6

For E ≤ 40 J

$$s_E = s_L, \text{ if } |s_E - s_L| \leq 0.5 \text{ J}$$

For E > 40 J

$$s_E = s_L, \text{ if } |s_E - s_L| \leq 1.0 \text{ J}$$

The probability of obtaining $s_E \neq s_L$ is very small with the two reference machines.

<u>Second step</u> : Comparison of the mean values

The following condition must be satisfied in order to state the identity of the mean values :

Condition (2) Table 6

For E ≤ 40 J

$$\bar{X}_E = \bar{X}_L, \text{ if } |\bar{X}_E - \bar{X}_L| \leq 2 \text{ J}$$

For E > 40 J

$$\bar{X}_E = \bar{X}_L, \text{ if } |\bar{X}_E - \bar{X}_L| \leq 3 \text{ \% E.}$$

When the condition (2) is satisfied, the mean energy value and the variance are respectively calculated by the following formulas :

$$\bar{E} = \frac{n_E\bar{X}_E + n_L\bar{X}_L}{n_E + n_L}$$

TABLE 6--Determination of reference energy and uncertainty

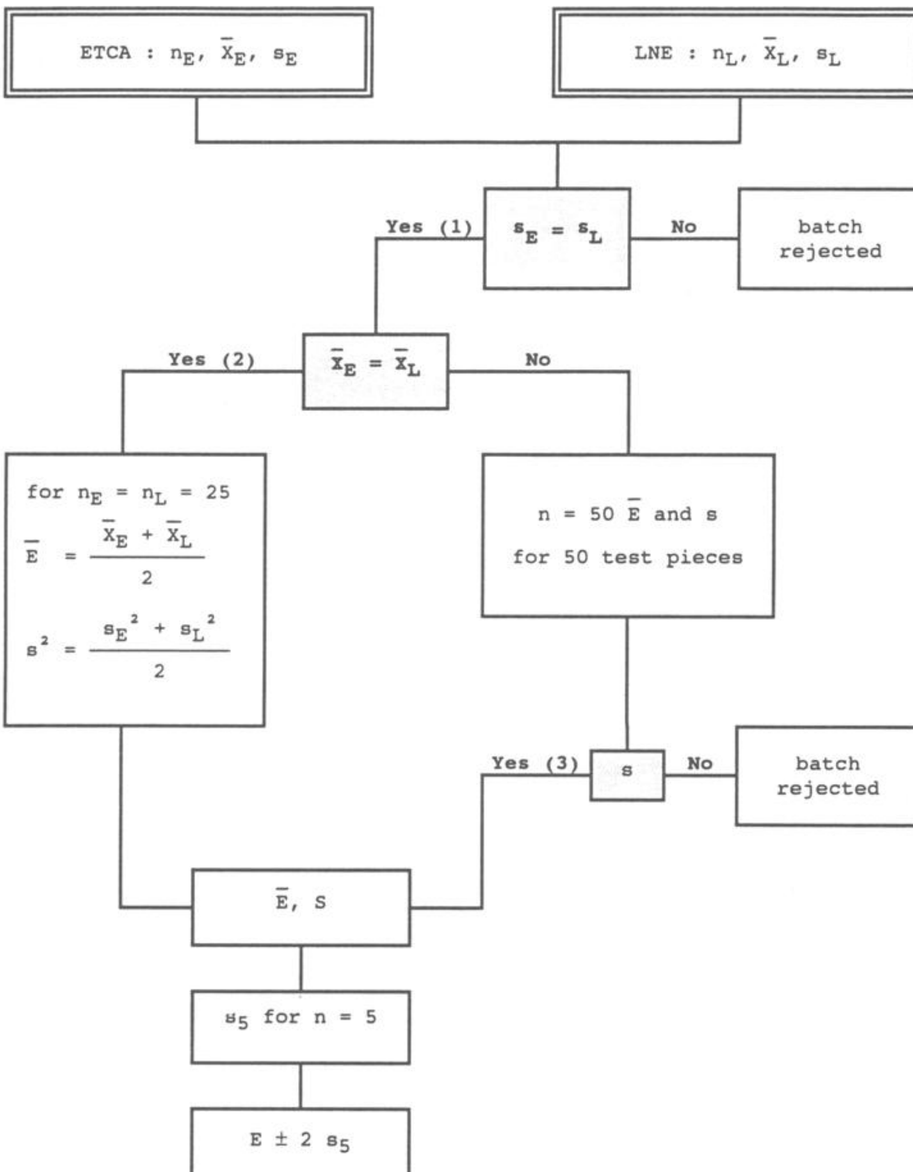

$$\bar{s}^2 = \frac{(n_E - 1)s_E^2 + (n_L - 1)\, s_L^2}{n_E + n_L - 2}$$

where $n_E = n_L = 25$

When the condition (2) is not satisfied, the mean energy value and the experimental standard deviation are determined for the 50 results.

Condition (3)

We verified that the experimental standard deviation fulfills the requirement of NF EN 10045-2:

$s < 2$ J, for $E < 40$ J
or $s < 5$ % E, for $E > 40$ J.

Reference value for the batches of 5 test pieces

The following values are determined for the verification sets of the industrial impact testing machines:

the mean value $\bar{E}$,
uncertainty determined by the experimental standard deviation s_5 for 5 test pieces (Student's t factor):

$$s = t\,(0{,}975/48)\; s / \sqrt{5}$$

$$S_5 = 2{,}011\; s / \sqrt{5}$$

The uncertainty associated with the energy value is equal to 2 s_5.

RESULTS

For example, Table 7 gives the results obtained for 3 batches:

batch 1A, level 20 J,
batch 2B, level 70 J, and
batch 5B, level 120 J.

We note that the conditions (1) and (2) are only satisfied for the two first levels (20 J and 70 J).

TABLE 7--Results for 3 batches at different energy levels

Batch	ETCA (E)	LNE (L)	Δ (E, L)	$\bar{E}$, s	Reference value (J)
1 A level 20 J	$\bar{X}_E$ = 20,8 s_E = 1,1 n_E = 25	$\bar{X}_L$ = 22,3 s_L = 1,0 n_L = 25	$\Delta(X_E, X_L)$ = 1,5 $\Delta(s_E, s_L)$ = 0,1 (1) Yes (2) Yes	$\bar{E}$ = 21,5 s = 1,05 s_5 = 0,9 for n = 5	E ± 2 s_5 21,5 ± 1,8
2 B level 70 J	$\bar{X}_E$ = 70,5 s_E = 2,7 n_E = 25	$\bar{X}_L$ = 72,6 s_L = 2,2 n_L = 25	$\Delta(X_E, X_L)$ = 2,1 $\Delta(s_E, s_L)$ = 0,5 (1) Yes (2) Yes	$\bar{E}$ = 71,5 s = 2,46 s_5 = 2,2 for n = 5	E ± 2 s_5 71,5 ± 4,4
5 B level 120 J	$\bar{X}_E$ = 112,3 s_E = 3,8 n_E = 25	$\bar{X}_L$ = 117,8 s_L = 4,1 n_L = 25	$\Delta(X_E, X_L)$ = 5,5 $\Delta(s_E, s_L)$ = 0,3 (1) Yes (2) No (3) Yes	$\bar{E}$ = 115,1 s = 4,82 for n = 5 s_5 = 4,35 for n = 5	E ± 2 s_5 115,1 ± 8,7

(1) (2) (3) Conditions of Table 6.

In the case of the third level (120 J):

condition (1) is satisfied,

condition (2) is not satisfied, however,

condition (3) is satisfied.

FINAL CONCLUSION

Thanks to a preliminary study, a procedure for the production and calibration of Charpy V reference test pieces was defined. The test pieces produced in France according to this procedure comply with all requirements of the EN 10045-2 standard. Valid calibration of these test pieces can be carried out by the French reference machines, which are qualified through periodic tests with the BCR certified reference test pieces.

Verification sets of this French production have been in use since the beginning of 1993. During 1993, 7,500 test pieces were produced: 500 were used for verification of the manufacturing process and for the determination of the reference energies; 4500 were used for the indirect verification of 300 industrial machines.

A regular production program is running and verification sets are available for potential users.

The process which has been described enables the French industry to satisfy the requirements of the EN 10045-2 standard.

REFERENCES

[1] French Standard NF A 03-508 (December 1985): Vérification des Machines de Flexion par Choc (Moutons-Pendules).

[2] G. Revise, "Influence of a Dimensional Parameter of a Test Machine on the Results of a Test," Charpy Impact Test - Factors and Variables: ASTM STP 1072 (1990).

[3] Impact Testing of Metals: ASTM STP 466 (1969)

[4] Instrumented Impact Testing: ASTM STP 563 (1974)

[5] ASTM E 23-91: Standard Test Methods for Notched Bar Impact Testing of Metallic Materials.

[6] EN 10045-2: Metallic Materials - Charpy Impact Test - Part 2: Verification of Pendulum Impact Testing Machines.

[7] ISO-DIS 442: Verification of Pendulum Impact Testing Machines for Testing Metallic Materials.

[8] H. Marchandise, A. Perez-Sainz, D. Counet: Certification of the Impact Toughness of V-notch Charpy Specimens, BCR report (European Community Bureau of Reference) EUR 12598 (1990).

[9] ISO 5725: Precision of Test Methods - Determination of Repeatability and Reproducibility by Interlaboratory Tests.

Testing Procedures and Other Topics

Rajesh G. Chandavale[1] and Tamal Dutta[2]

CORRECTION OF CHARPY IMPACT VALUES FOR KINETIC ENERGY OF TEST SPECIMENS

REFERENCE: Chandavale, R. G. and Dutta, T., "**Correction of Charpy Impact Values for Kinetic Energy of Test Specimens,** "Pendulum Impact Machines: Procedures and Specimens for Verification," ASTM STP 1248, Thomas A. Siewert and A. Karl Schmieder, Eds., American Society for Testing and Materials, Philadelphia, 1995.

ABSTRACT: The Charpy impact test was studied theoretically and experimentally, to learn how much of the pendulum energy is imparted to the test specimen. The fracture was separated from the subsequent collision, and the collision was studied kinematically. Materials are known to have a standard coefficient of restitution between any two bodies [1]. If this value is known, the behavior of the two bodies can be predicted after collision for any two initial velocities of the colliding bodies. This parameter was measured on U-type pendulum impact testing machine at a known initial velocity of the pendulum. The error based on velocities of V-notched test specimens and pendulum were calculated at several different initial velocities of the pendulum corresponding to different energy levels. The error was also measured by experiment at different energy levels on machine. The results were in reasonable agreement with the calculated values. Various test conditions and material properties of the specimen that cause such error are also discussed.

KEYWORDS: Collision, coefficient of restitution, velocity, kinetic energy, density.

Observations of a large number of Charpy V-notch impact test on different metals indicate that the test specimens do not always undergo complete fracture. This is because a specimen of a ductile material can bend and slip through the anvil before the crack has fully propagated. This results in an error in the absorbed

1 Metallurgist, Quality Assurance and Control Division, Thermax Ltd., Chinchwad, Pune 411 019, India.

2 Manager, Quality Assurance and Control Division, Thermax Ltd., Chinchwad, Pune 411 019, India.

energy, which is then used also for tossing the test specimen. This additional energy contributes to the scale reading as absorbed energy for fracture. The error is not significant for light metals and alloys, but is estimated to be significant for dense and moderately dense metals and their alloys. The error is of an intermediate value for the most commonly used metals and alloys. Because of the constraints such as radial notch (0.25 mm radius) and the large distance (40 mm) between the corners of the anvil, the specimen may be only partly fractured, particularly so for ductile metals. The problem was studied through the principles of kinematics. The behavior of the test specimens and pendulum was analyzed by theoretical calculations and experimental measurements. Three commonly used engineering metals: 99.5% pure copper, low carbon steel (ASTM A 516 Gr. 70), and 99.5% pure aluminum were selected to observe the kinetic energy effect. The conditions producing the error in the absorbed energy are also discussed in general.

THEORY

The Charpy impact test is composed of two separate events: 1) fracture and 2) the subsequent collision between the pendulum and the incompletely fractured test specimen. The calculations and measurements consider only a collision based on kinematics. Measurement of the coefficient of restitution (in this case, the elastic rebounding of the specimen from the striker) in a collision between two bodies on a given testing machine can be used to predict the behavior of the two bodies after the collision. The velocity of the pendulum immediately after fracture is the same as the initial velocity of the pendulum in collision:

$$V_{p2}-V_{s2} = -e\,(V_{p1}-V_{s1}) \qquad \text{....(1)}$$

Where

e = Coefficient of restitution.

V_{p1} = Initial velocity of the pendulum, m/s.

V_{p2} = Final velocity of the pendulum, m/s.

V_{s1} = Initial velocity of the test specimen, m/s

V_{s2} = Final velocity of the test specimen, m/s.

The system is considered isolated from any interferences from external sources. Irrespective of the value of the coefficient of restitution, the momentum of the system is conserved. Therefore, from the principle of conservation of momentum-

$$M_p\,V_{p1} + M_s\,V_{s1} = M_p\,V_{p2} + M_s\,V_{s2} \qquad \text{.....(2)}$$

Where

M_p = Mass of the pendulum, kg.

M_s = Mass of the test specimen, kg.

A simulated experiment was made as described below to calculate the value of the coefficient of restitution, "e". The two unknown variables V_{p2} and V_{s2} can be determined from the above two equations after substituting the value of "e".

EXPERIMENTAL PROCEDURE

A U-type pendulum impact machine with scale range of 300 J was used in the experiment. The standard size Charpy V-notch specimens were weighed before being fractured. The specimens were chosen after checking their rigidity so that no further fracturing occurred in tossing. The specimen was lightly placed in the anvils as shown in photograph 1. Friction between the specimen and the anvil was minimized during the toss so as to avoid material elasticity effects. Special supports were made and welded to the anvil, as shown. These platforms helped keep the specimen level with the anvil base.

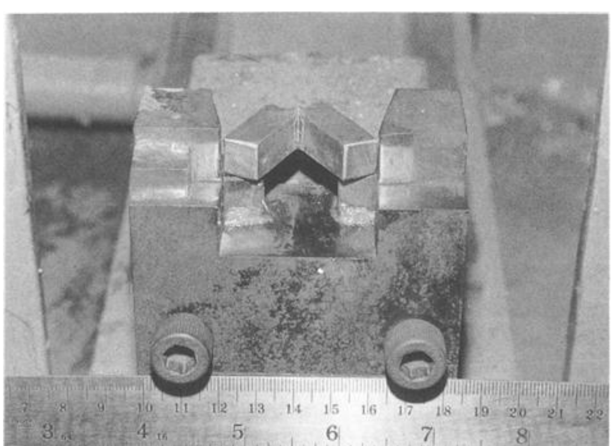

Photograph 1. Set up of the specimen.

The specimen was then tossed by dropping the pendulum from its full height, and the energy spent was measured on the scale. This energy is considered kinetic energy of the test specimen, and is given by

$$\text{Kinetic energy} = \tfrac{1}{2} M_s V^2_{s2} \tag{3}$$

Different energies thus recorded for copper, low carbon steel, and aluminum test specimens were 2.25 J, 1.90 J, and 0.45 J respectively. The corresponding velocities of the specimen were calculated from equation (3) as 9.57 m/s, 9.43 m/s, and 7.79 m/s.

Using these values in equation (1) and (2) the coefficient of restitution was found to be 0.7934, 0.7658 and 0.4574 respectively. We assume that this is a material property, and remains constant for given pair of bodies at all pendulum energy levels.

Based on these measurements of the coefficient of restitution, errors were calculated at evenly distributed pendulum energies, as given in Table 1. The errors were determined after calculating initial pendulum velocities from the machine data as per ASTM Standard Test Methods for Notched Bar Impact Testing of Metallic Materials (E 23). The initial velocity of the specimen (V_{s1}) was assumed zero at all energies.

TABLE 1 -- Results, theoretical and experimental.

Pendulum energy level in J	Error for Copper in J		Error for Low C Steel in J		Error for Aluminum in J	
	Calculated	Measured.	Calculated.	Measured.	Calculated.	Measured.
300	-	2.25	-	1.9	-	0.45
275	2.06	2.0	1.74	1.7	0.41	0.40
250	1.88	1.8	1.58	1.5	0.37	0.35
225	1.69	1.70	1.43	1.45	0.34	0.35
200	1.5	1.6	1.27	1.35	0.30	0.30
175	1.31	1.2	1.11	1.1	0.26	0.25
150	1.13	1.0	0.95	0.8	0.22	0.20
125	0.94	0.8	0.79	0.8	0.19	0.20
100	0.75	0.75	0.63	0.5	0.15	0.10
75	0.56	-	0.48	-	0.11	-
50	0.38	-	0.32	-	0.07	-
25	0.19	-	0.16	-	0.04	-
0	0	-	0	-	0	-

Table 1 also indicates the measured energies on a machine range of 300 J at different pendulum energies. An easily disengagable stand was used to support the pendulum at different heights. The pendulum was released smoothly and instantaneously for each trial. Measurements could only be made between potential energies of 100 J (200 J on scale) and 300 J (0 J on scale). Table 2 shows the masses of the individual specimens and the data used in calculations. Mass and the reference velocity of the pendulum were taken from the manufacturer's manual.

TABLE 2-- Data for theoretical calculations.

Copper	49.13 gm
Low C steel	42.77 gm
Aluminum	14.83 gm
Mass of pendulum (M_p)	20.97 kg
Reference velocity of pendulum (V_{p1})	5.349 m/s*

* Excluding the increase in velocity provided for compensating for the friction and windage losses.

RESULTS AND DISCUSSION

The experiment above uses the same impact testing machine for measuring the coefficient of restitution, but does not consider the energy losses in other forms such as by sound and heat.

The values from Table 1 are plotted in Figure 1. A plot of theoretical calculated values showed perfect linearity, with varying slopes for different metals. A small scatter in the measured values was observed as shown.

The curves indicate the highest energy losses are for copper, followed by low C steel, then aluminum. The coefficient of restitution and densities for these three materials were in decreasing order. Therefore, the error due to the kinetic energies obviously depends on both the density (representing the mass of the material) and the coefficient of restitution (representing the velocity of the specimen by collision). However, the coefficient of restitution and the density are independent of each other. The coefficient of restitution depends on both the materials involved in the collision. The curves can be expressed in equations as follows :

$$y = \frac{3x}{400} \quad \text{for copper} \qquad .....(4)$$

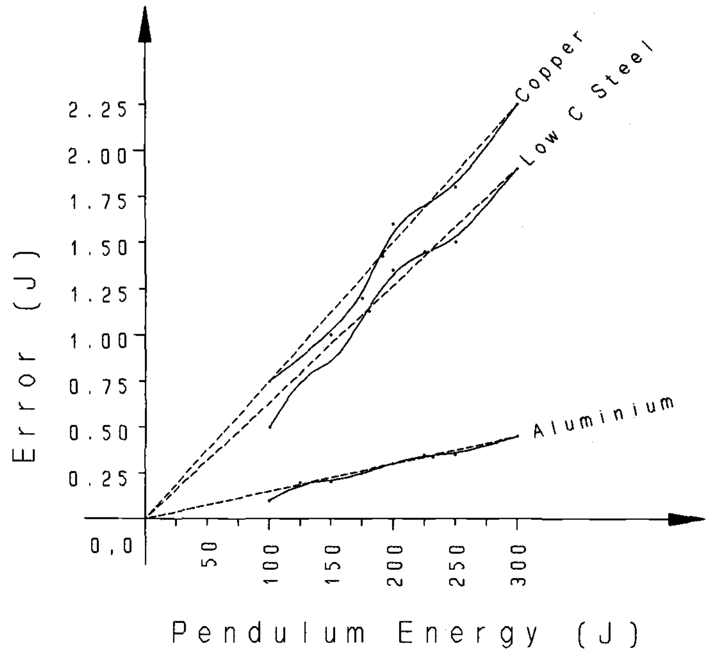

Figure 1. Calculated (dotted line) and measured (solid line) error at various pendulum energies.

$$y = \frac{19x}{3000} \quad \text{for low C steel} \qquad .....(5)$$

$$y = \frac{3x}{2000} \quad \text{for aluminum} \qquad .....(6)$$

Where,

y is the error in J

and

x is the pendulum energy in J, corresponding to the initial pendulum velocity

The slope of each curve describes the error completely. The curves are redrawn in Figure 2 to determine the error recorded on the scale during the actual test. Note that the pendulum (potential) energy is inversely related to the absorbed energy recorded in the test: a high pendulum energy following specimen fracture is a result of only a small amount of energy being absorbed during the fracture.

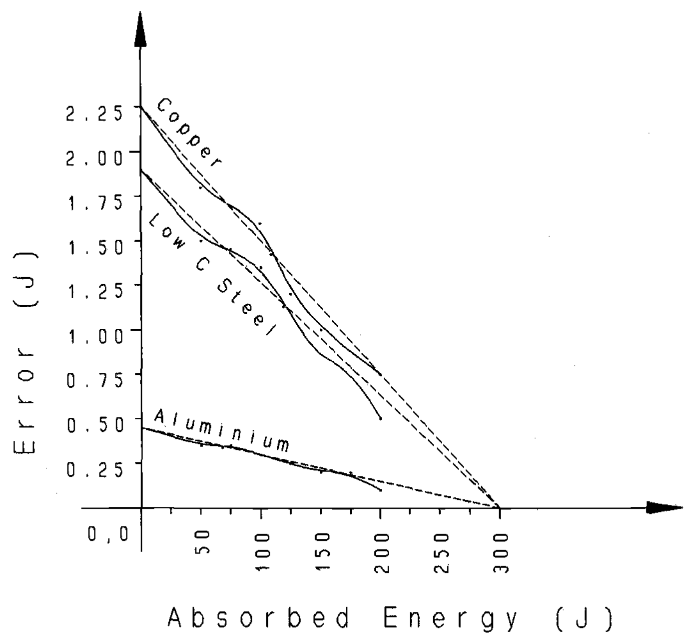

Figure 2. Calculated and measured error at various recorded energy levels on scale

The equations of each curve can be reinstated as -

$$Y = \frac{3(300\text{-}X)}{400} \quad \text{for copper} \qquad \text{....(7)}$$

$$Y = \frac{19(300\text{-}X)}{3000} \quad \text{for low C steel} \qquad \text{....(8)}$$

$$Y = \frac{3(300\text{-}X)}{2000} \quad \text{for aluminum} \qquad \text{....(9)}$$

Where,

the quantity 300 represents the scale range of the machine in J.

Y = Error in J

X = Recorded absorbed energy in J

Hence,

$$\text{True absorbed energy} = \text{Recorded absorbed energy - Error} = X - Y \qquad .....(10)$$

The error includes losses due to sound and heat which are estimated to be negligible compared to the main loss by kinetic energy in specimen. The other losses may not be significant even if the coefficient of restitution is low.

No energy was spent in further fracturing the test specimen as confirmed by numerous comparative measurements in a similar experiment on unnotched, merely bent specimens. A pendulum machine with a higher energy range than the one used in above experiment would give higher kinetic energy losses than that given in Table 1.

IMPORTANCE OF MATERIALS AND TEST CONDITIONS

a. Material density

Denser materials would give high kinetic energy loss due to the mass effect. The error described above is more for dense metals such as tungsten and precious metals, which are anticipated to give an error above 4 J.

Materials such as plastics and other composite materials of polymers are light in weight so would include only a very small error.

b. Coefficient of restitution

The kinetic energy loss will increase for elastic (in kinematical terms) bodies as the coefficient of restitution approaches 1.0. The kinetic energy decreases if the coefficient approaches 0, that is when the bodies are perfectly inelastic and have common velocities after collision. The earlier case would never be achieved and the later, very rarely [1].

The coefficient is also more likely to change with the material of the pendulum (striker). The coefficients of restitution would remain the same in all pendulum impact testing machines as long as the pendulum material is the same, irrespective of the range of scale in the machines.

c. Ductility

The toss error is important for the metallic materials with good ductility. Brittle materials are almost certain to completely fracture and a situation of collision among three bodies would occur. In such a case, the behavior of the three bodies can't be predicted. If a brittle material did not separate into halves, the high initial pendulum velocity could cause a large error. The ductile material will show lesser degree of error because of low initial pendulum velocity.

d. Mode of fracture

The mode of fracture is important because the specimen may not fracture into two separate halves. As shown in ASTM E 23 (Figure 15 - Fracture Appearance), even in low percent shear fracture test specimens, the specimens often undergo high shear deformation near the surface opposite to the notched surface [2]. This causes the specimen halves to remain joined even in the brittle test specimens.

A low-energy high-strength specimen, if it fails in a shear mode, would cause a large error as the kinetic energy is derived from the high velocity of the pendulum. A shear mode of fracture would involve large plastic deformation in fracture compared to the brittle crystalline fracture surfaces, and hence would tend to oppose complete fracture.

e. Modulus of elasticity

Materials of high modulus of elasticity are thrown with high kinetic energy in real impact tests. As reported in ASTM E 23, low-energy high-strength steel specimens are known to leave impact machines at speeds higher than 15.2 m/s [2]. The specimen stores large elastic stresses, which give high velocity to the test specimen. The combination of pendulum velocity and the reaction of the anvil creates a high velocity when the specimen squeezes through the anvil. Highly elastic materials undergo high reactive forces from the anvil. However, these forces can be taken as part of the energy absorbed to fracture, being a part of the area under elastic region of the stress-strain curve.

f. Yield strength

High yield strength materials would tend to reduce the size of the plastic zone given by

$$d_y = \frac{K^2}{\pi \sigma_y^2}$$

as per the mechanics of elastic-plastic fracture [3] near the crack. These materials generally undergo elastic fracture by breaking into two pieces and thus would have only a small error.

g. Test temperature

High test temperatures normally tend to result in incomplete separation of the specimen halves. Charpy values (CVN) of some metals and alloys such as fcc metals (Ag, Al, Au, Cu, Ni, Pb, and Pt, although Ir and Rh do cleave) increases from 0 K up to about 0.35 of the melting point (T_m) and do not normally cleave [reproduced from 3]. Steels also have a higher ductility above the ductile-brittle transition temperature. These materials would not tend to separate into two pieces after fracture at higher temperatures, depending on their toughness, thus contributing to the error.

h. Size of the specimen

Subsize test specimens tend to transform from plain strain to plain stress condition. In such a condition, the specimen has shear lips on the edge of fracture surfaces resulting from large plastic deformation [4]. This would tend to keep the specimen single after fracture. Also in proportion to the mass of the specimen, the specimen error due to kinetic energy will be reduced, but the coefficient of restitution remains unchanged.

CONCLUSIONS

The error due to kinetic energy effects of the test specimen is solely a function of density of the material of test specimen and the coefficient of restitution by collision. The value of both these vary widely in different materials, alloys, and composites, but largely depend on the properties and proportions of the base metal.

The relation between the error and the recorded impact values is found to be linear for a given material.

The behavior of three bodies after collision can not be predicted, a situation which occurs when the specimen halves separate.

This method of determining the toss error is valid for all types of materials and test specimens (when the halves do not separate) in Charpy impact testing.

ACKNOWLEDGMENTS

The authors would like to thank the management of Thermax Ltd., for permission and great support in carrying out this work. Particular thanks to Mr. R. K. Mittal and colleagues for the encouragement. The author also acknowledges the help of S. Raghavan for preparing the text and B. M. Rajput for the assistance. Special thanks to Mr. Nitin Konde and Raj Yeolekar for typing this manuscript.

REFERENCES

1. D. Titherington and J.G. Rimmer, Engineering Science, Vol. 2, Copyright 1982, McGraw Hill Book Co. (UK) Ltd., p. 29 and 30.

2. E 23-92, Standard test methods for notched bar impact testing of metallic materials, American Society for Testing and Materials, Philadelphia., p. 11 and 18.

3. A.G. Atkins and Y.W. Mai, Elastic and Plastic Fracture, 1985, Ellis Horwood Limited, England, p. 38 and 132.

4. E.J. Hearn, Mechanics of Materials, Vol. 2, 1985, Pergamon Press Ltd, UK, p 881.

Ken J. KarisAllen[1] and James R. Matthews[1]

LOAD DAMPING ABSORBERS AND THE DETERMINATION OF LOAD/DISPLACEMENT DATA FOR PRECRACKED CHARPY SPECIMENS

REFERENCE: KarisAllen, K.J. and Matthews, J.R, "**Load Damping Absorbers and the Determination of Load/Displacement Data for Precracked Charpy Specimens**", Pendulum Impact Machine: Procedures and Specimens for Verification, ASTM STP 1248, Thomas A. Siewert and A. Karl Schmieder Eds., American Society for Testing and Materials, Philadelphia, 1995.

ABSTRACT: A mechanical damping technique is described where a soft metal absorber attached to the leading edge of the striker is used to reduce the inertial oscillatory component of dynamic load time records. A technique is also presented which generates specimen load line displacement data indirectly from force/time information. A comparison of damped and undamped impact records indicates that the tested absorber configuration is an effective method of reducing inertial load oscillations. The experimental evidence indicates that the elastic and plastic machine load-displacement relationships can be accurately determined under the impact conditions generated in a precracked Charpy test. The procedure presented eliminates the requirement for using a dedicated device for the measurement of specimen displacement when absorbers are used to remove the inertially generated load oscillations.

KEYWORDS: Fracture, precracked Charpy, three point bend, machine compliance, mechanical damping, pendulum tester, impact testing.

NOMENCLATURE

B = specimen thickness
E = material elastic modulus
m = mass of hammer assembly
P_a = average force on load cell between time i and i+1
S = specimen span
U_{tot} = energy absorbed by the machine/specimen system
U_{em} = elastic energy absorbed by the machine
U_b = brinelling energy absorbed by the specimen at the load points
U_{eb} = elastic brinelling energy absorbed at the load points
U_{pb} = plastic brinelling energy absorbed at the load points
U_f = elastic and plastic energy absorbed by the fracture process
V_a = average hammer velocity between time i and i+1
V_i = velocity of hammer at time i
V_{i+1} = velocity of hammer at time i+1
W = specimen width
δ_b = specimen deflection due to bending
δ_{sh} = specimen deflection due to shear
δem_i = elastic machine deflection at time i

---

[1] Defence Scientist, Defence Research Establishment Atlantic, P.O. Box 1012, Dartmouth, Nova Scotia, Canada, B2Y 3Z7.

δem_{i+1} = elastic machine deflection at time i+1
δpm_i = plastic machine deflection at time i
δpm_{i+1} = plastic machine deflection at time i+1
δs_i = specimen deflection at time i
δs_{i+1} = specimen deflection at time i+1
ν = material Poisson ratio

Pendulum impact machines have been historically used for the qualitative assessment of metallic materials [1,2]. Recently, increased use is being made of instrumented impact machines to extend elastic and elastic-plastic fracture technology into the dynamic regime [3-5]. The determination of meaningful dynamic data is critically dependent on the ability to obtain accurate load/load point displacement data (load/LPD). It has been previously determined that, particularly during the early portion of the test, load sensors mounted on the anvils or striker do not reflect actual crack tip loading because of the vibrations present in the system [6]. Various specimen/system configurations and load transducer positions which mitigate or are unaffected by the oscillations have been investigated [7-12]. For the drop weight configuration, it was found that a soft metal absorber inserted between the load cell and specimen effectively removed the high frequency oscillatory component [13]. This configuration, however, while providing accurate specimen load response data from remotely located sensors, required a device for the direct measurement of specimen load point displacement (LPD).

A straightforward approach to obtaining a dynamic load/LPD record involves processing the force/time signal generated from an instrumented load cell attached to the hammer assembly [14]. In order to convert force time to force displacement, it is necessary to know the velocity at any time. For a pendulum configuration, as the specimen is contacted, there is a loss of energy and an associated loss of hammer velocity as follows:

$$m\int_{V_i}^{V_{i+1}} V dV - \int_{t_i}^{t_{i+1}} P_a V_a dt = 0 \tag{1}$$

When load/LPD is derived using equation (1) the area under the curve defines the energy absorbed by the entire impact system. The components of this energy are given by:

$$U_{tot} = U_{em} + U_b + U_f \tag{2}$$

over a given displacement interval, equation (1) can be expressed as:

$$\int_{t_i}^{t_{i+1}} P_a V_a dt = \int_{\delta em_i}^{\delta em_{i+1}} P_a d\delta em + \int_{\delta pm_i}^{\delta pm_{i+1}} P_a d\delta pm + \int_{\delta s_i}^{\delta s_{i+1}} P_a d\delta s \tag{3}$$

where:

$$U_b = U_{eb} + U_{pb} \tag{4}$$

Accurate specimen load/LPD data require that deformation from machine sources be removed. Machine deformation is the sum of the elastic deformations of the hammer and anvil assemblies and the plastic deformation sustained by the soft metal absorber.

A common method for determining machine compliance is by employing a specimen geometry where the non machine compliance portion of the load/LPD record is quantifiable and thus can be removed. For an unnotched, rectangular, three-point bend specimen, the elastic load line deflection is given by [15]:

$$\delta_{tot} = \delta_b + \delta_{sh} \tag{5}$$

Analytical expressions for these components are [16]:

$$\delta_b = \frac{PS^3}{4BW^3E} \tag{6}$$

and

$$\delta_{sh} = \frac{0.6(1+\nu)PS}{BWE} \tag{7}$$

For the loading portion of a test where the tension surface of an unnotched bend bar does not yield, total deflection is a combination of the elastic deformations due to machine and specimen compliance plus local plastic brinelling at the loading points. Under these circumstances, maximum load and the point of maximum plastic brinelling will coincide. Thus, the unloading portion of the load/LPD record can be considered an elastic event. Machine loading and unloading compliance relationships will therefore differ depending on the amount of plastic brinelling sustained by the soft metal absorber during the loading portion of the curve.

Previous studies [17,18] indicated that the unloading portion of a test on an unnotched specimen produced an accurate elastic machine deformation relationship for both static and dynamic conditions. Once the elastic machine compliance record is known, the plastic absorber load deflection relationship can be determined from the loading portion of the same record. The knowledge of both these relationships allows the indirect calculation of specimen deflection using equations (1) and (2). This paper details the procedures for the indirect calculation of LPD from a force/time signal when a soft metal absorber is used to damp the inertially generated load oscillations. The load train assembly used to investigate the accuracy of the procedure is an instrumented pendulum impact tester.

EXPERIMENTAL PROGRAM

Unnotched three point bend specimens (10 mm size as per ASTM E23) were machined from a 25 mm plate of quenched and tempered SAE 4340 steel (Table 1). The specimen material was heat treated to an average surface hardness of Rockwell C 47. These specimens were impacted at initial velocities of 0.74 m/s and 1.16 m/s with a 33.2 kg commercially manufactured instrumented pendulum striker. Dimensional specifications

TABLE 1--Chemical composition of SAE 4340 and CSA G40.21 350 WT.

	Chemical Composition (wt%)							
	C	Mn	Si	S	P	Mo	Ni	Cr
CSA 350 WT	0.09	1.3	0.23	0.006	0.013			<0.004
SAE 4340	0.42	0.91	0.17	0.031	0.009	0.23	1.78	0.83

for the striker and anvil assemblies were verified to be in accordance with standard ASTM E-23-92. The impact velocity was selected to ensure that the tension surface of the specimen did not yield and that the capacity of the instrumented tup was not exceeded. An annealed aluminum absorber (Figure 1) was loosely attached to the leading edge of the tup to dampen any load oscillation which may have otherwise been present. Machine compliance relationships for notched specimens impacted at 5.18 m/s with the absorber attached were generated by using duplicate

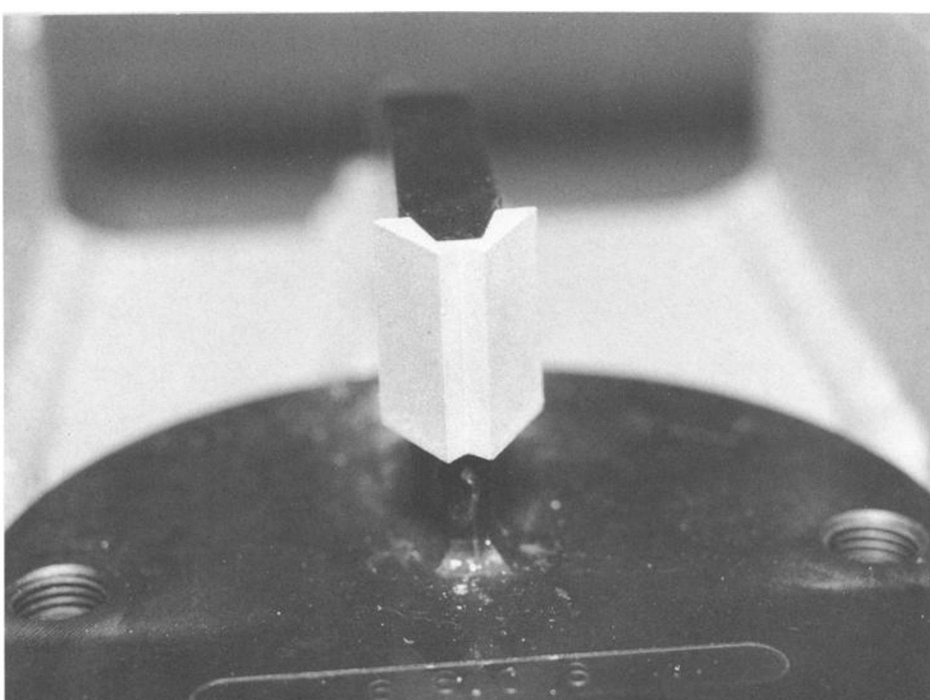

FIG. 1--Photograph of the pendulum striker assembly with an aluminum absorber attached.

specimens from two sets of commercially produced Charpy calibration specimens. Also, precracked 10 mm x 10 mm specimens of CSA G40.21 350 WT (Table 1) were cooled to -40 C and impacted at 5.18 m/s with the aluminum absorbers attached to the tup in order to evaluate the transferability of the determined machine compliance.

The strain signals from the tup were conditioned using a 100 kHz amplifier. Load/time signals for notched and unnotched specimens were captured using an eight-bit programmable digitizer. Force-time data was bussed to a microprocessor where it was converted to velocity/time, system load/LPD, and machine load/LPD.

RESULTS AND DISCUSSION

Figure 2 shows a typical system load deflection relationship for an unnotched bend bar impacted at 0.74 m/s without an absorber. The load-deflection relationship indicates the specimen and machine remained

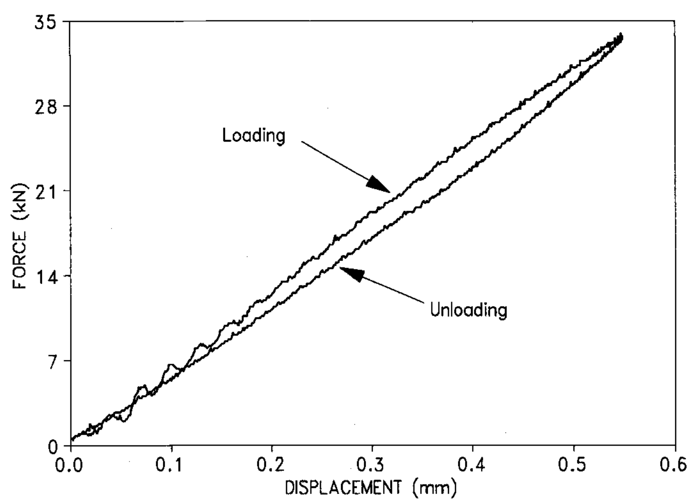

FIG. 2-- Typical load-displacement record from an unotched bar ipmacted at 0.74 m/s without an absorber attached to the striker.

elastic during the test. Inspection of the test pieces subsequent to testing revealed no visual evidence of brinelling at the loading points or limit load plasticity on the tension surface of the specimens. Figures 3 and 4 show typical load-deflection relationships for 0.74 m/s and 1.16 m/s respectively when the aluminum absorbers were attached to the leading edge of the striker. The load-displacement data indicates that significant plastic deflection was sustained by the system. Again, no evidence of plasticity was observed on the specimen or machine. Thus it has been inferred that plastic deflection was sustained only by the absorber. The load-displacement data at both velocities indicates highly nonlinear relationships during the loading portion of the curves. Initially, the major component of the plastic deflection was the axial

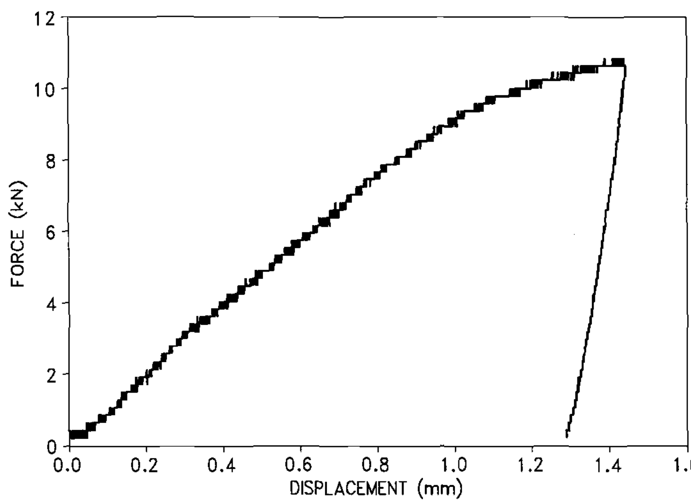

FIG. 3--Typical load-displacement record from an unnotched bar impacted at 0.74 m/s with an aluminum absorber attached to the striker.

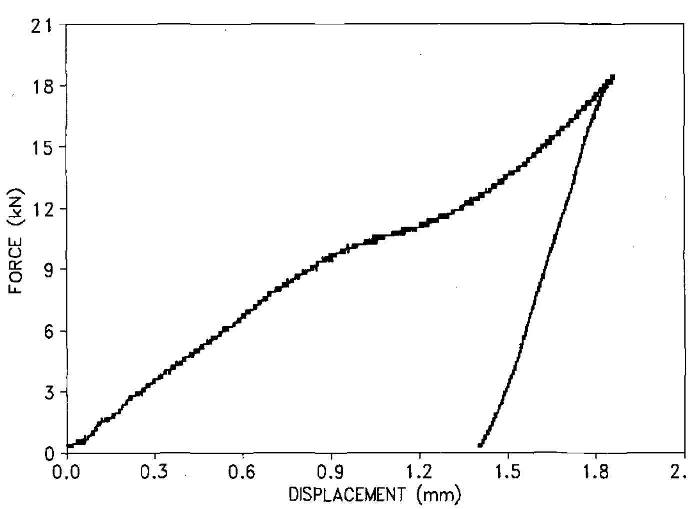

FIG. 4--Typical load-displacement record from an unnotched bar impacted at 1.16 m/s with an aluminum absorber attached to the striker.

compression of the leading edges of the absorber (Figure 5). As the system load increased above 11 kN, the bending stress generated from the effects of the curved striker surface and the two compressive contact points on the leading edge of the absorber combined to cause the back edge of the absorber to bend and conform to the leading surface of the striker. This effect was responsible for the plateau observed in Figures 3 and 4. Once the back face of the absorber had conformed to the surface of the striker, then the axial compression of the leading edges of the absorber was reestablished as the major component of plastic deflection.

Figure 6 compares the loading portions of the unnotched bar test with absorbers. Because of the difficulties in establishing the point

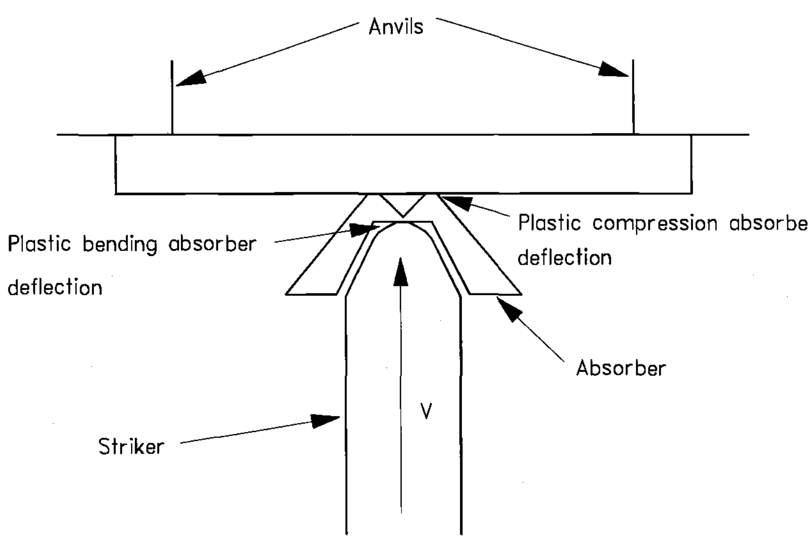

FIG. 5--Schematic representation of the experimental load train assembly showing the positions of plastic absorber deflection.

of impact in the load-time records, each data set has been shifted on the displacement axis to a common point at 2 kN. Figure 7 compares the unloading portion of all the unnotched bar tests(with and without absorbers). The unloading data was shifted to a common point at 0.5 kN. The good correlation between data sets indicates that the plastic absorber deflection was reproducible and was insensitive to velocity over the range tested. Also, the good correlation between unloading data sets with and without absorbers indicates that the unloading load-displacement relationship is independent of the presence of the absorbers.

Figure 8 shows typical system load-displacement data for low energy (brittle) and medium energy (ductile) commercial calibration specimens impacted at 5.18 m/s with absorbers. The reproducibility of

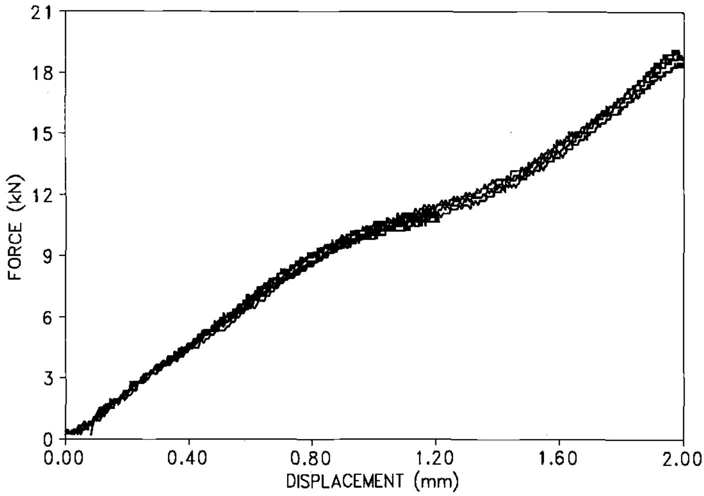

FIG. 6--A comparison of the loading load-displacement data from unnotched bars impacted at 0.74 m/s and 1.16 m/s with an aluminum absorber attached to the striker.

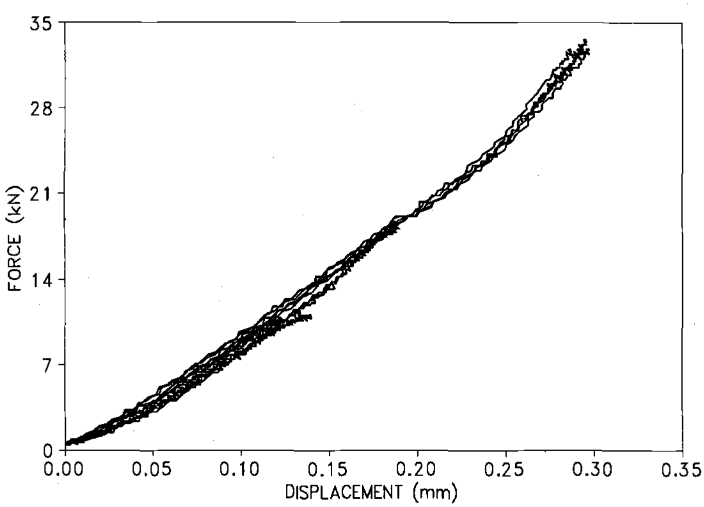

FIG. 7--A comparison of the unloading load-displacement data from unnotched bars impacted at 0.74 and 1.16 m/s with and without an aluminum absorber attached to the striker.

the load displacement data is good up until approximately 22 kN. The observed decrease in the system load at 22 kN results from the structural failure of the absorbers at this load. Thus this absorber design and material combination has been limited to tests not exceeding 20 kN. Figure 9 compares the machine deflection generated from notched specimens at 5.18 m/s and unnotched specimens at 1.16 m/s. During the initial portion of the test, the correlation between the two sets of data is relatively good. However, the load plateau occurs at a slightly elevated level in the notched specimens. The notched and unnotched data parallel each other subsequent to the plateau. The rate insensitivity of annealed 6061 aluminum and the velocity data presented combine to indicate that the presence of the notch changes the way the specimen rotates and thus slightly changes the direction of the forces which are acting on the absorber. This indicates that notched specimens should be used to generate the machine load-deflection relationships for precracked specimens.

Once the machine deflection data is calculated, it is common practice to perform some type of regression analysis to generate an expression which accurately represents the data. While a third order polynomial accurately describes the unloading machine compliance data, the highly nonlinear nature of the loading of the data limits the ability of linear fit to accurately fit the entire loading portion of the tests. The loading data was divided into two data sets and a third order polynomial was generated to describe each set. Thus, using the three generated third-order polynomials, machine compliance data can now be generated for the precracked charpy test, provided they do not exceed 20 kN.

Figure 10 shows an undamped CSA G40.21 350 WT precracked charpy specimen cooled to -40 C and impacted at 5.18 m/s. The load oscillations make it practically impossible to isolate and evaluate any critical event information. One of the major advantages of attaching

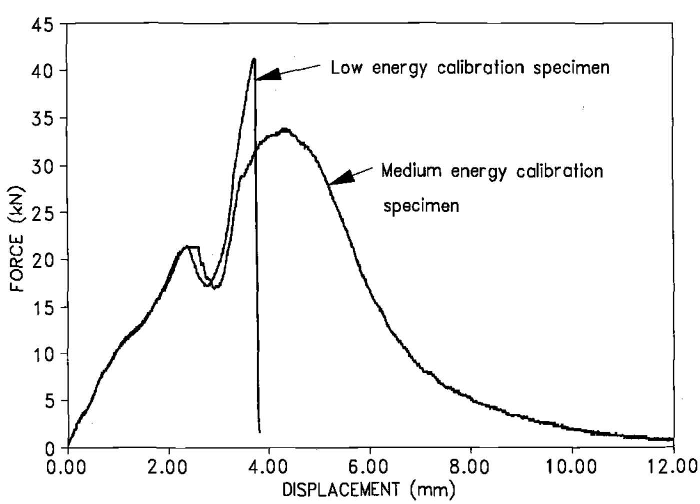

FIG. 8--Typical load-displacement records from notched calibration specimens impacted at 5.18 m/s with an aluminum absorber attached to the striker.

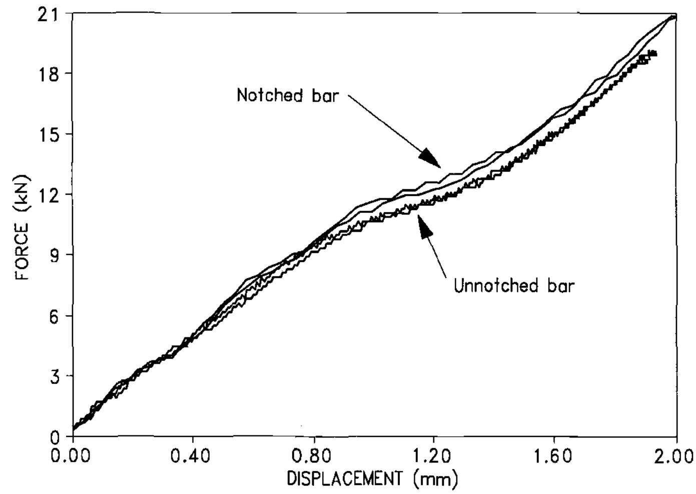

FIG. 9--A comparison of notched and unnotched specimen machine load-displacement relationships with absorbers attached.

the absorber to the leading edge of the striker and measuring displacement indirectly is the relative ease of performing low temperature experiments (the specimen can be cooled in a separate bath and moved to the anvils just prior to triggering the hammer). Figure 11 is the record of a specimen impacted under the same conditions as in Figure 10 except for the addition of the absorber to the leading edge of the striker. In comparison to Figure 10 the load oscillations have been dramatically reduced. The brittle initiation point becomes clearly evident. It is also evident that the addition of the absorber reduced the initial loading rate of the specimen. When the force-time was converted to force displacement and the machine compliance was subtracted according to the predetermined relationships (Figure 12) the resulting specimen load-deflection relationship was generated (Figure 13). The measured crack length for this specimen was 3.2 mm (three point average). The theoretical stiffness of the specimen compared favourably to the corrected load displacement data. The low frequency component in the corrected data results from the inability of lower order polynomial regression analysis to fully describe the minor oscillation present in the notched bar machine compliance data (Figure 9). Alternatives to describing machine compliance by regression analysis relationships has been identified as an area for future work.

Current work is focused on producing an absorber with a higher load range. This should be achievable by selecting a rate insensitive absorber material with a higher yield than the annealed aluminum used in this study. In addition, alterations to the design of the absorber are currently being considered to remove the load plateau observed in this study. Initial indications suggest that the load plateau can be removed by premoulding the back face of the absorber to the surface of the

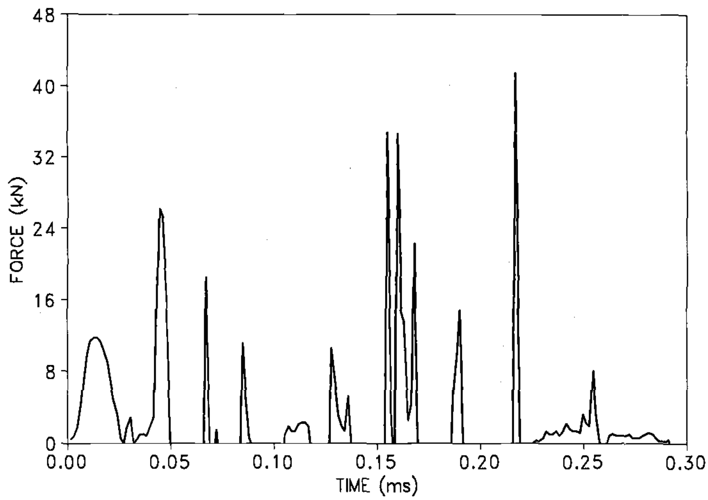

FIG. 10--Load-time record for a precracked CSA G40.21 350 WT Charpy specimen cooled to -40 C and impacted at 5.18 m/s without an absorber attached to the striker.

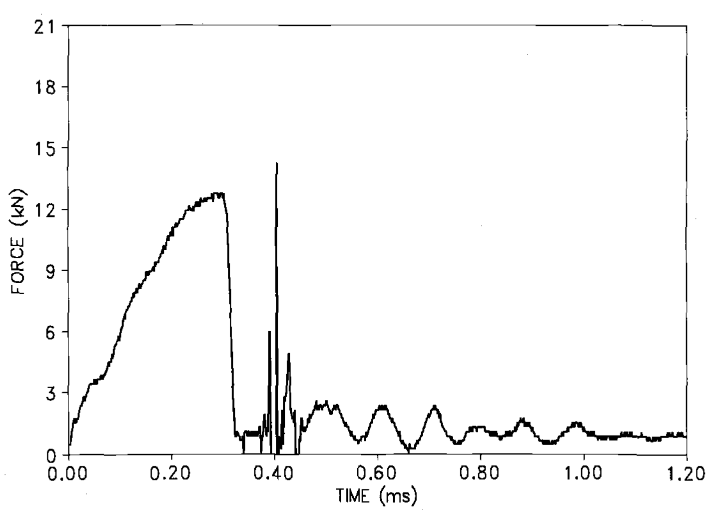

FIG. 11--As in figure 10 with an absorber attached to the striker.

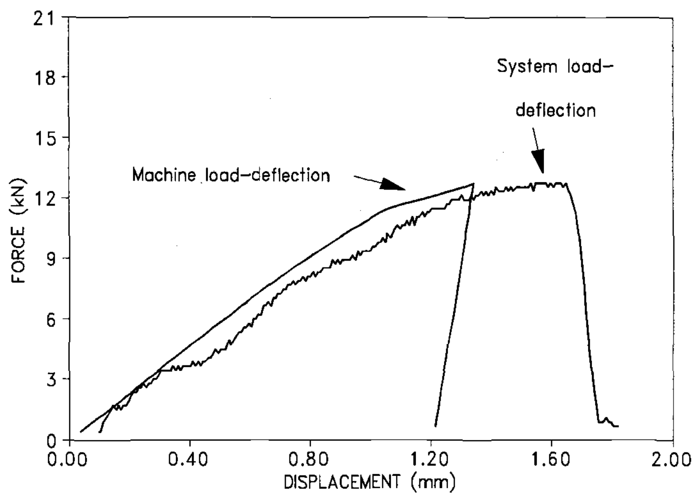

FIG. 12--System and machine load-displacement relationships for a precracked charpy specimen impacted at 5.18 m/s with an absorber attached to the striker.

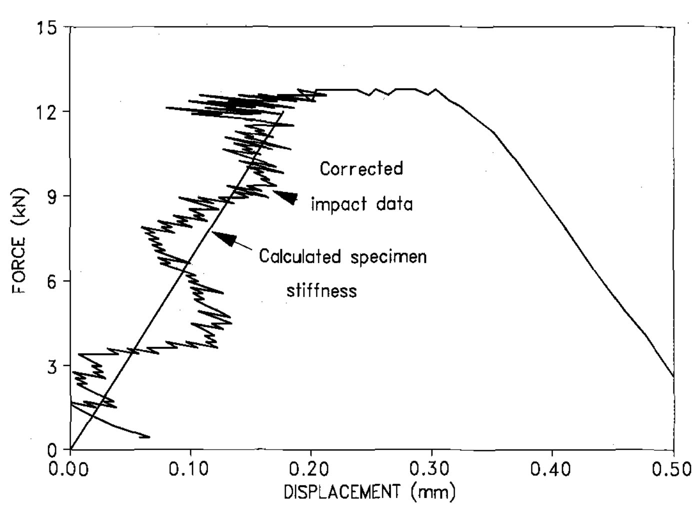

FIG. 13--Comparison of corrected load-displacement data and calculated specimen stiffness for a precracked charpy specimen impacted at 5.18 m/s with an absorber attached to the striker.

striker. A study into the significance, relevance, limitations and transferability of fracture data (such as J_c) obtained using the method outlined in this paper is ongoing.

CONCLUSIONS

1. The addition of a soft metal absorber inserted between the striker and the specimen dramatically reduces the oscillatory component of dynamic load-displacement data. These absorbers can also be used to reduce (control) the loading rate.

2. The unnotched specimen tests indicated that the loading and unloading portions of the tests which used absorbers were highly reproducible and insensitive to the velocity range between 0.74 and 1.16 m/s.

3. There was a good correlation between the unloading load-displacements data of the unnotched specimens impacted with and without absorbers.

4. The data indicates that the useful limit of this particular geometry and material combination for an absorber is approximately 20 kN. The data also indicates that a slightly elevated machine compliance relationship results from a notched specimen tested at 5.18 m/s.

5. Precracked Charpy data generated indirectly by defining and removing the machine compliance portion of the test is an accurate means of determining precracked Charpy load-displacement data.

REFERENCES

[1] Lange, E. A. and Loss, F. J., in "Impact Testing of Metals", ASTM STP 466, American Society for Testing and Materials, Philadelphia, 1970, pp. 241-258.

[2] Faheey, N. H., in "Impact Testing of Metals", ASTM STP 466, American Society for Testing and Materials, Philadelphia, 1970, pp. 76-88.

[3] Server, W. L., in "Elastic-Plastic Fracture", ASTM STP 668, American Society for Testing and Materials, Philadelphia, 1979, pp. 493-514.

[4] Kobayashi, T., Yamamoto, I. and Niinomi, M., "Evaluation of Dynamic Fracture Toughness Parameters by Instrumented Charpy Impact Test," Engineering Fracture Mechanics., Vol. 24, 1986, pp. 773-782.

[5] Logsdon, W. A., in "Elastic-Plastic Fracture", ASTM STP 668, American Society for Testing and Materials, Philadelphia, 1979, pp. 515-536.

[6] Venzi, S., Priest A. H., and Wylie, R. D., in "Impact Testing of Metals," ASTM STP 466, American Society for Testing and Materials, Philadelphia 1970, pp.165-180.

[7] Tredeau, L. P., "Dynamic Toughness - Its Relevance and Measurement,"Research Report R 275, Department of Energy, Mines, and Resources, Mines Branch, Canada, Oct. 1974.

[8] Turner, C. E., Culver, L. E., Radon, J. C. and Kennish, P., "An Analysis of the Notched Bar Impact Test with Special Reference to

the Determination of Fracture Toughness," presented at the Institute of Mechanical Engineers Conference, London, 3-5 May 1971, Paper C6/71, pp. 38-47.

[9] McGillivary, H. J. and Cannon, D. F., in "Rapid Load Fracture Testing", ASTM STP 1130, American Society for Testing and Materials, Philadelphia, 1991, pp.161-179.

[10] Bonenberger, R. J., Dally, J. W. and Irwin, G. R., in "Constraint Effects in Fracture", ASTM STP 1171, American Society for Testing and Materials, Philadelphia, 1993, pp.129-157.

[11] Böhme, W. and Kalthoff, J. F. "The Behaviour of Notched Bend Specimens in Impact Testing," International Journal of Fracture, Vol. 20, 1982, pp. R139-R143.

[12] KarisAllen K. J. and Morrison, J., in "Rapid Load Fracture Testing", ASTM STP 1130, American Society for Testing and Materials, Philadelphia, 1991, pp. 76-91.

[13] Joyce, J. A. and Hackett, E. M., in "Nonlinear Fracture Mechanics," ASTM STP 995, American Society for Testing and Materials, Philadelphia, 1989, pp. 298-317.

[14] Ewing, A. and Raymond L., in "Instrumented Impact Testing", ASTM STP 563, American Society for Testing and Materials, Philadelphia, 1974, pp. 180-202.

[15] Haggag, F. M. and Underwood, J. H., "Compliance of a Three-Point-Bend Specimen at Load Line," International Journal of Fracture, Vol 26, R63 - R65 (1984).

[16] Roark, R. J., Formulas for Stress and Strain, McGraw-Hill (1965).

[17] KarisAllen K. J. and Morrison J., "The Determination of Instrumented Impact Machine Compliance Using Unloading Displacement Analysis," Experimental Mechanics, Vol. 29, No. 2, June 1989.

[18] KarisAllen K. J. and Matthews J. R., "The Determination of Single Edge Notched Bend Specimen Load Line Displacement from Remotely Located Sensors in Elastic Plastic Fracture Testing," accepted for publication in Journal of Testing and Evaluation, November, 1994.

Christopher N. McCowan[1], James W. Dally[2], Daniel P. Vigliotti[1] and Ouk S. Lee[3]

LOW COST LOWER BOUND TOUGHNESS MEASUREMENTS

REFERENCE: McCowan, C.N., Dally, J.W., Vigliotti, D.P., Lee, O.S., "Low Cost Lower Bound Toughness Measurements," Pendulum Impact Machines: Procedures and Specimens for Verification, ASTM STP 1248, Thomas A. Siewert and A. Karl Schmieder, Eds., American Society for Testing and Materials, Philadelphia, 1995.

ABSTRACT: A method is proposed for determining the lower bound toughness of engineering steels based on impact loading of a modified Charpy specimen in a standard Charpy machine. The modified Charpy specimen employed here is nearly the same as the over-sized specimen studied previously by Bonenberger et al. The primary difference is that a sharp notch is employed to initiate the crack instead of pre-compression. A master curve is developed to relate the stress intensity developed at the tip of the notch to the time of crack initiation. An instrumented tup is then employed to give a force-time trace that can be interpreted to estimate the crack initiation time. Results are presented for the lower bound toughness of ASTM A 533, Type B, Class 1 steel over the temperature range from 0 to 40°C. These results are higher than the results reported by Bonenberger et al. for the same steel. The differences are attributed to the different techniques used to develop the starter crack in the modified Charpy specimen.

KEYWORDS: Charpy V-Notch, Instrumented Impact Test, Lower bound toughness

During the past 35 years, significant progress has been made in developing the theory of fracture mechanics, and in perfecting test methods for measuring crack initiation toughness. Nevertheless, failures of engineering structures continue to occur with serious consequences. Many of these failures are due to the fact that the material employed in the fabrication of the structure was not tested or certified

[1] Materials Reliability Division, NIST, Boulder Laboratories, Boulder, CO 80303
[2] Mechanical Engineering Department, University of Maryland, College Park, MD 20742
[3] Mechanical Engineering Department, University of Inchon, Inchon, Korea

prior to its use in construction [1]. In many instances, handbook values of fracture toughness were used in the fracture mechanics analysis. This practice is very dangerous because the fracture toughness varies markedly from heat to heat of steel, and the values quoted in handbooks for a particular alloy should only be considered as typical.

It is necessary to test the material specified in the design to establish the crack initiation toughness over the temperature range expected in the service of the structure. Test methods used to determine the toughness are well known, ASTM E399 [2] for example. What is less well known to the engineer performing the analysis, and the designer of the structure is the huge amount of scatter encountered in measuring the initiation toughness. Recent results by Link and Joyce [3] from an extensive series of tests with A 533, Type B reactor grade steel, presented in Fig. 1, illustrate the amount of scatter for steels commonly employed in pressure vessels.

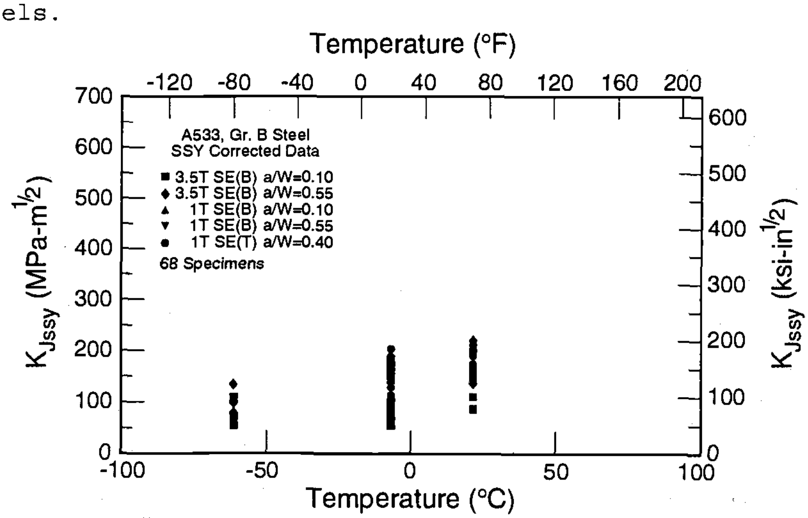

Figure 1: The scatter in the crack initiation toughness of A 533 Type B reactor grade steel is very large even near the nil ductility temperature. Data from Link and Joyce[3].

The scatter is so large (400% at the nil ductility temperature) that the only conservative method of design is to determine the lower bound, which is a curve of toughness as a function of temperature drawn below all of the test data. To establish this lower bound toughness, it is necessary to conduct many tests at each temperature to ensure that at least one or two "low" values are represented in the data set. It appears that the difficulty in measuring the lower bound, and the excessive time and expense involved in testing are important factors that are limiting the effectiveness of design against fracture.

This paper describes a low cost method of measuring the lower bound toughness of steels that has potential to be used to certify steels for a wide variety of structural applications. The method is based on testing an oversized Charpy specimen in a standard 240 J Charpy impact machine. The Charpy specimen, shown in Fig. 2, is oversized in cross section with a height of 19 mm and a thickness of 12.7 mm, but it is of standard length. Side grooves are cut into the specimen 2.0 mm deep with a sharp tip cutter having an included angle of 45°. The face groove, opposite the impact point, is also 2 mm deep as in the standard Charpy specimen, but the radius of the tip is approximately 0.06 mm. This approach is similar in many respects to the method described previously by Bonenberger et al. [4,5]; however, two important modifications have been made to improve the method.

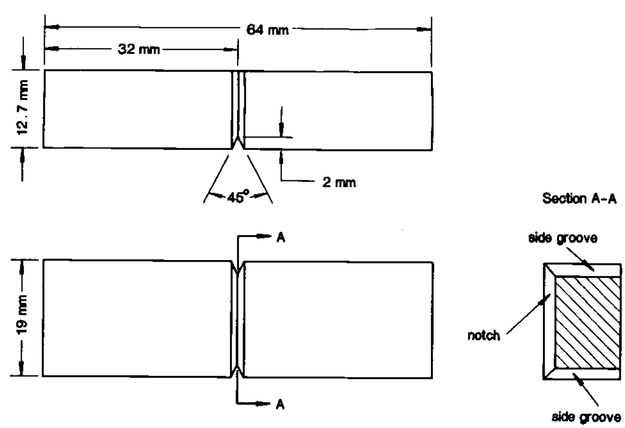

Figure 2: Geometry of the modified (oversized) Charpy specimen.

First, in preparing the modified Charpy specimens, Bonenberger subjected the specimens to axial pre-compression stresses well above the yield strength of the material. The purpose of the pre-compression was to deform the material in the local neighborhood of the notch thereby sharpening its tip. The practice of pre-compression may be objectionable, because the material local to the notch is strain hardened and its toughness may be degraded. In the method described in this paper pre-compression is not necessary because cleavage may be initiated at temperatures in the lower transition region if the machined notch is sufficiently sharp.

Second, Bonenberger employed four strain gages on each specimen that were located near the crack tip to record a strain relative to time during the impact period. The strain-time trace was interpreted to give the stress intensity factor as a function of time. The time of crack initiation was evident from the strain-time traces because of the rapid decrease in the strain at the gage location due to crack extension. The value of the stress intensity factor K_I, at the initiation time, was taken as K_{Id} which is an estimate of the lower bound toughness. The approach described in this paper, involved strain gaging and testing several modified Charpy specimens to develop a master curve showing the stress intensity factor K_I as a function of time. Strain gaging can then be discontinued for subsequent evaluations of the lower bound toughness. An instrumented tup is employed to establish the time of the initiation of the crack at the notch. Using the initiation time together with the (K_I-t) master curve, it is possible to measure the lower bound toughness without strain gaging at test temperatures in the lower transition region.

Eliminating the need for pre-compression removes the question of altering the material properties prior to testing. Eliminating the strain gages reduces the time and the cost of lower bound toughness measurements by at least a factor of ten.

SPECIMEN PREPARATION

The modified Charpy specimens were machined from A 533 B reactor grade steel. This particular lot of material was available from the round robin test series conducted to verify the arrest toughness testing procedure, ASTM E-1221 [2]. The properties of the material are well known and are described in reference [6]. It is important to note that the RT_{NDT} was -2°C, because it indicates the temperature range of interest in defining the lower bound toughness in the lower transition region. At room temperature this plate of A 533B exhibited a yield strength of 480 MPa, and an arrest toughness K_{Ia} of 83.4 MPa·m$^{1/2}$.

The specimens were machined in accordance with the drawing shown in Fig. 2. Of particular concern was the sharpness of the notch, since it was to act as a starter crack. The notch was machined with a multi-tooth carbide cutter with a 45° included angle. The tip of the cutter ground with a tip radius of 0.04 mm; however, we expected tool wear would increase that radius. We checked the profile of several notches using shadow projection with high magnification and found some variation in notch quality with radii varying from 0.05 to 0.07 mm. It was also noted that the notch tip was not a perfect circular arc. A typical profile of a notch tip, presented in Fig. 3, shows the quality typical of the geometry maintained at the notch tip.

Four bonded foil strain gages, with an active element 1.5 mm long, were installed on each specimen 5 mm from the tip of the notch as indicated in Fig. 4. This location is identical to that employed by Bonenberger [5] in the initial development of this approach. During the impact experiments, the strain gage signals were recorded on a four channel digital oscilloscope. The frequency response of the strain measuring system was controlled by the strain gage amplifiers which were essentially flat from d.c. to 100 kHz.

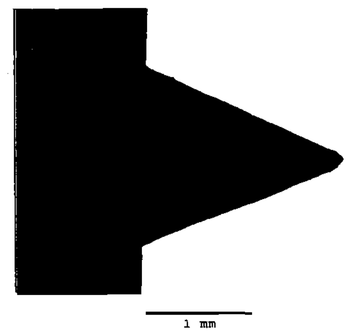

Figure 3: Micrograph of a replica of the notch.

CHARPY MACHINE MODIFICATIONS

The Charpy machine employed in the study had a standard U type pendulum with a capacity of 240 J, although we made two modifications to the machine. First, to accommodate the added height of the oversize specimen (19 mm versus 10 mm for the standard specimen), the rails supporting the specimen were reduced in thickness by 4.5 mm. This change maintained the position of the centerline of the specimen relative to the nose piece on the hammer.

The second change involved instrumenting the nose piece, to permit a signal representing the impact force to be recorded. Shallow slots were ground on both sides of the nose piece of the hammer to accommodate semi conductor strain gages. Cover plates were bonded to the nose piece to protect the gages from contact with the Charpy specimens during the fracture process. The sensitivity of the instrumented nose piece was very dependent on the location of the applied force along its height. We resolved this problem by an insitu calibration technique based on absorbed energy. We first calibrated the nose piece in a testing machine to obtain an approximation of the calibration constant for its load sensitivity. Subsequently, this first estimate was adjusted so that the absorbed energy as calculated from the force-time record coincided with the absorbed energy measured directly from the Charpy machine. The repeatability of this calibration technique was excellent.

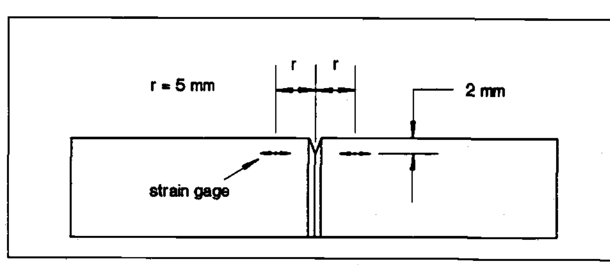

Figure 4: Location of the strain gages relative to the notch tip.

DEVELOPING THE MASTER CURVE

A typical set of strain-time traces recorded from the four gages is shown in Fig. 5. We note that each gage indicates a slightly different signal depending on the response of specimen. To accommodate these differences, the signals from the four different gages are averaged together to give a single strain-time trace as indicated in Fig. 6.

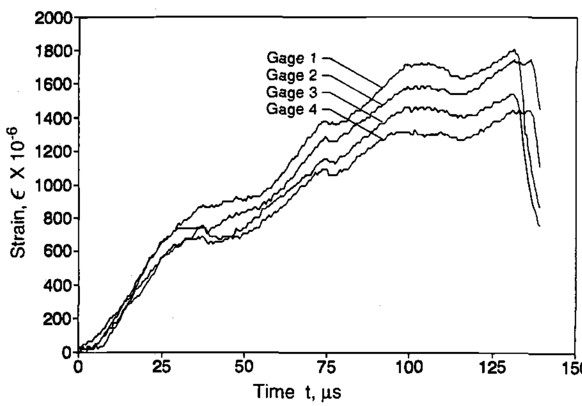

Figure 5: Typical strain-time traces showing gage to gage variation in strain.

The strain-time trace in Fig. 6 clearly indicates the dynamics of the modified Charpy specimen. The strain increases with time in a nearly linearly manner for the first 50 μs, then the trace becomes more non-linear. The non linearity is due to two effects. First, with increasing time the Hertzian load at the contact point produces local compressive stresses that exceed the yield strength of the A 533B steel, and a portion of the hammer displacement is accommodated by local plastic deformation at the contact point. Second, with the higher strains (1200 $\mu\epsilon$ and above) the regions near the notch tip have yielded, and the specimen deformation is accommodated by plastic deformation near the notch tip. It is evident that the non linearity in the strain-time trace is to be expected, and that it will be dependent on the yield strength of the material tested and the shape of the nose piece on the Charpy machine.

Oscillations are also evident in the strain-time record presented in Fig. 6. The first oscillation has a period of 40 μs and the second oscillation has a period of about 65 μs. The third oscillation begins, but it is damped beyond recognition and its period is not evident. Clearly, the specimen is under going vibration during impact; however, the magnitude of the oscillations are small compared to the mean strain later (after 70 μs) in the impact event. Since all of the specimens tested in this series of experiments failed at times longer than 95 μs, it appears that the effect of specimen vibration on the strain recorded at the time of crack initiation was relatively small.

The reproducibility of the strain-time traces is illustrated in Fig. 7, where the records for four different specimens tested at temperatures varying from 0 to 40°C are presented. Examination of these results show that the strain-time traces are almost identical for times less than about 75 μs and strains less than 0.0014. Later in the impact event larger record to record deviations are evident. It is believed that these deviations are due to the tearing that occurs at the notch tip before cleavage failure is initiated. We will show, in the section on Fractography, evidence of this tearing and describe the specimen to specimen variation of the extent of tearing observed at the tip of the notch.

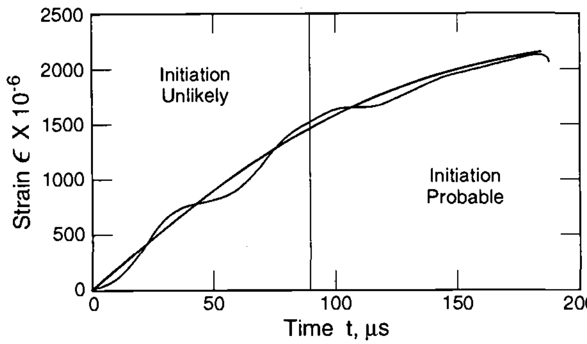

Figure 6: Dynamic characteristics of the strain-time trace.

The master strain-time curve, shown in Fig. 8, is representative of those individual traces presented in Fig. 7. It is necessary to convert this master strain-time curve to a corresponding stress-intensity-factor-time master curve. This conversion was made by employing the relationship derived by Bonenberger et al. [5]:

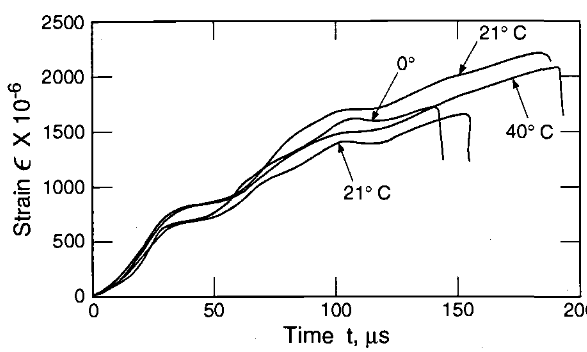

Figure 7: Four stress-time traces showing reproducibility.

$$K_{Id} = 38,880\epsilon^*_{yy} \tag{1}$$

where K_{Id} has units of $MPa \cdot m^{1/2}$, and ϵ^*_{yy} is the strain at the instant of cleavage initiation. We consider the dynamic initiation toughness K_{Id} as well as the crack arrest toughness K_{Ia} to be a good estimates of the lower bound toughness. Accordingly the value of K_{Id} is presented on the right hand ordinate of Fig. 8.

The smooth non linear shape of the master curve suggested that it would be possible to fit the curve with a relatively simple relation. We have selected a two term function of the form shown below to relate toughness with time.

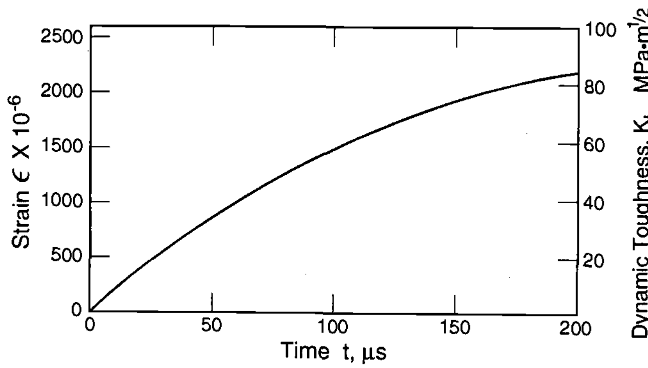

Figure 8: Master curve for ϵ-t and K_{Id}-t.

In Eq. (2) the time t is in μs and K_{Id} is in $MPa \cdot m^{1/2}$. The constants a and b were determine as 4.88 and 0.0758 by fitting the relation to data taken at t = 100 and 200 μs.

$$K_{Id} = at^{1/2} + bt \quad \textbf{(2)}$$

CRACK INITIATION TIME

The dynamic initiation toughness for A 533B reactor grade steel may be determined from the master curve shown in Fig. 8 or from Eq. (2), if some method is used to measure the time during the impact event when the crack initiates. There are three different methods for measuring the initiation time. Strain gages can be mounted near the crack tip and their signals will show a sharp decrease within a few μs after the crack initiates [4,5]. A second technique involves the placement of a coil near the Charpy specimen to sense the magnetic field. When the crack initiates the field suddenly changes. Recording the voltage v produced by the coil with respect to time gives a discontinuity in the v-t trace that indicates the initiation time [6]. The third technique involves measuring the impact force as a function of time during the impact event. The tup signal decreases rapidly with time when the crack initiates (in cleavage) and the specimen stiffness shows a corresponding decrease. We employed both the tup and strain gage signals in determining initiation time in this study.

Oscilloscope records of the average strain-time trace and the tup force-time trace are shown in Fig. 9. We include four records to show the effect of different testing temperatures. An examination of these records indicates that the tup signal oscillates with very large amplitude for the first cycle; however, in subsequent cycles the amplitude of the oscillation decreases markedly but does not vanish.

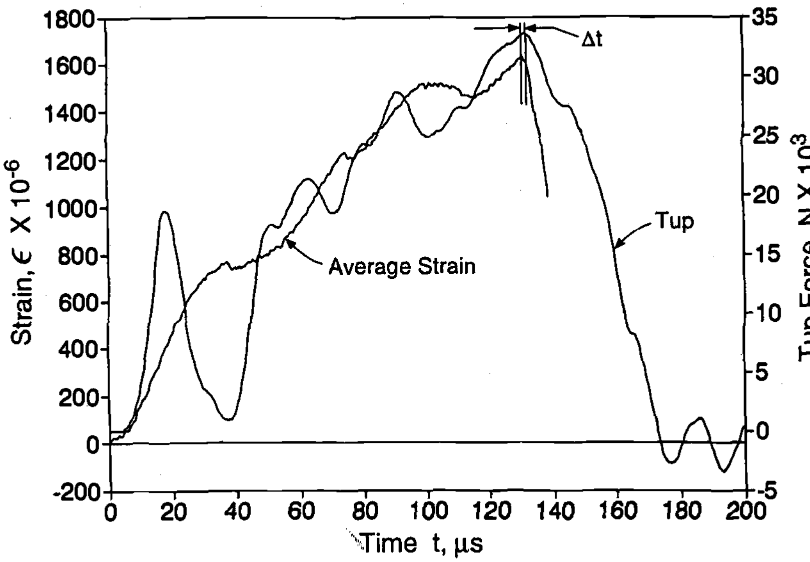

(a)

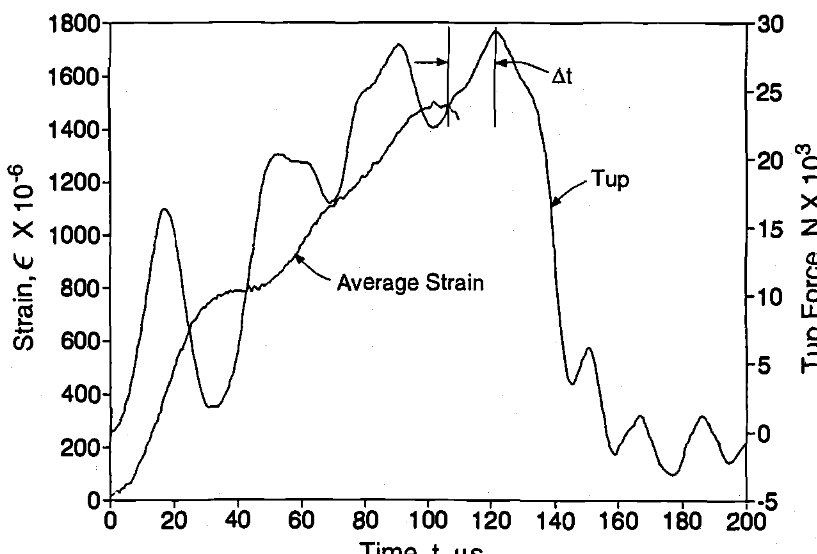

(b)

Figure 9: Four records showing correspondence between the strain gage signals (average) and the tup signal: (a) E3-11 at 0°C, (b) E3-3 at 10°C, (c) & (d) next page.

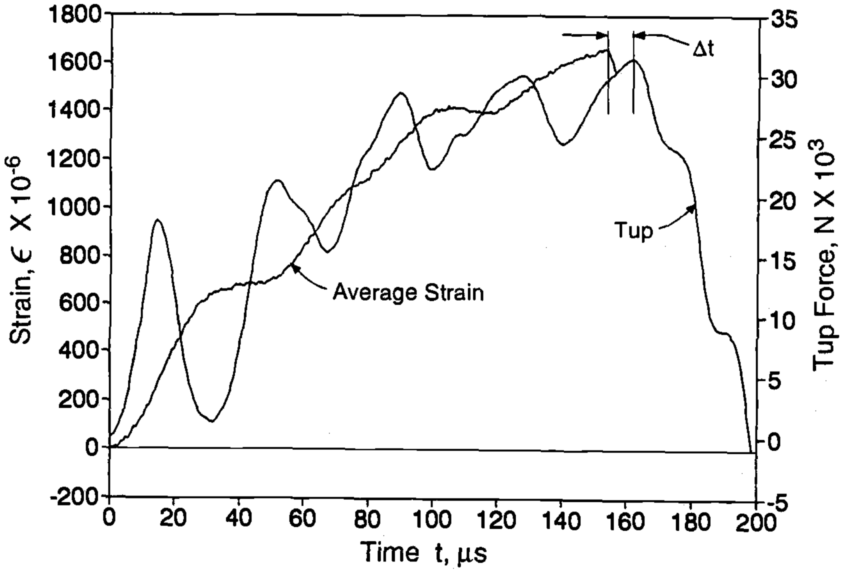

(c)

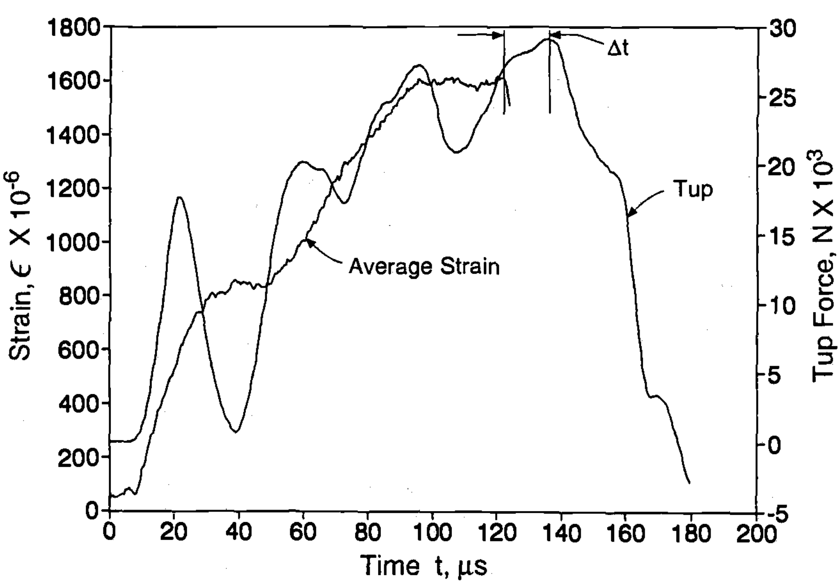

(d)

Figure 9 continued: (c) E3-16 at 21°C, and (d) E3-17 at 30°C.

The oscillations in the force-time records are due to several different harmonics. The fundamental harmonic, at 27 kHz, is probably due to the ringing of the nose piece at its natural frequency. The natural frequency of the specimen (about 2.5 kHz) is not evident in the tup record.

For times larger than about 50 to 60 μs, the tup signal appears to track the strain signal with oscillations producing the primary deviations between the two signals. When the crack initiated in the modified Charpy specimen, both signals decreased rapidly with respect to time. The difference in the indicated time of initiation varied from specimen to specimen. Reference to Fig. 9a shows a very close correspondence, because the oscillation of the tup signal was in phase with the initiation of the crack. That is the oscillation produced a decrease in the force signal at the same instant as the reduced stiffness of the failing Charpy specimen produced a decrease in the tup signal. On the other hand, Fig. 9b, c, and d show that the oscillation was producing an apparent increase in the force signal, at the instant of crack initiation. In this case, the force-time trace is delayed in its response to the reduced stiffness of the specimen after crack initiation.

It is clear then that differences occur in the estimate of the crack initiation time as measured from the strain-time traces and the force-time traces. The differences are indicated by the graph of initiation time as measured from the strain-time trace on the ordinate, and initiation time as measured from the force-time traces on the abscissa in Fig. 10. For ideal measurements, the initiation times associated with both methods should be equal and the data points should track the no delay line shown Fig. 10. However, neither measurement technique is without error, and we observe a dispersion of data points on both sides of the no delay line. Most of the points indicate that the indications from the force-time records are delayed relative to the time indicated from the strain-time trace. The delay in most cases is less than 10 μs. In three cases the force time record gives

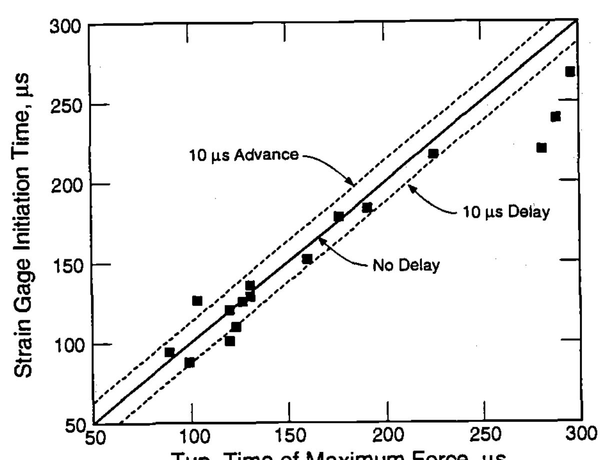

Figure 10: Comparison of initiation time determined from strain gage and tup signals.

an early indication of initiation, but the differences in these early signals is usually less than 5 μs. We note three data points in Fig. 10 that fall well outside the ±10 μs band. In two instances the specimen yielded, and the crack experienced a significant degree of tearing before cleavage initiated at times greater than 250 μs. The effects of tearing are to delay the fracture event and to produce an apparent toughness well above the lower bound toughness. In one case, Q3-21, a reasonable toughness was predicted with crack initiation time of 221 μs. In general one might disregard any test with a crack initiation time significantly greater than about 200 μs.

The effect of small errors in measuring the crack initiation time depends on the time of crack initiation. If the dynamic crack initiation toughness is relatively low (about 60 MPa·m$^{1/2}$), the specimen will fail early in the impact event, say at 100 μs. A delay error of 10 μs (10% in this instance) produces an error in K_{Id} of 6.0%. The mitigation of the error is due to the non-linearity of the master curve shown in Fig. 8. At higher toughness values (say 73 MPa·m$^{1/2}$) which corresponds to an initiation time of 150 μs, a delay error of 10 μs (6.7% in this case) produces an error in K_{Id} of only 4%. For the highest toughness, about 85 MPa·m$^{1/2}$, the time to initiation is 200 μs, and the error in the time measurement will be 5% and in the toughness measurement only about 3%. When compared to the scatter of several hundred per cent in toughness measurements typically observed in extensive and carefully controlled testing programs for K_{Ic}, these errors are very small.

We conclude that force-time records from instrumented Charpy machine can be interpreted to give a close estimate of the initiation time. The estimate will usually give an initiation time that is too long by 5 to 10 μs, but this error is small compared to the typical scatter in the measurement, and the error is in part mitigated by the non linearity of the master K_{Id}-t curve.

RESULTS

A total of 16 modified Charpy specimens were tested in this study. Each specimen was instrumented with strain gages, and simultaneous records of strain and force were made as a function of time during the impact event. Specimens were tested at temperatures of 0, 10, 21, 30 and 40°C. The results from the test series include the crack initiation time measured from the strain gage and the instrumented tup records, the dynamic crack initiation toughness K_{Id}, and the energy absorbed are shown in Table 1. Two specimens, E3-8 and -16, we considered to be invalid tests due to excessive tearing prior to cleavage initiation The results for the crack initiation toughness of the remaining specimens are also presented in Fig. 11.

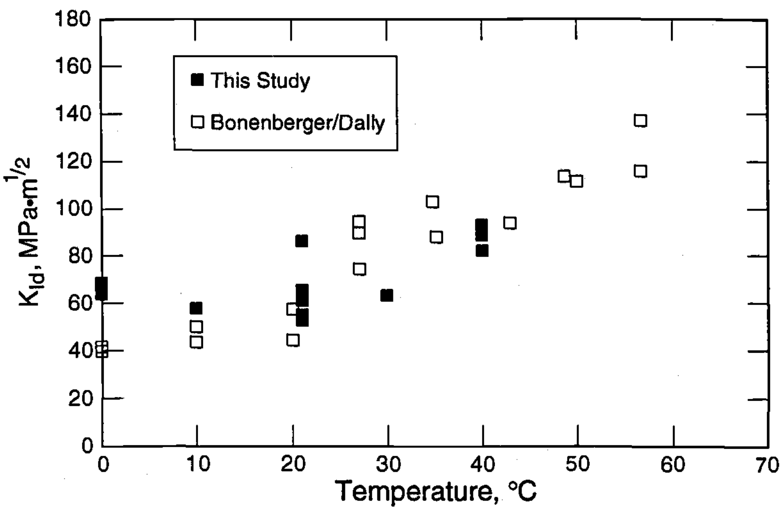

(a)

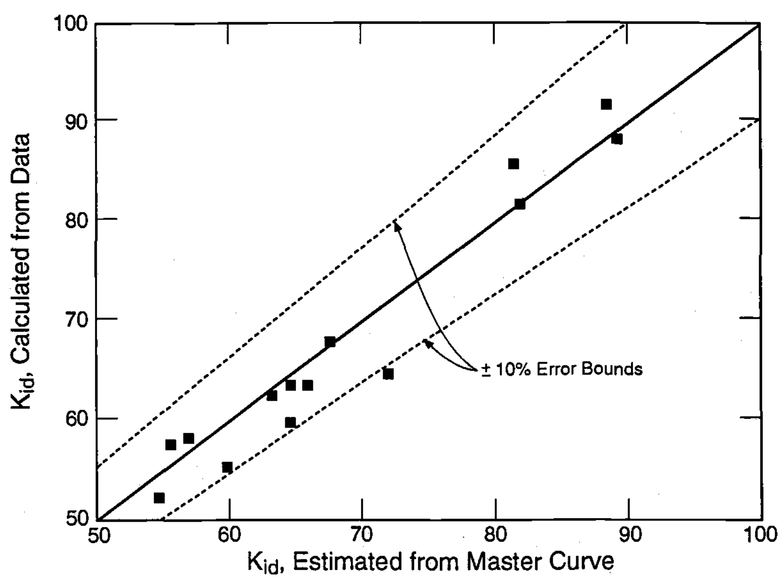

(b)

Figure 11: (a) The K_{Id} temperature relation for A553 B reactor grade steel, and (b) the correlation between K_{Id} values calculated from the data to K_{Id} values estimateed from the master curve.

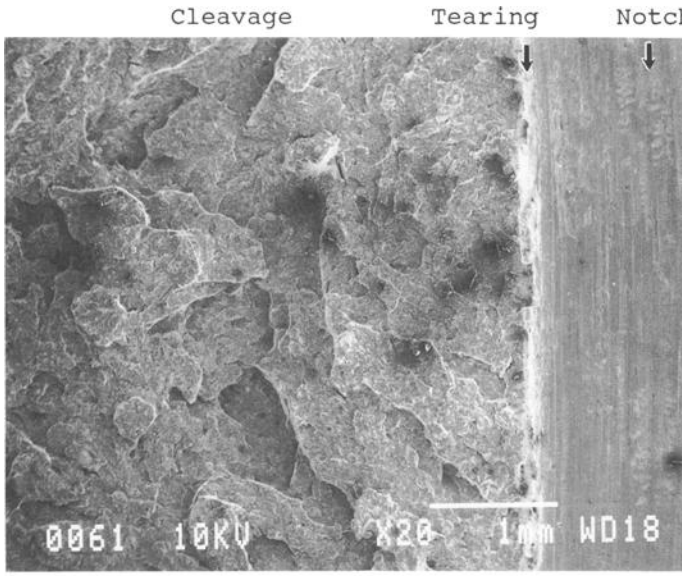

(A)

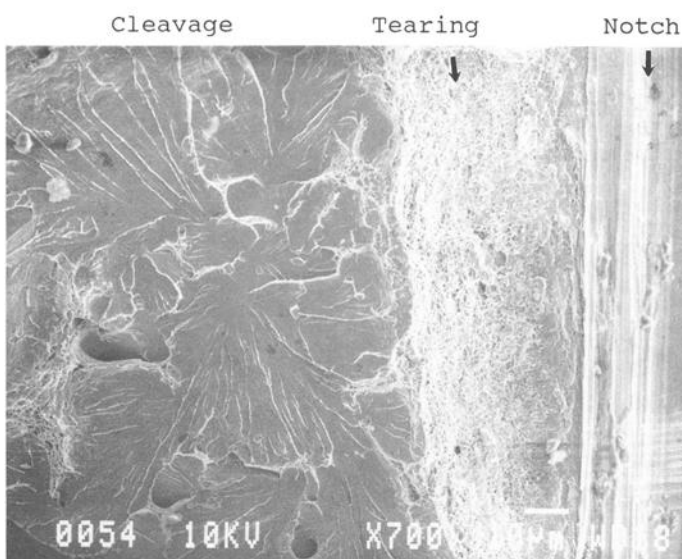

(B)

Figure 12: The tearing zone at the root of the notch in the E3-11 sample (0 C), is approximately 0.1 mm wide. Tearing was followed by cleavage intiation, which is more clearly shown at higher magnification, B.

TABLE 1--Results from the Modified Charpy Test Series

Spec. No.	Temp. °C	K_{Id} MPa·$m^{1/2}$	Strain Time μs	Force Time μs	Absorbed Energy J
E3-11	0	70.4	131	132	32.2
Q3-20	0	75.6	137	132	32.9
E3-3	10	71.2	102	121	44.8
E3-20	10	63.9	98	100	26.6
E3-1	21	60.4	127	139	29.4
E3-6	21	58.2	95	95	23.1
E3-10	21	61.5	111	124	35.0
E3-16	21	71.7	154	161	37.8
E3-18	21	70.4	127	128	28.0
Q3-17	21	95.4	131	132	55.3
E3-7	30	69.0	180	177	35.0
E3-17	30	69.3	122	121	29.4
E3-8	30	100.1	267	296	100.8
Q3-10	40	101.5	218	227	59.5
Q3-21	40	99.0	221	283	79.8
Q3-23	40	90.6	191	*	56.0

* Instrument malfunction on tup record.

FRACTOGRAPHY

The fracture surfaces from five different specimens were examined in a scanning electron microscope to study the initiation of fracture from the "sharp" notch tip. The results that were observed varied considerably from specimen to specimen. The smallest amount of tearing occurred in specimen E3-11 as illustrated in Fig. 12. An overall view of the notch region at 20X, presented in Fig. 12a, shows a narrow tearing zone at the notch tip prior to clevage initiation over a large region. It is important to note that the extent of tearing is not uniform, and the depth of the tear zone varies over the height of the specimen. This fact is better illustrated in Fig. 12 b, where the transition from ductile tearing to cleavage is presented at a magnification of 700X. We observe that the depth of the

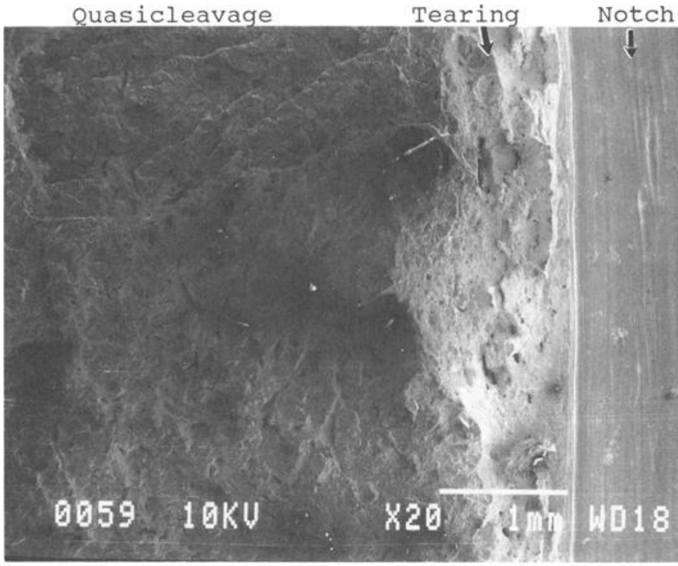

(A)

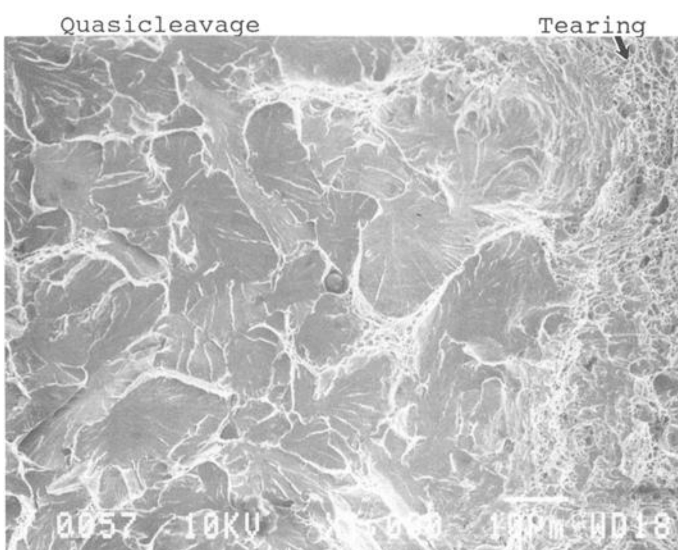

(B)

Figure 13: The tearing zone at the root of the notch in the E3-8 sample (30 C), is over 1 mm wide in some regions. Tearing was followed by cleavage initiation (mixed mode), which is more clearly shown at higher magnification, B.

tear zone varies from about 33 μm at the bottom of the fractograph to about 47 μm at the top. The cleavage region shows small areas of ductile hole joining at the ridge lines, which is typical for this type of steel when cleavage occurs at test temperatures close to the RT_{NDT}.

The most extensive tearing occurred for specimen E3-8 which was tested at 30°C. The fractograph shown in Fig. 13a, indicates that the depth of the tear zone exceeded 1 mm. The propagation of the crack front by the tearing mechanism is relatively slow in comparison to cleavage propagation. As a consequence, the time required for cleavage initiation is very long. In this case the time to initiation was 267 μs. With this large amount of tearing the test is considered invalid and the data is not used in the determination of the lower bound toughness. The transition from tearing to cleavage eventually occurs, as shown in Fig. 13 b. Again the cleavage region shows evidence of late breaking ligaments at the ridge lines of the cleavage facets. The ductile hole joining in these regions is typical of this steel when tested at 30 to 40°C above the RT_{NDT}.

The area of tearing at the tip of the notch varied from 1.8 mm^2 to 9.6 mm^2. The time to crack initiation was a function of this area as expected. The shorter initiation times (less than 150 μs) were associated with tearing areas of less than 2 mm^2, and the longer initiation times (more than 200 μs) were associated with areas in excess of 2.5 mm^2.

DISCUSSION AND CONCLUSIONS

The concept of determining crack initiation toughness from Charpy specimens is not new. Initial studies [8,9] coincided with the development of instrumented tups, and efforts were made to relate the toughness directly to the impact force. The method for determining K_{Id} from the tup records was described by Radon and Turner [10], and this method was employed by Server and Tetelman [11] in their studies of a reactor grade steel. Both of these investigations used standard Charpy specimens that had been precracked in fatigue and side-grooved. From these studies, guidelines [12] were developed to determine K_{Id} and J_{Id}.

The difficulty in using the standard Charpy specimen to determine toughness is that the small height (10 mm) of the specimen is sufficient to provide plain strain constraint for only those materials with extremely low toughness. For more commonly employed engineering steels, additional constraint is necessary to accommodate increased toughness. Hoyt [13] had suggested using double height specimens to increase constraint as early as 1938, but nothing was done to implement this suggestion until Bonenberger developed the modified specimen geometry [4] with a height of 19.2 mm.

This specimen offers sufficient constraint to permit testing of engineering steels with K_{Id} approaching about 100 MPa·m$^{1/2}$.

We have extended the work of Bonenberger et al. by modifying the procedures followed for specimen preparation and testing. We have employed a sharp notch instead of a precrack formed with precompression. The results obtained indicate that cleavage can be initiated from the sharp notch, but that the cleavage is preceded by a small amount of tearing. The depth of the tearing ranged from 30 to 50 μm for specimens exhibiting lower toughness (55 to 70 MPa·m$^{1/2}$) to as much as 1 mm for specimens with very high toughness (in excess of 100 MPa·m$^{1/2}$). The tearing transitions into cleavage even in the high toughness specimens; however, tearing is a slow process and the initiation time is extended to 200 μs or longer.

We have also shown that an instrumented tup can be employed to estimate the crack initiation time. There is usually a small delay in the response of the tup, when compared to the strain gage response; however, the error produced by the typical delay (5 to 10 μs) is negligible when compared to the scatter observed in carefully controlled and standardized tests for toughness.

A master curve relating crack initiation time to K_{Id} was developed in this investigation. This curve differs from the master curve developed by Bonenberger [5], even though the material was from the same plate. The curve presented in Fig. 8 is nearly identical to the curve in [5] for small strains but for the larger strains, the curve developed in this study shows more non linearity. We believe that part of the differences may be due to the different Charpy machines that were employed. Bonenberger employed a U type machine with a 400 J capacity. The machine was old (worn tup), used extensively by undergraduate students and not firmly mounted to the floor. The machine used in this study was a U type with a capacity of 250 J. It was in excellent condition; grouted and properly bolted to the floor with a suitable foundation. The nose piece on the hammer was new. We believe that a significant part of the non linearity in the master curve is due to the plastic deformation at the contact point due to Hertzian stresses that exceed the yield strength.

A second difference was in the material at the notch. Although the specimens were all from the same plate, Bonenberger pre-compressed the material in the local neighborhood of the notch. This pre-compression elevated the local yield strength and the specimen exhibited better resistance to the Hertzian contact stresses and required a longer time before yielding at the net section occurred. The precompession also introduces residual tensile stresses which were partially relieved by short cracks at the notch tip.

The third difference was in the depth of the side grooves. In this study we employed a depth of 2 mm compared to a depth of 1.9 mm used by Bonenberger. This difference would tend to cause yielding of the more deeply side grooved specimens at an early time and to accentuate the non linearities, although the effect would be small.

The results that we measured for K_{Id} were higher than those measured by Bonenberger at 0°C. We believe this difference is due largely to the method used to prepare the specimens. Precompression used by Bonenberger probably elevated the yield strength while suppressing the toughness. Also the precompression produced a residual tensile stress near the notch that was only partially relieved by the formation of a short crack at the crack tip. Accordingly Bonenberger measured K_{Id} values (40 to 50 MPa·m^{½}) that were significantly lower than the average crack arrest toughness of 83.4 MPa·m^{½} [7]. In this investigation the measurements of K_{Id} at room temperature varied from 58.2 to 95.4 MPa·m^{½} with an average value of 69.6 MPa·m^{½}, which is in better agreement with the average arrest toughness of the material.

We expect the arrest toughness of the steel K_{Ia} to be less than the dynamic crack initiation toughness K_{Id}. In this series of measurements the average value of K_{Id} was about 16.5% lower than the average value of K_{Ia}. However, in the round robin testing [7] of the same lot of A533 Type B steel the standard deviation for the crack arrest toughness was 10.6 MPa·m^{½}. If one defines the lower bound toughness as the mean less two standard deviations, the value from the round robin test program would be 83.4 - 2(10.3) = 62.2 MPa·m^{½}. It appears that the results from the sharp notched modified Charpy specimens are somewhat conservative when average values are considered. However, if one is attempting to determine the lower bound toughness to be used in a conservative design, then the results using the proposed method appear to be in reasonable correspondence with a arrest toughness measurements when the dispersion of the test results are taken into account.

It is important to eliminate the need to use strain gages in developing a measurement method for fracture toughness that is based on impact loading with Charpy machines. The strain gages require additional instrumentation, are expensive to install and require additional time in data reduction. Master curves can be developed for different alloys using a limited number of strain gages and then employed in subsequent certification testing to insure that the toughness of a particular heat of steel exceeds a minimum lower bound toughness. This approach requires that the initiation time be established with some degree of confidence. We have shown that the instrumented tup gives a reasonably close estimate of the initiation time. However, before we close this topic it should be noted that initiation is not an instantaneous event.

When a crack initiates, even from a fatigue sharpened crack, the initiation event is a series of many small initiation events. Initiation occurs at many cleavage initiation sites. Crack front stretch and even limited amounts of tearing (ductile hole joining) occur before all of the cleavage initiation site are triggered. Sometimes in the tougher steels, cleavage will extend across a few grains and then the fracture mechanism will transition back to ductile hole joining. The initiation process is a combination of many local initiation events which occur over a small amount of time, but not at the same instant. When we attempt to measure the initiation time, we should recognize that it is not a precise number, but an approximation of the time when a critical number of local cleavage initiation events are occurring.

ACKNOWLEDGMENTS

James W. Dally appreciates the support of the National Science Foundation during the later phase of this study.

REFERENCES

[1] Rosenfield, A.R. and Marschall , C.W., "Fracture Mechanics Based Failure Analysis," USNRC Report NUREG/CR-5860, June 1992.

[2] Anon, 1993 Annual Book of ASTM Standards, Section 3, Metals Test Methods and Analytical Procedures, ASTM E-399 and ASTM E-1221 Specification, ASTM, American Society of Testing Materials, Philadelphia, 1993.

[3] Link, R.E. and Joyce, J.A., "Experimental Investigation of Fracture Toughness Scaling Models," 2nd Symposium on Constraint Effects in Fracture, ASTM, November, 1993.

[4] Bonenberger, R.J. and Dally, J.W., "Further Studies of a Modified Charpy Specimen for Lower Bound Toughness," Fracture Mechanics: 25th Volume, ASTM STP 1220, F. Erdogan and R.J. Hartranft, Eds., American Society of Testing Materials, Philadelphia, 1993.

[5] Bonenberger, R.J., Dally, J.W., and Irwin, G.R., "Lower Bound Initiation toughness with a Modified Charpy Specimen," Constraint Effects in Fracture, ASTM STP 1171, E.M. Hackett, K.-H. Schwalbe, and R.H. Dodds, Eds., American Society of Testing Materials, Philadelphia, 1993, pp. 139-157.

[6] Winkler, S. Fraunhofer - Institut für Werkstoffmechanik 7800 Freiburg, Germany, Private Communication.

[7] Barker, D.B., Chona, R., Fourney, W.L., and Irwin, G.R., A Report on the Round Robin Program to Evaluate the Proposed ASTM Standard Test Method for Determining the Plane Strain Crack Arrest Fracture Toughness, K_{Ia}, of Ferritic Materials, NRC report, NUREG/CR-4996, ORNL/Sub/79-7778/4, January 1987.

[8] Irwin, G.R., Dally, J.W., Zhang, X-J, and Bonenberger, "Lower Bound Initiation Toughness of A 533B Reactor Grade Steel," Symposium on Rapid Load Fracture Testing, San Franciso, CA, April 1990, ASTM, Philadelphia, PA, 1990.

[9] Impact Testing of Metals, ASTM STP 466, ASTM, Philadelphia, PA, 1970.

[10] Radon, J.C. and Turner, C.E., "Fracture Toughness Measurement by Instrumented Impact Test," Engineering Fracture Mechanics, Vol. 1, 1969, pp. 411-428.

[11] Server, W.L. and Tetleman, A.S., "The Use of Pre-cracked Charpy Specimens to Determine Dynamic Fracture Toughness," Engineering Fracture Mechanics, Vol. 4, 1972, pp. 3673-375.

[12] Server, W.L., "Impact Three-Point Testing for Notched and Precracked Specimens," Journal of Testing and Evaluation, Vol. 6, No. 1, 1978, pp. 29-34.

[13] Hoyt, S.L., "Notched-Bar Testing and Impact Testing," Proceedings ASTM Part II, Vol. 38, ASTM, Philadelphia, PA, 1938, pp. 141-156.

Thomas J. Mackin[1] and David F. Tognarelli[2]

Design and Evaluation of a Verification System for Force Measurement Using Instrumented Impact Testing Machines

REFERENCE: Mackin, T. J. and Tognarelli, D. F., "Design and Evaluation of a Verification System for Instrumented Impact Testing Machines," Pendulum Impact Machines: Procedures and Specimens for Verification, ASTM STP 1248, T.A. Siewert and A.K. Schmieder, Eds American Society for Testing and Materials, Philadelphia, 1995.

ABSTRACT: A series of controlled impact experiments using a charpy pendulum were conducted to address the possibility of dynamic verification and calibration of instrumented tups. The methodology involved striking an instrumented pendulum tup against a rigidly fixtured transducer. The guiding principal is as follows: If a NIST traceable dynamic load cell is impacted by a service load cell, a comparison of the signals can be used to verify the performance of the service load cell. In this fashion, tups can be verified and calibrated electronically, without resorting to the use of standard test specimens. A relatively compliant Nylon bumper was placed between the pendulum tup and the fixed load cells to dampen the excitation of high frequencies during the impact event. During each impact, load-time signals measured by both the pendulum and fixtured tups were recorded, compared and Fourier analyzed. Results of the Fourier analysis justified a simple two-mass-two-spring model of the impact behavior. Results of the experiments are rationalized using the mass-spring model, and present guidelines for designing a verification system for both pendulum and drop-weight testing machines.

KEYWORDS: verifier tup, dynamic calibration, instrumented impact, Fourier analysis, viscous damping, stress waves, frequency spectrum, nylon alloy

INTRODUCTION

Charpy tests have found widespread use in the measurement of the fracture properties of materials. However, the dynamic effects associated with impact testing make accurate calculations of the energy partitioning quite difficult[1]. Additionally, stress wave

1 Assistant Professor, Department of Mechanical and Industrial Engineering, The University of Illinois at Urbana-Champaign, Urbana, IL 61801

2 Dynatup, GRC International Inc., 5383 Hollister Ave., Santa Barbara, CA 93106

reflections during a test affect the measured signals, and substantially alter the output of impact experiments [2,3,4,5]. This was clearly outlined by Sahraoui and Lataillade[3], who considered the vibrations of a charpy specimen throughout an impact test. Their work demonstrates that, depending upon the contact stiffness of the system, one can either substantially under- or over-estimate the failure load during charpy tests. These dynamic effects have made a complete understanding of impact testing an elusive goal, and created a need to dynamically calibrate and verify impact testing equipment.

The issue of dynamic calibration arises from the fact that impact transducers are calibrated quasi-statically, yet used dynamically. This has raised the issue of whether a static calibration is suitable for dynamic load measurements[1]. For the most part, the issue of dynamic verification has been addressed by conducting tests on standard test specimens (ASTM E 23). Using this approach, tests are conducted on a standard test material with a known energy absorption to failure. Samples of the material standard are tested according to the ASTM protocol (ASTM E 23), and their energy absorption recorded. The resulting value must agree with the known standard to within ±5%. Though this represents a viable methodology, it is always subject to statistical variability in sample properties, testing conditions, and experimental diligence. Furthermore, the fracture of materials is inherently non-linear and, therefore, extremely sensitive to initial conditions.

The present research presents an alternate verification technique that utilizes an entirely electronic verification scheme. This is accomplished by striking one load cell against another. A compliant nylon bumper was placed between the two load cells to damp out any high frequency excitations. Furthermore, since the modulus of the compliant bumper is several orders of magnitude lower than that of either the pendulum or the fixtured transducer, the compliant bumper becomes the dominant energy absorber throughout the impact event. Experiments were conducted over a range of impact energies and bumper thickness. A comparison of the signals, then, would allow one transducer to be verified against the output of another. Such a comparison, however, depends upon a thorough understanding of the impact event, accounting for any and all dynamic effects associated with the tests. With this in mind, a controlled study was conducted to guide the development of a verification system, the results of which are reported in this paper.

EXPERIMENTAL PROCEDURE

A Dynatup (Model POE2000) Instrumented charpy testing machine was configured with an impact transducer at the normal location of a test specimen, Figure 1. This transducer is considered as a reference (or verifier) for comparing the transducer output of the instrumented tup. In this investigation, both the instrumented tup and the verifier transducer were quasi-statically calibrated.† The verifier transducer was rigidly clamped to the base of the pendulum machine, all of which was attached to a 1600lb block of concrete. The verification transducer was a custom fabricated dynamic tup for use as a verifier transducer in both pendulum and drop-weight machines. A nylon bumper was affixed to the tip of the verifier transducer, as shown in Figure 2. The nylon is used as a compliant shock bumper that prevents high frequency excitations, and has a stiffness three orders of magnitude lower than that of the tups. As a result, the vast majority of the impact energy is absorbed in the compliant bumper, with very little elastic energy absorbed by the tups. This enables a simple analysis, whereby the tups are considered to be rigid, and all the impact energy is absorbed by the nylon bumper.

† In practice, it is proposed that the verifier tup be replaced with a NIST-traceable, dynamically calibrated load cell.

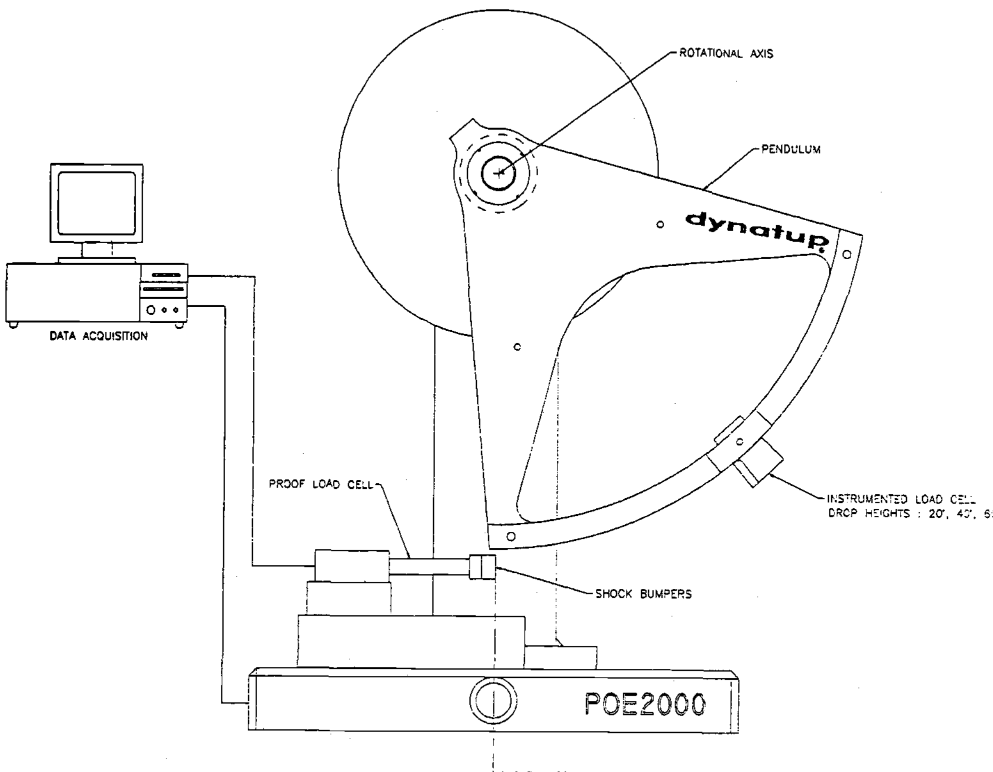

Figure 1. Schematic of the verification system. The verifier transducer is positioned at the bottom of the pendulum arc.

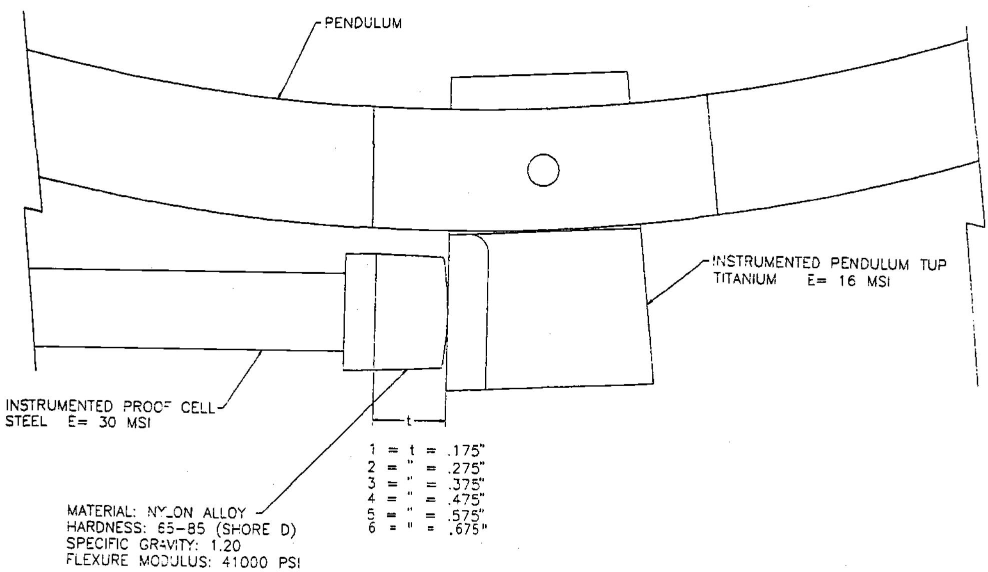

Figure 2. A nylon bumper is molded directly onto the verifier tup. Bumpers were fabricated with thickness ranging from 4.4 mm (0.175") to 17.0 mm (0.675").

The charpy pendulum is raised to a pre-determined height (drop angle) and released. As it approaches the verifier transducer, it activates a data acquisition system. Data is acquired from both the charpy and verifier tups at a 400kHz sampling rate. The experiment is repeated four times, at each drop angle, to assure statistical reliability. Three different drop angles (20°, 40° and 60°) were used for each of six different Nylon bumper thicknesses, as listed in Figure 2. This broad range of testing conditions was used to provide a breadth of experimental results to guide the subsequent modeling.

EXPERIMENTAL RESULTS

Overlays of typical signals from both the charpy and verifier tups are displayed in Figures 3 and 4. Figure 3 shows results of a drop test from an angle of 20°. Each of the curves show the same qualitative shape, with quantitative differences in the magnitude of the tup response. Note that the agreement between the signals improves with an increase in thickness of the nylon bumper , Figure 3b. Figure 4 shows a similar comparison of tup response for a drop angle of 60°. The thin nylon bumper results in substantial differences between the charpy and verifier signals (Fig 4a), while, again, improvements in signal agreement are obtained for the thick bumper (Fig 4b). Such differences are due to dynamic effects associated with the bumper material, and will be modeled in the next section.

A series of impact tests were conducted using bumpers ranging in thickness from 0.175" to 0.675", over each of the drop angles. The peak force measured by both the charpy and verifier tups is plotted as a function of bumper thickness and drop angle in Figure 5. Two items are of note in these figures: First, the peak impact force was found to increase with increasing bumper thickness. Second, the mean difference between the charpy and verifier signals decreases with increasing bumper thickness. These effects are attributed to the dynamic response of the bumper material. As will be shown in the next section, the stress wave amplitude has a greater effect for the thinner specimens, due, in part, to the increased viscous damping that accompanies the thicker bumpers.

The load-time signals of both the charpy and verifier tups were analyzed for their spectral content. Figure 6 contains representative results of the spectral analysis for both tups. Both tups show a dominant spectral component at 400Hz, the frequency associated with the elastic rebound. The power diminishes rapidly, showing only one additional frequency of any consequence in the verifier signal. This frequency is associated with stress wave propagation in the Nylon bumper material [6],

$$f = \frac{v}{t} \tag{1}$$

where $v = \sqrt{\frac{E}{\rho}}$

E = is the modulus of elasticity
p = is the density
and t = is the bumper thickness

For nylon, this results in a frequency of approximately 1600Hz. In each experiment the spectral content of the verifier was greater than that of the charpy tup. This effect is attributed to the fact that the Nylon bumper is securely fixed to the verifier, while it experiences only a pressure contact at the charpy side. The improved coupling at the verifier results in a different Fourier spectrum. This effect is not attributed to the differences in the tups themselves, since the content of the Fourier spectrum is well below the natural frequencies of the two tups.

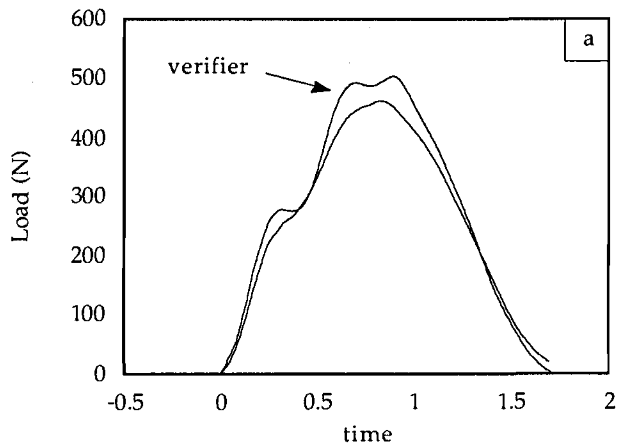

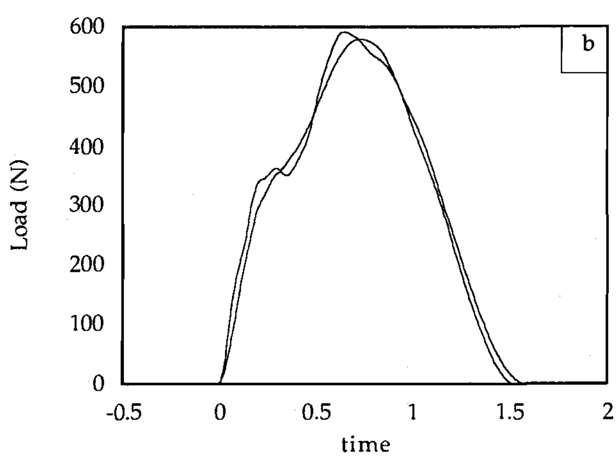

Figure 3. Overlays of the load-time response from both the verifier and charpy tups during impact from a drop angle of 20°.show quantitative differences. (a) A bumper thickness of 4.4 mm resulted in a verifier response greater than that of the charpy tup. (b) A bumper thickness of 17.1 mm resulted in better agreement between the charpy and verifier tups.

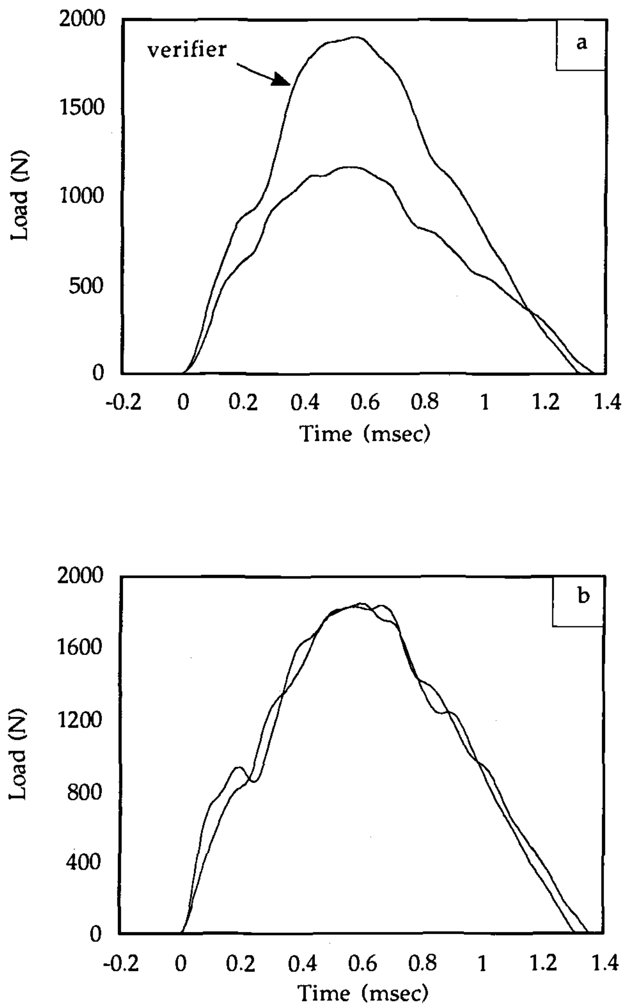

Figure 4. Overlays of the load-time response from both the verifier and charpy tups during impact from a drop angle of 60°. (a) The thin bumper (4.4 mm) resulted in large discrepancies between the charpy and verifier tups, while good agreement was found for the thick (17.1 mm) bumper.

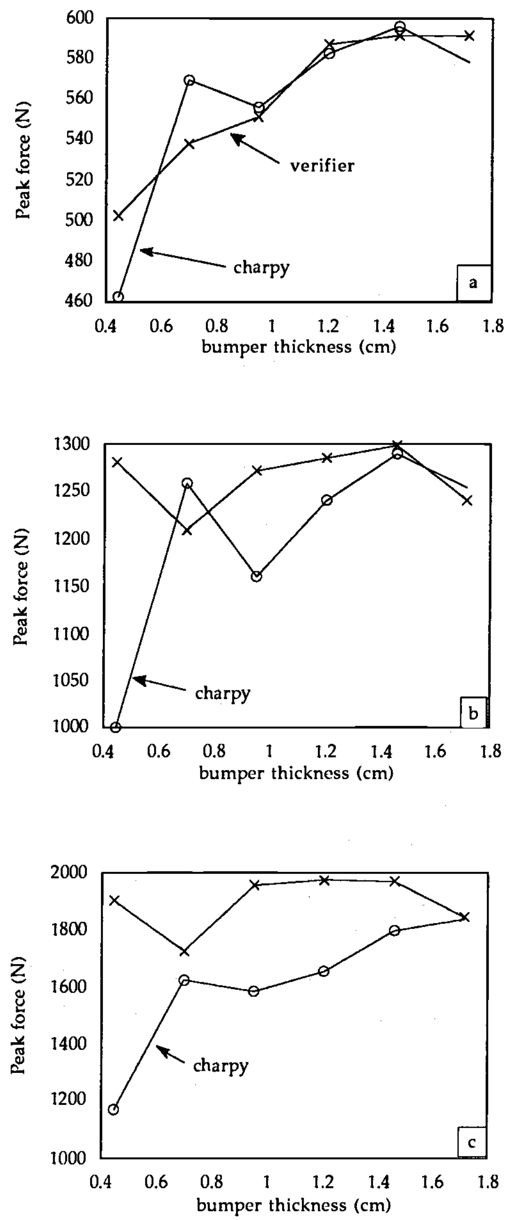

Figure 5. Both charpy and verifier response was found to vary with bumper thickness. (a) drop angle=20°, (b) drop angle=40°, and (c) drop angle=60°.

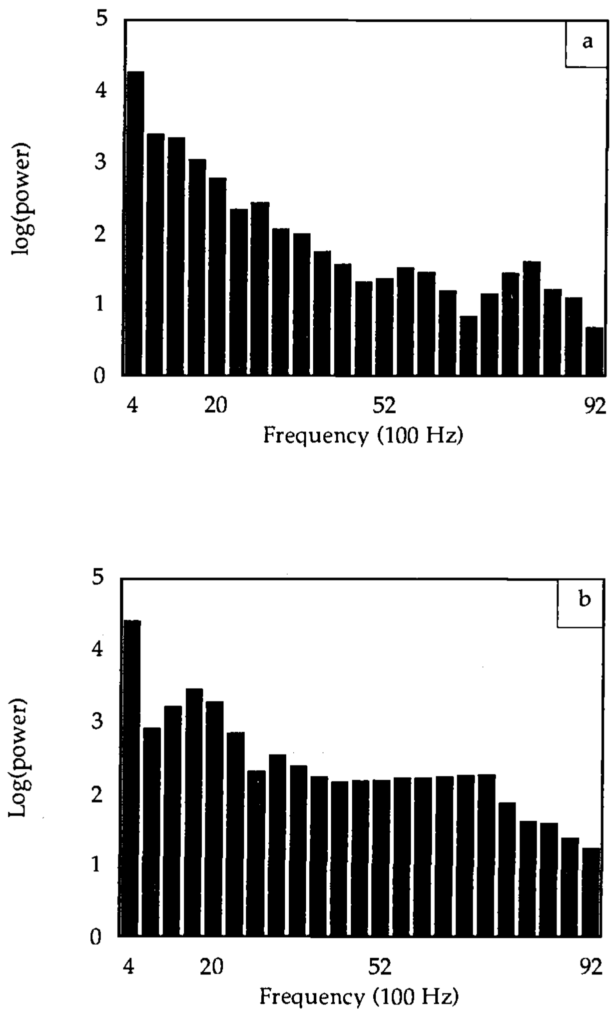

Figure 6. Plots of the power spectrum obtained from the Fourier transform of the (a) charpy and (b) verifier signals.

THEORY AND COMPUTER SIMULATION

Fourier analysis of the Impact signals revealed two dominant frequencies in the power spectra. As a result, a two-mass-two-spring model is used to provide a theoretical framework for interpreting the results, and is confined to modeling the behavior of the nylon bumper during the impact event. Given the relative stiffness of the tup and bumper materials, the Charpy and verifier transducers are considered to be rigid. Since polymers are notoriously viscoelastic, the nylon bumper model includes both elastic springs and viscous damping elements, Figure 7. The viscous damping element has the effect of diminishing the stress-wave amplitude, a result that is noted in the experimental impact results. Using the coordinate system indicated in Figure 7, a set of two coupled differential equations completely describes the dynamics of this system[7]:

$$\ddot{u}_1+\frac{c_1}{m_1}\dot{u}_1+\frac{k_1}{m_1}(2u_1-u_2)=0 \tag{2a}$$

$$\ddot{u}_2+\frac{c_2}{m_2}(\dot{u}_2-\dot{u}_1)+\frac{k_2}{m_2}(u_2-u_1-u_0)=0 \tag{2b}$$

where: $\underline{u}$ denotes the location of each mass
$\underline{c}$ is a damping coefficient
$\underline{m}$ is the associated mass
and $\underline{k}$ is the associated spring constant.

The subscripts correspond to each mass and spring element.

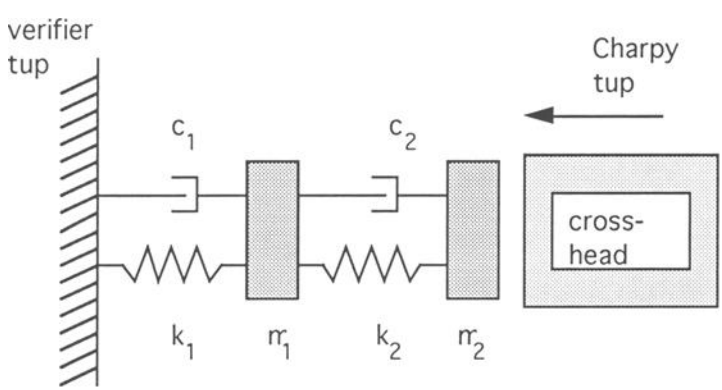

Figure 7. The response of the nylon bumper is modeled as a system of two masses connected by two springs and two dash pots. The tups are rigid in comparison to the nylon bumper. The verifier response is simply the reaction force at the wall, while the charpy response is equal to the crosshead mass times the deceleration of the crosshead.

In the following simulations, the damping coefficients and spring constants are equal, while m_1 is given by half the mass of the Nylon bumper, and m_2 is equal to the sum of half the bumper mass plus the cross-head mass. The spring constant is related to the modulus of the Nylon material through

$$k=\frac{AE}{L} \tag{3}$$

where A is the cross sectional area of the Nylon bumper
E is the modulus of elasticity of Nylon
and L is the bumper thickness

The damping coefficients, c, were systematically varied until a behavior similar to that observed in the experiments was obtained. It is important to note that these simulations are for the purpose of understanding the observed experimental trends, and are not intended to be quantitative models of the impact experiments. Thus, the numerical output is not calibrated to the experimental values measured by the charpy and verifier tups.

The proposed model captures the essence of the impact problem; it incorporates elastic and inelastic response, and it includes a stress wave component. As such, this model *can* be adjusted to accurately model the experimental traces.

For the purpose of completeness, higher order spring-mass models were also tested, resulting in an additional simultaneous equation for each mass that was added to the model. In all cases, the ensuing 2nd order coupled differential equations were written as two first order equations and solved using a 4th order Runge-Kutta technique. The accuracy of the Runge-Kutta was evaluated by iteratively refining the step size, until only small differences were noted in the resulting solutions. Increasing the number of springs and masses adds higher frequencies to the spectrum of vibrations. Since only two major frequencies were noted in the experiments, the higher order models were not needed, and all subsequent modeling was conducted using a two-mass two-spring system.

Figure 8 overlays the results of an impact simulation using the two-mass two-spring model with an experimentally measured impact curve. As can be seen in the figure, the model accurately captures the essential features of the impact event, wherein a dominant bell shaped curve is modulated by a damped sinusoid. The damped sinusoid corresponds to oscillations of the center mass in the model material, in direct analogy to the modulations brought about by stress waves in the nylon bumper material.

The configuration of the experimental set-up has the charpy tup measuring the load on one side of the nylon bumper, while the verifier measures the load on the opposite side. Using the proposed model, simulations were conducted to compare such loads. The force associated with crosshead deceleration models the charpy load, while the reaction force at the wall models the verifier load, Figure 7. In contrast to quasi-static loading, dynamic loading contains inertial and stress wave effects that result in different loads simultaneously occurring on each side of the sample. This is clearly revealed in Figure 9, where, first, the stress waves are out of phase, and, second, inertial effects have diminished the relative peak loads at both the front and back sides of the bumper (Fig 9a). Thus, the results of simulated impacts show differences in front and back-side loads that arise due to stress waves, inertial effects and viscous dissipation. As a result, comparison of one tup to another, *during the same impact event,* must account for both stress waves and viscous dissipation effects.

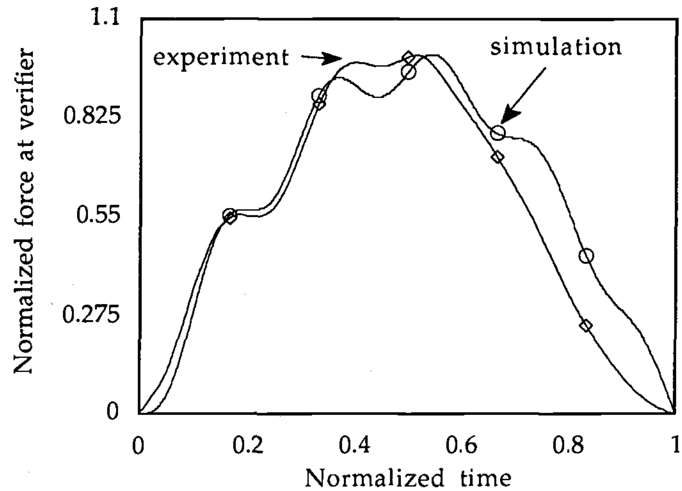

Figure 8. A comparison of simulated and measured impact response at the verifier tup show good qualitative agreement.

The impact experiments conducted led to several surprising results. First, increasing the nylon bumper thickness improved the agreement between the charpy and verifier transducers. Second, as the nylon bumper thickness increased, the peak load measured by both the charpy and verifier tups were found to increase. Simulations were conducted to determine the response of the mass-spring analog as the sample thickness was increased. Changes in the sample thickness were modeled in two ways: (1) the sample was doubled in thickness by doubling the total number of masses and springs, and, (2) the sample was doubled in thickness by doubling the mass and the equilibrium length of the two spring system. As expected, doubling the total number of masses and springs causes a decrease in the peak load for a given impact condition. However, the frequency spectrum is dramatically altered, resulting in a load-time trace that does not resemble the experiments. Doubling the masses and equilibrium spring lengths, while changing the spring constants results in simulations that are in good qualitative agreement with the experiments, Figure 9. That is, increasing the specimen thickness increased the peak load measured at both sides of the bumper. It is postulated that, over the range of thickness tested, an increase in thickness increases the inertial effects, resulting in an increased peak load.

CONCLUSIONS

The experiments presented in this study reveal the possibility of designing a verification system for tups used under daily service testing. The service machine would be verified against a known standard impact transducer by striking the verifier with the service tup. The procedure for verification would mimic the procedures outlined in this study. In brief, a verification tup would be mounted onto a Pendulum machine to receive a blow from the pendulum tup. The verifier tup would be positioned at the bottom of the charpy arc, and fixtured with a compliant bumper material. Several impact tests would be conducted at several drop heights, and the signals from both tups would be recorded and overlaid. If the charpy tup is functioning properly, the resulting signals should agree to within a specified tolerance, determined through a round-robin set of experiments. A compliant bumper material should be chosen with specific elastic and geometric properties, based, again, upon the results of round-robin testing.

It is important to note that, due to inertial, stress wave, and viscous effects, even perfectly calibrated transducers will record differences in the load on each side of a compliant bumper. Thus, verification must consider the dynamic response of the bumper material. An excessively hard bumper will partition a greater share of the impact energy to both the striking and verifier tups, resulting in the need to include the tup response in the dynamic modeling. Thus, a compliant bumper is preferred. However, one must also consider the viscous damping and thickness related effects inherent in the choice of a bumper material. The experiments presented herein demonstrate that a 0.675" thick nylon alloy bumper allows for good agreement between the charpy and verifier tups. Though further testing is required, it is clear that the proposed verification system can be the basis of a useful and reliable verification system.

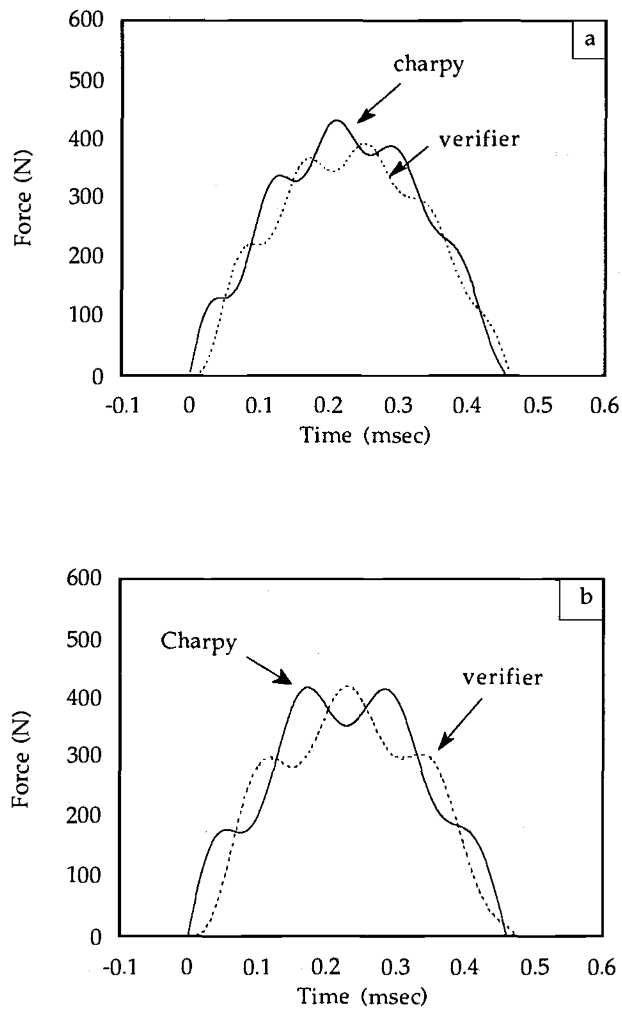

Figure 9. Simulations of the charpy and verifier tup response show differences at both the front and back sides of the nylon bumper. (a) A thin bumper material shows relatively large differences between the front and back-side response. (b) A thick bumper material results in better agreement between the peak force, but still shows substantial phase shifts in the two signals.

REFERENCES

[1] Ireland, D. R., "Procedures and Problems Associated with Reliable Control of the Instrumented Impact Test," Instrumented Impact Testing, ASTM STP 563, American Society for Testing and Materials, 1974, pp. 3-29.

[2] Jemian, W. A., Jang, B. Z., and Chou, J. S., "Testing, Simulation and Interpretation of Materials Impact Characteristics," Instrumented Impact Testing of Plastics and Composite Materials," ASTM STP 936, S. L. Kessler, G. C. Adams, S. B. Driscoll, and D. R. Ireland, Eds., American Society for Testing and Materials, Philadelphia, 1987, pp. 117-143.

[3] Sahraoui, S. and Lataillade, J. L., "Dynamic Effects During Instrumented Impact Testing," Engineering Fracture Mechanics Vol. 36, N0. 6, pp. 1013-1019, 1990.

[4] Kobayashi, Y., Koide, Y., Daicho, Y., and Ikeda, R., "Dynamic Fracture Toughness Testing of Epoxy Filled with SiO_2 Particles," Engineering Fracture Mechanics Vol. 28, N0. 1, pp. 21-19, 1987.

[5] Kobayashi, Y., "Analysis of Impact Properties of A533 Steel for Nuclear Reactor Pressure Vessel by Instrumented Charpy Test," Engineering Fracture Mechanics Vol. 19, N0. 1, pp. 49-65, 1984.

[6] Graff, K. F., Wave Motion in Elastic Solids, Dover Publications, Inc., NY 1975.

[7] Goldstein, R., Classical Mechanics, 2nd Edition, Addison Wesley, 1981.

Jörg F. Kalthoff[1], and Gerd Wilde[2]

INSTRUMENTED IMPACT TESTING OF POLYMERIC MATERIALS

REFERENCE: Kalthoff. J. F. and Wilde, G., **"Instrumented Impact Testing of Polymeric Materials,"** Pendulum Impact Machine: Procedures and Specimens for Verification, ASTM STP 1248, Thomas A. Siewert and A. Karl Schmieder, Eds., American Society for Testing and Materials, Philadelphia, 1995.

ABSTRACT: Measuring techniques and evaluation procedures for determining impact energies of polymeric specimens in instrumented impact tests are discussed. In particular, high sensitivity striker tups capable of measuring small loads with high accuracy are introduced and the importance of sufficiently fast electronic measuring systems for obtaining true load traces are illustrated. But even when determined with appropriate test techniques the measured impact energy might not in all cases represent the true fracture energy for breaking of the specimen. Kinematographic recordings of the movement of the broken specimen halves after the impact process show that a considerable portion of the measured impact energy is transferred into kinetic energy of the moving specimen halves. The difference of the conventionally measured impact energy and the kinetic energy of the moving specimen halves is introduced as the true impact fracture energy.

KEYWORDS: impact testing, measuring techniques, dynamic material behaviour, polymers, electronic frequency response

INTRODUCTION

The most widely used property for quantifying the impact strength of polymers is the energy to break a specimen in a

[1]Professor, Experimental Mechanics, Ruhr-University Bochum, 44780 Bochum, Germany

[2]Product Manager, Amsler Otto Wolpert-Werke GmbH, 67014 Ludwigshafen, Germany

pendulum impact device. The measuring technique and the evaluation procedure follow in principle the methodology of the Charpy-test [1] originally developed for testing of steel specimens. Because of the low load and energy values that apply in testing of polymeric specimens certain modifications of the test techniques, however, are usually needed. Furthermore, the obtained results require special interpretation and consideration as regards their validity to represent true material properties that indeed characterize the actual failure behaviour of the material. This paper addresses some aspects relevant to the impact testing of polymeric specimens.

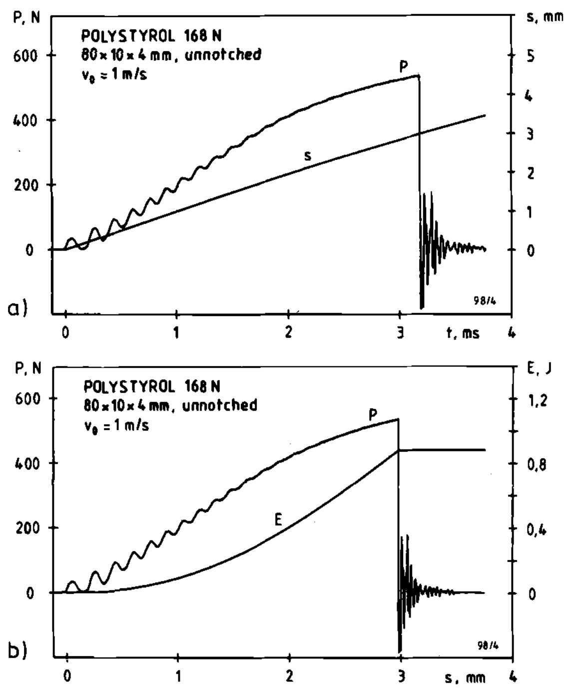

FIG. 1--Typical instrumented impact test data, (P = load, t = time, s = displacement, E = energy).

MEASUREMENT OF IMPACT LOADS

With the modern version of the impact test in its instrumented form, the energy to break a specimen is not determined by the difference of the heights of the pendulum hammer before and after the test; instead, with a load sensor at the tup of the striking hammer the load the specimen is subjected to is measured during the entire loading and subsequent failure process of the specimen. Then, following Newton's law, integration of the measured load-time-trace determines the position of the striking hammer during the impact process; this position is equivalent to the displacements the specimen has undergone

$$s(t)=\int[v_\circ-\frac{1}{m}\int P(t)dt]dt \tag{1}$$

with
P = measured load
t = time
m = mass of hammer
$v_\circ$ = (initial) impact velocity
s = specimen displacement

A plot of the measured load P as function of the calculated displacement s and another integration with respect to displacement gives the energy E to break the specimen

$$E(s)=\int P(s)ds \tag{2}$$

If the integration is not carried out over the entire impact process, partial energy values are obtained by integration up to or in between characteristic parts of the load-time-curve. A typical load-time-record and the derived displacement-time-, load-diplacement-, and energy-displacement-traces obtained in a test with a polymeric specimen are shown in Fig. 1.

It is evident from Eqs 1 and 2 that the load is the essential quantity controlling the final measuring result.

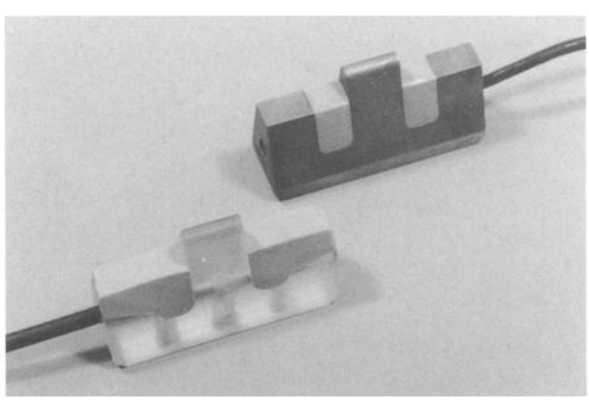

FIG. 2--High sensitivity striker tup made of epoxy resin Araldite B (left) and conventional steel tup (right).

Therefore, certain aspects regarding the experimental techniques for measuring loads in impact tests shall be considered first.

Usually foil strain gauges at the tup of the striking hammer are used as sensors for measuring the load. Since the loads for breaking polymeric specimens are rather small (several 100 N) the resulting strains in tups which are usually made of steel are very low. As a consequence, the resulting signals are difficult to measure and often disturbed by electronic noise. Larger signals can be obtained using semiconductor strain gauges but difficulties may arise from nonlinearities and/or temperature effects, which one usually wants to avoid completely in precision measuring techniques. The author introduced a high sensitivy striker tup [2] which is based on the principle that the tup is made from a material having a Young's modulus lower than of steel: the resulting strains thus become larger and can easily be measured with conventional foil strain gauges. Tups from titanium-, aluminium-, or magnesium-alloys or from the epoxy resin Araldite B are used. The lower the Young's modulus the larger the strains, and consequently, the higher the sensitivity. The sensitivity of these tups is thus enlarged by factors ranging from 2 to about 100. Because of its relatively high strength, strongly linear-elastic and rate insensitive behaviour Araldite B represents a material very well suited for machining tups that allow accurate measurements of very small load values. Figure 2 shows an Araldite B tup in comparison to an equivalent steel tup. The tup has been calibrated up to loads of 1000 N (see Fig. 3), a strongly linear response is obtained.

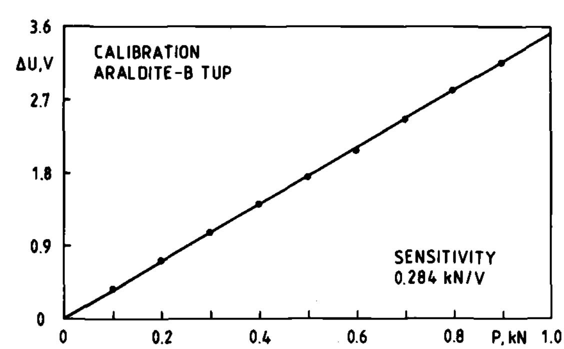

FIG. 3--Calibration of an Araldite B tup.

High sensitivity striker tups in combination with instrumented test techniques represent another advantage: In the usual non-instrumented test, pendulum devices of sufficiently low energy capacity are needed for the testing of low strength materials: sufficiently large differences in the pendulum heights before and after the test are thus obtained and impact energies with sufficient accuracy are determined. As a consequence, pendulum devices of different sizes with energy capacities ranging from 750 J down to 0.5 J and maximum impact velocities from 5.5 m/s down to 2.9 m/s are used. With the instrumented test and high sensitivity striker tups, however, the accuracy in determining impact energy values is only determined by the accuracy of the load measurement - regardless of the energy capacity of the pendulum. Thus, without any disadvantages oversized (high energy) pendulum devices can also be applied for testing of low strength materials if a striker tup of sufficiently high sensitivity is used. Oversized pendulum devices can actually be advantageous since 1.) impact velocities higher than usual can be used (if wanted) for the testing of low strength materials, 2.) the loading rate during the impact and subsequent failure process of the specimen stays practically constant, and 3.) only one pendulum device is needed for tests of any kind of material of any strength property. A high energy (300 J or 50 J) pendulum device with interchangeable striker tups of different sensitivity represents a Universal Impact Pendulum Test System [2,3].

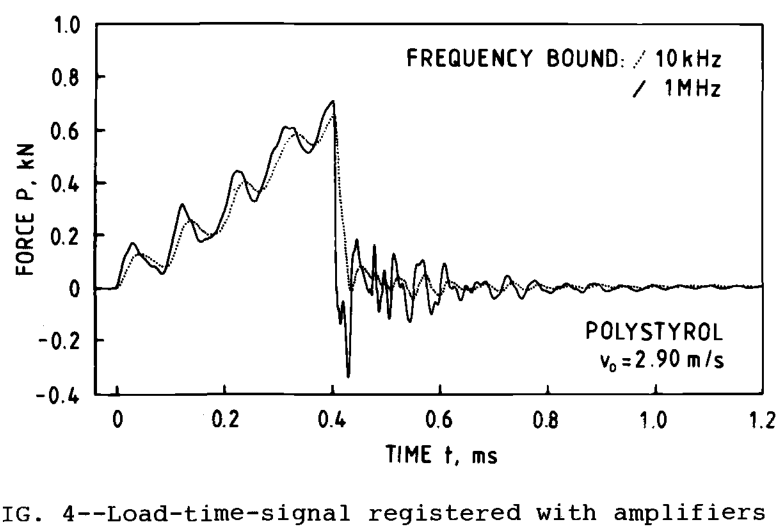

FIG. 4--Load-time-signal registered with amplifiers of different upper frequency bound.

As shown by Fig. 1 the load signal measured in impact tests shows characteristic oscillations. These oscillations do not represent disturbances due to an insufficient measuring technique but result from the sudden loading the specimen is subjected to by the impacting hammer. Thus, these oscillations represent true mechanical behaviour of the specimen and, consequently, must correctly be measured, recorded, and analyzed. Foil strain gauges because of their small dimensions are capable of correctly recording very fast signals (up to about 1 MHz). It is often overlooked, however, that the overall response of the load measuring device is determined by the entire measuring chain, in particular also by the strain gauge amplifier. Since the oscillations in load signals recorded with polymeric specimens of sizes used in pendulum test devices are in the range of about 20 kHz (partly larger) the upper frequency bound of the amplifier should be around 50 kHz, better 100 kHz (or even higher if the rapid load drop due to brittle failure processes shall correctly be recorded). Figure 4 shows load-time-traces of one experiment recorded with a dual channel oscilloscope with one channel attached to a 1 MHz amplifier and the other channel attached to a 10 kHz amplifier. The signal obtained with the 10 kHz channel shows smaller oscillations and, additionally, a slower increase of the load when compared to the signal obtained with the 1 MHz amplifier (see also the different recordings of the rapid load drop). The signal of a 100 kHz amplifier would practically be the same as obtained with the 1 MHz amplifier; these signals represent the true specimen response.

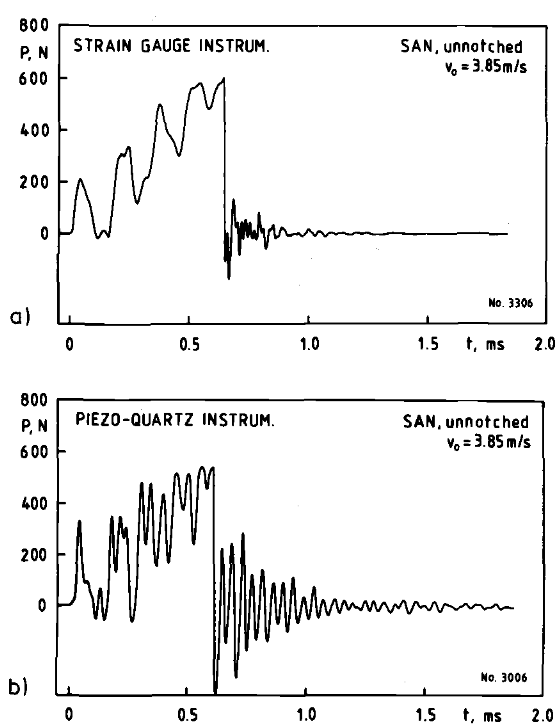

FIG. 5--Load-time-signals recorded with a) strain gauge and b) piezo-quartz instrumented tup.

Sometimes piezo-quartzes, positioned between the striker tup and the hammer, are used as load sensors. Since piezo-quartzes have their own natural eigenfrequency (in the range of 40 - 70 kHz for the fastest piezo-quartzes available) only signals with frequencies below these limit values can accurately be measured and, furthermore, superimposed disturbing eigenoscillations of the piezo-quartz can eventually show up in the measured load signal - if the eigenoscillations are excited by the event to be recorded. Figure 5 shows load-time-traces recorded with a piezo-quartz sensor on the one hand and with a strain gauge instrumented tup on the other hand, for two experiments for which all test parameters were identical [3]. A comparison of the two records shows higher frequency oscillations in the signal recorded by the piezo-quartz, resulting from eigenoscillations of the quartz.

Care is also needed in choosing impact velocities that yield load-time-traces which can reliably be used as a basis for energy calculations. Figure 6 shows load-time-traces obtained with specimens of the same material tested at various impact velocities [3]. The higher the velocity the more pronounced the oscillations, i.e., the larger the amplitude of the oscillations and the lower the number of oscillations up to a certain displacement, as is expected. Thus, the higher the impact velocity, the less reliable the derived energy value.

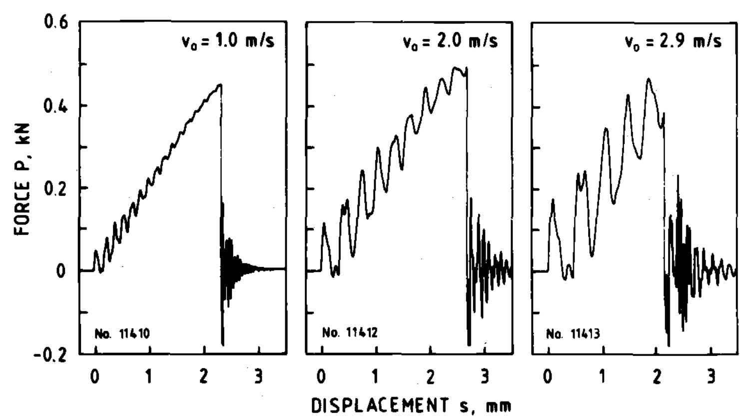

FIG. 6--Load-time-signals obtained at various impact velocities.

In conclusion, for impact testing of polymeric materials load measuring systems of sufficiently high sensitivity in combination with sufficiently fast electronic processing systems are needed to correctly record load traces with their natural oscillations. Only by correct recordings of the load-time-traces can the accuracy of the determined energy values be assessed and can indications on possible erroneously determined energy quantities be obtained.

KINETIC ENERGY OF THE MOVING SPECIMEN HALVES

Precautions in the measuring techniques must be taken to overcome the problems addressed in the previous chapter; with sufficient care, however, the energy absorbed by the specimen during the impact process can accurately be determined. The second part of this paper addresses the question whether this energy in all cases represents the true fracture energy for breaking the specimen. In particular, it is investigated how much effect the kinetic energy of the moving specimen halves after the impact process, i.e., after the specimen has been broken into two separate halves, will have on the results. Especially when specimens fail in a brittle manner, the specimen halves obviously exhibit certain kinetic energy quantities, which is easily recognized, since the broken parts are often found large distances away from the test machine.

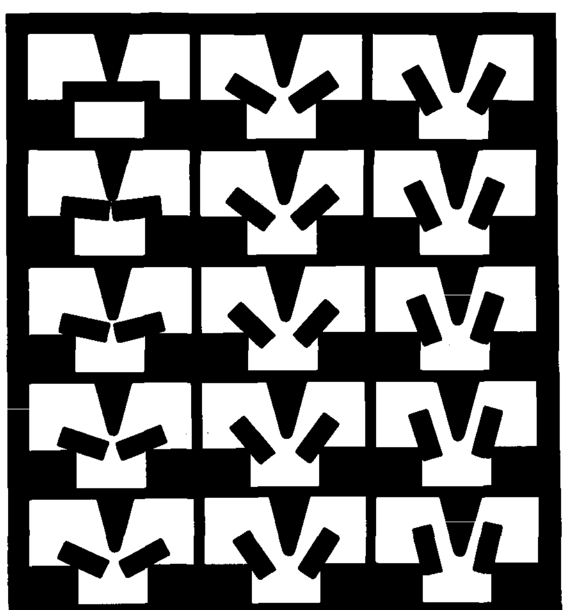

FIG. 7--High speed photographs of the movement of the broken specimen halves after impact.

In order to quantify the magnitude of these kinetic energies, experiments were performed for which the movement of the specimen halves after the impact process has been photographed with a high speed camera [4,5]. A Cranz-Schardin 24 spark high speed camera was utilized for these investigations; the camera was operated in a special recording mode by which shadow images of the object, i.e. the striking tup, the specimen, and the anvils are photographed. To allow for an open view field these experiments were performed with a drop weight tower instead of a pendulum device, but all test parameters were kept the same. Figure 7 shows 15 of the 24 photographs total obtained for a typical experiment. The picture interval time in this series of photographs is 0.64 ms. The graphical representation in Fig. 8 shows the subsequent positions of the moving specimen halves relative to each other in one picture.

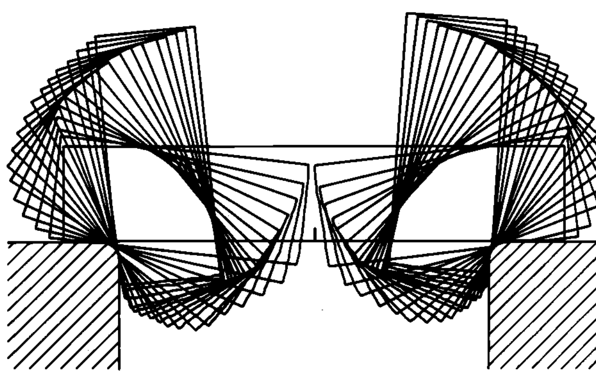

FIG. 8--Position of the broken specimen halves after impact for subsequent times.

For each photograph, i.e. time step, the local coordinates of the specimen halves have been quantitatively determined, and from these data the translational and rotational velocities of the specimen halves, v_T and ω_R, were calculated. With these velocities the kinetic energy for translation, $T_T = \frac{1}{2}m(v_T)^2$, and for rotation, $T_R = \frac{1}{2}\Theta(\omega_R)^2$, and also the total kinetic energy, $T_G = 2(T_T+T_R)$, were determined. Although the translational velocity v_T and the rotational velocity ω_R showed some variations wit time (obviously the free movement of the specimen halves is hindered by the anvils) the total kinetic energy of the specimen halves was - within experimental scatter - determined constant within the time range investigated.

Quantitative data were obtained for the material polystyrene (BASF Polystyrol PS 168 N). Unnotched specimens measuring 80 x 10 x 4 mm were tested at a support span of 60 mm. Experiments were performed with impact velocities ranging from 0.4 to 5 m/s. In the experiments the total impact energy, A, was determined by the described integration procedures from the recorded load-time-traces; the kinetic energy of the moving specimen halves after the impact process, T_G, was determined from the high speed photographs. The data are shown in Fig. 9. The following phenomena are observed: First, the measured impact energy, A, shows a decreasing trend with increasing loading rate, obviously the material embrittles with increasing loading rate. Secondly, and most importantly, the kinetic energy, T_G, of the specimen halves after the impact process represents a very considerable portion of the measured impact energy A.

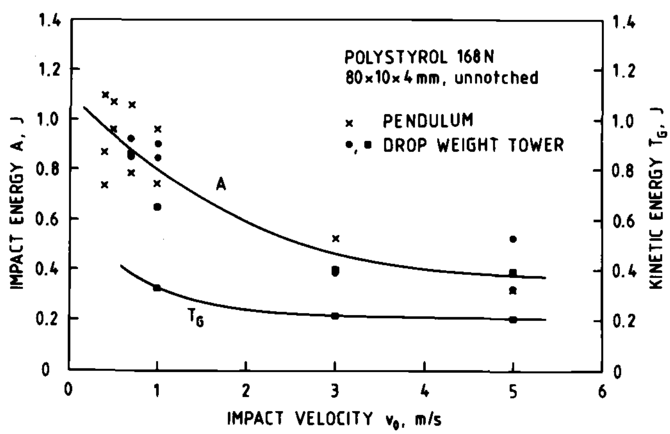

FIG. 9--Measured impact energy and kinetic energy of the broken specimen halves after impact for various impact velocities.

It must be concluded therefore that the measured impact energy, now denoted A^{MEAS} for clarity ($A = A^{MEAS}$), does not represent a true material property, i.e. a property that correctly characterizes the resistance of the material against failure. Obviously, only a certain portion of the measured impact energy is used as fracture energy for breaking the specimen, another obviously very large portion is converted into kinetic energy of the moving specimen halves. As a true and reliable material strength characterization, therefore, the difference of the conventionally measured impact energy and the resulting kinetic energy of the moving specimen halves is proposed

$$A^{TRUE} = A^{MEAS} - T_G \tag{3}$$

This difference energy is denoted impact fracture energy, A^{TRUE}. Regardless of whether the conventional impact energy, A^{MEAS}, or the true impact fracture energy, A^{TRUE}, is considered, a decreasing trend with increasing loading rate results for the data shown in Fig. 9.

Only for specimens that fail in a brittle manner are kinetic energy quantities T_G of considerable magnitude observed, more ductile failure processes result in considerably smaller or negligible kinetic energy quantities. Different to the reported behaviour, specimens in the latter case often even do not break completely into two separate halves but still remain connected by certain unbroken parts of the ligament. Also, when compared to other, non-polymeric types of materials, the magnitude of the kinetic energy, T_G, of the moving specimen halves with respect to the conventional impact energy, A, is of predominant importance for polymeric materials only and of much less importance for other materials. With steels, for example, even if they fail in a brittle manner and kinetic energies are observed, these kinetic energies are small with respect to the impact energies since the strength and ductility properties of steels are higher than of polymers and, consequently, impact energies of considerably higher magnitudes result.

SUMMARY AND CONCLUSIONS

Several aspects of measuring techniques and evaluation procedures for determining impact energies of polymeric specimens in instrumented impact tests have been addressed and requirements for obtaining valid data that correctly characterize the true failure behaviour of the material have been presented. In particular, it has been shown that the load measuring system must meet certain requirements: the load sensing striker tup must be of sufficiently high sensitivity and the electronic measuring system must exhibit a sufficiently high upper frequency bound in order to allow for a correct recording of the forces the specimen is subjected to during the impact process. Only correct recordings of the load allow for the correct and reliable determination of impact energy values.

Furthermore, impact energies, although correctly determined, do not necessarily represent the actual fracture energy for breaking the specimen. Kinematographic recordings of the movement of the broken specimen halves after the impact process have shown that a considerable portion of the measured impact energy is transferred into kinetic energy of the moving specimen halves. Thus, only the difference of the measured impact energy and the kinetic energy of the specimen halves, denoted impact fracture energy, can serve as a reliable quantity characterizing the true failure property of the material. Estimates on the magnitude of these kinetic energy quantities for various conditions are given.

An appropriate consideration of these kinetic energy quantities requires further clarification and additional research. When impact energies for polymers that fail in a ductile manner are compared to those that fail is a brittle manner, however, the different magnitudes of kinetic energies involved should at least in principle be taken into account.

REFERENCES

[1] ESIS-Document "Proposed Standard Method for the Instrumented Charpy-V Impact Test on Metallic Materials", Draft 11, prepared by Working Party "European Standard on Instrumented Charpy Testing" of the European Structural Integrity Society (ESIS) TC 5, Technical Sub-Committee on Dynamic Testing at Intermediate Strain Rates, Chairman H. MacGillivray, Imperial College, London, U.K., 1994.

[2] Kalthoff, J.F., and Achterfeldt, K., "Hochsensitive Schlagfinne zur Prüfung von Kunststoff- oder Keramikproben im instrumentierten Kerbschlagbiegeversuch", Proceedings 13. GESA-Symposium Experimentelle Mechanik in Forschung und Praxis, Bremen, 10./11. May 1990, VDI-Berichte 815, VDI-Verlag, Düsseldorf, Germany, 1990, pp 389-402 and Proceedings Werkstoffprüfung 1990, 6./7. Dec. 1990, Bad Nauheim, DVM, Deutscher Verband für Materialforschung und -prüfung, Berlin, Germany, 1990, pp 43-54.

[3] Kalthoff, J.F., "Ermittlung des Werkstoffverhaltens von Kunststoffen unter schlagartiger Beanspruchung mit dem instrumentierten Schlag-Biege-Versuch", Bericht der Wolpert Forschung und Entwicklung, FE 1/93, Amsler Otto Wolpert-Werke GmbH, Ludwigshafen, Germany, 1993.

[4] Kalthoff, J.F., and Takahashi, S., "Characterization of the Strength of Ceramic and Polymeric Materials by Instrumented Impact Testing", Proc. IMEKO/GESA Symposium on Risk Minimization by Experimental Mechanics, Düsseldorf, April 28-30, 1992, VDI-Berichte 940, VDI-Verlag Düsseldorf, Germany, 1992, pp 333-344.

[5] Kalthoff, J.F., and Takahashi, S., "On the Measurement of the True Impact Energy of Polymeric and Ceramic Specimens in Instrumented Impact Tests", Proc. Int. Symp. on Impact Engineering, Ed. I. Maekawa, Sendai, Japan, Nov. 2-4, 1992, pp 538-545.

Author Index

Subject Index

ISBN 0-8031-2018-4